



University of HUDDERSFIELD

University of Huddersfield Repository

Tesfa, Belachew Chekene

Investigations into the Performance and Emission Characteristics of a Biodiesel Fuelled CI Engine under Steady and Transient Operating Conditions

Original Citation

Tesfa, Belachew Chekene (2011) Investigations into the Performance and Emission Characteristics of a Biodiesel Fuelled CI Engine under Steady and Transient Operating Conditions. Doctoral thesis, University of Huddersfield.

This version is available at <http://eprints.hud.ac.uk/id/eprint/11072/>

The University Repository is a digital collection of the research output of the University, available on Open Access. Copyright and Moral Rights for the items on this site are retained by the individual author and/or other copyright owners. Users may access full items free of charge; copies of full text items generally can be reproduced, displayed or performed and given to third parties in any format or medium for personal research or study, educational or not-for-profit purposes without prior permission or charge, provided:

- The authors, title and full bibliographic details is credited in any copy;
- A hyperlink and/or URL is included for the original metadata page; and
- The content is not changed in any way.

For more information, including our policy and submission procedure, please contact the Repository Team at: E.mailbox@hud.ac.uk.

<http://eprints.hud.ac.uk/>

Investigations into the Performance and Emission
Characteristics of a Biodiesel Fuelled CI Engine under
Steady and Transient Operating Conditions

Belachew Chekene Tesfa

A Thesis Submitted to the University of Huddersfield
in Partial Fulfilment of the Requirements for
the Degree of Doctor of Philosophy

May 2011

TABLE OF CONTENTS

TABLE OF CONTENTS	2
LIST OF FIGURES	7
LIST OF TABLES.....	17
LIST OF ABBREVIATIONS AND NOTATIONS	18
ABSTRACT	22
DECLARATION	24
COPYRIGHT	25
ACKNOWLEDGEMENTS.....	26
PUBLICATIONS	27
CHAPTER ONE	29
1. INTRODUCTION	29
1.1 Background.....	30
1.2 Biodiesel Production and Physical Characterisation.....	33
1.3 Performance and Emission Characteristics of CI Engines Running with Biodiesel	35
1.4 Emission Regulations	37
1.5 Research Problem and Aims	38
1.6 Organisation of Thesis.....	41
1.7 Summary on Chapter One	43
CHAPTER TWO	44
2. BIODIESEL CHARACTERISATION AND PERFORMANCE AND EMISSION CHARACTERISATION OF CI ENGINES RUNNING WITH BIODIESEL	44
2.1 Biodiesel Characterisation.....	45

2.1.1	Density of Biodiesel	47
2.1.2	Viscosity of Biodiesel	48
2.1.3	Heating Value of Biodiesel	50
2.1.4	Effects of Physical Properties of Biodiesel on Fuel Supply System.....	53
2.1.5	Summary of Knowledge Gaps in Biodiesel Characterisation Research	54
2.2	Combustion, Performance and Emission Characteristics of CI Engines Running with Biodiesel.....	55
2.2.1	Combustion Characteristics of CI Engines Running with Biodiesel	55
2.2.2	Performance Characteristics of CI Engines Fuelled by Biodiesel	57
2.2.3	Emission Characteristics of CI Engines Running with Biodiesel	61
2.2.4	Summary on Knowledge Gaps on Combustion, Performance and Emission Characteristics of CI Engines Running with Biodiesel	66
2.3	NOx Measurement Techniques and Prediction Models.....	67
2.4	Techniques to Reduce NOx Emission.....	68
2.4.1	NOx Formation in Diesel Engines	68
2.4.2	Methods of NOx Reduction	70
2.4.3	Summary and Knowledge Gaps on NOx Emission Reduction Techniques and Predicting Models.....	74
2.5	Scope and Objective of the Study	75
2.5.1	Scope of the Study.....	75
2.5.2	Objectives of the Study	76
2.6	Summary on Chapter Two.....	77
 CHAPTER THREE.....		78
3. TEST RIG INSTRUMENTATION AND TEST PROCEDURES.....		78
3.1	Biodiesel Characterisation Facilities	79
3.1.1	Materials-Biodiesel and Diesel	79
3.1.2	Density measurement: Apparatus and Procedures	79
3.1.3	Viscosity measurement: Apparatus and Procedures	79
3.1.4	Lower Heating Value: Apparatus and Procedures	80
3.2	CI Engine and Test Bed Facilities	81
3.2.1	Engine Dynamometer Specifications	81
3.2.2	Oil and Coolant System.....	83

3.2.3	Measurement System for Operating Parameters of the Test Engine.....	84
3.3	Test Procedures	92
3.3.1	Biodiesel Blend Preparation.....	92
3.3.2	Engine Test Cycles.....	94
3.3.3	Testing Procedures and the Details of the Measured Parameters	96
3.3.4	Transient Testing Cycles	98
3.3.5	Water Injection System	100
3.3.6	Water Injection Test Procedures	102
3.3.7	Procedure to Ensure Accuracy of Measurement	104
3.4	Summary on Chapter Three.....	104
 CHAPTER FOUR.....		106
4.	BIODIESEL CHARACTERISATION	106
4.1	Effect of Biodiesel Fraction and Temperature on Density.....	107
4.2	Effect of Biodiesel Fraction and Temperature on Viscosity	111
4.3	Effect of Biodiesel Fraction on Lower Heating Value.....	117
4.4	Development of integrated Mathematical Models of Fuel Supply System.....	122
4.5	Computational Procedures used for Models of Fuel Supply System	124
4.6	Effect of Density and Viscosity of Biodiesel on the Fuel Supply System Performance.....	126
4.7	Summary on Biodiesel Charactersation	130
 CHAPTER FIVE		131
5.	PERFORMANCE AND EMISSION CHARACTERISTICS OF A CI ENGINE RUNNING WITH BIODIESEL BLENDS DURING STEADY STATE.....	131
5.1	In-Cylinder Pressure and Heat Release Rate of the CI Engine	132
5.2	Performance Characteristics of the Test CI Engine Running with Biodiesel Blends during Steady State Operating Condition.....	139

5.2.1	Effects of Biodiesel Feedstock Sources on the Engine Performance Parameters	139
5.2.2	Effects of Biodiesel Feed Sources on the Engine Emission Parameters	143
5.2.3	Effects of Biodiesel Blend Fraction on Engine Performance Parameters..	147
5.2.4	Effects of Biodiesel Blend Fraction on Engine Emissions Parameters.....	151
5.2.5	Effects of Physical Properties of Biodiesel on Engine Performance Parameters	155
5.3	Summary on the Performance and Emission characteristics of the test CI engine during Steady State Operation.....	158
CHAPTER SIX		160
6.	PERFORMANCE AND EMISSION CHARACTERISTICS OF THE TEST CI ENGINE DURING TRANSIENT OPERATION	160
6.1	Performance Characteristics during Transient Operation	161
6.1.1	Fuel Consumption Rate	161
6.1.2	Emission Characteristics of CI Engine during Transient Operation	171
6.2	Effects of Engine Parameters on Transient Emissions.....	195
6.3	Quantitative Dependence of Emissions on Engine Operating Parameters.....	208
6.4	Summary on the Performance and Emission Characteristics of the Test CI Engine during Transient Operation	213
CHAPTER SEVEN.....		215
7.	PREDICTION OF NO_x EMISSION FROM THE TEST CI ENGINE BASED ON THE IN-CYLINDER PRESSURE MEASUREMENT	215
7.1	NO _x Prediction Model Development.....	216
7.2	Computational Procedures for NO _x Prediction from in-cylinder Pressure.....	219
7.3	Parametric investigations (In-cylinder temperature and NO _x)	220
7.4	Validation of the NO _x Prediction Model	225
7.5	Summary on NO _x Prediction from In-cylinder Pressure	228

CHAPTER EIGHT	229
8. MANAGEMENT OF NO_x EMISSIONS FROM A CI ENGINE OPERATING WITH BIODIESEL USING A WATER INJECTION SYTEM	229
8.1 Effects of Water Injection on NO _x and CO Emissions.....	230
8.2 Water Injection Effects on Cylinder Pressure and Heat Release Rate	234
8.3 Effects of Water Injection on Engine Performance.....	240
8.4 Summary on Effects of Water Injection on CI engine Performance.....	243
 CHAPTER NINE	 245
9. CONCLUSIONS AND FUTURE WORKS	245
9.1 Review of Research Objective and Achievements.....	246
9.2 Conclusions	248
9.2.1 Conclusions on Biodiesel Characterisation	249
9.2.2 Conclusions on Combustion, Performance and Emission Characteristics of the Test CI Engine during Steady and Transient Operations	250
9.2.3 Conclusions on NO _x Prediction Model.....	251
9.2.4 Conclusions on Effects of Water Injection on NO _x Reduction	252
9.3 Thesis contribution to the Knowledge.....	252
9.4 Recommended Future Work.....	254
 APPENDIX	 256
Appendix A: Heating Value Measurement.....	256
Appendix B: Power and Torque Curves of CI engine.....	258
References.....	264

Total Pages: 270

Total word count: 65,422

LIST OF FIGURES

Figure 1-1 Total number of cars manufactured in the world [6]	30
Figure 1-2 Biodiesel production trend of EU countries [14], [15]	32
Figure 1-3 Biodiesel Production Process [22]	33
Figure 1-4 General equation of transesterification process [10]	34
Figure 1-5 Speed and Torque transient profile a) acceleration, b) deceleration.....	36
Figure 2-1 Passengers cars NO _x emission overview of past and future requirements.....	71
Figure 3-1 Capillary viscometer apparatus.....	80
Figure 3-2 Bomb calorimeter apparatus	81
Figure 3-3 Experimental engine facilities.....	82
Figure 3-4 Engine test facilities lay out.....	83
Figure 3-5 In-cylinder pressure measurement system.....	85
Figure 3-6 FMS-1000 Gravimetric fuel meter apparatus and its specifications.....	86
Figure 3-7 Hot-film air mass flow meter with its specification.....	87
Figure 3-8 Torque measurement system with its specification	88
Figure 3-9 DRUCK PMP-4010 series sensors and RS-249-3943 pressure transducer	88
Figure 3-10 HORIBA EXSA-1500- Emission analyser.....	90
Figure 3-11 Analogue to Digital Converter (ADC) and measured parameters	92
Figure 3-12 Biodiesel blends prepared in the laboratory for performance and emission investigations	93
Figure 3-13 Range of engine speeds and engine loads for steady state testing cycle	95
Figure 3-14 Speed transient profiles a) Acceleration 1000-1500rpm b) Deceleration (1500-1000rpm).....	98
Figure 3-15 Torque transition profiles a) Positive torque transition 210-420N b) Negative torque transition 420-210Nm.....	99
Figure 3-16 Scheme of water injection system at intake manifold	101
Figure 3-17 Water injection system configuration	102
Figure 4-1 Variation of density of biodiesel with biodiesel fraction for different biodiesel source feeds.....	107
Figure 4-2 Variation of density of biodiesel with temperature for different biodiesel source feeds.....	110
Figure 4-3 Variation of kinematic viscosity of biodiesel with biodiesel fraction for different biodiesel source feeds	112

Figure 4-4 Variation of kinematic viscosity of biodiesel with temperature for different biodiesel sources feeds.....	113
Figure 4-5 Variation of predicted kinematic viscosity of rapeseed biodiesel with temperature	116
Figure 4-6 Variation of kinematic viscosity of biodiesel with temperature	117
Figure 4-7 Temperature change in Bomb calorimeter for various biodiesel source feed.	118
Figure 4-8 Variation of lower heating value of biodiesel with biodiesel fraction for different biodiesel source feeds.	119
Figure 4-9 Flow rate of fuel through filter with time for different kinematic viscosity values	127
Figure 4-10 Variation of fuel pump head loss with fuel flow rate for various kinematic viscosity	128
Figure 4-11 Variation of sauter mean diameter with kinematic viscosity using Hiroyasu and Arai Model [184].	129
Figure 4-12 Variation of sauter mean diameters with temperature using Hiroyasu and Arai Model [184].	129
Figure 5-1 P-V diagrams for CI engine running with diesel and biodiesel blends at speed of 1300rpm and range of engine loads.....	133
Figure 5-2 Variation of in-cylinder pressure with crank angel for CI engine running with 50B, 100B and diesel at engine speed of 1300rpm and range of engine loads	134
Figure 5-3 Variation of rate of in-cylinder pressure increase with crank angle for CI engine running with 50B, 100B and diesel at engine speed of 1300rpm and range of engine loads	135
Figure 5-4 Variation of heat release rate with crank angle for CI engine running with 50B, 100B and diesel at engine speed of 1300rpm and range of engine loads.	137
Figure 5-5 Variation of cumulative heat release rate with crank angle of CI engine running with 50B, 100B and diesel at engine speed of 1300rpm and range of engine loads	138
Figure 5-6 Variation of peak in-cylinder pressure with engine speed for CI engine running with ROB, COB, WOB and diesel at load of 420Nm.....	140

Figure 5-7 Variation of brake specific fuel consumption (BSFC) with engine speed of CI engine running with ROB, COB, WOB and diesel at load of 105Nm and 420Nm	141
Figure 5-8 Variation of thermal efficiency with speed for CI engine running with ROB, COB, WOB and diesel at load of 420Nm.....	142
Figure 5-9 Variation of CO ₂ emission of CI engine running with ROB, COB, WOB and diesel at load of 420Nm	144
Figure 5-10 Variation of NO _x emission with engine speed for CI engine running with ROB, COB, WOB and diesel at load of 420Nm and range of engine speeds	145
Figure 5-11 Variation of THC emission with engine speed for CI engine running with ROB, COB, WOB and diesel at load of 420Nm	146
Figure 5-12 Variation of CO emission with speed for CI engine running with ROB, COB, WOB and diesel at a load of 420Nm	147
Figure 5-13 Variation of in-cylinder pressure with speed of CI engine running with biodiesel blends at load of 420Nm	148
Figure 5-14(a,c) Variation of BSFC with engine speed for different biodiesel blends at 105Nm and 420Nm (b,d) Variation of BSFC increment with engine speed for biodiesel blends at load of 105 and 420Nm.....	149
Figure 5-15 (a) Variation of BSFC with biodiesel fraction at engine speed of 1500rpm and various engine loads (b) Variation of BSFC percentage increment with biodiesel fraction at engine speed of 1500rpm and at various engine loads.	150
Figure 5-16 (a) Variation of CO ₂ emissions with engine speed for CI engine running with biodiesel blends at load of 420Nm (b) Variation of CO ₂ emissions percentage reduction with engine speed for CI engine running with biodiesel blends at load of 420Nm	151
Figure 5-17 Variation of NO _x emissions with engine speed for CI engine running with biodiesel blends at load of 420Nm (b) Variation of NO _x emissions percentage reduction with engine speed for CI engine running with biodiesel blends at load of 420Nm.....	153
Figure 5-18 Variation of NO _x emissions with engine speed for CI engine running with biodiesel blends at load of 420Nm (b) Variation of NO _x emissions percentage	

reduction with engine speed for CI engine running with biodiesel blends at load of 420Nm	154
Figure 5-19 Variation of CO emissions with engine speed for CI engine running with biodiesel blends at load of 420Nm (b) Variation of CO emissions percentage reduction with engine speed for CI engine running with biodiesel blends at load of 420Nm	155
Figure 5-20 Variation of BSFC with density of biodiesel at engine speed of 900rpm and 1500rpm and various engine loads	156
Figure 5-21 Variation of BSFC with viscosity of biodiesel at engine speed of 900rpm and 1500rpm and various engine loads	157
Figure 5-22 Variation of BSFC with density of biodiesel at engine speed of 900rpm and 1500rpm and various engine loads	158
Figure 6-1 (a) Variation of Fuel flow rate with time for CI running with biodiesel during speed transient at 420Nm (b) Variation of Fuel flow rate percentage increment with time by using biodiesel blends during speed transient at 420Nm	162
Figure 6-2 (a) Variation of Fuel flow rate with time for CI running with biodiesel during torque transition at 420Nm (b) Variation of Fuel flow rate percentage increment with time by using biodiesel blends during torque transition at 420Nm	163
Figure 6-3 (a) Variation of exhaust temperature with time for CI engine running with biodiesel during speed transient at 420Nm (b) Variation of exhaust temperature percentage increment with time by using biodiesel blends during speed transient at 420Nm.....	165
Figure 6-4 (a) Variation of exhaust temperature with time for CI running with biodiesel during torque transition at 420Nm (b) Variation of exhaust temperature percentage increment with time by using biodiesel blends during torque transition at 420Nm	166
Figure 6-5 (a) Variation of in-cylinder peak pressure with time for CI engines running with different fuels during speed positive transient (b) Variation of rate of change in-cylinder peak pressure with time for CI engines running with different fuels during negative speed transient.....	168

Figure 6-6 (a) Variation of In-cylinder peak pressure with time for CI engines running with different fuels during negative speed transient (b) Variation of rate of change in-cylinder peak pressure with time for CI engines running with different fuels during negative speed transient	169
Figure 6-7 (a) Variation of In-cylinder peak pressure with time for CI engines running with different fuels during torque positive transient (b) Variation of rate of change in-cylinder peak pressure with time for CI engines running with different fuels during negative torque transient.....	170
Figure 6-8 (a) Variation of in-cylinder peak pressure with time for CI engines running with different fuels during negative torque transient (b) Variation of rate of change in-cylinder peak pressure with time for CI engines running with different fuels during negative torque transient.....	171
Figure 6-9 (a) Variation of CO ₂ emission of CI engines with time for running with different fuels during positive speed transient (b) Variation of rate of change CO ₂ emission with time for CI engines running with different fuels during positive speed transient.....	172
Figure 6-10 (a) Variation of CO ₂ emission of CI engines with time for running with different fuels during negative speed transient (b) Variation of rate of change CO ₂ emission with time for CI engines running with different fuels during negative speed transient.....	173
Figure 6-11 (a) Variation of CO ₂ emission of CI engines with time for running with different fuels during positive torque transient (b) Variation of rate of change CO ₂ emission with time for CI engines running with different fuels during positive torque transient.....	174
Figure 6-12 (a) Variation of CO ₂ emission of CI engines with time for running with different fuels during positive torque transient (b) Variation of rate of change CO ₂ emission with time for CI engines running with different fuels during positive torque transient.....	175
Figure 6-13 Variation of CO ₂ emission percentage reduction of CI engine with time by using different biodiesel blends during speed transient condition.....	176
Figure 6-14 Variation of CO ₂ emission percentage reduction of CI engine with time by using different biodiesel blends during torque transient condition.....	177

Figure 6-15 (a) Variation of NO _x emission of CI engines with time for running with different fuels during positive speed transient (b) Variation of rate of change NO _x emission with time for CI engines running with different fuels during positive speed transient.....	178
Figure 6-16 (a) Variation of NO _x emission of CI engines with time for running with different fuels during negative speed transient (b) Variation of rate of change NO _x emission with time for CI engines running with different fuels during negative speed transient.....	179
Figure 6-17 (a) Variation of NO _x emission of CI engines with time for running with different fuels during positive torque transient (b) Variation of rate of change NO _x emission with time for CI engines running with different fuels during positive torque transient.....	180
Figure 6-18 (a) Variation of NO _x emission of CI engines with time for running with different fuels during negative torque transient (b) Variation of rate of change NO _x emission with time for CI engines running with different fuels during negative torque transient.....	181
Figure 6-19 Variation of NO _x emission percentage reduction of CI engine with time by using different biodiesel blends during speed transient condition.....	182
Figure 6-20 Variation of NO _x emission percentage reduction of CI engine with time by using different biodiesel blends during torque transient condition.....	183
Figure 6-21 (a) Variation of CO emission of CI engines with time for running with different fuels during positive speed transient (b) Variation of rate of change CO emission with time for CI engines running with different fuels during positive speed transient.....	184
Figure 6-22 (a) Variation of CO emission of CI engines with time for running with different fuels during negative speed transient (b) Variation of rate of change CO emission with time for CI engines running with different fuels during negative speed transient.....	185
Figure 6-23 (a) Variation of CO emission of CI engines with time for running with different fuels during positive torque transient (b) Variation of rate of change CO emission with time for CI engines running with different fuels during positive torque transient.....	186

Figure 6-24 (a) Variation of CO emission of CI engines with time for running with different fuels during negative torque transient (b) Variation of rate of change CO emission with time for CI engines with different fuels during negative torque transient	187
Figure 6-25 Variation of CO emission percentage reduction of CI engine with time by using different biodiesel blends during speed transient condition.....	188
Figure 6-26 Variation of CO emission percentage reduction of CI engine with time by using different biodiesel blends during torque transient condition.....	188
Figure 6-27 (a) Variation of THC emission of CI engines with time for running with different fuels during positive speed transient (b) Variation of rate of change CO emission with time for CI engines running with different fuels during positive speed transient.....	189
Figure 6-28 (a) Variation of THC emission of CI engines with time for running with different fuels during negative speed transient (b) Variation of rate of change CO emission with time for CI engines running with different fuels during negative speed transient.....	190
Figure 6-29 (a) Variation of THC emission of CI engines with time for running with different fuels during positive torque transient (b) Variation of rate of change CO emission with time for CI engines running with different fuels during positive torque transient.....	191
Figure 6-30 (a) Variation of THC emission of CI engines with time for running with different fuels during negative torque transient (b) Variation of rate of change CO emission with time for CI engines running with different fuels during negative speed transient.....	192
Figure 6-31 THC emission percentage reduction of CI engine by using different biodiesel blends during speed transient condition.....	193
Figure 6-32 THC emission percentage reduction of CI engine during torque transition condition	193
Figure 6-33 CO ₂ emission of CI engine running with various fuels during speed transient of 1000-1500rpm at range of engine loads	195
Figure 6-34 CO ₂ emission of CI engine running with various fuels during speed transient of 1500-1000rpm at range of engine loads	196

Figure 6-35 CO ₂ emission of CI engine running with various fuels during torque transition of 210Nm to 420Nm and at range of engine speeds.....	197
Figure 6-36 CO ₂ emission of CI engine running with various fuels during torque transition of 420Nm to 210Nm and at various engine speeds	198
Figure 6-37 NO _x emission of CI engine running with various fuels during speed transient of 1000-1500rpm at range of engine loads	199
Figure 6-38 Variation of the NO _x emission with respect to the engine speed for the test engine operating with different fuels during a negative speed transient of 1500 rpm to 1000 rpm at different engine torques.	200
Figure 6-39 NO _x emission of CI engine running with various fuels during torque transition of 210Nm to 420Nm and at various engine speeds	201
Figure 6-40 NO _x emission of CI engine running with various fuels during torque transition of 420Nm to 210Nm and at various engine speeds	202
Figure 6-41 THC emission of CI engine running with various fuels during speed transient of 1000-1500rpm at range of engine loads	203
Figure 6-42 THC emission of CI engine running with various fuels during speed transient of 1500-1000rpm at range of engine loads	203
Figure 6-43 THC emission of CI engine running with various fuels during torque transition of 210Nm to 420Nm and at various engine speeds	204
Figure 6-44 THC emission of CI engine running with various fuels during torque transition of 420Nm to 210Nm and at various engine speeds	205
Figure 6-45 CO emission of CI engine running with various fuels during speed transient of 1000-1500rpm at range of engine loads	206
Figure 6-46 CO emission of CI engine running with various fuels during speed transient of 1500-1000rpm at range of engine loads	207
Figure 6-47 CO emission of CI engine running with various fuels during torque transition of 210Nm to 420Nm and at various engine speeds	207
Figure 6-48 CO emission of CI engine running with various fuels during torque transition of 420Nm to 210Nm and at various engine speeds	208
Figure 6-49 Accuracy of prediction models for CO ₂ emission estimation.....	209
Figure 6-50 Accuracy of prediction models for NO _x emission estimation.....	211
Figure 6-51 Accuracy of prediction models for THC emission estimation.....	212
Figure 6-52 Accuracy of prediction models for CO emission estimation.....	213

Figure 7-1 Flow chart for NO _x prediction from in-cylinder pressure	217
Figure 7-2 In-cylinder temperature versus crank angle of CI engine running with diesel during: (a) engine speeds of 1300 rpm and various loads (b) engine loads of 420Nm and at various engine speeds.....	221
Figure 7-3 In-cylinder temperature versus crank angle of CI engine running with biodiesel(100B) during: (a) engine speeds of 1300 rpm and various loads (b) engine loads of 420Nm and at various engine speeds.	222
Figure 7-4 In-cylinder temperature versus crank angle of CI engine running with diesel and biodiesel for engine loads of 420Nm and range of speeds	223
Figure 7-5 Variation of predicted NO _x emission with crank angle of CI engine running with biodiesel at various loads and range of engine speeds	224
Figure 7-6 Variation of predicted NO _x emission with crank angle of CI engine running with biodiesel and diesel at engine load of 210Nm and various engine speeds	225
Figure 7-7 Variation of predicted NO _x emission with crank angle of CI engine running with biodiesel and diesel at engine load of 315Nm and various engine speeds	226
Figure 8-1 NO _x emission values of CI engine running with biodiesel(100B) and water at range of engine speeds and engine loads	230
Figure 8-2 Reduction of NO _x emission from CI engine running with biodiesel(100B) due to the effects of water injection at range of engine speeds and engine loads	231
Figure 8-3 CO emission values from CI engine running with biodiesel(100B) and water at range of engine speeds and engine loads.....	232
Figure 8-4 Percentage increase in CO emission from CI engine running with biodiesel(100B) due to the effects of water injection at range of engine speeds and engine loads.....	233
Figure 8-5 P-V diagram of CI engine running with biodiesel(100B) and water at an engine speed of 1300rpm at various engine loads	234
Figure 8-6 In-Cylinder pressure versus crank angle of CI engine running with biodiesel(100B) and water at engine speed of 1300rpm and various engine loads	235
Figure 8-7 In-Cylinder pressure versus crank angle of CI engine running with biodiesel(100B) and water at loads 420Nm and various engine speeds.....	236

Figure 8-8 Heat releases rate of CI engine versus crank angle running with biodiesel(100B) and water at range of engine speeds and engine loads.....	238
Figure 8-9 Cumulative heat release of CI engine versus crank angle running with biodiesel(100B) and water at range of engine speeds and engine loads.....	239
Figure 8-10 Brake specific fuel consumption (BSFC) of CI engine running with biodiesel(100B) and water at range of engine speeds and various engine loads	240
Figure 8-11 Brake specific fuel consumption (BSFC) change of CI engine due to water injection at range of engine speeds and engine loads	241
Figure 8-12 Thermal efficiency values of CI engine running with biodiesel(100B) and water at range of engine speeds and engine loads	242
Figure 8-13 Thermal efficiency change of CI engine due to water injection at range of engine speeds and engine loads	243

LIST OF TABLES

Table 1-1 EU emission standard for passenger diesel cars [38].....	38
Table 2-1 Standard Specification Biodiesel, B100 and diesel fuel [1], [54].....	46
Table 2-2 The heating value predication correlations developed by previous authors	52
Table 2-3 Estimated share of literature (in % number of publications) on effect of pure biodiesel on engine performance and emission in comparison with Diesel [91] 59	59
Table 2-4 Rate constants for thermal NO _x formation [140].....	69
Table 3-1 Characteristics of JCB engine	82
Table 3-2 Cooling system specification	84
Table 3-3 The emission analyser type and measuring range.....	90
Table 3-4 Physical and Chemical properties of Biodiesel and its blends.....	94
Table 3-5 Transient profiles values of previous research studies.....	96
Table 3-6 Measured and calculated parameters during the engine test.....	97
Table 3-7 Quantity of water injected by previous researchers	103
Table 3-8 Engine operating conditions and water mass flow rate.....	103
Table 4-1 Density of biodiesel blend by experimental methods, mixing equation and correlation equation at 15.6°C.....	109
Table 4-2 Kinematic viscosity of biodiesel and its blends at 40°C.	115
Table 4-3 Lower heating value prediction from the density of rapeseed oil biodiesel blends	121
Table 4-4 Lower heating value prediction from the viscosity of rapeseed oil biodiesel blends	121
Table 4-5 Input parameters for fuel supply system analysis	125
Table 6-1 Summary of the maximum emission reduction when using biodiesel blends as compared with diesel.....	194
Table 6-2 The effects of transient operation on of the post- transient operation.....	194
Table 6-3 Emission predicting models coefficients of CI engine running with diesel and biodiesel blends.....	210
Table 7-1 Rate constants for thermal NO _x formation [140].....	218
Table 7-2 Measured and Predicted NO _x emission values of CI engine running with biodiesel (100B).....	227
Table 7-3 Measured and Predicted NO _x emission values of CI engine running with biodiesel (100B).....	227

LIST OF ABBREVIATIONS AND NOTATIONS

Through the thesis abbreviations have been defined. The abbreviations and descriptions with units (where require) have been listed below.

List of Abbreviations

<i>0B</i>	0% Biodiesel	[%]
<i>5B</i>	5% Biodiesel	[%]
<i>20B</i>	20% Biodiesel	[%]
<i>50B</i>	50% Biodiesel	[%]
<i>100B</i>	100% Biodiesel	[%]
<i>BSFC</i>	Brake specific fuel consumption	[g/kWh]
<i>CI</i>	compression ignition	[-]
<i>CO:</i>	Carbon monoxide	[ppm]
<i>CO₂:</i>	Carbon dioxide	[%]
<i>EGR</i>	Exhaust gas recirculation	[-]
<i>ETBE:</i>	Ethyl tertiary butyl ether	[-]
<i>EU</i>	European Union	[-]
<i>FT</i>	Fischer-tropsch	[-]
<i>HCLD</i>	Heated chemiluminescent detector	[-]
<i>LHV</i>	lower heating value	[J/kg]
<i>NO_x</i>	Nitrogen oxides	[ppm]
<i>PM</i>	Particulate material	[ppm]
<i>THC</i>	Total hydrocarbon,	[ppm]
<i>SG</i>	Specific gravity	[-]
<i>HHV</i>	Higher heating value	[J/kg]

<i>CN</i>	Carbon number	[-]
<i>NDIR</i>	Non-dispersive infrared	[-]
<i>HCLD</i>	Heated chemiluminescent detector	[-]
<i>HFID</i>	Heated flame ionisation detector	[-]
<i>BDC</i>	Bottom dead centre	[deg]
<i>TDC</i>	Top dead centre	[deg]
<i>DIN</i>	Germany Institute for Standardization	[-]
ΔT	Temperature change	[K]
<i>ADC</i>	Analogue to Digital Converter	[-]
<i>PID</i>	proportional–integral–derivative controller	[-]
<i>Re</i>	Reynolds number	[-]
<i>SCR</i>	Selective catalytic reduction	[-]

List of Notations

M_w	Water mass flow rate	[kg/s]
C_{pw}	Specific heat capacity of water	[J/kg]
a	Crank radius	[m]
A	Area	[m ²]
A	Stoichiometric air fuel ratio	[-]
a, b	Specific gravity correlation constants	[-]
b	Bore diameter	[m]
<i>bio</i>	Biodiesel	[-]
<i>corr</i>	Correlation	[-]
<i>die</i>	Diesel	[-]
D_p	Piston head diameter	[m]

e_1	Correction heat produced by burning the fuse	[J/kg]
Em	Engine emission	[% , ppm]
Ep	Engine parameter	[rpm, Nm]
h_e	Enthalpy of evaporation	[J/kg]
I	Refractive index	[-]
k_1, k_2, k_3	Rate constants of NOx formation	[m ³ /g ¹ om s]
K_{sens}	Sensor sensitivity constant	[mV/MPa]
l	Rod length	[m]
M_a	Air mass flow rate	[Kg/s]
m_b	Mass of the benzoic acid	[kg]
m_{bd}	Mass of biodiesel	[kg]
m_f	Fuel mass rate of injection	[kg/s]
mix	Mixture	[-]
N	Number of cycles	[cycles/s]
N_R	Rotational speed of engine	[rev/s]
P	In-cylinder pressure	[Pa]
P	Power	[W]
P_{offset}	Offset in-cylinder pressure	[Pa]
P_{real}	Actual in-cylinder pressure	[kg/s]
Q	Heat	[m]
q	Heat supply factor	[-]
R	Ratio of connecting rod length (l) to crank radius (a).	[-]
R	Regression correlation	[-]
R_g	Gas constant	[J/kg K]
S	Stroke	[m]

T	Temperature	[K]
t	Time	[s]
T_l	Ambient temperature	[K]
T_b	Water boiling temperature	[K]
V	In-cylinder volume	[m ³]
V_d	Engine displacement volume	[m ³]
W	Energy equivalent of the calorimeter	[J/k]
X	Biodiesel fraction	[%]
β	Cut-off fuel ratio	[-]
γ	Ratio of specific heats	[-]
η	Thermal efficiency	[%]
μ	Kinematic viscosity	[mm ² /s]
σ	Surface tension	[N/m]
μ	Dynamic viscosity	[Pa s]
ρ	Density	[Kg/m ³]
θ	Crank angle	[deg]

ABSTRACT

The stringent emission laws, the depletion of petroleum reserves and the relation of fuels with politics have forced the world to find alternatives to fossil fuels. Biodiesel is one of the biofuels which is renewable and environmentally friendly and can be used in diesel engines with little or no modifications. For the last two decades, many researchers have reported extensive work on the performance and emission characteristics of engines running with biodiesel during steady state operation. However, there are numbers of knowledge gaps that have been identified which include limited information on biodiesel physio-chemical properties and their effects on combustion behaviour and performance and emission characteristics of the engine. In this study after an exhaustive literature review, the following four research areas have been identified and investigated extensively using available numerical and experimental means.

The initial focus was to investigate the most important properties of biodiesel such as density, viscosity and lower heating value using experimental and numerical techniques. The effects of biodiesel blend content on the physical properties were analysed. For each property, prediction models were developed and compared with current models available in literature. New density and viscosity prediction models were developed by considering the combined effect of biodiesel content and temperature. All the empirical models have showed a fair degree of accuracy in estimating the physical properties of biodiesel in comparison to the experimental results. Finally, the effects of density and viscosity on the fuel supply system were investigated. This system includes the fuel filter, fuel pump and the engine combustion chamber in which air-fuel mixing behaviour was studied numerically. These models can be used to understand the effects of changes in the physical properties of the fuel on the fuel supply system. In addition, the fuel supply system analysis can be carried out during the design stage of fuel pump, fuel filter and injection system.

The second research objective was the investigation into a CI engine's combustion characteristics as well as performance and emissions characteristics under both the steady and transient conditions when fuelled with biodiesel blends. The effects of biodiesel content on the CI engine's in-cylinder pressure, brake specific fuel consumption, thermal efficiency and emissions (CO_2 , NO_x , CO , THC) were evaluated based on experimental results. It has been seen that the CI engine running with the biodiesel resulted in acceptable engine performance as well as reduction in main emissions (except NO_x). Following this study, a detailed analysis on the transient performance and emission output of the CI engine has been carried out. During this analysis, the emission changing rate is investigated during speed transient and torque transition stages. Further to this, a transient emission prediction model has been developed using associated steady and transient emission data. The model has been shown to predict the transient emission reasonably accurately.

The third research objective was to develop a method for on-line measurement of NO_x emission. For this purpose the in-cylinder pressure generated within a CI engine has been measured experimentally along with mass air flow and these parameters have been used in the development of a NO_x prediction model. This model has been validated using experimental data obtained from a NO_x emission analyzer. The predicted data obtained from NO_x prediction model has been compared with measured data and has shown that the deviation is within acceptable range.

The final research objective was to develop a simple, reliable and low-cost novel method to reduce the NOx emission of the CI engine when using biodiesel blends. A potential solution to this problem has been found to be in the form of direct water injection which has shown to be capable to reduce NOx emission. Using a water injection technique, the performance and emission (NOx and CO) characteristics of a CI engine fuelled with biodiesel has been investigated at varying water injection flow rates. Intake manifold water injection reduces NOx emission by up to 40% over the entire operating range without compromising the performance characteristics of the CI engine

DECLARATION

No portion of the work referred to in this thesis has been submitted in support of an application for another degree or qualification of this or any other university or institute of learning.

COPYRIGHT

1. Copyright in text of this thesis rests with the Author. Copies (by any process) either in full, or extracts, may be made only in accordance with instructions given by the Author and lodged in the University Library of Huddersfield. Details may be obtained from the Librarian. This page must form part of any such copies made. Further copies (by any process) of copies made in accordance with such instructions may not be made without the permission (in writing) of the Author.
2. The ownership of any intellectual property rights which may be described in this thesis is vested in the University of Huddersfield, subject to any prior agreement to the contrary, and may not be made available for use by third parties without the written permission of the University, which will prescribe the terms and conditions of any such agreement. Further information on the conditions under which disclosures and exploitation may take place is available from the Head of the School of Computing and Engineering.

ACKNOWLEDGEMENTS

Firstly and foremost, I would like to thank Almighty God for providing the strength to complete my PhD and His guidance throughout my life.

This work has been carried out within the School of Computing and Engineering, Department of Mechanical engineering at the University of Huddersfield, UK. It was financially funded by the Fee-waiver Scholarship scheme from the University through the Energy, Emission and Environment Research Group (E3RG) within and Centre for Diagnostic Engineering (CDE). E3RG and CDE are gratefully acknowledged for their support during this project.

I would first like to thank my director of studies Dr Rakesh Mishra at the University of Huddersfield for all his guidance, encouragement and support throughout the three years duration of this research project. This work would never have been accomplished without his very often interesting discussions and multi-disciplinary research expertise.

I would also like to thank my second supervisor Dr Fengshou Gu of the University of Huddersfield for his help and guidance throughout. Dr Fengshou's help in engine test design, instrumentation, and data analysis was commendable.

Also my thanks go to Christopher Stubbs and Oliver Gilkes at the University who helped me in experimental design and development of the test rig. Further thanks go to Dr Vihar Malviya and Gareth Colley for their friendship and support. My thanks are also extended to Simret Ab and Hirut for their encouragement and help.

I also give thanks to my mum, Felku, my dad, Chekene and my brothers and sisters for their love, support and motivation throughout my life.

Finally, I would like to thank my wife Melat for her love, patience and unlimited encouragement throughout my study. My deepest thanks go to my lovely daughter Yordanos for her love towards her father.

PUBLICATIONS

I. Journals

1. B.C. Tesfa, R. Mishra, F. Gu, A.D.Ball. '*Effects of Biodiesel Physical properties on CI Engine Performance and Emission*, Fuel, 2011 (In progress).
2. B.C. Tesfa, R. Mishra, F. Gu, A.D.Ball. '*Evaluation of CI Engine Performance and Emission Fuelled with biodiesel during Transient Operation*, Environmental Science & Technolog, 2011 (In progress).
3. B.C. Tesfa, R. Mishra, F. Gu, A.D.Ball. '*NOx Emission Measurement using the Air Flow Rate and In-cylinder Pressure during Transient Operation*, Renewable Energy, 2011 (In progress).
4. B.C. Tesfa, R. Mishra, F. Gu, A.D.Ball. '*Water Injection Effects on the Performance and Emission Characteristics of a CI Engine Operating with Biodiesel*, Renewable Energy, 2011 (Accepted).
5. B.C. Tesfa, R. Mishra, F. Gu, N.Powles. '*Prediction models for density and viscosity of biodiesel and their effects on fuel supply system in CI engines*. Renewable Energy, 2010,35(12), pp.2752-2760.
6. Tesfa, Belachew, Mishra, Rakesh and Gu, Fengshou (2010) '*Behaviour of a CI Engine Running by Biodiesel under Transient Conditions*. 2010 SAE 2010-01-1280
7. Tesfa, Belachew, Mishra, Rakesh, Gu, Fengshou and Ball, Andrew (2009) '*Condition Monitoring of CI engine running on Biodiesel using Transient Process*. Key Engineering Materials, 413-414. pp. 495-503. ISSN 1013-9826.

II. International Conference and Presentation

1. B.C. Tesfa, R. Mishra, F. Gu, A.D.Ball. '*NOx Emission Prediction Based on Cylinder Pressure Measurement for Engine Emission Monitoring*, COMADEM 2011 ISBN 0-9541307-2-3, Norway 30 May 1st Jun 2011.
2. B.C. Tesfa, R. Mishra, F. Gu, A.D.Ball. '*Combustion Characteristics of CI Engine Running with Biodiesel Blends*, ICREPQ'11, Canaria, Spain, 13 -15 April 2011.
3. B.C. Tesfa, R. Mishra, F. Gu, A.D.Ball. '*Prediction Models for Density and Viscosity of Biodiesel and their Effects on Fuel Supply System in CI Engines*'. Renewable Energy, 35(12), 2010.

-
4. Tesfa, Belachew, Mishra, Rakesh and Gu, Fengshou (2009) *Performance of Compression Ignition (CI) Engine Running on Biodiesel during Transient Condition*. In: Thirty Sixth National Conference on Fluid Mechanics and Fluid Power, 17- 19 December 2009, Pune, India.
 5. Tesfa, Belachew, Mishra, Rakesh, Gu, Fengshou and Ball, Andrew (2009) *Predicting specific gravity and viscosity of biodiesel fuels*. In: Proceedings of Computing and Engineering Annual Researchers' Conference 2009: CEARC'09. University of Huddersfield, Huddersfield, pp. 38-44.
 6. Tesfa, Belachew, Mishra, Rakesh, Gu, Fengshou and Ball, Andrew (2009) *Transient process modelling for condition monitoring of compression ignition (CI) engine*. In: Proceedings of the 12th EAEC European Automotive Congress 2009. European Automotive Congress. ISBN 9788096924387
 7. Tesfa, Belachew, Mishra, Rakesh, Gu, Fengshou and Fieldhouse, John D. (2009) *Investigation Of Transient Characteristics For Performance Improvement And Health Monitoring For a CI Engine Running Biodiesel*. In: University of Huddersfield Research Festival, 23rd March - 2nd April 2009, University of Huddersfield.

CHAPTER ONE

1. INTRODUCTION

This chapter provides a brief introduction into the general application of biodiesel as a fuel. In particular, it considers biodiesel production and its physical characterisation, engine performance and emission characteristics during steady and transient operations and current emission legislations. From a general review, the research problems have been identified, from which the aim of this study was set.

1.1 Background

Globally, over the past several years, considerable efforts have been made to develop renewable and alternative fuels for transportation industries. The primary drives for such growing interest are the stringent regulations in form of automotive emission laws and the international efforts to reduce reliance on petroleum fuels which are available largely from potentially vulnerable regions [1]. In addition, biofuels also have the properties of both biomass and carbon neutral sources and can reduce atmospheric carbon dioxide which is the main greenhouse gas that causes global warming [2]. It is also forecasted that current fossil fuel reserves may become depleted in the coming four decades [3] which the world relies heavily on for energy needs. The automotive sector uses limited alternative energy sources compared to that used in power generation and its 98% of the energy sources depend on oil [4]. Currently, growth in world energy consumption stands at approximately 2% per annum [5]. Presently there are more than 600 million passenger cars in world; production of new cars increased by 20% between 1999 and 2009 [6], as shown in Figure 1-1. These figures are increasing rapidly, especially in India and China [7].

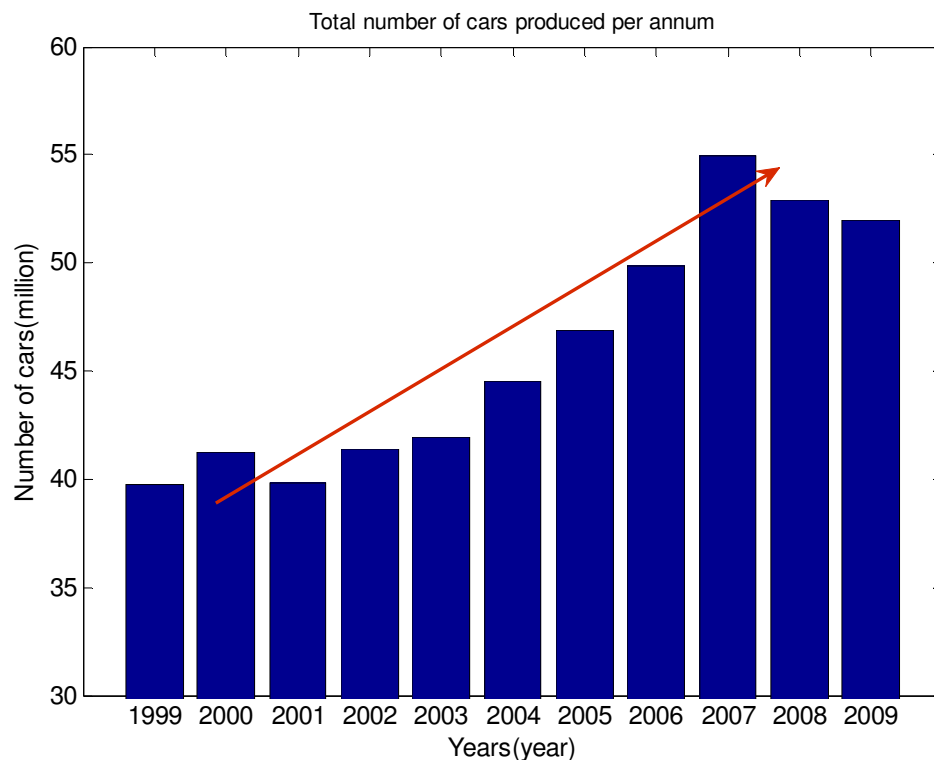


Figure 1-1 Total number of cars manufactured in the world [6]

In order to meet such increasing energy demands and to supplement fossil fuel reserves, biofuel application in the transport sector is being promoted heavily. Biofuel is defined as

a solid, liquid or gaseous fuel obtained from lifeless biomass and developed into fuel within a short time span. The major types of biofuel include biodiesel, bioethanol, ethyl tertiary butyl ether (ETBE), fischer-tropsch (FT) and developmental bioethanol [8]. The dominant products in the current market are bioethanol and biodiesel. Due to the dominance of the diesel engines in the automotive sector and the usage of biodiesel in such engines without requiring modification, biodiesel is now the most common biofuel used in diesel engines [9]. Biodiesel is one of the renewable energy sources produced from vegetable-based oils by the transesterification process which consists of short chain alkyl (methyl or ethyl) esters. Biodiesel is used in compression-ignition (CI) diesel engines without requiring any engine modification and can be used in different percentage blends [1], [10-12].

The use of vegetable-based oils in transportation is not new. In 1895, Dr Rudolf Diesel developed the first CI engine to run specifically on peanut oil. During that time due to easily availability and the low cost of mineral oil, biodiesel use was unsuccessful: Dr Diesel commented that ‘...*there will be time when it will be important...*’ [3]. However, vegetable oils were being used in diesel engines up until the late 1920s. During this period, a number of diesel engine manufacturers modified engines to use lower viscosity petrodiesel, rather than biodiesel [1].

On August 31st 1937, Chavane of the University of Brussels was granted a patent for “*Procedure for the transformation of vegetable oils for their uses as fuels*”. Due to the mid-1970s petroleum crisis, the fuel prices have increased alarmingly and environmental pollution laws have become more stringent. Early in 1980, the use of vegetable oil as an alternative renewable fuel was proposed. The 1990s saw many European countries opening biofuel plants and launching different usage legalisations. In 1991, the first biodiesel standard was set by the Austrian Standardisation Institute. In 2007, EU energy ministers agreed to increase the share of bio-fuels used in transport to 10% by 2020[13].

Furthermore, in 2008, a total of 214 biodiesel production facilities were ready to produce up to 16 million tonnes of biodiesel per year. The overall annual growth of the biodiesel sector in European Union (EU) countries is shown in Figure 1-2. Compared to Italy, Germany and France, the UK biodiesel production is very slow. In 2002 the total biodiesel

production in EU was 1,065,000 tonnes, while in 2010 the production rate growth is almost up by 20 times to 21,904,000 tonnes [14].

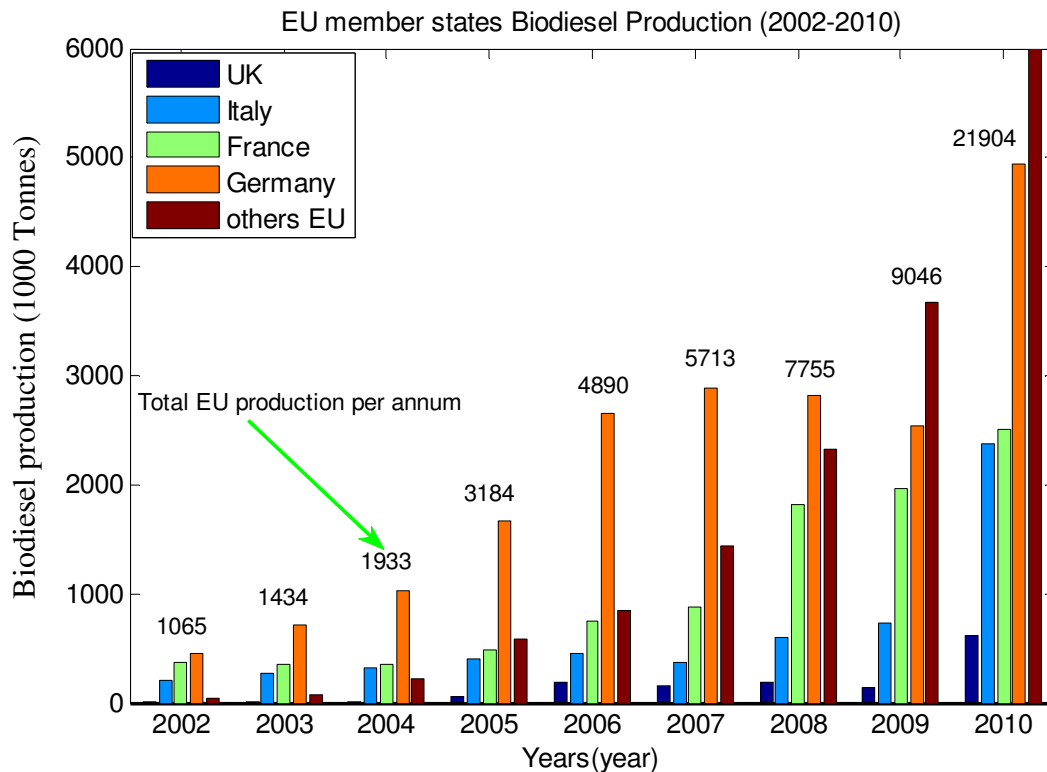


Figure 1-2 Biodiesel production trend of EU countries [14], [15]

At present, most countries are maximising their use of biodiesel as an alternative energy source. China has planned to produce 12 million tonnes of biofuel in 2020 [16] and USA and EU are planning to use 20% blend by 2017 [17] and 2020 [18] respectively. The UK has set a target of 5% of fuel sales to be from renewable resources by 2010–2011; currently the UK government supports the uptake of biofuel through the use of 20 pence per litre fuel duty differential for biodiesel produced from waste oil [19].

To meet these targets a lot of research work has been carried out throughout the world on the biodiesel production, physical properties, engine performance, engine emission and engine durability. It has been reported that biodiesel is technically viable, economically acceptable and environment friendly. Currently, extensive research is being conducted in different countries in the areas of: optimisation of biodiesel production, characterisation of biodiesel, facilitation of transportation, storage, and improvement of engine performance and emission characteristics, while using biodiesel as fuel.

1.2 Biodiesel Production and Physical Characterisation

Researchers and scientists have developed various methods of biodiesel production using different biofuels, with the main objective being to reduce oil viscosity. As a straight replacement for petroleum oil, vegetable oils have too high a viscosity for use in most existing diesel engines [10], [20], [21]. Furthermore, plant oils usually contain free fatty acids, phospholipids, sterols, water, odorants and other impurities. In order to utilise plant oils in car engines, purification of such impurities is mandatory. There are a number of ways to reduce vegetable oils' viscosity. Dilution, microemulsification, pyrolysis, and transesterification are the four techniques applied to solve problems encountered with high fuel viscosity. Currently, the major method used in the production of biodiesel from oil-seed crops (rapeseed, sunflower, soybean and animal fats), is transesterification [10], [22-24]. Transesterification is a sequential chemical conversion of oil into its corresponding fatty acid methyl esters (FAME), as described in [22]. Fossil methanol and ethanol have been used in the transesterification process. Transesterification is a base-catalysed, acid-catalysed, enzyme catalysed or non-catalysed process [25]. The biodiesel production process from vegetable oils is shown Figure 1-3.

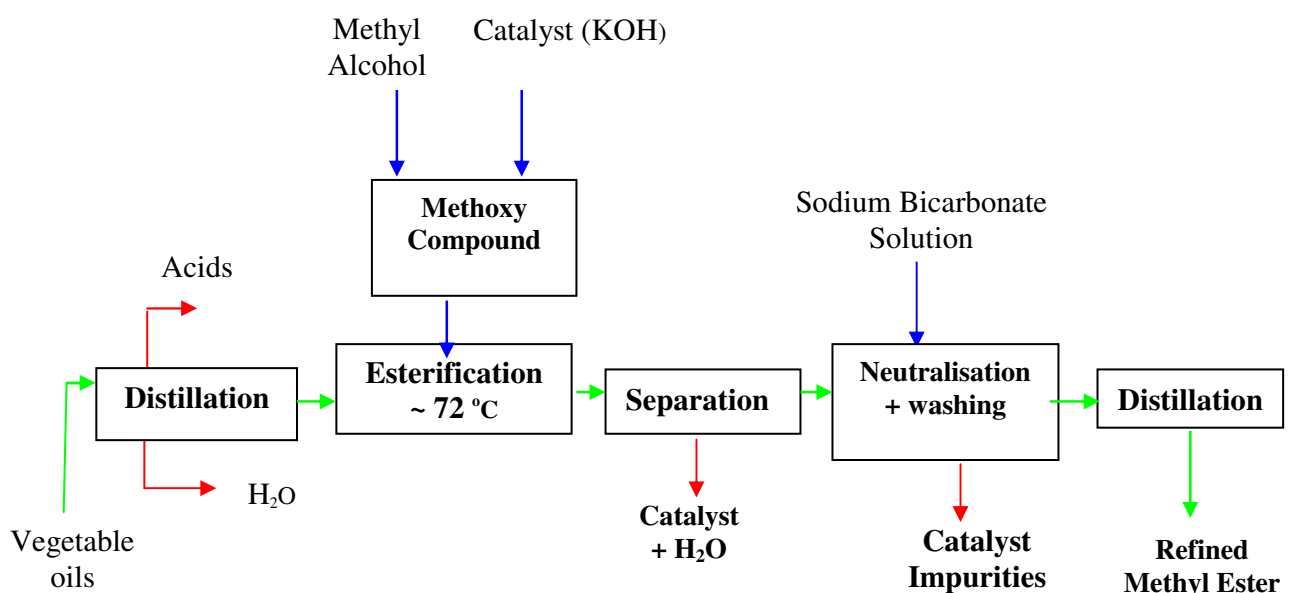


Figure 1-3 Biodiesel Production Process [22]

Today, most biodiesels are produced using the base-catalysed reaction [22], [23] due to its low temperature and pressure reaction as well as capability of yielding high oil

conversion and requiring simple production facilities. In the production process methyl alcohol and base-catalysed (KOH) has been used. As the Stoichiometric material balance shows, the ratio of ester to alcohol is 100:11 and the ratio of biodiesel to Glycerol is 100:10[26] in the transesterification process described in Figure 1-4. Transesterification of triglycerides produces fatty acids, alkyl esters and glycerol. Due to density differences, the glycerol layer settles down at the bottom of the reaction vessel. Diglycerides and monoglycerides are the intermediates in this process.

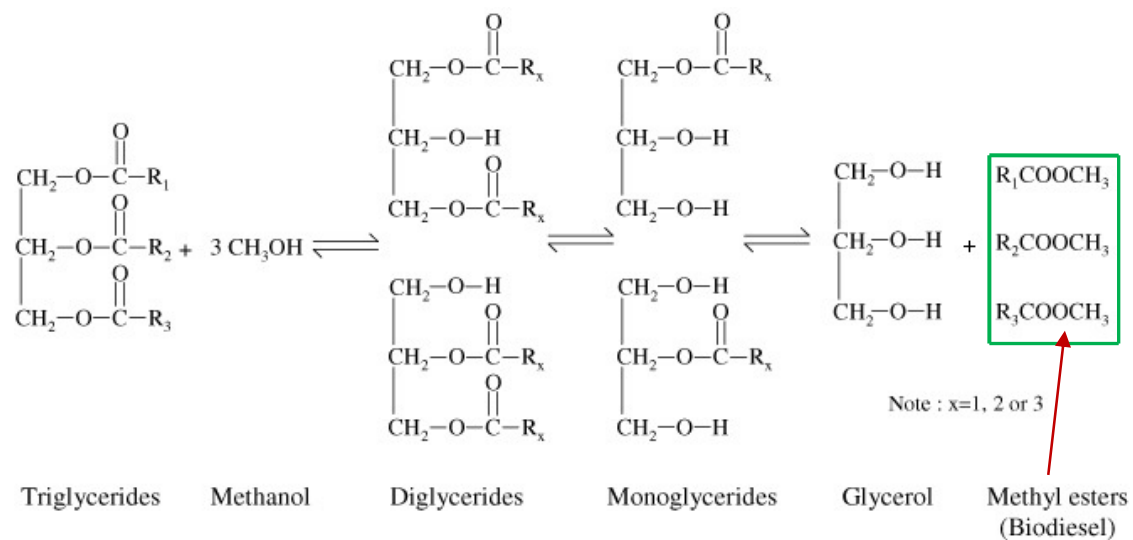


Figure 1-4 General equation of transesterification process [10]

To facilitate the formation of the esters, different types of techniques can be used, for example, adding more alcohols to shift equilibrium towards the formation of ester and also using alkali or acid catalysts [10].

Biodiesel properties depend heavily on various plant feed stocks, growing climate conditions, soil type, plant health and plant maturity upon harvest. These parameters affect the physical and chemical properties which also have a direct relationship with performance and emission characteristics of the engine [20]. Among the biodiesel properties, kinematics viscosity, density and heating value are the most important parameters which affect engine performance and emission characteristics [27]. Viscosity is one of the most important properties of biodiesels since it affects the operation of fuel supply systems, such as fuel pumps, fuel filters and fuel injectors. Higher viscosity leads to poor atomisation of fuel spray and less efficient operation of the fuel injectors. The

conversion of triglycerides into methyl or ethyl esters through the transesterification process reduces viscosity by a factor of eight. Biodiesel's viscosity decreases with an increase in temperature. The second important property of biodiesel is density. The density of biodiesel is slightly higher than diesel (860-895kg/m³ at 288K). Due to the availability of 11% oxygen molecule in biodiesel, the lower heating value (calorific value) of biodiesel is less than petrol-diesel [20], [24], [28], [29]. In relation to the physical properties, the basic problems with biodiesel are its higher density and viscosity as well as its lower heating values.

1.3 Performance and Emission Characteristics of CI Engines Running with Biodiesel

The inventions of different internal combustion engines and subsequent developments in engine technology have led to extensive exploitation of the petroleum reserves, which are being depleted at a rapid rate [9]. Currently, biofuels are being investigated in detail for application in IC engine with exciting potential opportunities to increase energy security and reduce gas emissions. This could have significant effects on economic development and poverty reduction programmes throughout the world. The main findings from the literature reviewed indicate that biofuels, when used in engines, have comparable power, brake specific fuel consumption (BSFC) and brake thermal efficiency, as compared to engines running with diesel. Biodiesel also has advantages of significant portability, higher combustion efficiency, lower sulphur and aromatic content, a higher cetane number and higher lubrication effects. Moreover, it has unique advantages of being available around the world. Furthermore, it has been observed that the use of biofuel in an engine produces lower emission of total hydrocarbon (THC), carbon monoxide (CO) and carbon dioxide (CO₂) as well as lower exhaust gas temperatures [30-32]. Biodiesel has been shown to emit lower values of non-regulated emission which cause mutagenic and carcinogenic problems in human [33]. One of the unique disadvantages of biodiesel is its higher nitrogen oxides (NO_x) emission, when used as fuel in CI engines [34]. Suitable mechanisms are therefore required to be developed to reduce NO_x emissions associated with biodiesel.

In the most of the reviewed papers, extensive investigations have been reported on the engine performance and the emissions of the engine running with biodiesel during steady state operation. However, in passenger cars, both steady and transient conditions occur

frequently. Transient, in engines, is the change of engine speed and/or torque as a function of time. The transient phenomena can be observed in most automotive drive routes, such as engine start, warm up, accelerations and decelerations. The examples of acceleration and deceleration transient phenomenon for an engine for the speed and torque) are shown in Figure 1-5. The profiles include three parts, which are pre-transient steady state condition, transient conditions and post-transient conditions.

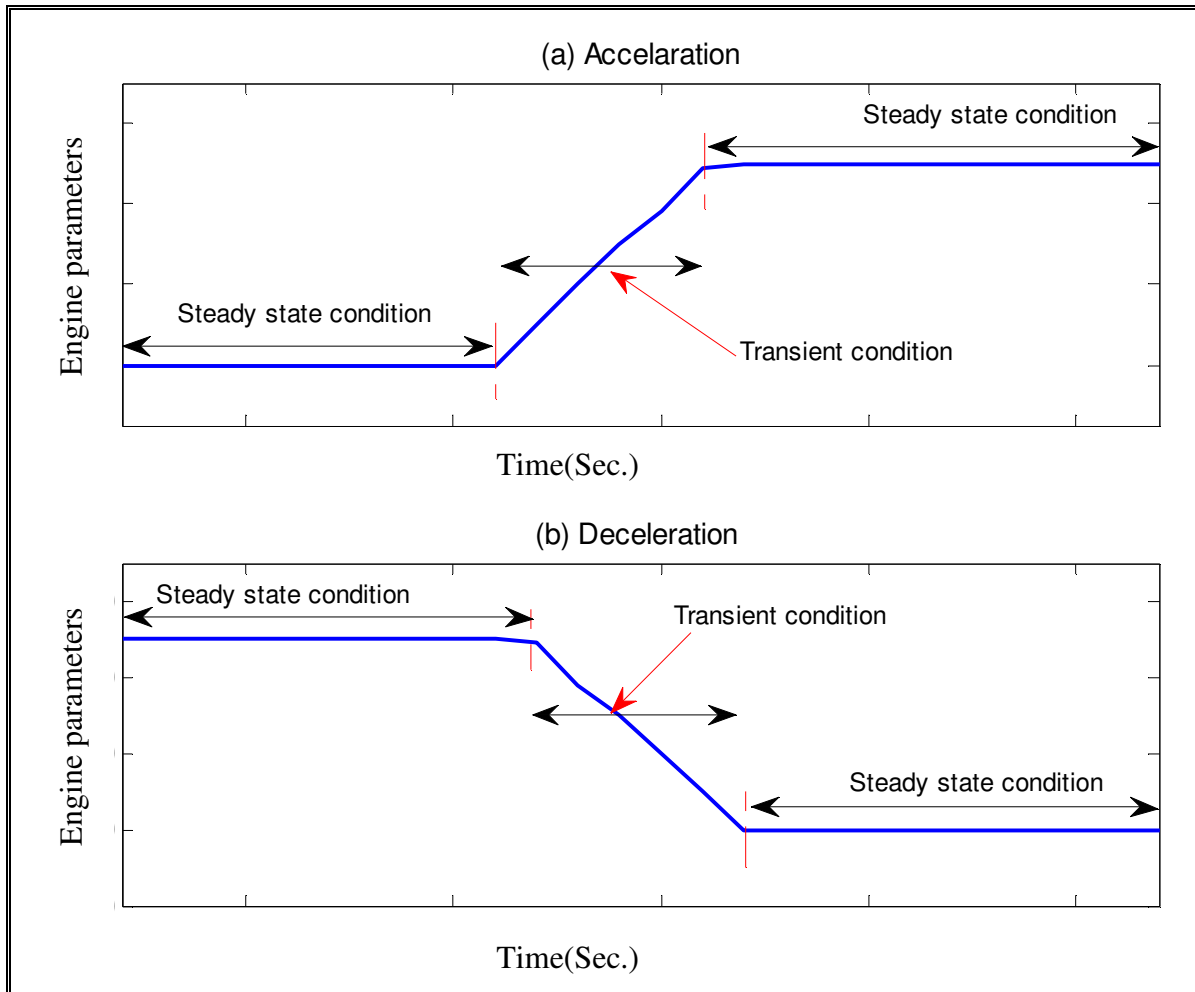


Figure 1-5 Speed and Torque transient profile a) acceleration, b) deceleration

These driving phenomena can be initiated by driver's driving behaviour and the slopes and geometric features of the road [35]. It has been reported that road's geometric features, such as road gradients and horizontal road curvatures (roundabouts), considerably influence the performance and emission characteristics of engines [36]. Bazari [37] reported that during the transient process, the performance and emissions

characteristics of turbo-charged diesel engines are significantly worse than those under steady conditions. This is mainly because of the difficulties associated with optimising the transient response of the intake, injection and combustion systems [37]. Armas[35] *et al.* also investigated the effects of biodiesel blends on the smoke-opacity reduction during transient conditions [35]. They reported that the use of biodiesel blends in diesel engines reduces the smoke-opacity significantly, not only in steady conditions, but also during transient engine operation.

1.4 Emission Regulations

The first emission legislation was introduced in California in 1959, in order to control carbon monoxide (CO) and hydrocarbon (HC) emissions from gasoline engines [38]. In Europe, concerns surrounding atmospheric pollution have been rising steadily since the 1980s and since January 1993, all new petrol passenger vehicles sold within European countries have been fitted with catalytic converters [39]. The major diesel exhaust emissions, regulated in many areas of the developed world, are CO, NO_x, HC and particulate matters (PM). Carbon monoxide (CO) is a colourless, odourless and tasteless gas which is slightly lighter than air, and which when combined with haemoglobin, reduces the blood's capacity to carry oxygen (O₂) to vital organs in the body[40]. NO_x is generic term for the mono-nitrogen oxides, NO and NO₂, which are produced from the reaction of N and O₂ at higher temperature during the combustion process. In this process, 90% of NO_x is contributed by NO. Exposure to high levels of nitrogen dioxide (NO₂) has been linked to respiratory problems and long term exposure may affect lung function and increase the response to allergens [40]. Moreover, HCs contribute to ground level ozone formation which may lead to damage of the respiratory system [40]. The fine particles of PM also have an adverse effect on the respiratory system and have been associated with advancing the deaths of those suffering from respiratory illness [40]. Although CO₂ is not directly harmful to human health, it is the most significant of the greenhouse gases which contributes to climate change. In response to these concerns, at the Kyoto Conference on Climate Change in December 1997, many developed countries agreed to legally binding targets in order to reduce greenhouse gas emissions of 1990, by 5.2% in 2010 [41]. A number of measures have been introduced in the UK to incentivise the purchase and use of efficient vehicles in order to lower CO₂ emission. Since March 2001, a system of gradual vehicle excise duty has been in operation for new cars, based

on the level of CO₂ emission and since April 2002, company car tax has also been based on the CO₂ emissions of vehicle provided to employees for their private use [42]. Table 1.1 shows the permissible limits for past, present and future exhaust emissions for diesel passenger cars [38]. The emission standard's trend shows that stringent regulations are being set for NO_x and PM in Euro VI to be effective from 2014 compared with the previous emission standards. To approve new cars, various driving test cycles have been set for both steady and transient operating conditions for new engines [39].

Table 1-1 EU emission standard for passenger diesel cars [38]

Stage	Date	CO	HC	HC+NO _x	NO _x	PM
g/km						
Euro I	1992.07	2.72 (3.16)	-	0.97 (1.13)	-	0.14 (0.18)
Euro II,	1996.01	1.0	-	0.7	-	0.08
Euro II, DI	1996.01	1.0	-	0.9	-	0.10
Euro III	2000.01	0.64	-	0.56	0.50	0.05
Euro IV	2005.01	0.50	-	0.30	0.25	0.025
Euro V(a)	2009.09 ^a	0.50	-	0.23	0.18	0.005
Euro V(b)	2011.09 ^b	0.50	-	0.23	0.18	0.005
Euro VI	2014.09	0.50	-	0.17	0.08	0.005

a - 2011.01 for all models

b - 2013.01 for all models

1.5 Research Problem and Aims

Puppàn[3] has reported that the world's available oil reserves may deplete in 30-79 years. Such reserves are concentrated in certain regions that are vulnerable to political, economic, social and military instability which could potentially pose serious problems in future [3]. It has also been observed that petrol prices have fluctuated considerably over the past few years depending on the political situations in countries rich in fossil oil reserves. Such trends will continue to adversely affect the world's economy in the future. On the other hand, engine

design and manufacturing companies have largely concentrated on petroleum dependent engine research instead of research on sustainable and alternative energy source driven engines [43]. To alleviate these problems biodiesel is being considered as one such alternative fuel which has the potential to become a carbon neutral fuel. For the last two decades the number of research publications has increased exponentially in the areas of: biodiesel, blends and sustainability, life cycle assessment, production, development, performance and emission. Most of the works have been reported on performance and emission characteristics of diesel engines operating under steady state conditions [44]. There are still many operational problems associated with biodiesel physical properties, engine performance and emissions which have hardly been addressed by the research community. Some of these challenges have been described in the following.

The direct utilisation of biodiesel within diesel engines, particularly in direct injection systems has been reported to result in problems of coking and trumpet formation on the injectors. This formation occurs to such an extent that fuel atomisation does not occur properly or is largely prevented [10], [45]. This may be due to the occurrence of plugged orifices due to carbon deposits and the thickening or gelling of the lubricating oil as a result of contamination by vegetable oils. In addition, biodiesel is easily oxidised with air at high temperatures [14], [46], [22]. All these problems are directly or indirectly related to the physical and chemical properties of the biodiesel. To understand the influence of physio-chemical properties of biodiesel on engine health, performance and emission, further research is required and this forms the first facet of this work. In particular, the higher density and viscosity of biodiesel can be attributed to the majority of these problems.

Stringent environmental regulations on climate change are one of the driving forces for seeking alternative methods to reduce emissions from all sectors, specifically the transport sector. Currently, 98% of the transport sector uses fossil fuel energy sources which contribute more than 30% to the total global emissions [8]. Biodiesel is known to significantly affect the performance characteristics of engines designed for diesel fuel. The research conducted in this area has highlighted both the positive and negative effects of using this fuel. Most of the existing work is limited to analysing the effectiveness of biodiesel under steady state operation of diesel engines. However, the most frequent operation of automotive vehicles in urban environments is in the transient mode. Emission characteristics during the transient mode are considerably worse than those generated during steady state conditions [35]. Measuring engine performance and emission characteristics during transient operation is

more difficult as both the speed and/or load of the engine change as a function of time and this time span is relatively short [47]. It is therefore necessary to understand the effectiveness of biodiesel as a fuel under the transient condition of operation, both on engine performance as well as emissions. This forms the second facet of the present research.

It is observed that an engine fuelled with biodiesel provides comparable engine performance and significant reductions in CO₂, CO and THC emission. However a considerable number of researchers have reported that the engines running with biodiesel emit higher NO_x concentrations in exhaust [44], [48], [49]. NO_x and PM are the major toxic emissions that need to be regulated [50]. This highlights need for online measurement of NO_x emissions. The currently available methods of measuring/predicting NO_x emissions include: analyser (direct measuring), engine map methods and artificial neural network. Measurement of oxides of nitrogen on a dry basis, by means of a heated chemiluminescent detector (HCLD) with a NO₂/NO analyser is widely used. However, the analyser has disadvantages of higher associated costs, requiring large space, demanding frequent calibration and the possible effects of soot. In addition, its responses are very slow, which affect the transient NO_x emission measurement [51]. The development of a method to predict NO_x emissions online forms the third section of this present research.

The regulatory requirement to have NO_x emission within a prescribed limit has resulted in major research and development works being undertaken in order to reduce NO_x emissions. Various methods have been used to reduce NO_x emissions successfully that are emitted from compression-ignition when engines running with diesel as a fuel. Some of these methods include: exhaust gas recirculation (EGR), catalytic conversion (post combustion method) and water injections/emulsion [52]. In present work, a technically viable and economically acceptable method would be developed in order to alleviate NO_x emission problem of engines running with biodiesel. This forms the fourth section of this present research.

The general aim of this study is to investigate, both experimentally and numerically, the physical property of biodiesel and the performance and emission characteristics of compression ignition (CI) engines running on biodiesel and its blends during steady and transient operations. It is also aimed at developing new method for the reduction of NO_x emission and to develop NO_x emission predicting models from the in-cylinder pressure measurement. The objective of this study has been set in Chapter two which includes the literature review on different facets discussed above. This has been done to identify the

knowledge gaps in the identified research areas. In Chapter two extensive literatures reviews have been done and the spesfic problems have been identified. Based on the identified problems, the objectives of this study have been listed in section 2.5.2.

1.6 Organisation of Thesis

The basic outline of the thesis is as follows:

Chapter one: Brief introduction of the current scenario of biodiesel, biodiesel production and physical characterisation, performance and emission characteristics of engine running with biodiesel during the steady and transient operation conditions, and the emission legislation are given. Finally, the research problem has been identified from the general review and the aim of this study was identified.

Chapter two: This chapter presents the literature review on the biodiesel characterisation, performance and emission characteristics of CI engines running with biodiesel, NOx emission reduction techniques and NOx prediction models. In the first section the basic physical properties of biodiesel, such as the density, the viscosity and the heating value of the biodiesel have been discussed and the effects of temperature and biodiesel fraction on the physical properties are highlighted. The prediction models of the density, viscosity and heating value of the biodiesel are discussed in detail. In second section reviews on the CI engine combustion characteristics, break specific fuel consumption, brake effective power, thermal efficiency and emissions (NOx, CO₂, CO, THC and PM) have been included. It also highlights the factors affecting combustion, performance and emission characteristic of CI during steady and transient operations running with biodiesel. The third section provides methods on NOx formation, and available methods of NOx reduction in diesel engines. The NOx formation section discusses three well known methods of NOx formation in diesel engines in detail. In addition, this chapter discusses the NOx predicting models available in literature. Finally the scope and specific objective of this research was presented depending on the literature review and lists out the specific objectives of the study.

Chapter three: This chapter gives a brief description of the biodiesel characterisation facilities, the test engine's characteristics and specifications, and also describes the test rig and instrumentation. The list of measured parameters, data acquisition system and application software are described in this chapter. It also outlines measurement procedures for density, viscosity, and lower heating value of biodiesel and its blends.

Chapter four: This chapter provides the results and discussions of biodiesel characterisation. It outlines the effects of biodiesel fraction and temperature on the main fuel properties, such as density, viscosity and lower heating value based on experimental investigation. It also includes new predicting models developed to predict these properties.

Chapter five: This chapter is focused on the experimental investigation carried out on a CI engine, which is fuelled by biodiesel and its blends during steady state operation. In particular engine's combustion performance and emission characteristics have been evaluated. The effects of feedstock source and the biodiesel blend fraction on the engine performance and emission are discussed in the first section. Furthermore, the effects of biodiesel physical properties on the engine performance are also reported.

Chapter six: This chapter provides the performance and emission characteristics of the test CI engine running with biodiesel during transient operation. The effects of transient operation on fuel flow rate, exhaust temperature and emission characteristics of CI engine fuelled with biodiesel and its blends have been investigated in detail. In addition, the engine parameters effects on engine emissions have been quantified and an emission prediction model during transient operation has been developed.

Chapter seven: This chapter presents the development of NO_x predicting model from the experimentally measured in-cylinder pressure. The accuracy of the predictive model has also been established in this chapter.

Chapter eight: This chapter provides the experimental results as well as analysis and discussion on effects of water injection in a CI engine running with biodiesel. It includes the effects of water injection on fuel combustion parameters, engine performance and emission in a CI engine.

Chapter nine: This chapter presents the conclusions and future work based on this research. The conclusions have been categorised in different sections for biodiesel characterisation, engine performance and emission during both steady and transient operation, the effects of water injection on the engine performance and emission and the newly developed NO_x emission prediction model.

1.7 Summary on Chapter One

Chapter one is presents a brief introduction regarding the research conducted in this study. It presents general introduction about the importance of biofuel in the transport industries, the production process and physical characterisation of biodiesel, the engine performance and emission characteristics. In addition, the general research problems have been identified and the aim of the study has been set. In the next chapter, previous researchers' works, industrial technical reports and standards have been reviewed and the specific research problems have been identified.

CHAPTER TWO

2. BIODIESEL CHARACTERISATION AND PERFORMANCE AND EMISSION CHARACTERISATION OF CI ENGINES RUNNING WITH BIODIESEL

Chapter two presents the literature review on various facets of the research discussed in chapter one. Its main objective is to review the previous works on the biodiesel characterisation, performance and emission characteristics of CI engines running with biodiesel, NO_x emission reduction techniques and NO_x prediction models. Depending on the extensive review the specific research problems have been identified. In the first section basic physical properties of biodiesel, such as the density, the viscosity and the heating value of biodiesel have been reviewed and the effects of temperature and biodiesel fraction on the physical properties have been highlighted. The prediction models of the density, viscosity and heating value of the biodiesel are reviewed in detail. The second section reviews the CI engine's combustion characteristics, break specific fuel consumption, brake effective power, thermal efficiency and emissions (NO_x, CO₂, CO, THC and PM). It also highlights the factors affecting combustion, performance and emission characteristic of CI engines during steady and transient operations when running with biodiesel. The third section provides review of methods on NO_x formation, and available methods for NO_x reduction in diesel engines. The NO_x formation section discusses three well known methods of NO_x formation in diesel engines in detail. In addition, this chapter discusses the details of NO_x predicting models available in literatures. Finally the scope and specific objective of the present research is presented based on the literature review and lists out the specific objectives of the study.

2.1 Biodiesel Characterisation

Biodiesel fuels are characterised by a number of physio-chemical properties. Some of these are: viscosity, density, cetane number, cloud and pour points, flash point, ash content, sulphur content, carbon residue, acid value and lower and higher heating values. Although most of the biodiesel properties are similar to those of diesel fuels, there are considerable differences in some of the basic fuel properties such as density, viscosity and lower heating values [1], [45]. The parameters, which define the quality of biodiesel, can be divided into two groups. The first group contains the general physical parameters used for characterising mineral oil based fuels. The second group parameters describe the chemical composition of biodiesel and purity of fatty acid alkyl esters [10]. Austria was the first country in the world to define and approve the standards for biodiesel to use as a fuel in 1991[45]. Other countries, such as Germany, Italy, France, the Czech Republic and the United States have also developed standards to maintain the quality of the biodiesel to be used in Diesel engines. Currently, in order to use biodiesel in diesel engines, biodiesel properties should meet the EN-14213 specifications in Europe [53] and D-6751 specifications in United States of America [54], both of these are presented in Table 2-1.

Biodiesel characteristics depend heavily on: various feed stock plants, growing climate conditions, soil type, plants health and plants maturity upon harvest [20], [55]. These parameters affect the physical and chemical properties, which also have direct bearing on performance and emission characteristics of the engines [56]. In addition, the molar ratio of alcohol to vegetable oil and the reaction temperature significantly affect the biodiesel characteristics [1]. Of all biodiesel properties, kinematics viscosity, density and heating value are the most important parameters which affect engine performance and emission characteristics considerably [6], [27], [20], [56], [57]. One of the major shortcomings of the biodiesel when used in a diesel engine is the detrimental effects caused by the high viscosity of the fuel. Higher viscosity causes poor fuel atomisation during the spray, increases the carbon deposition on fuel filter, demands more energy from the fuel pump and wears the fuel pumps and injectors [27], [20].

Furthermore, higher viscosity causes the mixture to burn lean in the engine as fuel moves slowly through the fuel filter and fuel lines [58]. In addition, higher viscosity of biodiesel fuel affects the start of injection, injection pressure and the fuel spray characteristics. All these parameters affect engine performance and exhaust emissions considerably [59]. The density

of diesel fuel is also a very important parameter which has been correlated against other crucial performance parameters of engine, such as cetane number and heating value [28].

Table 2-1 Standard Specification Biodiesel, B100 and diesel fuel [1], [54]

Property	Units	EN-14214		ASTM-D6751	
		Biodiesel	Diesel	Biodiesel	Diesel
Specific gravity		0.86-0.90	-	-	0.82 -0.86
Viscosity	Mm ² /s	3.50-5.00	1.3 – 4.1	1.9-6.0	2 – 4.5
Calorific value	MJ/Kg	37-40	42.7	-	-
Flash point	°C	120 min		130 min	
Cetane number		51		47	
Sulphur	mg/kg	10.0 max		15.0 max	
Phosphorus content	mg/kg	10.0 max		10.0 max	
Acid number	mg KOH/g	0.50 max		0.80 max	
Free glycerine	% mass	0.02 max		0.02 max	
Total glycerine	% mass	0.25 max		0.24 max	
Sulphated ash content	% mass	0.02 max		0.020 max	
Methanol content	% mass	0.02 max			
Mono-glycerides	% mass	0.80 max			
Di-glycerides	% mass	0.20 max			
Ester content	% mass	0.20 max			
Linolenic acid ME	% mass	96.5 min			
Carbon residue	% mass			0.050	
Iodine value				120 max	

The density and viscosity of the fuel affect the power output and the fuel spray characteristics of the engine. In order to improve viscosity and density of the biodiesel, the available techniques being used are mixing the diesel with biodiesel and/or pre-heating the biodiesel [10], [58],[60].

The effects of mixing biodiesel with diesel on density and viscosity of biodiesel blends, effect of temperature on biodiesels' density and viscosity and the chemical structure of biodiesels (fatty acid, position and number of double bond), are well reported. Different empirical correlations have been developed which relate various performance parameters

with density and viscosity of biodiesel [28], [20], [56], [57], [61], [62], [63]. Previous researchers' works on biodiesel density, viscosity and lower heating value have been summarised below.

2.1.1 Density of Biodiesel

Density is an important property of biodiesel fuel. It is defined as its mass per unit volume, whereas the specific gravity of biodiesel is defined as the ratio of its density to the density of water at a specific temperature and pressure, typically at 4°C and 1atm. The specific gravity of biodiesel has been investigated by many researchers. Density of biodiesel has values between 0.848 and 0.885g/cm³ at 311.15 K, according with previous reports [27], [64]. Tat and Garpen[28] measured experimentally the specific gravity of 20%, 50%, 75%, and 100% soybean biodiesel as a function of temperature in the temperature range of crystallization temperature to 100°C, using the standard hydrometer method. The results indicate that the biodiesel and its blends demonstrate temperature dependent behaviour. A first degree linear regression equation (2-1) was developed which is shown below:

$$SG = a + bT \quad (2-1)$$

Where SG is the specific gravity of blended biodiesel, T is the temperature in °C, and a and b are constants that depend on different percentages of biodiesel blends.

Tat et al. [56] also reported similar linear equation for three different biodiesels namely, canola oil biodiesel, soybean oil biodiesel and fish oil biodiesel. These equations were developed based on the data obtained from a capacitance type liquid level meter over a temperature range from 20°C to 300°C. Clements (referenced in [56]) suggested that equation (2-2) could be used to determine the specific gravity of different biodiesel blends at a standard temperature. In this equation, the specific gravity of the blends has been considered to be proportional to mass fractions of the constituents:

$$SG_{blend} = \sum SG_i M_i \quad (2-2)$$

Where SG_{blend} is the specific gravity of the blend, SG_i is the specific gravity of the component i , and M_i is the mass fraction of the component i .

Alptekin and Canakci [27] carried out experimental tests on different biodiesels made from soybean oil, waste palm oil, sunflower oil, corn oil, canola oil, and cotton seeds. They

suggested a first degree empirical equation, which relates the density of a biodiesel blend with the percentage of biodiesel used in the fuel as shown in equation (2-3):

$$\rho = Ax + B \quad (2-3)$$

Where ρ is density (g/cm³), A and B are constants which vary with the type of the biodiesel and X is the biodiesel fraction.

Benjumea *et al.* [65] measured the densities of palm oil biodiesel and diesel fuel blends at various temperatures (from 289 to 373 K) and at five biodiesel concentrations (B0, B5, B20, and B100). These authors reported that, for a given temperature, there is a linear variation of density relative to the biodiesel content in the mixtures. Also, they found that density was a linear function of temperature for the palm oil biodiesel, diesel and different biodiesel blends.

Currently, biodiesel is blended with petroleum diesel and then used within diesel engines with no or minor modifications in engine systems. These engines are also subjected to a wide variety of operating temperatures. The most of the available temperature dependent density prediction models have been developed for pure biodiesel only. In this study, appropriate models will be developed to correlate the density of biodiesel blends as a function of the biodiesel fraction and the operating temperature. These newly developed models can then be used to predict density values for a given biodiesel blend at wide variety of operating temperatures. This information will be of considerable use in characterising fuel supply systems, engine combustion and evaluating the engine performance and emissions.

2.1.2 Viscosity of Biodiesel

Viscosity is the property of a fluid by virtue of which it offers resistance to the flow. As the temperature of a fluid substance is increased, its viscosity decreases and it is therefore able to flow more readily. Viscosity affects the operation of fuel injection equipment, especially at low temperatures. High viscosity fuel leads to poorer atomisation of the fuel spray and less than desirable operation of the fuel injectors [1]. The viscosity of a typical biodiesel is higher than the viscosity of fossil-diesel and some researchers have reported that the biodiesel viscosity can be up to 1.6 times that of diesel at 40°C [66]. This ratio increases especially when the temperature is below 25°C. Blending of biodiesel with diesel and preheating of biodiesel improves the viscous characteristics significantly [58]. The viscosity of biodiesel can be estimated from well known mixing laws such as the Grun-Nissan and Katti-Chaudhri laws, which were originally proposed by Arrhenis [67]. The laws are expressed in mathematical form as written in form of equation (2-4).

$$\ln(\eta_{\max}) = x_1 \ln(\eta_1) + x_2 \ln(\eta_2) \quad (2-4)$$

Where, η_{\max} is the kinematic viscosity (mm²/s) of the mixture, η_1 and η_2 are kinematic viscosities (mm²/s) of components 1 and 2 and X_1 and X_2 are the volume fractions of components 1 and 2.

Alpetekin and Canakci investigated the variation of the viscosity as a function of different percentages of blends of biodiesel. The tests were conducted at 40°C for a wide variety of biodiesels, such as waste palm oil, sunflower oil, soybean oil, corn oil, cotton seed oil and commercial diesel. They developed a second degree empirical equation (2-5) to calculate the viscosity of blended biodiesel, as a function of the fraction of biodiesel in the mixture. It was found that the estimated values from the equation were fairly close to the measured values:

$$\eta_{blend} = A_1 x^2 + B_1 x + C_1 \quad (2-5)$$

Where η is the kinematic viscosity (mm²/s), A_1 , B_1 and C_1 are coefficients and X is the biodiesel fraction.

Riazi and Al-Otaibi developed equation (2-6) for estimating the viscosity of liquid hydrocarbons and petroleum mixtures at various temperatures from their refractive index values (I). However, in this model the equation needs the values of molecular weight, specific gravity, boiling temperature and refractive index of compounds as inputs:

$$\frac{1}{\mu} = A_2 + \frac{B_2}{I} \quad (2-6)$$

In the above equation, μ is the dynamic viscosity (cP), A_2 and B_2 are constants specific to each component and I is the refractive index.

A modified equation was proposed by Tat and Van Gerpen[20] to determine the viscosity of biodiesel at different temperatures. The equation is shown below:

$$\ln(\eta) = A_3 + \frac{B_3}{T} + \frac{C_3}{T^2} \quad (2-7)$$

Where A_3 , B_3 and C_3 are constants, T is temperature in K, and η is the kinematic viscosity (mm²/s).

In Tat and Van Gerpen's equation, the constants A_3 , B_3 and C_3 , vary with the biodiesel type and the biodiesel fraction and this limits the general use of this equation. Pegg *et al.* [68] developed the equation 2-8 to calculate the dynamic viscosity of B100 as a function of temperature in the temperature range of 277K to 573K:

$$\ln(\mu) = -2.4343 + \frac{216.66}{T} + \frac{293523}{T^2} \quad (2-8)$$

Where η is the dynamic viscosity (mPa s) and T is the temperature (K). By considering the carbon number, Krisnangkura *et al.*[69] proposed equation 2-9 and equation 2-10, to determine viscosity of biodiesels with long and short carbon structure at different temperatures:

$$\ln(\eta_{C_{12}-C_{18}}) = -2.177 - 0.202CN + \frac{403.66}{T} + \frac{109.772}{T} CN \quad (2-9)$$

$$\ln(\eta_{C_6-C_{12}}) = -2.915 - 0.158CN + \frac{492.12}{T} + \frac{103.35}{T} CN \quad (2-10)$$

Where $\mu_{C_6-C_{12}}$ and $\mu_{C_{12}-C_{18}}$ are the kinematic viscosities of biodiesels with number of carbon atoms varying from 6 to 12 and 12 to 18, respectively, in mm^2/s , T is the temperature in K, and CN is carbon number.

In Krisnangkura's [69] equations, number of the carbon atoms is required *a-priori* which limits the use of the equation. Most of the available methods for the estimation of biodiesel viscosity at different temperatures are fairly complicated and depend on a number of different input parameters. In addition, these empirical correlations vary depending on the biodiesel source [70]. In this study, simple and comprehensive viscosity prediction models are developed by considering the effects of biodiesel blend percentage and temperature. Furthermore, in this research a new model is developed by correlating the density and viscosity of biodiesel.

2.1.3 Heating Value of Biodiesel

Heating value can be defined as the energy content of the biodiesel. In other words, the heating value is the amount of heat released during the combustion of one gram of fuel to produce CO_2 and H_2O at its initial temperature and pressure [63]. It is one of the most important parameters for estimating the design parameters and is vital for numerical

simulation of combustion [71], [57], [62]. The design and operation of biodiesel combustion systems significantly relies on biodiesel characteristics, such as the heating value, moisture content, elemental composition, ash properties etc. The heating value of fuel can be reported in two ways: the higher heating value (HHV), or gross calorific value, and the lower heating value (LHV), or net calorific value. HHV refers to the heat released from the fuel combustion with the original and generated water in a condensed state, while LHV is based on gaseous water as the by product [72]. Though the term higher heating value has wider acceptance in the fuel characterisation, the engine performance estimation models usually use lower heating values of the fuel [73]. For this reason, in this study the lower heating values of the biodiesel blends have been used in further investigation.

Many researchers have reported the measurement of the heating value of the fuel from experimental results using an adiabatic bomb calorimeter, proximate and ultimate analyses. The conventional analysis is a complicated and time consuming process which requires specialised set-up, measurements and calculation procedures [72]. Therefore, many attempts have been made to estimate the heating values based on correlating heating value of fuels from the experimental values obtained from bomb calorimeter [23], [24], [71], [72], [73], [74]. Various correlation for predicting heating value which were proposed by previous authors have been summarised in Table 2-2. The gross heats of combustion of different biodiesel fuels have been measured and calculated by Freedman *et al.*[57] and Krisnangkura[62] using a parr adiabatic calorimeter according to ASTM D240 and D2015 standards. They developed a linear correlation between the heating value, carbon number and molecular weight. They concluded that the HHV of triglycerides increased with increasing carbon number and molecular weight. Demirbas[75] has reported that the heating value of vegetable oils can be calculated using saponification point and iodine data of oils. He also determined the HHV of vegetable oils, alcohols and alkane experimentally and correlated these with their density and viscosity values [1], [74]. Sadrameli *et al.* [63] measured the heating values of pure fatty acids using a Parr bomb calorimeter. They developed a correlation of LHVs of fatty acids with their molecular weight, density and carbon number. They also found that the heating value increases with increasing molecular weight and density of saturate fatty acid. The heating values of the vegetable oils and biodiesel were predicted based on the bond energies of their fatty acid/methyl ester constituents.

Table 2-2 The heating value predication correlations developed by previous authors

Author	Correlations	Accuracy	Remark
Freedman and Bagby, 1989 [57]	HHV=76.71+154.77CN, HHV(kg.cal/mole) HHV=-431.08+11.03Mw	R ² =0.99 R ² =0.99	HHV calculated from Carbon number(CN), and Molecular weight of methyl esters
Demirbas, 2000 [74]	HHV = 79.014 - 43.126ρ, HHV(kJ g ⁻¹), ρ(g cm ⁻³) HHV=37.945+0.0491μ, HHV(kJ g ⁻¹), μ(mm s ⁻²)	R ² =0.938 Average difference =0.01% R ² = 0.998	HHV calculation calculated from density and viscosity of vegetable oils
Sheng and Azevedo, 2005[72]	HHV = -1.3675 + 0.3137C + 0.7009H + 0.0318O HHV (MJ kg ⁻¹), C, H, O (wt%)	90% predictions, +- 5% error	HHV calculation from composition of main elements
Sadarameli et al., 2008 [63]	HHV = 0.0518Mw + 29.76, HHV(MJ kg ⁻¹) HHV = -93.4ρ + 122.67, ρ(kg m ⁻³) HHV=0.7271CN+31.419	R ² = 0.9895 R ² = 0.9798 R ² = 0.9895	HHV calculation from molecular weight(Mw), density(ρ) and carbon number(CN) of fatty acids
Demirbas, 2009[75]	HHV = -0.0382ρ + 74.468, HHV(MJ kg ⁻¹), ρ(kg m ⁻³) HHV = 0.6154μ + 38.998, μ(mm s ⁻²)	R ² = 0.8922	HHV calculation from biodiesel density
Mehta and Anand, 2009 [73]	LHV=0.0109(C/O) ³ - 0.3516(C/O) ² + 4.2000(C/O) + 21.066 - 0.11N _{DB} LHV=0.0011(H/O) ³ - 0.0785(H/O) ² + 2.0409(H/O) + 20.992 - 0.100N _{DB}	R ² =0.99 R ² =0.99	LHV calculation from carbon to oxygen ration and number of double bond

They measured 17 different vegetable oils and 15 differently processed fuels of which has heating values of 37MJ/kg and 38MJ/kg, respectively [73]. Most of the heating value correlations have been developed for pure fatty acids or biodiesel fuels. However, currently, biodiesel used in the transport sector is blended with petrol diesel. To investigate the combustion characteristics, performance and emission of the engine, the LHV of the blended biodiesel is required. This problem has also been addressed in the present investigation.

2.1.4 Effects of Physical Properties of Biodiesel on Fuel Supply System

It is well documented that biodiesel and diesel fuels have almost similar thermodynamic properties, although differences in physical properties such as density, viscosity and the bulk modulus have been reported [27], [20], [56], [57]. These physical properties strongly affect fuel pump performance, injection pressure, injection rate and fuel air-characteristics. These effects also extend to the performance and emission characteristics of the engine. Limited numbers of authors have investigated the effects of the physical properties of biodiesel fuels on the fuel pump performance characteristics, fuel injection operation and air-fuel mixing behaviour[76-80]. Bannikov et al. [76] studied the effects of viscosity of the fuel on fuel pump performance characteristics by testing sunflower oils and biodiesel blends. The authors reported that the engine fuelled with more viscous blends could not develop its rated power. Yamane et al. [77] investigated the influence of the physical properties of fuels on the injection characteristics using computer simulation. They reported that when biodiesel fuels were used, the fuel injection pressure increased and furthermore the injection timing advanced with a decrease in fuel temperature. The spray characteristics of inedible oil which include spray penetration, spray cone angle, spray tip speed and Sauter mean diameter (SMD) were studied by Gao et al.[78] using both numerical and experimental techniques for various biodiesel fractions. Their experimental results showed that as the ratio of biodiesel in the blends increased, spray penetration and spray speed increased, but the spray cone angle decreased. Furthermore, the SMD of blend fuels was found to be greater than that of diesel. Lee et al.[79] investigated the atomization characteristics of biodiesel-blended fuels, including spray tip penetration, SMD and mean velocity distribution using a spray visualization system and phase Doppler particle analyzer. The authors concluded that the biodiesel blended fuels had similar spray tip penetrations to conventional diesel but higher SMD. This

phenomenon was explained on the basis that viscosity and surface tension of the biodiesel were higher than those of the conventional diesel fuel.

Bannikov et al. [76] studies were focused on the investigation of biodiesel with a viscosity of almost 5 times that of a commercial biodiesel. It was concluded that use of highly viscous biodiesel resulted in highly distorted performance characteristics of the fuel pump.

This review highlights the lack of research in considering the effects of biodiesel viscosity and density on the fuel pump. Therefore, further investigation is required to understand fuel pump characteristics at different operating conditions when fuelled with different biodiesel blends. Even though the effects of high viscosity and density of biodiesel results in fuel filter clogging and fuel flow rate variations [58], [81], [82], there is a lack of numerical and experimental investigations to quantify such effects. In order to overcome problems experienced with the fuel filter, further work is required in adapting traditional fuel filter designs to suit biodiesel physical properties.

The effects of density and viscosity on the SMD have been reported by previous authors mentioned in above [77-79]. However, these studies were carried out over a limited range of engine operating conditions. Under normal operating conditions the engine operates at various engine speeds and loads in which the effects of density and viscosity of the fuels need to be investigated further.

2.1.5 Summary of Knowledge Gaps in Biodiesel Characterisation

Research

In this chapter the research works on physical properties of biodiesels, such as density, viscosity and heating value were reviewed from the published literature. The prediction models for the density, viscosity and heating value of biodiesel have been analysed in detail. Most of the empirical correlations described above are dependent on some constants and vary with type of biodiesel and percentage of blends. It is very important to adopt a simple, stable and reliable estimation method of viscosity as a function of biodiesel fraction, temperature and density of biodiesel. These relations will be of immense use in engine intake, combustion, and exhaust modelling. Furthermore, the properties of biodiesels affect the dynamic flow phenomena in the fuel pump; the fuel filter and injector spray [77]. Based on

the above requirements, following two objectives have been formulated which need further investigation.

1. Identify the effect of temperature and biodiesel fraction on density and viscosity of biodiesel blends, as well as develop correlations to predict the density, viscosity and heating value from biodiesel fraction or/and temperature values. Further, an attempt will be made to inter-relate density, viscosity and heating values as density of the fuels can be measured relatively easily.
2. Investigate and quantify the effect of density and viscosity of biodiesel and its blends on the fuel supply system, such as fuel pump, fuel filter, fuel injector and spray characteristics.

2.2 Combustion, Performance and Emission Characteristics of CI Engines Running with Biodiesel

2.2.1 Combustion Characteristics of CI Engines Running with Biodiesel

Combustion of fuels is one of the most important processes which affect the performance and emission characteristics as well as engine durability. The important parameters that signify the combustion process effectiveness are in-cylinder pressure, ignition delay, combustion duration, heat release and cumulative heat release rate [83], [84]. The other important combustion parameters, such as combustion duration and intensity, can be easily estimated from the heat release rate (HRR) variation over an engine cycle. The HRR diagram provides key input parameters, for example temperature and pressure values, in the prediction models for NO_x emissions. The heat release rate is estimated from the first law of thermodynamics as given below:

$$\frac{dQ}{d\theta} = p \cdot \frac{\gamma}{\gamma-1} \frac{dV}{d\theta} + \frac{1}{\gamma-1} V \frac{dP}{d\theta} \quad (2-11)$$

$$V(\theta) = \frac{V_d}{\gamma_c-1} + \frac{V_d}{2} [R + 1 - \cos\theta - (R^2 - \sin^2\theta)^{1/2}] \quad (2-12)$$

Where, $dQ/d\theta$ is rate of heat release (kJ/deg), P is the in-cylinder gas pressure, V is the in-cylinder volume, γ is the ratio of specific heats, V_d is the engine displacement, θ is crank angle and R is the ratio of connecting rod length (l) to crank radius (a).

In equation (2-11), the cylinder content is assumed to be a homogeneous mixture of air and combustion products. It is further assumed that a uniform temperature and pressure

exists at any moment during the combustion process. In order to determine the heat release rate within the internal combustion engine (equation 2-11), the engine geometry specifications, as described in Table 3-1, and cylinder pressure values recorded during the tests, were used. Furthermore, the cumulative heat release (Q_{cum}) is calculated by the equation (2-13):

$$Q_{cum} = \int dQ = \int P \frac{\gamma}{\gamma-1} dV + \frac{1}{\gamma-1} V dP \quad (2-13)$$

Most of the researchers have reported that the engines running with biodiesel blends result in an advancement in injection timing and the start of combustion as the biodiesel content in the blends increases [83], [77], [78], [81], [85]. Gao *et.al*[78] investigated the spray penetration, spray cone angle and spray tip speed characteristics using a high-speed camera for different biodiesel blends. The experimental result showed that as the ratio of biodiesel in the blends increased, the spray penetration and spray speed increased. The spray cone angle, however, decreased. They also reported that the Sauter mean diameter of blended fuels was greater than that of diesel under similar operating conditions. Furthermore, Zhang and Van Gerpen[86] investigated the effects of blends of methyl esters of soya bean oil and diesel in a turbo-charged, four-cylinder, direct injection diesel engine. They found that these blends gave a shorter ignition delay and combustion characteristics were found to be similar to diesel [86]. Yusuf and Milford [87] studied the in-cylinder pressure and heat release rate characteristics of a six-cylinder, direct injection 306 kW diesel engine, using blends of esters of methyl as a fuel. The peak rate of heat release, peak cylinder pressure, indicated mean effective pressure (IMEP) and charge of temperature for this blend were found to be lower than that of diesel, [87] Recently, Gumus [83] reported results of an investigation into the combustion and heat release characteristics of biodiesel fuelling direct-injection compression ignition engines. The tests were conducted for different biodiesel blends and the in-cylinder pressure was measured. The combustion duration, heat release rate and cumulative heat release were calculated from the in-cylinder pressure values. It was concluded that the engine running with biodiesel did not show any significant deviation from the engine fuelled with diesel in parameters characterising combustion [83]. Modifications, such as increasing the injection timing, compression ratio, and injection pressure, provided significant improvements in combustion and the heat release characteristics.

However, as the biodiesel content in the blend increased, shorter ignition delays and pre-mixed stage durations were observed. As this review highlights, the studies in combustion characteristics on Biodiesel blends are fairly in-consistent. There is a lack of systematic investigation to quantify biodiesel characteristics and combustion characteristics interdependence. More investigations are required in order to understand the phenomena of combustion and to improve the performance and emission characteristics of engines running with biodiesel blends.

2.2.2 Performance Characteristics of CI Engines Fuelled by Biodiesel

The performance of engines is represented by a number of different parameters. The common parameters includes: brake specific fuel consumption, brake effective power and thermal efficiency. Many researchers have investigated the performance characteristics of engines running with biodiesel and its blends and compared it against its performance when running with normal diesel.

2.2.2.1 Brake Specific Fuel Consumption (BSFC)

Brake specific fuel consumption (BSFC) is the ratio of the engine fuel consumption to the engine power output, as measured at the flywheel. Many authors reported the BSFC of biodiesel as being higher than the diesel during the steady state operation of engines. Canakci [30] carried out extensive tests on a John Deere 4276T, 4-cylinder, 4-stroke, variable speed, turbo-charged direct injection diesel engine, to obtain performance and emission characteristics when running with 20 % soybean oil methyl ester (SME), under steady state operating conditions. The analysis showed that the use of SME resulted in higher BSFC than the commercial diesel. He further reported that the neat SME and 20 % SME resulted in 13.9% and 2.8% increase in BSFC, respectively. Dorado *et al.* [88] used transesterfied waste olive oil on a 3-cylinder, 4-stroke, water-cooled, direct injection diesel engine. Their results revealed a slight increase in BSFC. Monyem and Gerpen [89] also tested neat biodiesel, 20% blend, and a base diesel fuel on a John Deere 4276T turbo-charged DI diesel engine at a single speed of 1400 rpm, with 100% and 20% loads. The biodiesels used were both oxidised and un-oxidised. They reported that the oxidised and un-oxidised neat biodiesels resulted in 15.1% and 13.8% higher BSFC than the diesel fuel, respectively. Ramadhas *et al.* [90] tested rubber seed oil on a four-stroke direct injection, naturally aspirated single cylinder diesel engine at a speed of 1500 rpm under various loads. They reported that when the applied load increased, the BSFC decreased

until the engine attained a 60–70 % load condition. In the same analysis, it was seen that as the percentage of biodiesel increased the BSFC of the engine also increased. Lin C and Lin H [50] reported that the BSFC of fuels decreased with increasing speeds of the engine under a constant engine torque. Lapuerta *et al.*[44] and Xue *et al.*[91] carried out a thorough review of publications on the BSFC of engines using biodiesel and its blends. They found that in excess of 87.1% of researchers agreed that the fuel consumption of an engine fuelled with biodiesel was higher than that of engines run with diesel as shown in Table 2-3.

It can be concluded from the reviewed literature that engines running with biodiesel result in a higher BSFC than when running with diesel, as the former has lower heating value and hence higher amount of fuel is consumed in order to maintain the same brake power [30], [89], [88]. These studies indicate that the fuel consumption is, on average, proportional to the loss of heating values, irrespective of whether heavy-duty or light-duty engines were tested. For example, Hasimoglu *et al.* [92] obtained 13% higher BSFC with a biodiesel having LHV 13.8% lower as compared to diesel on a 4-cylinder, TU and DI diesel engine. Armas *et al.* [93] found that the BSFC of B100 biodiesel, with a LHV (low heating value), 12.9% lower than that of diesel, had increased approximately by 12%, compared to the diesel on a 2.5L, DI and TU, common-rail diesel engine operating at 2400rpm and 64Nm. Furthermore, Lin *et al.* [94] investigated the BSFC of eight different types of biodiesel on a single-cylinder, 4-stroke, DI diesel engine and found the diesel engine had a higher BSFC within the range of 9.45–14.65% than that of diesel which had (12.9–16%) higher value of LHV as compared to the biodiesels.

In some papers it is reported [95], [32] that the increased fuel consumption was not proportional to the loss of heating value for biodiesel. For example, Gumus and Kasifoglu [95] found that the brake specific energy consumption (BSEC) for B100 was higher than that of diesel by 4.8%, due to a lower heating value (about 7.4%) and higher viscosity. Some works have also reported [96-99] decrease in fuel consumption for biodiesel, compared to diesel. For instance, Ulusoy *et al.* [96] observed that the fuel consumption of frying oil biodiesel was 2.43% less than that of diesel on a 4-cylinder, 4-stroke 46kW diesel engine under similar operating conditions. Other than the effects of heating value on BSFC, some researchers have also reported that the BSFC of biodiesel could be affected by the biodiesel content [100-102], biodiesel physical properties[94], [103], [104], engine type and operating

conditions[101], [102] and additives[105], [106]. In addition, some researchers have reported that the BSFC may increase due to changes in combustion timing caused by biodiesel's higher cetane number, as well as the injection timing [89]. Lapuerta *et al.* [44], [91] and Xue *et al.* [87] reviewed 158 and 162 articles respectively about biodiesel engine performance and emissions, published by highly rated journals in scientific indexes covering up to 2010.

Table 2-3 Estimated share of literature (in % number of publications) on effect of pure biodiesel on engine performance and emission in comparison with Diesel [44], [91]

Parameters	Increasing trend		Similar trend		Decreasing trend	
	number of papers		number of papers		number of papers	
	($\%$)		($\%$)		($\%$)	
	Lapuerta <i>et al.</i>	Xue <i>etal.</i>	Lapuerta <i>et al.</i>	Xue <i>et al.</i>	Lapuerta <i>et al.</i>	Xue <i>et al.</i>
Power performance	0	7.4	2	22.2	96	70.4
BSFC	98	87.1	2	3.2	0	9.7
Thermal efficiency	8	NR	80	NR	4	NR
NOx emission	85	65.2	10	5.8	5	29.0
PM emission	3	9.6	2	2.7	95	87.7
THC emission	1	NR	3	NR	95	NR
HC emission	NR	5.3	NR	5.3	NR	89.5
CO emissions	2	10.6	7	3.0	90	84.4
CO ₂	NR	46.2	NR	15.4	NR	38.5
Aromatic compounds	NR	0	NR	15.4	NR	84.6
Carbonyl compounds	NR	80.0	NR	0	NR	20.0

NR: not reported

It is shown in Table 2-3 that from total reports reviewed on the engine running with biodiesel, 98% and 87.1% of them agreed that the engine running with biodiesel resulted in higher BSFC as per Lapuerta *et al.* [44], [91] and Xue *et al.* [87] reports respectively.

2.2.2.2 Brake Effective Power

The brake power is the measure of the engine power available, at the flywheel, to perform work [107]. Many authors report that the power output delivered with biodiesel is lower than diesel during steady state condition of operation. Kaplan *et al.* [43] compared the performance with sunflower methyl esters and diesel on a 2.5 litre, 4-cylinder Peugeot

XD3P157 engine at full and partial load conditions. The loss of the torque and power for biodiesel ranged in between 5% -10%, compared to diesel. Cetinkaya *et al.* [108] investigated the engine performance on a 4-stroke, 4-cylinder, 75 kW Renault Megane diesel engine in winter conditions, using 'used' cooking oil and diesel. The torque and power of the engine with cooked fuel was less by 3-5% as compared to when used with diesel fuel. Utlu and Kocak [97] found that the respective average decrease of torque and power values of an engine running with waste frying oil methyl ester (WFOME), was 4.3% and 4.5% (due to a higher viscosity and density and lower heating value (8.8%)) as compared to when used with diesel fuel. Hansen *et al.* [109] observed that the brake torque loss was 9.1% for B100 biodiesel, relative to D2 diesel at 1900rpm as a result of variations in heating value (13.3%), density and viscosity. Moreover, Murillo *et al.* [110] reported a 7.14% loss of power for biodiesel, compared to diesel on a 3-cylinder, naturally aspirated (NA), submarine diesel engine at full load. In the above investigations the heating value of the biodiesel used was about 13.5% lower as compared to diesel.

Some authors have investigated the effects of biodiesel blends and have reported that the use of biodiesel blends in different percentages did not necessarily follow the above trends. For instance, Gumus and Kasifoglu [95] found that the power increased with addition of biodiesel content in blends up to the B20 (20% biodiesel, 80% diesel) blend. When the biodiesel content continued to increase in the blends, the power started to decrease and reached below that of the diesel fuel and reached minimum value for B100. Likewise, Usta *et al.* [111] showed that the power initially increased with the addition of biodiesel, reached a maximum value, and then decreased with a further increase in the biodiesel content. The aforementioned researchers explained this decrease of power in biodiesel, in relation to the higher viscosity and lower heating value of the biodiesel [97], [98], [110].

Some researchers have also reported that biodiesel delivered more torque and power, in comparison to diesel under similar engine operating conditions [98], [112], whilst others also reported of no significant power loss due to the biodiesel application on engines. Xue *et al.* reviewed 27 papers published in between 2000 and 2010 on the biodiesel power performance, and reported that 70.4% of them reported that the brake power of the engine fuelled with biodiesel decreased.

2.2.2.3 Thermal Efficiency

Thermal efficiency is a dimensionless parameter that indicates the effectiveness of energy conversion process in thermal devices, such as internal combustion engines etc. It is calculated by comparing the power output at the flywheel with the theoretical power available from fuel combustion. Canakici [30], based on his experiments concluded that the thermal efficiency of the engine running with the soybean oil methyl ester (SME) and SME blends had almost the same thermal efficiency when running with diesel. Similarly, Monyem and Gerpen [89] in their research found that the thermal efficiency of the engine running with biodiesel and its blends had the same thermal efficiency as the base diesel. Ramadhas *et al.* [32] tested rubber seed oil on a 4-stroke direct injection, naturally aspirated single cylinder diesel engine at a speed of 1500 rpm and at various load. They reported that when the applied load increased, the thermal efficiency also increased. Contrary to the other authors, they reported that 10% biodiesel blend had more thermal efficiency than the other blends and base diesel. Lin C. and Lin H [50] also reported that the brake thermal efficiency obtained with biodiesel was higher than that obtained with diesel. They reasoned that as biodiesel has higher oxygen content, it improves its burning characteristics. A number of researchers have also reported similar findings when using biodiesel fuels [44], [113].

2.2.3 Emission Characteristics of CI Engines Running with Biodiesel

Current and future emission regulations are, and will become, more stringent and as a consequence, the transport sector is undergoing rapid transformation in order to comply with these regulations. In addition, fossil fuel demand is continuously increasing globally, the result of which is the rapid depletion of fossil fuel deposits [114]. Such problems are compelling countries to now focus on developing or finding alternative fuels [115]. The major alternative fuels being used in automotive transport are ethanol, hydrogen and biodiesel. Ethanol technology is successfully established and commercialised in both developing and developed countries. However, ethanol use is limited only to spark ignition engines. Furthermore, ethanol use is also limited to maximum blend strengths of up to 15% only because higher blend strengths result in fuel injection system problems [116]. Hydrogen- based fuel cells could become a viable alternative to fossil fuels. However, to make its use commercially viable, many technical challenges need to be addressed, for example, complexity in hydrogen production, requirements of special infrastructure for its storage, and high fuel cell production costs. In spite of research advances on hydrogen-powered fuel cells, diesel engines are expected to remain in use for high-power applications,

such as rail road locomotives, ships and over land transport trucks [4]. A large number of studies have shown that biodiesel is one of the most promising renewable, alternative and environmentally friendly biofuels which could be used in diesel engines, with little or no requirement of engine modifications [90], [117-120]. It has also been shown that biodiesel has significant potential to reduce CO₂, CO, THC and PM emissions [88], [97].

2.2.3.1 Nitric oxides(NO_x)

Oxides of nitrogen are chemical compounds formed by the combination of nitrogen and oxygen under extremely high temperatures which occur during a combustion event in an internal combustion engine. Most of the literature reviewed showed that the use of biodiesel fuels caused increases in NO_x emission[23], [60], [96], [100], [109-111], [121], [122] [123], [124], [125]. As presented in Table 2-3 Lapuerta *et al.*[44] and Xue *et al.*[91] carried out a thorough review of publications on the NO_x emission of engines using biodiesel and its blends. Lapuerta *et al.*[44] and Xue *et al.*[91] reported that in excess of 85% and 65% of researchers agreed that the NO_x emission of an engine fuelled with biodiesel was higher than that of engines running with diesel respectively. Candace [125]carried out a test on a John Deere 4276T, 4-cylinder, 4-stroke, variable speed, turbo-charged DI diesel engine, for engine performance and emission analysis when running with 20% soybean oil methyl ester (SME) under steady conditions. The test analysis showed that NO_x emissions of the CI engine were higher for biodiesel and its blends than for diesel. The 20% and 100 % biodiesel blends had increased the engine emissions by 0.6% and 11.2 %, respectively. Marshall *et al.*[124] tested a Cummins L10E engine under transient conditions, with diesel fuel, and 20% and 30% biodiesel blends. They reported that the NO_x emission increased by 3.7% and 1.2% for 20% and 30% biodiesel blends, respectively over and above the diesel emission. Furthermore, a maximum of 15% increase in NO_x emissions for B100 was observed at a high load condition which may be because of 12% oxygen content of the B100 and higher gas temperature in combustion chamber [93]. Lin *et al.* [23] compared 8 kinds of biodiesel as mentioned earlier and observed that using biodiesels in the diesel engine yielded higher NO_x emissions. This NO_x emission ranged from an increase of 5.58% to an increase of 25.97% when compared to petrol diesel over a wide range of operating conditions. Three main arguments have been used in previous works to explain the observed increase in NO_x emissions when using biodiesel fuels [44], [91]. The first reason behind this observation is advanced engine combustion when running with biodiesel as a consequence of the

advanced injection derived from the physical properties of biodiesel such as viscosity, density, compressibility and speed of sound [126]. When biodiesel is injected, the pressure rise produced by the pump is quicker as a consequence of its lower compressibility (higher bulk modulus) and the pressure wave propagates more quickly towards the injectors as consequence of its higher sound velocity [77], [89], [126], [127]. This causes earlier ignition which results in higher temperature peaks and NO_x formation rates. The second argument frequently proposed to explain the higher NO_x emissions of engine running with biodiesel is the increased cetane number of biodiesel which leads to an advanced combustion by shortening the ignition delay [89], [112], [128], [129]. However, the argument of higher cetane number for higher NO_x emission is questionable. The higher cetane number will not only lead to early burn, but will also lower premixed combustion which will lead to smaller changes in cylinder pressure and temperature, which may lower NO_x formation [91]. The third argument is related with oxygen content of biodiesel which enhances the formation of NO_x. The relationship between NO_x values and the mass percent of oxygen in fuel had been investigated experimentally by Laybacks and Slavinskis [130] on a 4-stroke, 4-cylinder, direct injection diesel engine. The results showed that the NO_x emissions increased proportionally with the mass percent of oxygen in the rapeseed methyl ester diesel blends

A small number of researchers have reported that the NO_x emissions are reduced when biodiesel is used as a fuel [9], [88], [93], [97], [101], [128], [131]. For example, Dorado *et al.* [88] ran transesterified waste olive oil in a 3-cylinder, 4-stroke, water-cooled, 18.5:1 compression ratio, direct-injection diesel engine Perkins AD 3-152. In this test, the NO_x emission of the engine had reduced by 32%, compared to when used with diesel fuel. Puhan *et al.* [128] found that the average reduction of NO_x in the case of biodiesel was around 12% compared with the diesel fuel over the whole range of loads. Qi *et al.* [9] carried out emission analysis on a single cylinder, naturally aspirated, four stroke, and high speed diesel engine with a bowl in piston combustion chamber which was run with biodiesel produced from soybean. They reported NO_x emission was reduced by 5% compared with the normal diesel.

Insignificant numbers of researchers have reported that engines running with biodiesel do not show significant difference in NO_x emission between biodiesel and diesel fuels [12], [132], [133].

2.2.3.2 Carbon monoxide (CO)

CO is a toxic gas which forms due to inadequate oxygen amount present in combustion chamber. In diesel engines, CO is formed during the intermediate combustion stages. CO discharged from the engine into the exhaust manifold is oxidised to form CO₂, if adequate oxygen is present and the gases remain hot enough with a sufficient residence time.

Most of the previous works have indicated that the CO emissions of engine running with biodiesel are lower than that engine running with diesel [60], [96], [100], [109-111], [121], [122] [123], [124], [128], [129], [134]. The Lapuerta *et al.* [44] and Xue *et al.* [91] have reported that 90% and 84% of the reviewed papers shows decrease in CO emissions, when the engines ran with biodiesel. Krahl *et al.* [134] found about 50% reduction in CO emissions for biodiesel from rapeseed oil compared to diesel. A higher reduction in CO emissions was shown by Raheman and Phadatare [101], who observed that the CO emission reduced in the range of 73–94% for the karanja methyl ester (B100) and its blends (B20, B40, B60 and B80) as compared to diesel. Canakci [30] reported that for biodiesel and its blends, the CO emission was observed to be lower than that of normal diesel in the aforementioned test. He further added that the emission decreased with an increase in the blend percentage. Ramadhas *et al.* [32] tested rubber seed oil on a 4-stroke direct-injection, naturally aspirated single cylinder diesel engine. The carbon monoxide emission rose with increasing load levels, due to an air-fuel ratio decrease. Durbin *et al.* [12] experimented with biodiesel, biodiesel blends and synthetic diesel in four Ford and Dodge light heavy-duty diesel vehicles. CO emissions of the engine were significantly lower for all alternative biodiesel blends compared to diesel in this test. Wang *et al.* [132] conducted field work on Heavy Duty Chassis Dynamometer with Cummins 855 engines at West Virginia University using 35 % biodiesel blend under steady and transient conditions. The authors reported that during acceleration, CO increased in the engine running on biodiesel and decreased during the deceleration process. The main reason for reduction of CO emission is due to the extra oxygen content of biodiesel which enhances the complete combustion and leads to the reduction in CO emissions [9], [111-113], [123], [124], [127], [128], [131], [135].

2.2.3.3 Carbon dioxide (CO₂)

CO₂ is one of the gases emitted during combustion of carbon in fuel. There is no universal consensus on the effect of biodiesel on emission of CO₂ from CI engines. Some authors have reported that when a CI engine runs with biodiesel the CO₂ emission increases as compared to petrol diesel [30], [32], [96], [128]. Ramadhas et al. [32] measured the CO₂ emissions of the engine running with biodiesel and its blends over a wide range of loads. For all blends of biodiesel used in this work, the CO₂ emissions of the engine rose with increasing load. For lower percentages of biodiesel blends, the CO₂ emission of the engine running with biodiesel was lower than that of the emission of engine running with diesel. However, when 100% biodiesel was used, CO₂ emission of biodiesel was higher than diesel. Canakci [30] reported that the CO₂ emissions of the biodiesel and its blends were slightly higher than that of diesel. The 100% and 20% blends of biodiesel increased the CO₂ emissions from the engine by 0.5 and 0.1 %, respectively. The researchers suggested that this was due to biodiesel having a lower carbon-hydrogen ration than diesel fuel. In contrary to this some researchers reported that the CO₂ emission rise when CI engines run with biodiesel as compared to when used with diesel [50], [97], [104], [136]. Lin C. and Lin H [50] experimented using soybean biodiesel (Sample 1 and 2 biodiesel, commercial biodiesel) and ASTM No. 2D in a 4-cylinder, 4-strokes, naturally aspirated, direct-injection diesel engine with a displacement volume of 3.856 litre, under constant torque and variable engine speeds of 850 to 2000 rpm. The CO₂ emission index decreased with an increase in engine speed for diesel and biodiesel blends.

2.2.3.4 Total Hydrocarbon (THC)

The incomplete combustion of fossil fuels and fuel evaporation from the open areas are being the major sources of hydrocarbons (HC) in the atmosphere. When hydrocarbons combine with NO_x and sunlight, ozone is formed. This is a serious form of air pollution and a key component of smog. Most reviewed literatures show a sharp decrease in the THC emissions when substituting conventional diesel fuel with biodiesel fuels in engines [30], [32], [60], [96], [100], [109-111], [121], [122], [123], [128], [134]. For example, Puhane et al. [128] reported that the HC emissions reduced by an average of around 63% of when the CI engines run with biodiesel as compared to diesel. Durbin et al. [12] reported that THC emissions were generally lower for biodiesel and synthetic diesel, compared to California Diesel. The 100% biodiesel fuel resulted in the lowest THC. Monyem and Gerpen [89] tested neat biodiesel, 20% blends, and the diesel on a John Deere 4276T turbo-charged

DI diesel engine. The HC emissions for all the biodiesel fuels were less than that of the base fuel. Several researches also showed that there was no significant difference in THC emission caused by biodiesel and diesel [91], [130], [137]. Also the trend of THC emissions increase with the use of biodiesel was found in several publications [54,112,113]. Most authors have agreed that the primary cause of the formation of THC is the presence of oxygen content in the biodiesel molecule, which leads to a more complete and cleaner combustion [9], [111-113], [128], [124], [127], [128], [131], [135]. The higher cetane number of biodiesel reduces the combustion delay, and such a reduction results in reduction of THC [89], [112], [128], [129], [138].

2.2.4 Summary on Knowledge Gaps on Combustion, Performance and Emission Characteristics of CI Engines Running with Biodiesel

The performances of the CI engines running on biodiesel and its blends under steady conditions have been reported extensively in the aforementioned literature review. The main performance parameters, such as brake power, specific fuel consumption and thermal efficiency, variations with biodiesel blending percentage, engine speed, engine load, and engine types, have not been investigated in-depth. It can be concluded from this discussion that BSFC shows complex behaviour with biodiesel use in comparison to diesel and more investigations are required to understand these effects thoroughly. As per the knowledge of the researcher, there are limited works available on systematic investigation on engine performance when running with biodiesel and its blends during transient operations. The transient conditions of operation are mainly observed in urban area due to the ‘stop and go’ nature of vehicular traffic. This study, therefore, includes the investigation on the usefulness of biodiesel and its blends during such transient conditions of operation.

Detailed research has been conducted on the emissions of biodiesel during steady operations, considering different operating conditions. The effect of biodiesel blending fraction and the impact of speed and load variation on the engine have been investigated in detail. Most of the reports are focused on the steady state operations. Furthermore, established mathematical models for diesel and biodiesel emissions during transient conditions are yet to be developed. This study, therefore, will focus on the investigating the engine emissions during transient conditions. In addition, a mathematical model will be developed for prediction of emissions during transient conditions. Prediction of performance and emission characteristics of the engine running with biodiesel during transient operations is therefore will be attempted in the

present work. Furthermore, attempts will be made to test usefulness of steady state data (commonly available) in predicting transient behaviour of the engine running on biodiesel. The literature review clearly identified that the engine running with biodiesel resulted in significant reduction in emissions of CO₂, CO and THC. However, the engines running with biodiesel emit more NO_x than the engine running with conventional diesel. So it is very important to develop on-line measuring methods for monitoring NO_x emission as well as to develop novel NO_x reduction techniques. Therefore, the next section focuses on the NO_x emission measurement, NO_x formation in combustion chamber and NO_x reduction techniques.

2.3 NO_x Measurement Techniques and Prediction Models

The current available methods of measuring/predicting NO_x emissions are: analyser use (direct measuring), engine map method and artificial neural network. Measurement of nitrogen oxides on a dry basis, by means of a heated chemiluminescent detector (HCLD) with a NO₂/NO analyser, is widely used. However, the analyser has disadvantages of higher initial costs and larger space requirement well as it demands frequent calibration and can be affected by soot. In addition, its responses are very slow, which affect transient NO_x emission measurements [51]. However, the formation of NO_x is the most significant phenomena under transient engine operations especially when biodiesel is used as a fuel. These effects are mainly seen during engine acceleration or load increases, owing to the momentary increase in fuel injection which contributes to higher cycle temperatures and, hence NO production [35], [36]. An engine map method includes a NO_x database generally based on measurements of a series of settings of engine speed and torque, or power of the engine, under stationery conditions. Most maps have the disadvantages of not considering the effects of all the significant variables on NO_x emission levels. This causes deviations between real NO_x emissions estimated from the engine map. In addition, it estimates the transient conditions from discrete steady state values [51]. The third method, which needs the artificial neural network (ANN) system, has the advantage of training from real life data taken under transient conditions. However, in the neural network there is no explicit mathematical representation of the physical process, and the predicting capability is limited only to the specific engine type for which the neural network is trained [139].

NO_x formation is the thermal mechanism, which occurs in the post-flame burned gases, and as described by the extended Zeldovich mechanism, which is described by equations (2-14 to 2-16), and includes the reactants, products and rate constants. In order to derive the rate of

change of NO concentration in equation (2-17), it was assumed that the concentration of the N is minor in comparison to the concentrations of the other species, so that the rate of change in N can be set equal to zero. This assumption has been made due to the smallest value of the activation energy for oxidation of N atoms [140], [141]. During fuel-lean flame, the rate of consumption of free nitrogen atoms becomes equal to the rate of its formation and therefore an equilibrium state can be established and rate of change of N can be assumed almost zero. The rate constants for equation (2-17) have been measured in numerous studies and critically evaluated [137], [140], [142], [143], [196]. The reaction rates used in this NOx model are given in Table 2-4. In Table 2-4 the (-) sign indicate the backward reaction. The $[N_2]$ and $[O_2]$ concentrations were determined at ambient condition of the atmospheric air.

2.4 Techniques to Reduce NOx Emission

2.4.1 NOx Formation in Diesel Engines

NOx formation process in IC engines can be categorised as, prompt NOx formation process, fuel NOx formation process and the thermal NOx formation process. Although the NOx emission release amount varies, each of the three pathways of NOx formation contributes to the overall NOx emission into the environment [52]. Prompt NOx is produced when hydrocarbon fragments (mainly CH and CH₂) react with nitrogen in the combustion chamber to form fixed nitrogen species, such as HCN. HCN reacts with the atmospheric nitrogen to form NOx. Prompt NOx formation is only common in fuel-rich combustion. Diesel engines run fuel lean; therefore, the probability of prompt NOx formation is limited. In addition, in biodiesel the carbon to hydrogen ratio is lower as compared to carbon to hydrogen ratio in diesel fuel. Therefore, the contribution of prompt NOx formation from biodiesel within fuel engines can be ignored. The second method of NOx formation occurs when nitrogen which has been chemically bound in the fuel, combines with excess oxygen during the combustion process. This is not a problem for biodiesel again, which does not contain nitrogen inherently [140].

The thermal NOx formation process is the main contributor to NOx emissions from diesel engines. It occurs during fuel combustion in combustion cylinders when the atmospheric oxygen and nitrogen combines at higher temperature. The possible kinetic reaction mechanisms of emissions generation in the engine cylinder are described as the Zeldovich extended mechanism [144] equations (2-14 to 2-16):



Table 2-4 Rate constants for thermal NOx formation [140]

Rate constants	Values [(m ³ /(gmol s))]
k_1	$1.8 \times 10^8 e^{-38370/T}$
k_{-1}	$3.8 \times 10^7 e^{-425/T}$
k_2	$1.8 \times 10^4 T e^{-4680/T}$
k_{-2}	$3.8 \times 10^3 T e^{-20820/T}$
k_3	$7.1 \times 10^8 e^{-450/T}$
k_{-3}	$1.7 \times 10^8 e^{-24560/T}$

Where k_1 , k_2 and k_3 are the rate constants for the forward reactions as given in Table 2-4. Assuming quasi-steady state for the formation of N, the net rate of the NOx formation through the above reactions is given by the following formula (equation (2-17)):

$$\frac{dNO}{dt} = 2k_1[O][N_2] \frac{\left(1 - \frac{k_{-1}k_{-2}[NO]^2}{k_1[N_2]k_2O_2}\right)}{\left(1 + \frac{k_{-1}[NO]}{k_2[O_2] + k_3[OH]}\right)} \quad \text{gmol}/(\text{m}^3 \text{ s}) \quad (2-17)$$

To solve equation (2-17), in addition to the concentration of N₂ and O₂, both concentrations of O and OH are needed. The concentration of O radicals can be calculated from either an equilibrium approach or partial-equilibrium approach equation (2-18) and equation (2-19), respectively.

$$[O] = 3.97 \times 10^5 T^{-1/2} [O_2]^{1/2} e^{-31090/T} \quad \text{gmol}/\text{m}^3 \quad (2-18)$$

$$[O] = 36.64 T^{1/2} [O_2]^{1/2} e^{-27123/T} \quad \text{gmol}/\text{m}^3 \quad (2-19)$$

The concentration of OH molecules can be calculated from the following equation (2-20):

$$[OH] = 2.129 \times 10^2 T^{-0.57} e^{-4595/T} [O_2]^{1/2} [H_2O]^{1/2} \quad \text{gmol}/\text{m}^3 \quad (2-20)$$

For most fuel lean cases, such as in diesel engines, the thermal NO_x formation equation (2-16) can be neglected and [OH] is no longer needed. This is due to the equilibrium constant of [O₂] being much higher than the equilibrium constant of [OH].

The thermal NO_x formation rate is primarily a function of temperature and the residence time of nitrogen at that temperature. These reactions occur at high temperatures, usually in the range 300-5000K [59]. In addition, turbulence and amount of excess oxygen are two other important factors to consider. In order to reduce the rate of NO_x formation by thermal method in the cylinder, the only possible way to do so is by reducing the reaction rate in equation (2-17). The rate of reaction can be reduced by lowering the combustion chamber temperature. The chamber temperature can be reducing by a number of methods.

There are different methods used to reduce NO_x emission from compression-ignition engine, such as exhaust gas re-circulation (EGR), catalytic conversion (post-combustion method) and water injections/emulsion [52]. The following section highlights the merits and demerits of each method.

2.4.2 Methods of NO_x Reduction

Biodiesel is one of the renewable energy sources, which consists of short chain (methyl or ethyl) esters, produced from vegetable-based oils by transesterification. A large number of studies have shown that biodiesel is one of the most promising renewable, alternative and environmentally friendly biofuels which could be used in diesel engines with little or no requirement of engine modifications [117-120], [90]. It has also been shown that biodiesel has significant potential to reduce CO₂, CO, THC and PM emissions [88], [97].

Although biodiesel provides engine performances comparable to engine performances using diesel, a considerable number of researchers have reported that engines running with biodiesel emit higher NO_x concentrations in exhausts [44], [48], [49]. NO_x and PM emissions are major toxic emissions which are being regulated with emission regulations which are becoming increasingly more stringent [50], as shown in Figure 2-1[145]. This regulatory requirement has resulted in major research and development works being undertaken in order to reduce NO_x emissions. Different methods have been used to reduce NO_x emission successfully from compression-ignition engine. Some of these include: exhaust gas re-circulation (EGR), catalytic conversion (post-combustion) and water

injection/emulsion [52]. The working principles, advantages and disadvantages of these methods are summarised below.

2.4.2.1 Exhaust Gas Recirculation (EGR)

The main principle employed in EGR is re-circulation of a portion of an engine's exhaust gas back to the engine cylinders. The re-circulated exhaust gas decreases the local temperature in the combustion chamber. It is mostly effective in particular time/space zones during which NO_x emissions are produced, specifically during fuel injection and after the end of injections [146].

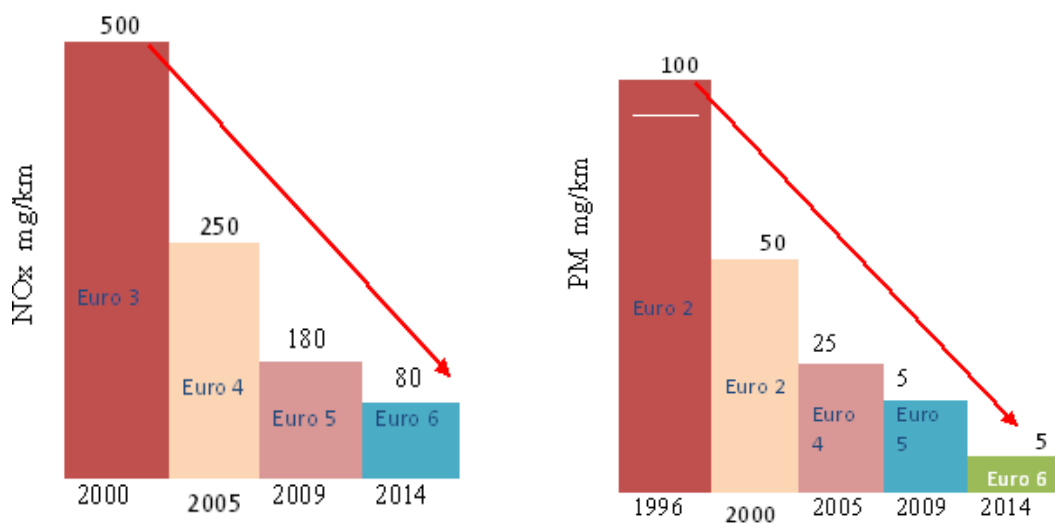


Figure 2-1 Passengers cars NO_x emission overview of past and future requirements [38]

In an EGR system, the heat of combustion from the fuel is used to heat the exhaust gas. The exhaust gas is essentially inert and therefore does not react in the combustion chamber and only absorbs heat [52]. Although EGR has a potential of reducing NO_x by 50%, it has an inherent drawback of increasing the PM emissions [115], [147], [148]. In addition, the heat absorption by exhaust inert gas in the cylinder chamber also results in small amounts of power loss from the engine.

2.4.2.2 Post-Composition Control Method

The other method used to reduce NO_x emissions is the post-composition control of exhaust gas. One such method being used for SI engines is a three-way catalytic converter. The catalytic-converter changes NO_x to N₂, CO to CO₂ and unburned hydrocarbons (HC) into H₂O and CO₂. However, the materials used in catalytic converters include platinum,

palladium, and rhodium, which are expensive. In addition, the catalytic converters work best at a stoichiometric air-fuel ratio of about 14.1:1. Most of diesel engines tend to run lean which makes the catalytic converter less effective in reducing NO_x emission [149]. Running lean also produces more NO_x emission due to an increase in engine temperature. The other catalytic method used to reduce NO_x is selective catalytic reduction (SCR). This method has been used for several years in stationary combustion installations to reduce NO_x, by injecting ammonia in the presence of the catalyst. In vehicles applications, however, instead of ammonia, an aqueous solution of urea (NH₂CONH₃) is used. The SCR can result in NO_x reductions by 90% [150]. However, the application of SCR is used mainly in heavy vehicles and is rarely in use in passenger cars. This is due to exhaust gas temperatures in diesel car being low that makes SCR less effective. In addition, urea/ammonia management is quite costly and requires modification of the exhaust system for catalyst space. Furthermore, provisions for a new urea/ammonia infrastructure and maintenance of the system need to be made [151].

2.4.2.3 Water Injection/Emulsion

The third method used to reduce local combustion temperature and, consequently, NO_x emission is the injection of water into an engine system [152-156]. One of the advantages of the water injection, as compared to the EGR and the catalytic converter, is the enhanced possibility of reduction of NO_x over the entire engine load range, without affecting the PM emission negatively [115]. Although water is inert, in the combustion cylinder it decreases the local adiabatic flame temperature by absorbing heat of water vapour [157-159]. As a result, the NO_x emission, which depends on the peak flame temperature, is reduced [15], [160], [50]. In addition to the reduction of NO_x, water emulsion also reduces the HC, soot and particulate matter. There are three main methods that are used to introduce water into a diesel engine. These are direct water injection into the cylinder using separate injectors, injecting water/diesel emulsion and spraying/injecting water into the intake manifold [154] [161], [162].

The first water-based injection system involves direct injection of water within the combustion cylinder. This method provides an option of controlling the water and fuel ratio [163]. Southwest Research Institute and Delphi Diesel Systems have developed a real-time water injection system for application in heavy-duty diesel engines. The system is integrated with an electronic control unit which controls the pump that delivers metered volumes of water to an electronic injector, forming a diesel and water mixture at the injector tip. It has

been reported that this method enables NO_x emission to be reduced by up to 42%, and in combination with EGR, this method enables NO_x emission to be reduced by up to 82% [164]. The drawbacks of this method, however, is the level of complexity involved in integrating additional components into the existing engine system, and further requirements needed in the re-design of a fuel supply system integrated within the engine.

The second water-based injection system involves the use of emulsification of water and fuel in the presence of some surfactants in an appropriate mixer. It has been also shown that adding water to the fuel improves atomisation and the mixing characteristics which are attributed to droplet micro-explosions. Micro-explosions phenomena are induced by volatility differences between the water and the fuel [162]. The water-fuel emulsion methods, however, have several shortcomings which impede emulsion fuels from becoming widely used in the practice. The effects of water emulsion on the performance of the engine vary with the operational modes of the engine. In most of the previous studies, water emulsion has been shown to have a positive effect on engine performance parameters [160], [165]. The water diesel emulsion, however, has some drawbacks. First, the emulsions needs a more advanced and well developed infrastructure for the implementation of a complex on-board, water-in-diesel emulsion production system integrated with the engine. This increase the engine cost [115]. In order to produce smaller and well-scattered water droplets, the engine operating parameters need to be controlled with very high degree of accuracy [162]. Second, the physical properties (viscosity, density and bulk modules) of the fuel emulsion may change. It was observed that the viscosity and density of water-emulsified fuel have higher values, than the normal fuel [166]. Changes in these parameters can significantly affect the performance of the fuel injection system.

The third method of water-based injection systems is intake manifold water injection. Currently, this method is widely used in large marine diesel engines. Water can be injected either downstream or upstream of the compressor [152-155],[156], [163]. Tauzia *et.al* [115] investigated the effects of water injection into the intake manifold of a HDDI diesel engine. They reported a NO_x reduction of up to 50% at an injection rate of between 60-65 % of water based on fuel consumption over a wide load range. The main advantage of water injection into the intake manifold is the simplicity and ease with which it can be integrated within existing engines and also with any new design. Since in this system water is injected through a separate valve and does not mix with fuel directly, it does not affect the fuel flow properties

in fuel supply line. It can be seen from the above discussion that water injection into the intake manifolds, has the potential to be the most effective method of NO_x reduction.

The reasons behind temperature reduction in combustion chamber because of water injection/emulsion can be one or more of the following [115], [152]:

- Decrease of the cylinder gas temperature due to the absorption of heat by water to form vapour.
- Water cooling effects due to evaporation of water from combustion chamber surfaces
- Increase of heat capacity due to higher trapped mass
- Increase of specific heat capacity due to air dilution with vapour
- Increase of heat losses at the cylinder wall, lining and piston head
- Combustion delay due to increase in ignition delay
- Decrease of the chemical reactions rate due to the inert ‘chemical’ water

For an adequate control of the reduction of NO_x emission by using water injection in diesel engines, a tool has to be available to accurately and quickly measure or predict the NO_x emissions during both steady and transient conditions. In next section a summary on detailed reviews has been presented on the available NO_x prediction models and corresponding merits and demerits.

2.4.3 Summary and Knowledge Gaps on NO_x Emission Reduction Techniques and Predicting Models

In this chapter available technologies for NO_x reduction were reviewed. It can be seen that the application of water injection to an engine running with diesel in order to reduce NO_x emission, has been reported extensively. However, little attention has been paid to understanding and investigating the effects of water injection on engines’ performance and emission when running with biodiesel and biodiesel blends. To use the water injection system for NO_x reduction, thermodynamic effects of water injection on the combustion behaviour, the performance and emission characteristics of a CI engine need to be investigated. The available NO_x measurement or predicting methods such as heated chemiluminescent detector (HCLD), engine map and artificial neural (ANN) system, are limited either only for steady state operations or limited for only some engine operations. Therefore, it is vital to develop new real-time NO_x emission prediction models for engine transient study and on-line diagnosis.

2.5 Scope and Objective of the Study

2.5.1 Scope of the Study

It has been reported that Biodiesel and its blends differ from diesel and have different physio-chemical properties. These properties are a function of operating temperature. The available literature does not provide complete information regarding this. Furthermore, there is no model which indicates the effect of such properties on filter, fuel pump and air-fuel mixing behaviour. Hence, the first facet of this work is to investigate the most important properties of biodiesel such as density, viscosity and lower heating value, both experimentally and numerically. The effects of the biodiesel blend content on the physical properties are also proposed to be analysed. For each property mentioned above it is proposed to develop accurate predicting models which will be validated through models available in literature and experimental results. It is proposed to develop new density and viscosity predicting models by considering the combined effect of biodiesel content and temperature. Finally the effect of the density and viscosity on the fuel supply system such fuel filter, fuel pump and air-fuel mixing behaviour will be established through numerical investigations.

The second facet of this research is to investigate the combustion as well as engine performance and emission characteristics of a CI engine under both steady and transient conditions of operation when operating with biodiesel. The knowledge available in this regard is sketchy and a systematic investigation is required in this regard. The effects of the biodiesel properties and the biodiesel content on the CI engine's in-cylinder pressure, brake specific fuel consumption, thermal efficiency and emissions (CO_2 , NO_x , CO , THC) will be discussed on the basis of the experimental results. For each parameter the effects of the biodiesel blends will be quantified. A detailed analysis on transient performance and emission characteristics of CI engines would be also carried out.

During the literature search, it has been noticed that there is a lack of available methods to predict and measure NO_x emission during transient state of engine operation. Hence the third facet of this work is to predict NO_x by using the measured in-cylinder pressure and air flow rate. The NO_x emissions are well known drawbacks of using biodiesel as a fuel. In absence of any well known method for NO_x reduction for engines running with biodiesel, research is necessary to investigate existing methods used for diesel engines to understand their suitability in reducing NO_x . Hence, the final facet of this dissertation is to develop a simple, reliable and inexpensive method (water injection) to reduce the NO_x emission from the CI

engine fuelled by biodiesel. By varying the water injection flow rates, the performance and emission characteristics (NO_x and CO) of CI engine fuelled with biodiesel would be investigated.

2.5.2 Objectives of the Study

In the literature review four research problems have been identified in areas of biodiesel physical properties, engine performance and emission behaviour during transient operation as well as NO_x emission measurement technique and complexity of NO_x emission during the utilization of biodiesel in CI engine. Taking the identified specific problems into account, this study has the following specific objectives:

1. To analyse the physical properties such as density, viscosity and lower heating value of biodiesel and its blends experimentally by considering biodiesel content and temperature variation.
2. To develop predictive models for physical and chemical properties of biodiesel and its blends from the experimental data which can correlate the physical properties with biodiesel content and temperature.
3. To investigate numerically the effects of the biodiesel physical properties on the fuel supply system such as fuel filter, fuel pump and engine combustion chamber.
4. To analyse experimentally, the combustion characteristics such as in-cylinder pressure, heat release rate and cumulative heat release of CI engine fuelled by biodiesel and its blends during both steady and transient conditions.
5. To examine analytically the brake specific fuel consumption, thermal efficiency and in-cylinder peak pressure of CI engine systems from experimental data obtained from engine using biodiesel and its blends during both steady and transient conditions.
6. To examine, numerically and experimentally the emissions of CI engine systems, from engine running on biodiesel and its blends during both steady and transient conditions.
7. To develop a method to estimate NO_x emission under steady and transient operation using in-cylinder pressure, specific heat and mass air flow rate.
8. To develop direct water injection system for use in CI engine running with biodiesel and investigate the combustion characteristics, performance and NO_x emission of the engine during steady mode of operation.

2.6 Summary on Chapter Two

In Chapter two an extensive literature review work on the biodiesel characterisation, performance and emission characteristics of CI engines running with biodiesel, NOx emission reduction techniques and NOx prediction models have been carried out. The reviews have identified the specific research problems. Depending on the research problems, the specific objectives of this study have been identified. In the next Chapter the test apparatus and test procedures have been explained in detail.

CHAPTER THREE

3. TEST RIG INSTRUMENTATION AND TEST PROCEDURES

This chapter gives a detailed description of the experimental facilities required for biodiesel characterisation, the test engine's characteristics and specifications, and also describes the test rig and instrumentation. The details of measured parameters, data acquisition system and application software are also provided. In addition, test procedures have been described in detail. Under test procedures the methodology of biodiesel blending, the new steady and transient test procedures, water injection system and injection procedures have been developed. Finally, methods to ensure accuracy of measurements have been discussed. The test apparatus and procedures have been selected after reviewing previous similar works and specification of various instruments.

3.1 Biodiesel Characterisation Facilities

3.1.1 Materials-Biodiesel and Diesel

In this study, three common types of commercially available biodiesels (corn oil biodiesel, rapeseed oil biodiesel, and waste oil biodiesel), obtained from a local company, have been used for analysis. The corn oil biodiesel and rapeseed oil biodiesel were produced by the transesterification process from ‘virgin’ oil using methanol. The waste oil biodiesel was produced by the same process, although the raw feed was from cooking oil waste. Normal diesel fuel was obtained from a local fuel supplier. The red diesel, which is exactly the same as regular diesel by its combustion, performance and emission behaviour, was used in all tests. The red diesel was selected due to its low fuel tax for off-road engines. The biodiesel was blended with diesel fuel at 5%, 10%, 20%, 50%, 75% and 100% on a volume basis. Six samples were prepared for each biodiesel. In total, (including diesel) 19 samples were used in density and viscosity measurements.

3.1.2 Density measurement: Apparatus and Procedures

In order to measure the density, standard procedures: BS EN 3675, have been followed [167]. A glass hydrometer with specific gravity in the range of 0.7 to 1.0 with an accuracy of three decimal places was used. To collect the temperature-dependent data, a 100ml graduated cylinder containing a biodiesel sample was placed in a temperature controlled bath. The water bath temperature varied from room temperature to 95°C. The test was repeated twice and the average values were taken as the representative value. In addition to the hydrometer measurements, the mass/volume method for density measurement was also used for comparison at 15.6°C.

3.1.3 Viscosity measurement: Apparatus and Procedures

The Standard Method [Petroleum products: Determination of kinematic viscosity and calculation of dynamic viscosity, the European standard EN ISO 3104:1996] [168] was used to measure the viscosity of the biodiesel samples. This method is commonly used to measure the kinematic viscosity of liquid petroleum products. Since biodiesel fuels also have similar properties as fossil fuel, this method was considered appropriate for the measurement of viscosity of the samples. Kinematic viscosity is determined by measuring the time taken for a known volume of fuel flowing under gravity to pass through a calibrated glass capillary viscometer tube. A Cannon-Fenske Viscometer tube (size B) and Selecta viscosity bath were used for this purpose. The size B viscometer had

approximate constants of 0.01 and kinematic viscosity ranged from 2-10mm²/s. The water bath temperature used had a temperature range from room temperature to 85°C. The viscosity values below room temperature were determined from the regression correlation developed from the data obtained from this study and previous reports. For the experimental data to be acceptable, the EN ISO 3104:1196 standards required the tests to be performed twice and that the first and second measurements to be within an accuracy of 0.02mm²/s. If the accuracy condition was satisfied, the average of the two tests was taken. The tests were repeated twice and the average value was taken as representative value. The viscosity measurement apparatus is shown in Figure 3-1.

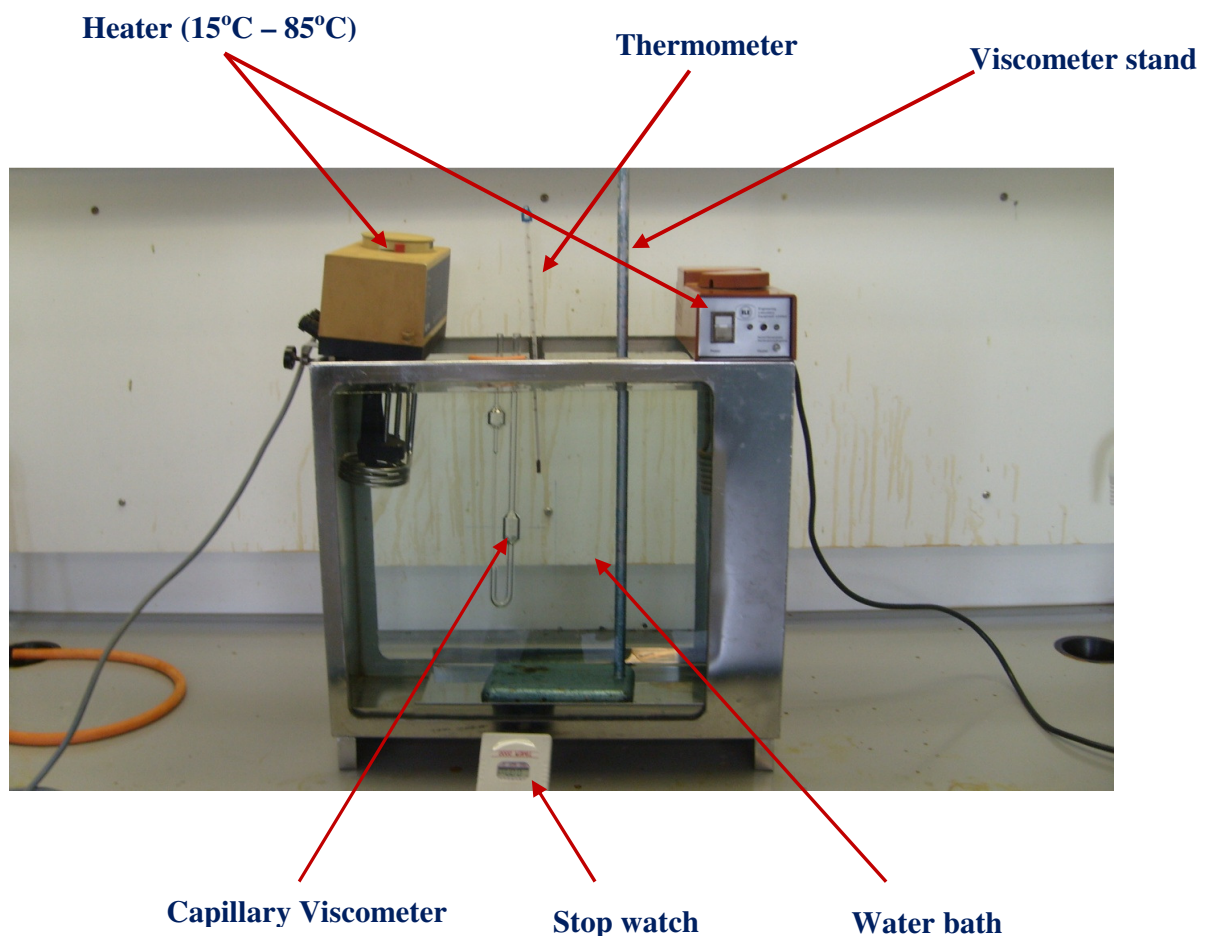


Figure 3-1 Capillary viscometer apparatus

3.1.4 Lower Heating Value: Apparatus and Procedures

The heating value of the diesel and biodiesel blends (0B, 10B, 20B, 50B, 75B and 100B) was determined in a Parr Adiabatic Oxygen Bomb Calorimeter, Model 230/5. The Auxiliary equipment included a bucket-filling system, a temperature-controlled reservoir and automatic pipette for dispensing repeatable 2000ml of distilled water at pre-set temperature into a

stainless-steel bucket, digital thermometer and ignition switch. The water heater maintained and delivered hot water at a controlled temperature to allow adjustment of the calorimeter jacket temperature. The water cooler provided a uniform supply of cooled water for adjusting the jacket temperature. The main components of the bomb calorimeter are shown in Figure 3-2. The heating value was measured using the official standard, DIN 51900 as explained in appendix A.

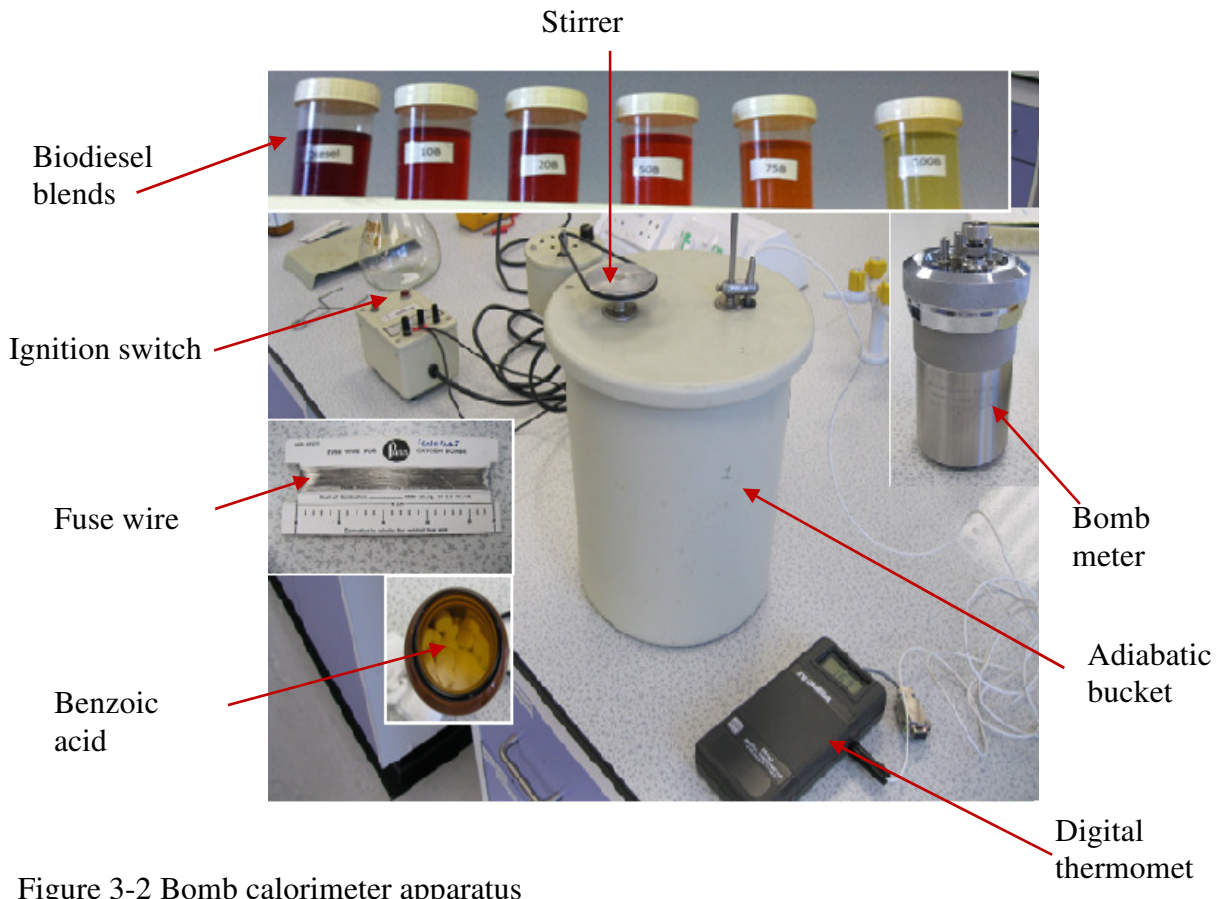


Figure 3-2 Bomb calorimeter apparatus

3.2 CI Engine and Test Bed Facilities

3.2.1 Engine Dynamometer Specifications

The CI engine test setup is available within the Automotive Laboratory, Huddersfield University, U.K. It has a transient test unit with a 200kW AC Dynamometer, 4 Quadrant Regenerative Drive with Motoring and Absorbing Capability. It is integrated with speed sensors, pressure transducers, thermocouples, air flow metres, fuel flow metres and an in-line torque meter. It has a four-cylinder, four-stroke, turbo-charged direct injection engine with a bore of 103 mm, a stroke of 132 mm, a displacement of 4.4 litre and a compression ratio of 18.3. Full engine characteristics of the engine are described in Table 3-1. The layout of the experimental set up and the experimental facilities are depicted in Figure 3-3 and

Figure 3-4 respectively. The engine was fully instrumented, and the steady state and transient cycle was programmed using the CADET software integrated within the engine system. The power and torque curves of the JCB engine have been presented in Appendix B.

Table 3-1 Characteristics of JCB engine

Technical parameters	Technical data
Engine type	Turbo charged diesel engine
Number of cylinders	4
Bore	103mm
Stroke	132mm
Inlet valve diameter	36.5mm
Exhaust valve diameter	33.2mm
Compression ratio	18.3:1
Number of valves	16
Injection system	Direct injection
Displacement	4.399 litre
Cooling system	Water
Nominal Idling speed	800 rpm
Maximum rating gross intermittent	74.2 @ 2200rpm
Maximum torque	425Nm @ 1300rpm

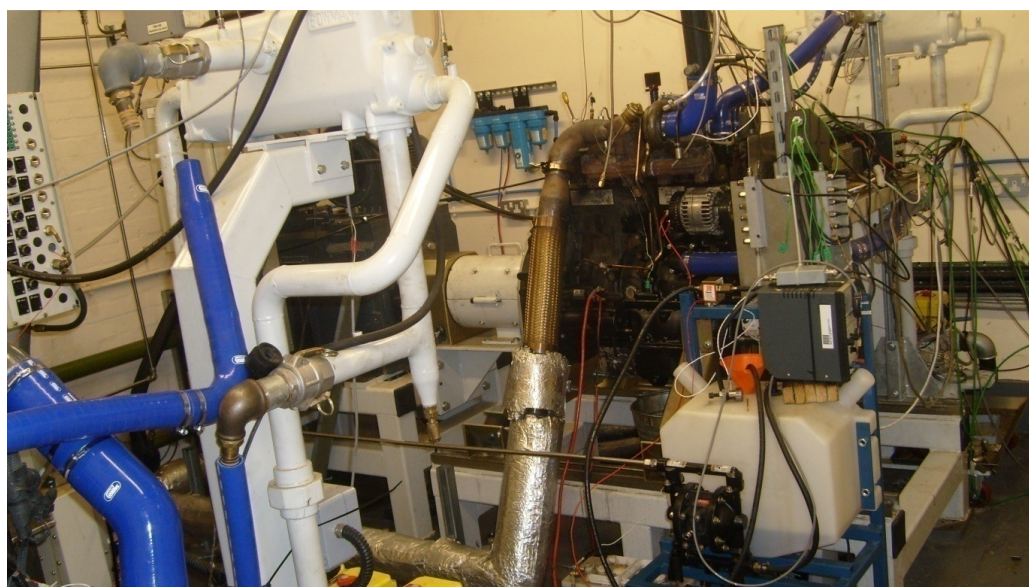


Figure 3-3 Experimental engine facilities

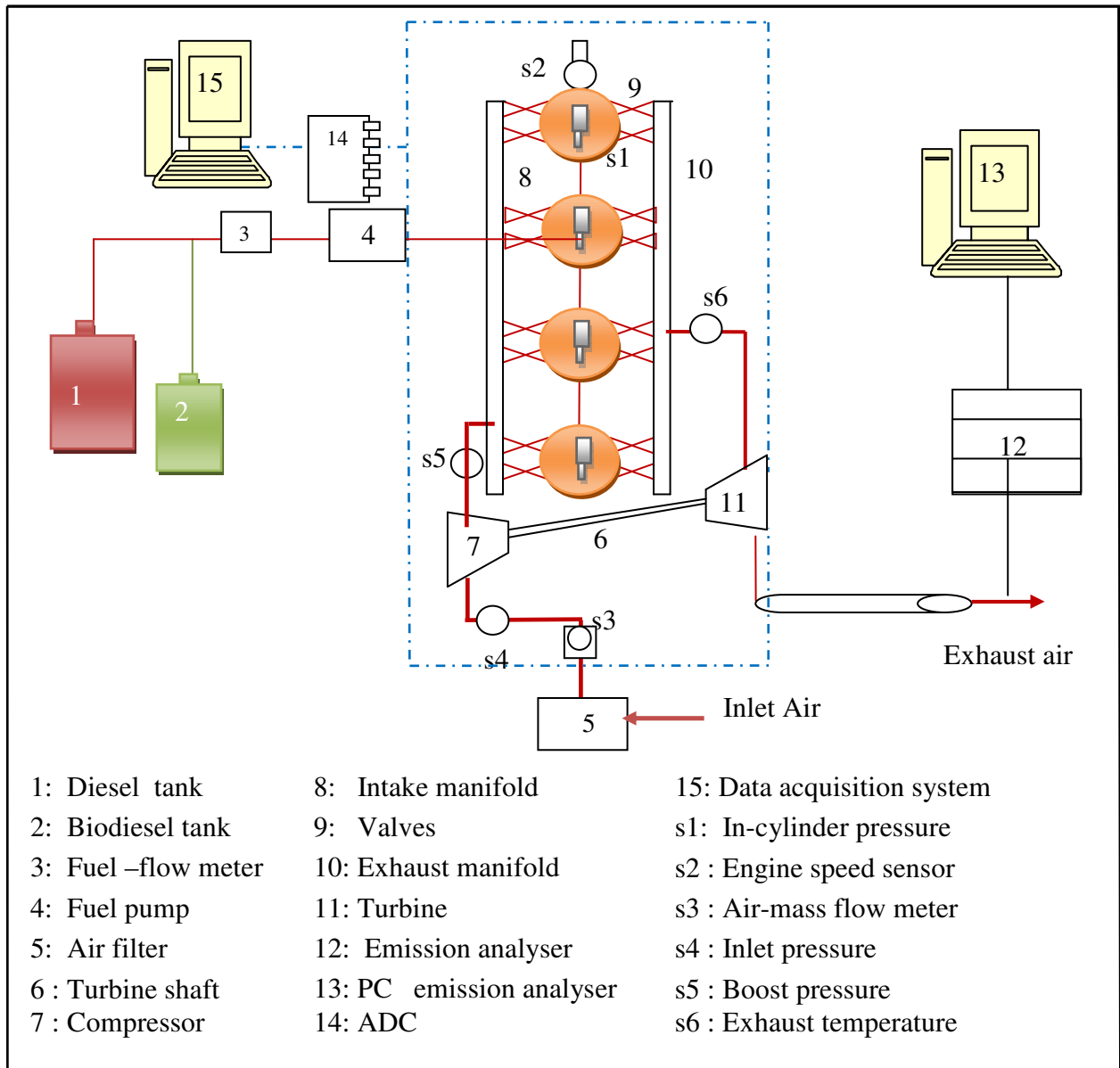


Figure 3-4 Engine test facilities lay out

3.2.2 Oil and Coolant System

A water cooling system was fitted to the JCB engine. In order to avoid cold starts and to help maintain the running temperatures of the engine, the facility had two Eltron Chromalox oil heaters mounted in the engine sump and one Watlow Industries 3kW domestic immersion water heater mounted within the coolant circuit. These had dedicated pumps and could be activated without the need to have the engine running. Both the coolant and oil circuits contained thermostatically controlled valves, which allowed the fluids to be circulated only in the engine until pre-set temperature of 90° C was attained. When the oil or coolant

temperatures surpassed this limit, the respective thermostats opened and the fluid was diverted through two separate heat exchangers, where heat generated by the engine was rejected to a constant water supply from cooling tower. This system replaced the standard vehicle radiator. The engine coolant was a 50:50 mixture of water and anti-freeze, ethylene glycol. The specification of the cooling system has been presented in Table 3-2.

Table 3-2 Cooling system specification

Parameters	Values
Coolant capacity –engine only	7ltrs
Water pump flow rated speed	200ltr/min
Heat to reject by heat exchanger at maximum power	52kW
Thermostat temperature	90°C
Cooling liquid maximum temperature	110°C
Maximum pressure in the cooling circuit	1bar
Coolant specification approved	ASTM D6210

3.2.3 Measurement System for Operating Parameters of the Test Engine

In order to acquire accurate and repeatable engine test data for diesel engine combustion, performance and emission characteristics, the engine system was instrumented with state-of-the-art measuring facilities as shown in Figure 3-4. The combustion pressure, temperature, engine speed, engine load, crank angle, air flow rate, fuel flow rate and TDC position were the main parameters measured. The signal from the outlined instruments required some form of signal conditioning prior to being connected to the data acquisition system. It was, therefore, necessary to use amplification in order to increase the resolution of low level signals and to distinguish them from background noise. In order to achieve the highest clarity, the signals needed to be amplified so that the maximum voltage range of the conditioned signals was equal to the maximum input range of the analogue-to-digital converter (ADC). This was used for transformation of the acquired data from analogue to digital form, enabling a computer to read, save and process the collected data.

3.2.3.1 In-cylinder Pressure

The in-cylinder pressure was measured using a Kistler 6125A11 model air-cooled piezo-quartz pressure sensor mounted on the cylinder head. The cylinder pressure signal was passed

through a Bruel & Kjaer 2635 charge amplifier to give outputs of 0-10volts for the calibrated pressure range of 0-25MPa. It was calibrated to read a maximum pressure of 25MPa. The configuration of the in-cylinder pressure measurement system is presented in Figure 3-5. Since the piezo-electric pressure measurement system does not supply absolute values, it is AC coupled and the signal must be referenced to the intake manifold pressure in order to eliminate the signal drift. The reference in-cylinder pressure can be obtained by averaging the signals at 100°CA around BDC at the end of the air intake stroke. At the end of air intake stroke, it was safe to assume that the in-cylinder pressure was same as the intake manifold pressure. As the manifold pressure was measured in absolute terms, it was used to calculate the offset for the in-cylinder pressure around BDC.

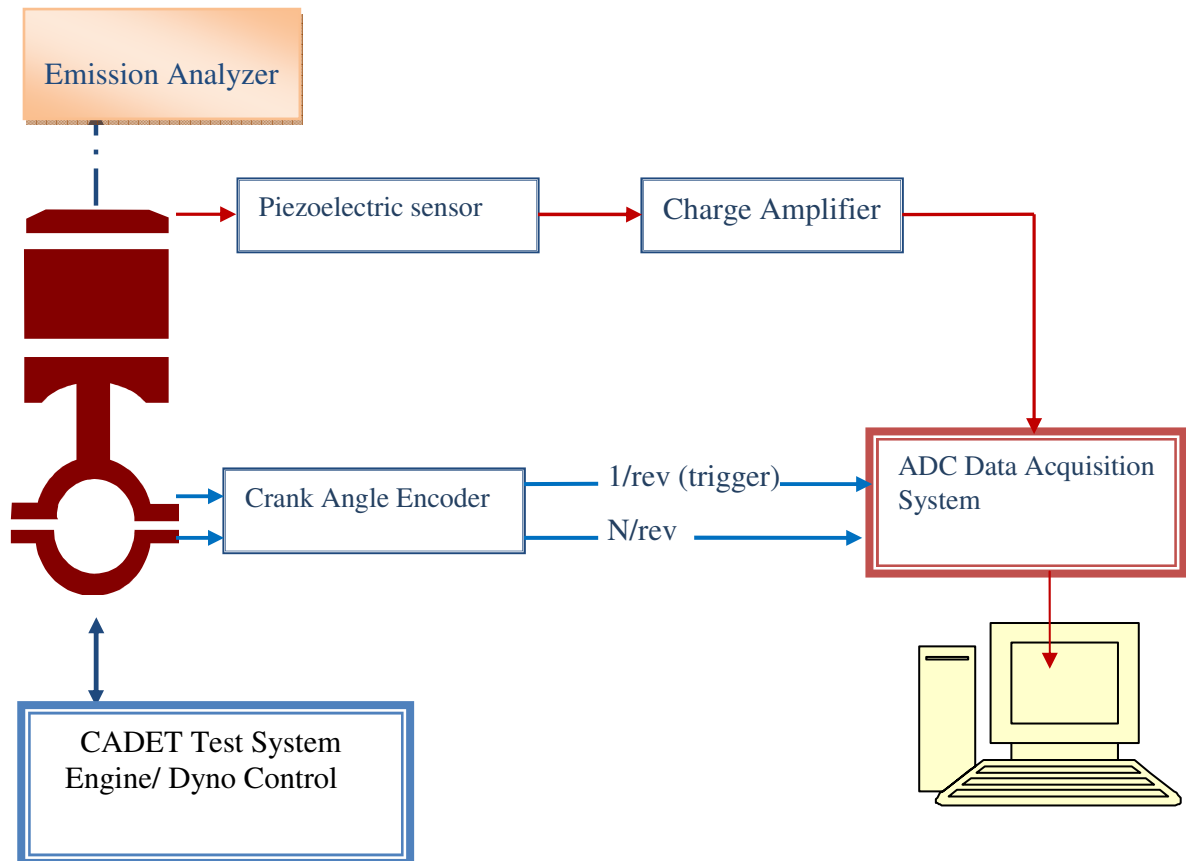


Figure 3-5 In-cylinder pressure measurement system

This offset was then applied, during post processing of the data, across the whole cycle to give the absolute normalised in-cylinder pressure values as shown in equation 3-1[169]:

$$P_{real} = P_{offset} + K_{sens}P_{measured} \quad (3-1)$$

Where P_{real} is the actual in-cylinder pressure, P_{offset} is offset in-cylinder pressure due to the ambient conditions, K_{sens} is the sensor sensitivity constant which is given by the sensor producer, and $P_{measured}$ is the pressure measured in the cylinder.

3.2.3.2 Fuel Flow

The specific fuel consumption was measured using a 2 litre FMS-1000 Gravimetric fuel meter which was controlled and monitored by a CADETV12. The FMS-1000 works on the gravimetric measuring principle and has a measuring accuracy of 0.05% for the readings. The fuel meter apparatus with its specification is shown in Figure 3-6.

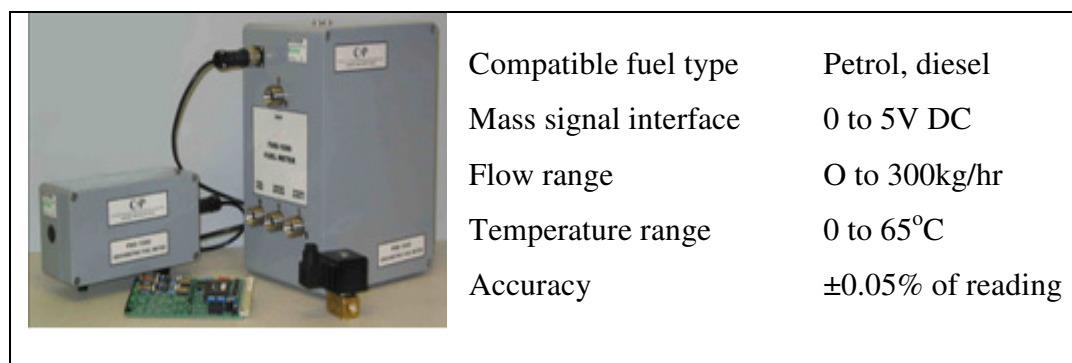


Figure 3-6 FMS-1000 Gravimetric fuel meter apparatus and its specifications

The entire section of the fuel meter was made of stainless steel which is compatible with biofuels. The fuel temperature variation due to the return fuel was conditioned by Fuel Conditioning Unit (FCU). It also cancelled out any vibration mechanically, as the construction is stiff and it has no moving parts. The fuel weigher used a 20N load-cell to measure the consumed fuel. The FMS-1000 was capable of monitoring fuel during a period of a transient cycle, for a specific time as short as 100ms. It has a measuring range of 0 - 300kg/hr.

3.2.3.3 Air Flow

The air-consumption was measured using the standard BOSCH-HFM5 hot-film air-mass meter, part number 0280217123. The basic principle of this method is that the heated sensor element in the air-mass meter dissipates heat to the incoming air. The higher the air flow, the more heat is dissipated. The resulting temperature differential is a measure of the air mass flowing past the sensor. An electronic hybrid circuit was used to condition the signals that the

air-flow quantity could be measured precisely. The air mass flow meter with its specification has been shown in Figure 3-7.

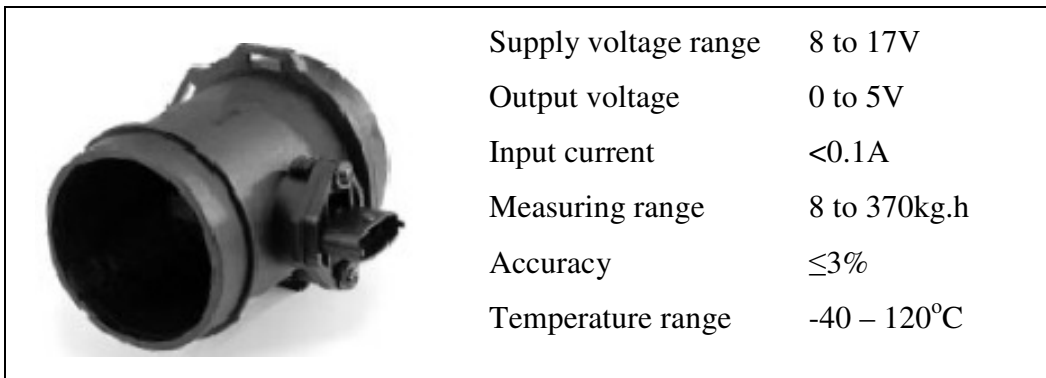


Figure 3-7 Hot-film air mass flow meter with its specification

3.2.3.4 Engine Speed, TDC Mark and Crank Angle Position

A Hengler RS58 speed sensor was used to measure the engine speed and was triggered simultaneously with the cylinder pressure sensor. The crankshaft position was obtained using a crank angle sensor to determine the cylinder pressure as a function of the crank angle. A reference point was required to compare the collected data and to perform time domain and angular domain averages of the signals. This was achieved by using an HED-6000 optical encoder, which was connected to the crankshaft (at the engine's front) using a rubber tube. Consisting of a rotating disk, a light source, and a photo detector, the encoder enabled data collection to start at exactly the same crank angle position and also gave a pulse for every complete turn of the crankshaft, allowing the time domain averaging to be performed.

3.2.3.5 Engine Torque

The engine torque measurement was carried out from the load cell mounted on the dynamometer and amplified by a Nobel Elektronik AST 3P analogue signal transmitter. The amplifier incorporated an analogue output filter with variable bandwidths, which was adjusted in order to reduce the unwanted, naturally oscillating torque profile produced by the engine. The torque measurement system with its specification has been shown in Figure 3-8.

3.2.3.6 Pressure Measurement

Air intake pressure measurements were made using DRUCK PMP-4010 series sensors pressure transducer, with a range of 0-5bar, which were mounted in the air intake manifold.

An amplifier was built in-house for these transducers and the arrangement was calibrated within the data acquisition system to give the required output pressure ranges.


Nominal Torque	1000Nm	
Nominal sensitivity (Frequency output)	5kHz	
Sensitivity	-49984 to 4998.4Hz	
Linear deviation	0.006 to 0.002%	
Nominal output signal (positive torque)	15kHz	
Nominal output signal (negative torque)	5kHz	

Figure 3-8 Torque measurement system with its specification

A pressure transducer (RS sensors with part number 249-3943) has been used to measure low fuel pressure, with a range of 0-6 bar, mounted before the high pressure pump in order to ensure that the low pressure fuel supply was maintained by the high pressure pump. A second pressure transducer, with a range of 0-6bar, was mounted in the oil circuit and was used to monitor oil pressure. An amplifier was built in-house for these transducers and the arrangement was integrated within the CADET system to give the required output pressure ranges. The pressure measurement transducers have been shown in Figure 3-9.

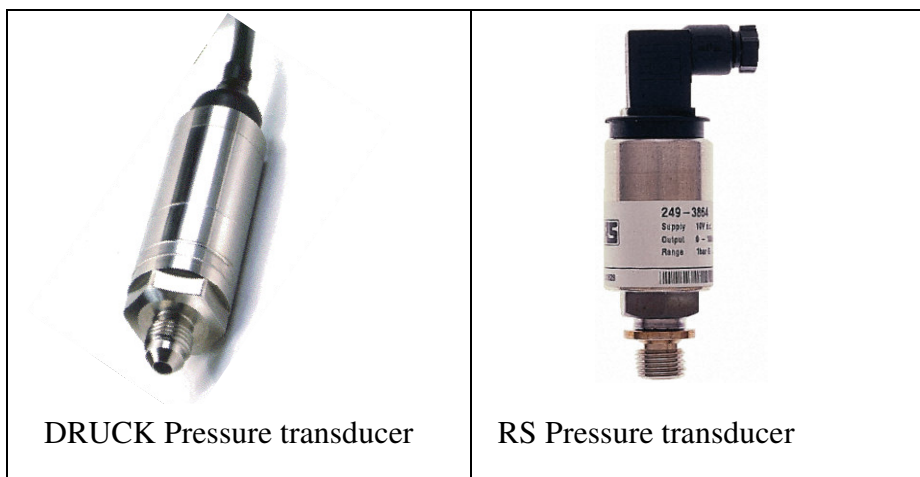


Figure 3-9 DRUCK PMP-4010 series sensors and RS-249-3943 pressure transducer

3.2.3.7 Temperature Measurement

The exhaust temperature has been measured by K-type thermocouple with stainless steel wire. The exhaust, air intake, water, oil and the fuel circuit temperatures were measured using PRT K type Chomel-Alumel thermocouple probes. The micro-voltage outputs from these thermocouples were processed by the CADET software to give values in degrees centigrade for data logging and engine monitoring purposes. Three thermocouples were included in the fuel system. This was required between: the intercooler and the input to the high pressure pump, between the return from the high pressure pump and the plate cooler, and after the plate cooler, to ensure that the fuel returning to the fuel meter had sufficiently reduced in temperature.

3.2.3.8 Emission Measurement

For the measurement of gaseous emissions, a gas test bench HORIBA EXSA – 1500, which is shown in Figure 3-8 has been used. The sample line of the equipment has been connected directly to the exhaust pipe and it has been heated to maintain a wall temperature of around 191°C to avoid the condensation of hydrocarbons into the line. The insulated line has been extended from the exhaust pipe to the equipment's unit where the analysers have been located. All emission analysers (NO_x, CO, CO₂ and THC) have been set on one bench. However, each emission analysers uses different principles in order to measure emissions. The hydrocarbon emission has been measured by using a flame ionisation detector (HFID), Oxides of nitrogen were measured on dry basis, by means of a heated chemiluminescent detector (HCLD) with a NO₂/NO converter. The carbon monoxide and carbon dioxide have been measured with an analyser of the non-dispersive infrared (NDIR) absorption type, whilst a paramagnetic detector was employed for the measurement of O₂ concentration in the exhaust flow. The exhaust gas sample line is connected directly to the exhaust pipe and it is heated to maintain a wall temperature of around 191°C and avoid the condensation of hydro carbons into the five meter long line. The sample flow rate is approximately 3litre/min. In order to minimise the misalignment of the measured emission gas concentration, due to the difference between the sampling transport time and the analyser's response time, 20 seconds duration was used as per manufacturer specification. The data from the analyser bench have been acquired using high speed data acquisition system ADC. The emission analyser type and measuring range is provided in Table 3-3

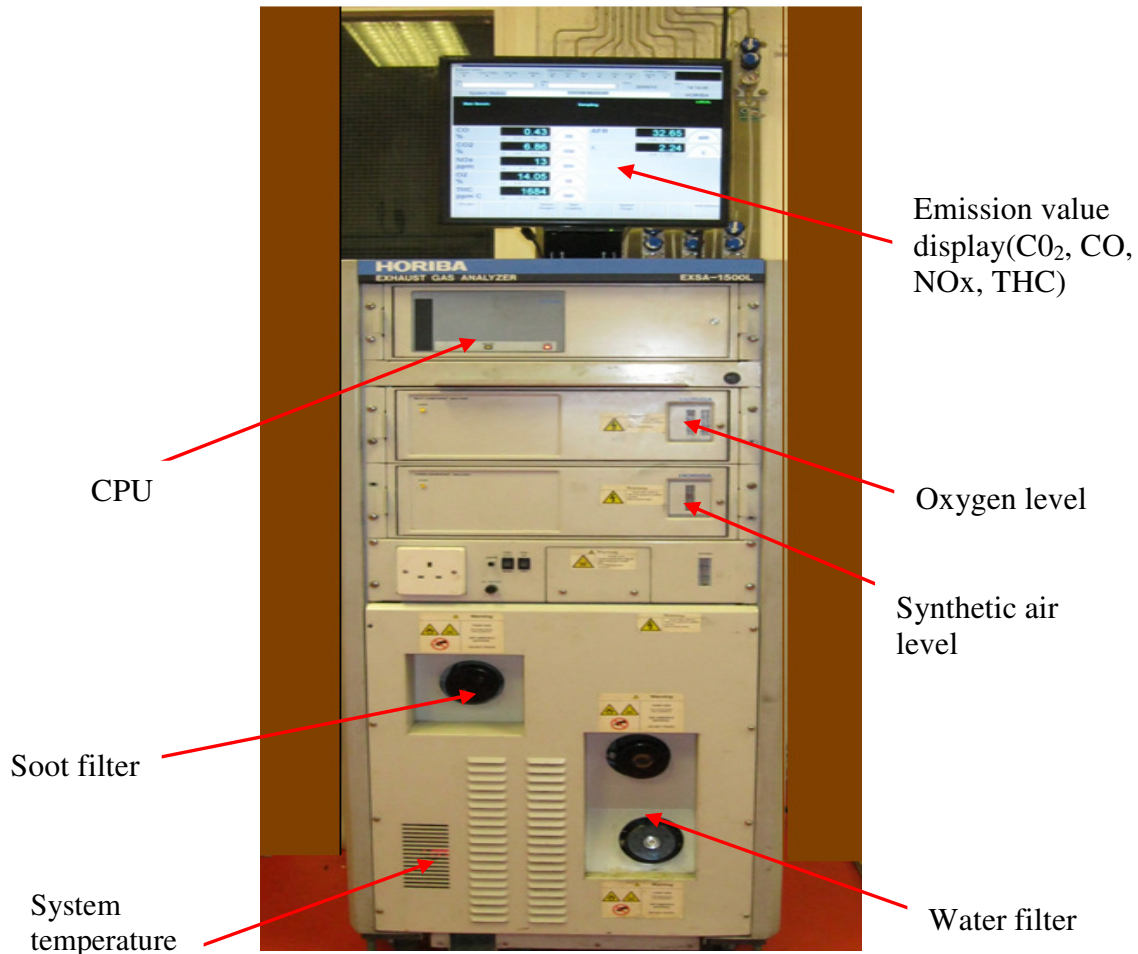


Figure 3-10 HORIBA EXSA-1500- Emission analyser

Table 3-3 The emission analyser type and measuring range

Emission type	Emission analyser type	Measuring range	Accuracy
CO	non-dispersive infrared (NDIR)	0 – 2000ppm	±2%
CO ₂	non-dispersive infrared (NDIR)	0 –100% ^a	±2%
NO _x	heated chemiluminescent detector (HCLD)	0 – 5000ppm	±2%
THC	heated flame ionisation detector (HFID)	0 – 100ppm	±1%
O ₂	paramagnetic detector	0 – 25% ^a	±1%

(a) the % is from the total exhaust gas

3.2.3.9 Data Acquisition System

All the signals collected from the test rig needed to be converted from an original analogue form to a digital form. This has been achieved by using CED Power 1401 Analogue to Digital Converter (ADC) interface between the transducers and the computer. The Analogue to Digital Converter (ADC) had 16 channels and 500MHz bandwidth. The ADC and measured parameters are shown below in Figure 3-11.

3.2.3.10 CADET V12 Software

CADET V12 software is a fully integrated Windows 2000-XP based engine and vehicle test system designed and built to meet the exact needs of automotive and associated industries. CADET V12 supports direct digital control of up to 16 high speed PID control loops, and in addition, supports User-Definable Control Functions suitable for more complex non-linear control requirements. The digital proportional integral derivative (PID) controller system is supplied with a low level hardware and software device driver developed by CP Engineering, to provide the required real-time environment underneath Windows 2000-XP. The PID system currently supported 16 PIDs at up to 320 Hz control frequency. Through the CADET V12, the engine power, fuel flow rate, the coolant temperatures, exhaust temperature were measured in this study.

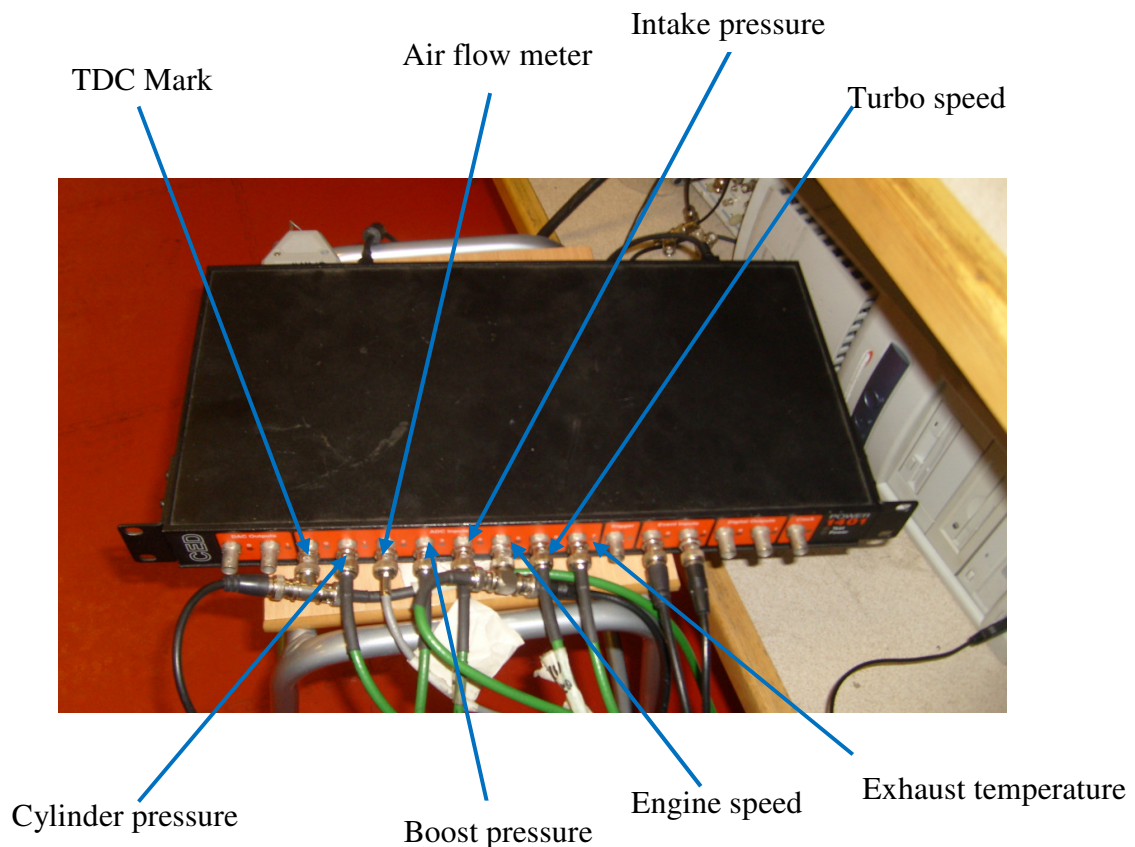


Figure 3-11 Analogue to Digital Converter (ADC) and measured parameters

3.2.3.11 Calibration of Instruments

The measuring sensors and instruments which have been shown in Figure 3-11 were calibrated through the data acquisition system before the test was conducted. To achieve this, readings were taken by the data acquisition as the input signals were swept through their operating ranges, in order to calculate the gain and offset values for each individual signal. The Kistler in-cylinder pressure transducer was calibrated by applying a known pressure to the sensor and measuring the voltage from the charge amplifier. The dead weight system used had an accuracy of 0.1%. These figures were then used to calculate the gain and offset values for the transducer. As the Kistler pressure transducer only generated a signal with a change in pressure, the cylinder pressure was referenced to the atmospheric pressure during the exhaust stroke, with the resulting offset being applied automatically in the data acquisition software. All other pressure transducers were calibrated using a Druck model portable pressure measurement instrument, capable of applying variable pressure to each sensor, to within an accuracy of 0.1%. The pressure measurements were taken through the data acquisition system and the appropriate gain and offset values for each transducer calculated. All emissions measurement equipment were calibrated daily prior to any experimental work according to the emission measurement procedures.

3.3 Test Procedures

In this section the testing procedures which have been applied in this study by using the apparatus and instruments in section 3.1 and 3.2 have been discussed in detail. The major testing procedures have been grouped into three categories, namely biodiesel blends preparation, steady state and transient test cycle's development and water injection system and procedures. In the next section procedure for biodiesel blend preparation has been discussed.

3.3.1 Biodiesel Blend Preparation

In this study, three neat biodiesels (rapeseed biodiesel, corn oil biodiesel and waste oil biodiesel) and petroleum diesel have been used in different proportions. The biodiesel percentage volumetric fraction of 0%, 10%, 20%, 50%, 75% and 100%, formed the blends

0B, 10B, 20B, 50B, 75B and 100B respectively. The biodiesel was purchased from No-Fossil Fuel Corporation, Huddersfield, U.K. The corn oil biodiesel and rapeseed oil biodiesel were produced by the transesterification process from ‘virgin’ oil using methanol, and waste oil biodiesel was produced from local cooking oil waste. Normal diesel fuel was obtained from a local fuel supplier. Currently, there are three major techniques used to produce biodiesel blend, which are splash blending, in-line blending and in-tank blending [175]. These techniques are used to blend biodiesel with petrol diesel to a required volumetric fraction. Splash blending is an operation where biodiesel and diesel fuels are loaded into a vessel separately, with relatively little mixing occurring as the fuels are placed in the vessel. Once in the vessel, during driving, the two fuels gain sufficient agitation to allow the biodiesel and diesel fuel to mix thoroughly. The second method is in-line blending. In this method, biodiesel is added to a stream of diesel fuel as it travels through a pipe or hose, in such a way that the biodiesel and diesel fuel become thoroughly mixed by the turbulent movement through the pipe. The biodiesel needs to be added slowly and continuously into a moving stream of diesel fuel via a smaller line inserted in a large pipe. Biodiesel can also be added in small slug or pulsed quantities spread evenly throughout the time the petro-diesel is being loaded.

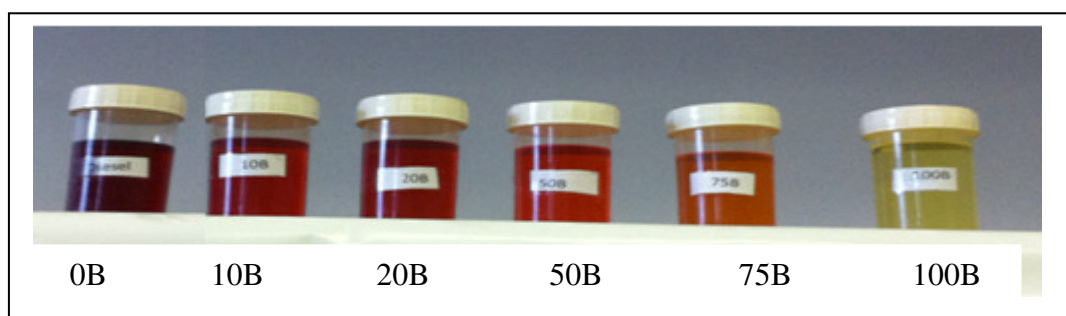


Figure 3-12 Biodiesel blends prepared in the laboratory for performance and emission investigations

In-take blending is the third method in which biodiesel and diesel fuel are loaded separately, or, in some cases, at the same time through different incoming sources. The high fill rate results in sufficient mixing without the need for additional recirculation or agitation. Comparing these three methods, splash blending is an effective and efficient technique which is widely used for commercial purposes.

The biodiesel blends, for the purpose of the experiments, needed high measurement accuracy, large number of testing batches and lower quantities of biodiesel. Hence, in this study, the in-

tank blending method was used with some modifications. The following procedures were followed to prepare the biodiesel blend:

- I. The biodiesel and diesel were prepared in different PVC tanks.
- II. Based on the blend fraction, the volume of the biodiesel and diesel were calculated. For example, to prepare 25 litres of biodiesel blends, 20B, 20% biodiesel (5 litres) and 80% diesel (20 litres) was used.
- III. The diesel was measured by volume basis as per procedure II and the diesel was poured into empty tanks. The biodiesels were poured on the diesel surface evenly. This technique enhanced the mixing of diesel and biodiesel and avoided settling of biodiesel at the bottom of the tank due to its higher density [175].
- IV. The preparation tank cap was closed firmly and the tank was agitated for 3 minutes. The prepared biodiesel blend was added to the fuel tank, which was connected to the fuel supply system.

The physical properties of the blend biodiesel which have been discussed in detail in Chapter four have been summarized in Table 3-4.

Table 3-4 Physical and Chemical properties of Biodiesel and its blends

Property		Diesel	10B	20B	50B	75B	100B
Composition (%)	C	87	86	85	82	79.5	77
	H	13	12.9	12.8	12.5	12.25	12
	O	0	1.1	2.2	5.5	8.25	11
Density(kg/m ³)		853.36	859.00	865.00	871.76	872.50	879.30
LHV (MJ/Kg)		42.67	42.26	41.84	40.58	39.54	38.500
Viscosity (mm ² /s)		3.55	3.91	4.28	4.68	4.74	5.13

3.3.2 Engine Test Cycles

Both steady and transient processes were designed to evaluate the performance and emission characteristics of the engine which was run using biodiesel and its blends as a fuel. The engine speed and load were the two parameters to be controlled in the test programme. The transient processes were programmed using the CADET program. More emphasis was given to represent the zones in the engine torque-speed map where the engine emissions restrictions were most important.

The engine performance and emissions (CO₂, NO_x, CO and HC) parameters for various biodiesel feedstock and blends have been measured according to the modified 13-mode European stationery Cycle (ESC) [38]. ESC has 13 modes of test points in engine speed and load curves which have been set for engine speed range of 62 – 95% engine and load range of 25 to 100%. The ESC mode does not consider the low speed range effects on the engine emissions. However, in real driving behaviour the lower engine speed ranges is very important especially in urban driving where stop-go traffic phenomena is dominant. Therefore, to analyse the emission characteristics of the lower engine speed range nine more testing points have been included in this study. As it is shown in Appendix B, the maximum rated speed and maximum torque of the test engine is 2200rpm and 425Nm. The modified steady state cycle is shown in Figure 3-13. The speed percentage and load percentage which have been shown in Figure 3-13 are based on the rated engine speed and maximum load. The CI engine power and torque curves have been shown in Appendix B. Each steady state was conducted for 2 minutes and the NO_x emission and the fuel consumption have been used as stability control parameters for data acquisition. After reviewing the transient categories of previous researchers [33], [35], [37], [43], [50], [136],[170], [171], [139], [35], [172-174], [37], [175-177], [49] which are presented in Table 3-5 and a pilot test in the laboratory, the transient test cycles have been developed in order to study the effects of transient operations on the performance and emission characteristics of the engine.

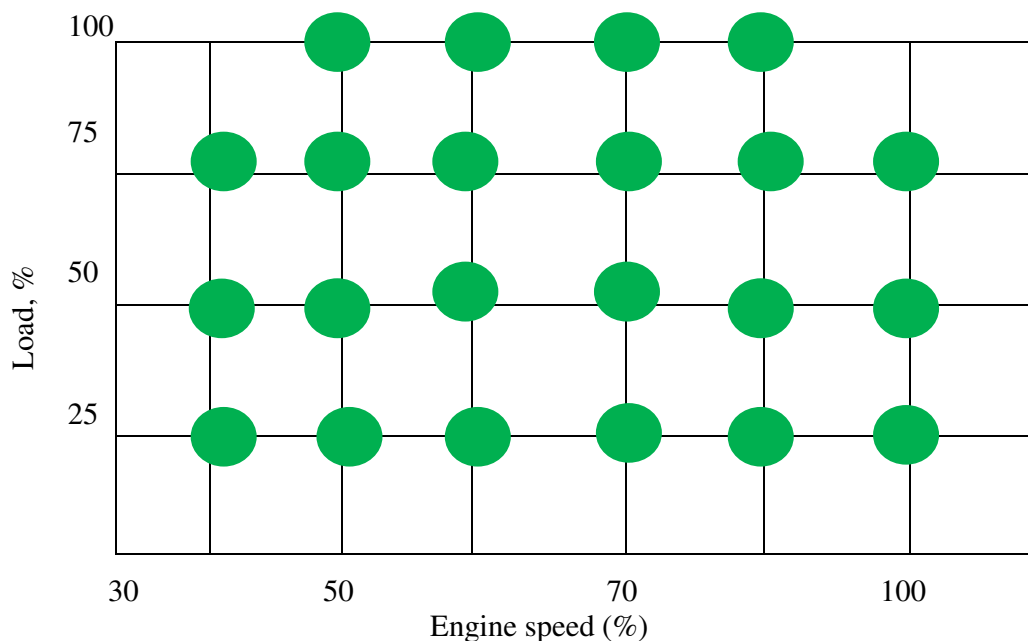


Figure 3-13 Range of engine speeds and engine loads for steady state testing cycle

Based on previous researchers and the pilot transient test, the transient operations in this study were developed by varying engine speed at constant load and varying load at a constant speed. Four different categories of transient operations were developed and CI engine's performance and emission characteristics were analysed experimentally. The details of the transient categories have been explained in section 3.3.4.

Table 3-5 Transient profiles values of previous research studies

Authors	Time(Sec)	Engine speed(rpm)	Torque (Nm)
Lui <i>et al.</i> [170]	2.5 Sec	1100 – 2200	250 – 63.7
	1.6 Sec	2000 – 867	250 - 69
Benajes <i>et al.</i> [171]		1250, 1750, 2250	
		1200 – 2500	50, 100, 150
Chan <i>et al.</i> [139]		1500	5 – 150
		2000	5 – 150
		2500	5 – 150
		0- 830	0
Armas <i>et al.</i> [35]		1661	26 -90
		2398	26 - 90
		2398 – 1661	90

3.3.3 Testing Procedures and the Details of the Measured Parameters

The experimental investigations have been carried out using the test rig explained in chapter three. The experiments have been carried out for a wide range of biodiesel feed sources, blends types and the test modes (steady and transient). The types of tests carried out in this investigation are listed below:

1. Steady state test at different load values of 105Nm, 210Nm, 315Nm and 420Nm for engine speeds in the range of 900 to 1900rpm at 100rpm increment using COB, ROB, WOB and diesel fuels as per the testing cycle that has been shown in Figure 3-13.
2. Steady state test at different load values of 105Nm, 210Nm, 315Nm and 420Nm for speeds in the range of 900 to 1900rpm at 100rpm increments using blends of diesel and ROB with blend fraction values of 0%(0B), 10%(10B), 20%(20B), 50%(50B) and 100%(B100) as per the testing cycles described in Figure 3-13.
3. Speed transients of 1000-1500rpm and 1500-1000rpm for different engine load values of 105Nm, 210Nm, 315Nm and 420Nm.

4. Torque transitions of 210-420Nm and 420-210Nm for different engine speeds of 100rpm, 1250rpm and 1500rpm. The details of the transient operation procedures have been described in the transient data analysis sections (section 3.3.4)

Using these tests cycles for different biodiesels blends, the CI engine's combustion, performance and emission parameters have been measured using the apparatus described in Chapter 3. The parameters are listed in Table 3-6. These parameters have been selected due to their importance of engine design and performance and emission evaluation.

Table 3-6 Measured and calculated parameters during the engine test

Measured parameters	Calculated parameters
In-cylinder pressure	Heat release rate
Crank angel	Cumulative heat release rate
Engine speed	Thermal efficiency
TDC mark	Power
Inlet pressure	
Boost pressure	
Fuel mass flow rate	
Brake specific fuel consumption	
Exhaust temperature	
Exhaust emissions(CO ₂ , CO, NO _x , THC)	

During the testing process, after each test run the fuel lines were drained prior to filling them with the next fuel blend. The engine was operated using newly filled fuel for 10 minutes without collecting data. This was done to ensure that all previous fuel in flow meter, fuel filter and fuel pipes had been removed. On the day prior to the testing day, and in between each biodiesel blend test, a pre-conditioning procedure of high speed and high load operation was applied in order to purge any of the remaining previously tested fuel from the engine fuel system, and also to remove deposited hydrocarbons from the sample line. A computer-based data acquisition system was used to record the parameters of interest.

The rated frequency of the data acquisition system was 37 kHz and the sampling time used was 60 seconds. This time duration was selected to ensure that the data is representative. All the signals collected from the test rig needed to be converted from an original analogue form to a digital form. This was achieved by using Analogue to Digital

Converter (ADC) interface between the transducers and the computer. The CED 1401 power ADC is able to record waveforms data, digital (event) data and marker information. It can also generate waveform and digital outputs simultaneously for real-time, multi-tasking experimental system using its own processor, clocks and memory under the control of the host computer. The Analogue to Digital Converter (ADC) has 8 channels, 500 MHz bandwidth and 4Gs/s sampling rate.

3.3.4 Transient Testing Cycles

For the purpose of this, synthetic speed and torque test cycles were developed in order to study the effect of transients on CI engine performance and emission characteristics. The transients were studied during both acceleration and deceleration events independently for both speed and torque transient, as shown in Figure 3-14 and Figure 3-15.

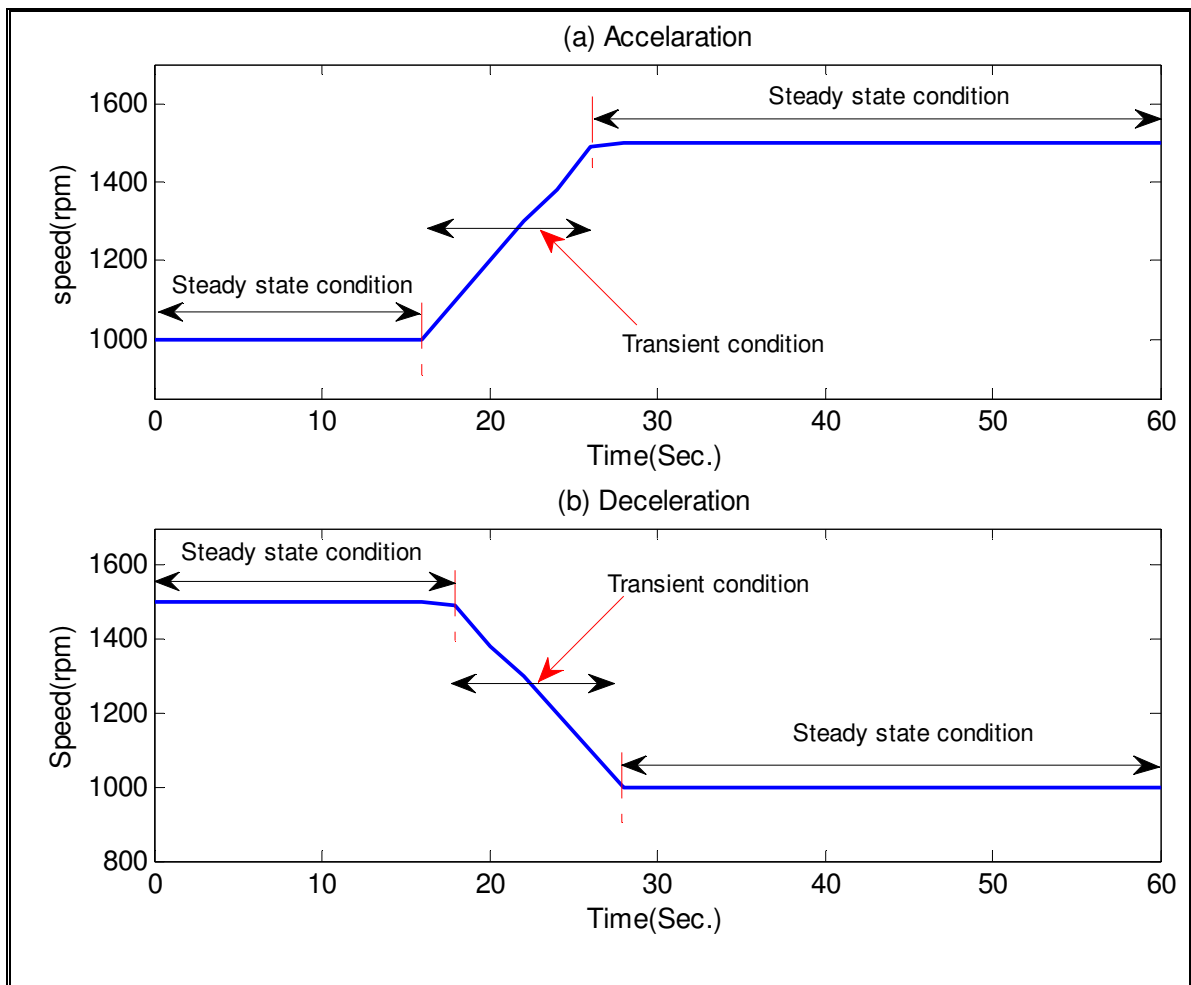


Figure 3-14 Speed transient profiles a) Acceleration 1000-1500rpm b) Deceleration (1500-1000rpm)

Figure 3-14(a) shows the engine speed acceleration profile for a load value of 420 Nm. Before data collection, the engine was allowed to run for 10 minute to stabilize the operating conditions. During the transient engine test, the acceleration duration normally reported is in the range of 1.0 to 10 seconds [178].

The steady and transient duration used in this test is 17 seconds and 8 seconds respectively, which are within the range specified. Finally, it was run at 1500 rpm for 35 seconds at steady conditions. The deceleration of the CI engine operation is shown in Figure 3-14(b). The engine was run steadily for 17 seconds, then decelerated for 8 seconds and then run for 35 seconds at steady conditions. The post-transient steady operation of the engine used was longer than the pre-transient steady operation. This was done in order to study the effects of transient operations on the next steady operation.

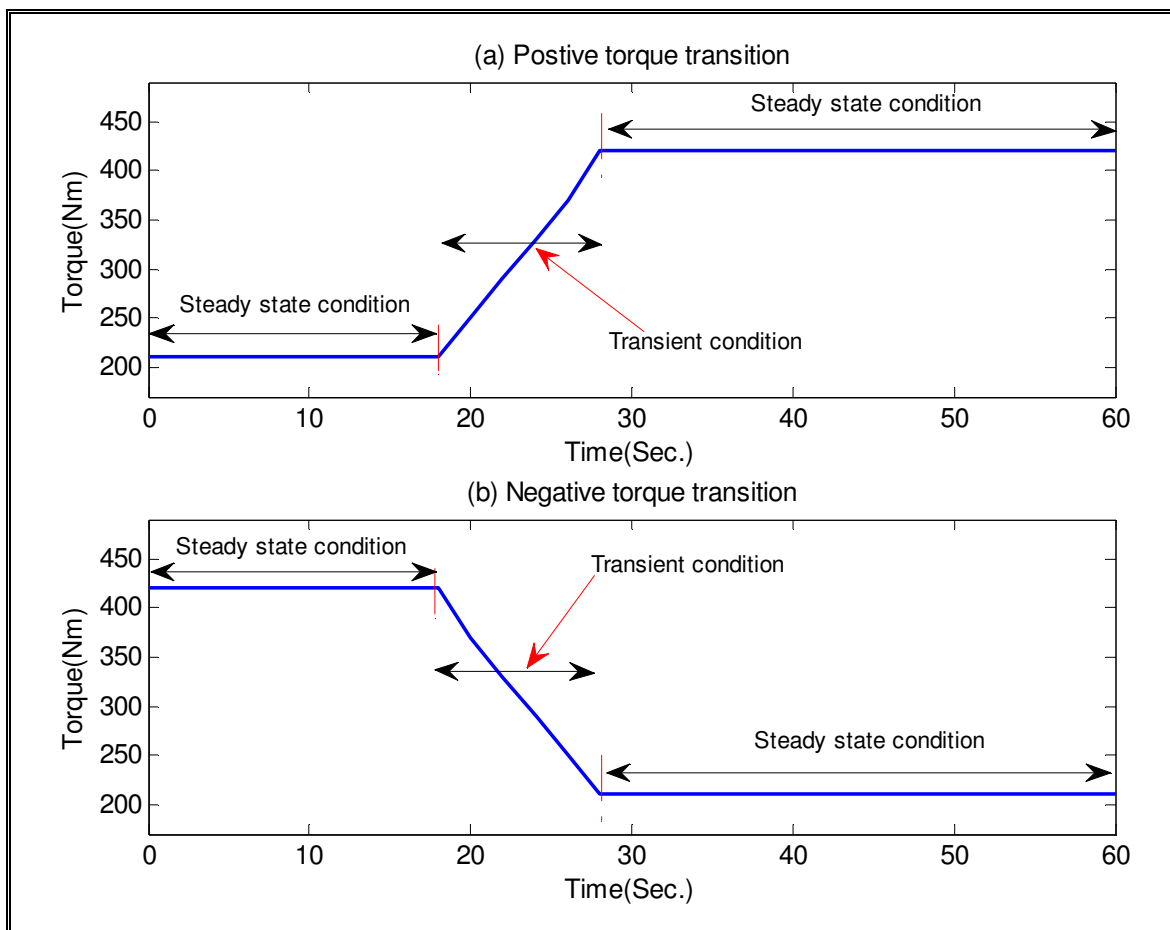


Figure 3-15 Torque transition profiles a) Positive torque transition 210-420N b) Negative torque transition 420-210Nm

The positive and negative torque transition profiles at 1500rpm engine speed are shown in Figure 3-15. In this condition, the engine was run for 17 seconds under steady state conditions, then it was run for 8 seconds in transition mode during which torque changed from 210Nm to 420Nm and finally engine was run at 420 Nm for 35 seconds, as presented in Figure 3-15(a). Similarly, the engine negative torque transition is shown in Figure 3-15(b). In the negative case apart from the torque value, the time segment values are similar to the positive torque transition condition.

The rate change of the parameters during trainient operation has been calculated by equation (3-2). This equation is drived from the definition of transient phenomena, which state as transient is change of specified parameter in the given span of time.

$$\dot{y} = \frac{y_i - y_{i-1}}{t_i - t_{i-1}} \quad (3-2)$$

Where \dot{y} the rate change of species y , y_i is the measured value of parameter at time t_i , y_{i-1} is the measured value of parameter at time t_{i-1} , t_i is latest time step, and t_{i-1} is the previous time-step.

3.3.5 Water Injection System

The water injection tests were carried out with the engine facilities and measuring instruments which are described in Chapter 3. This system was integrated with an additional water injection system to manage the performance and emission characteristics of the test CI engine. There are three methods of water-based injection system that have been used in the past: such as direct water injection to the combustion cylinder, emulsification of water and fuel in the presence of surfactant and injection of water at intake manifold. As it has been discussed in section 2.4, the direct injection to the combustion cylinder needs complex integration with the fuel supply system and it seems difficult to integrate this system with other existing engine systems. The water-fuel emulsion needs a more advanced and well developed infrastructure to be integrated with the engine which increases the engine cost [115]. In addition, the water-fuel emulsion process changes the physical properties (viscosity, density and bulk modules) of the fuel [166]. These changes negatively affect the performance of the fuel injection system. This may be a greater problem for biodiesel fuel which has higher density and viscosity than the diesel fuel. In this study a feasible and manageable technique: intake manifold water injection has been selected.

The main advantage of water injection into the intake manifold is its simplicity and ease with which it can be integrated within existing engines and any new designs. In this system, since water is injected through a separate valve and does not mix with fuel directly, it does not affect the fuel flow properties in the fuel supply line.

The water injection system has been designed in order to inject the required amounts of water in the intake manifold. The system has been installed downstream of air compressor at the middle of the intake manifold. A 1mm diameter nozzle was connected to the intake manifold. The water injection was carried out by using AKL603 Seko diaphragm dosing electric pump. The pump has flow rate in the range of 1-20l/h. The water was injected downstream of the compressor into the intake manifold.

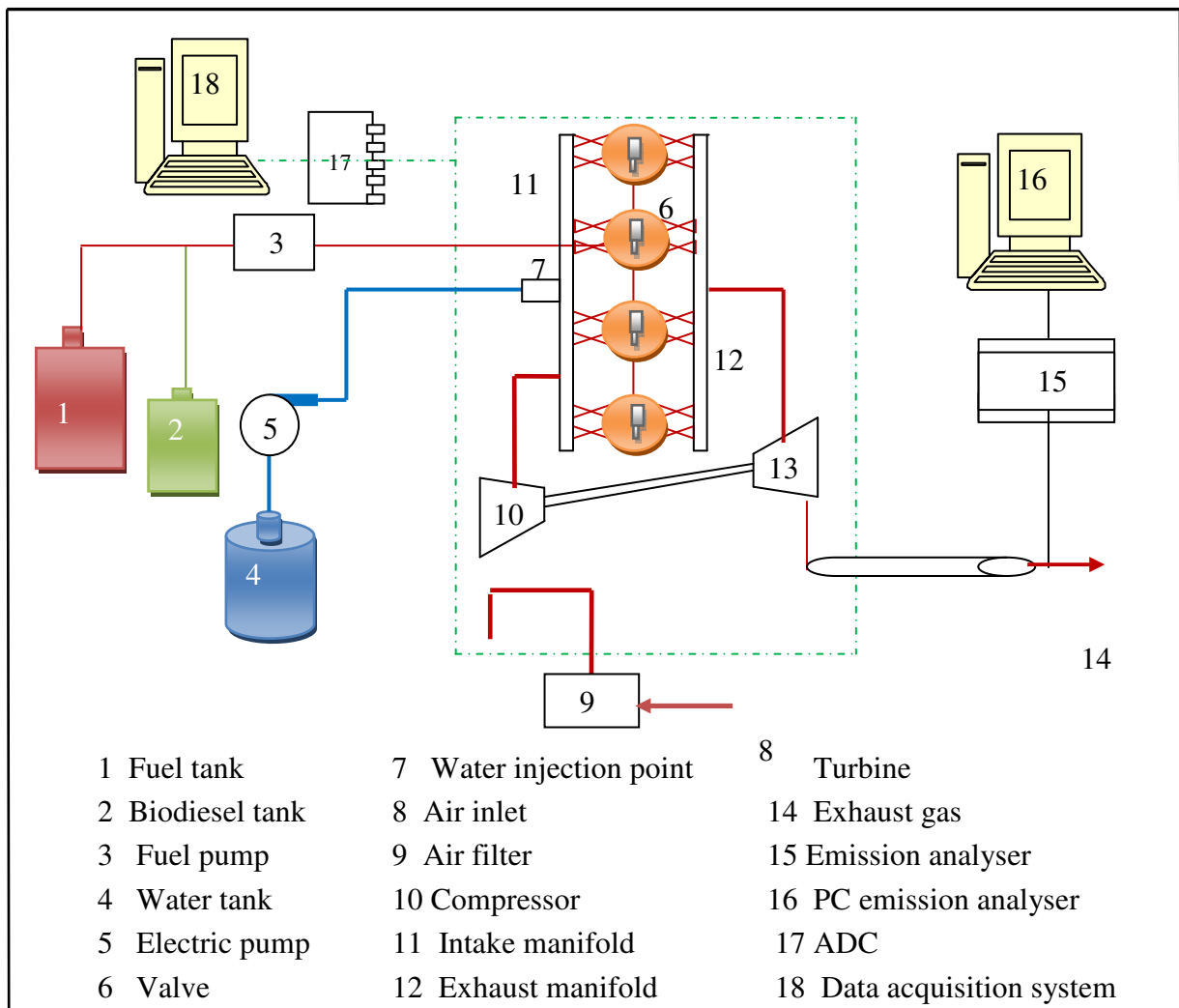


Figure 3-16 Scheme of water injection system at intake manifold

The water flow rate was measured using two methods: the electric pump and a calibrated burette with stop watch. The scheme and photograph of water injection system is shown in Figure 3-16 and Figure 3-17.

3.3.6 Water Injection Test Procedures

The water injections have been carried out with the same engine steady state operational procedures described in section 3.3.2 and 3.3.3. The main controlled parameters were the engine speed, engine load and mass flow rate of water. The operating conditions were selected with an aim to cover main engine operating speeds and loads.

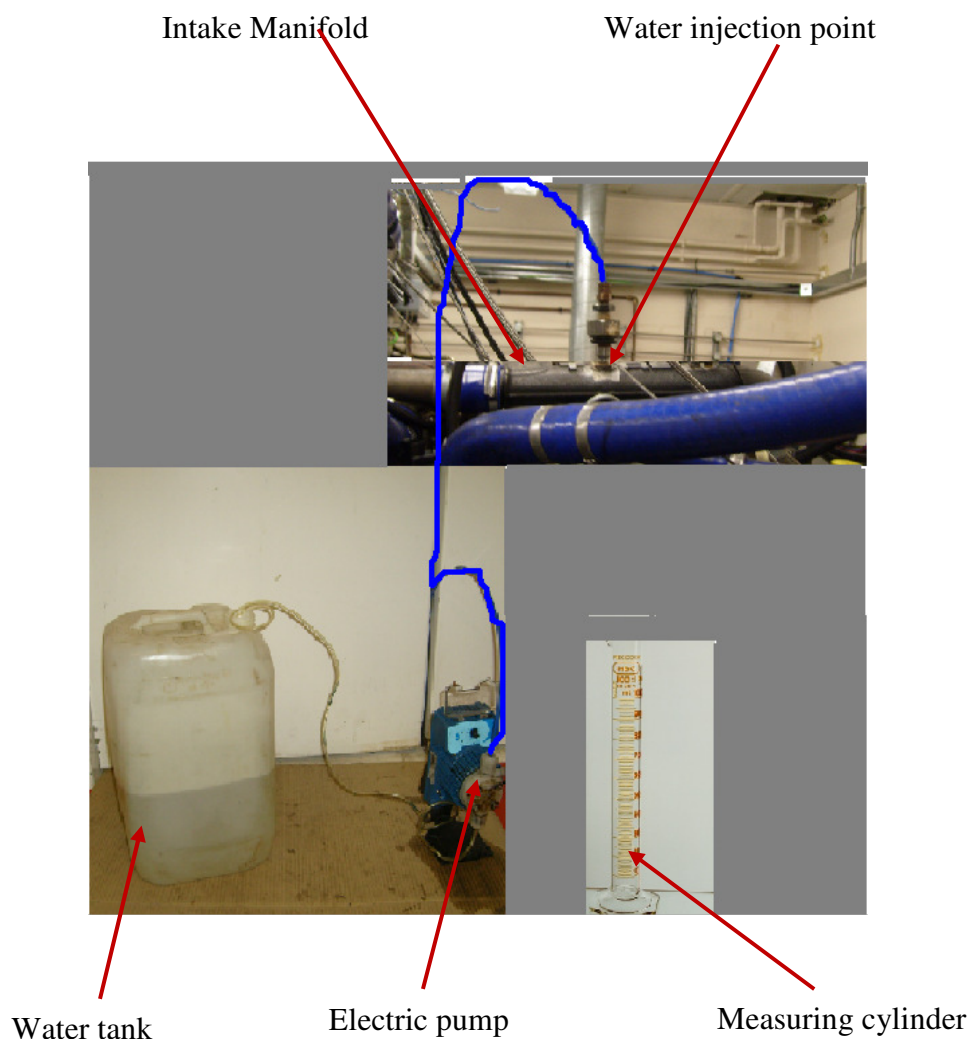


Figure 3-17 Water injection system configuration

The in-cylinder pressure, brake specific fuel consumption and the emissions (NO_x, CO, CO₂, THC) have been measured with the measuring system described in section 3.1. To decide the amount of water to be injected into the CI engine previous works have been

reviewed and summarized in Table 3-7. The limitations of water injection are its effects in the cylinder chamber parts and its significant influence on the CO emission[156], [158], [179]. In addition, the author has suggested that the higher water injection may cause higher plume smoke in in exhaust due to the formation of vapour in the cylinder. In Table 3-7, it can be seen that the minimum water added to the engine has been 0% and the maximum value has been 40%. In this study four water flow rates (0%, 10%, 15% and 25%) have been investigated.

Table 3-7 Quantity of water injected by previous researchers

Author	Water quantity
Lin and Chen [179]	0%,15%
Tauzia et al.[180]	0%, 3kg/h for 2liter engine
Chadwell and Dingle[164]	0%, 10%, 20%, 30%
Kegal and Pehan[156]	0%, 10%, 20%
Park et al.[158]	0%, 20%, 40%

The test engine has average fuel consumption rate of 12kg/h. Based on the average fuel consumption rate, the mass flow rate of the water has been calculated and presented in Table 3-8. During the data analysis in Chapter eight 10% water injection has been neglected due to insignificant effects on engine performance and emission.

Table 3-8 Engine operating conditions and water mass flow rate

Condition	Speed(rpm)	Load(Nm)	Water mass flow rate
A	900 – 1800	105	0kg/h ,1.2kg/h, 1.8kg/h, 3kg/h
B	900 – 1800	210	0kg/h, 1.2kg/h, 1.8kg/h, 3kg/h
C	900 – 1800	315	0kg/h , 1.2kg/h,1.8kg/h, 3kg/h
D	900 – 1600	420	0kg/h , 1.2kg/h,1.8kg/h, 3kg/h

The fuel from biodiesel tank was pumped to the fuel meter and then passes through the fuel pump to the fuel injector. The water injection was carried out by using an electric pump. The water was injected downstream of the compressor at intake manifold. The water flow rate was measured using two methods: the electric pump and calibrated burette with stop watch.

3.3.7 Procedure to Ensure Accuracy of Measurement

During engine testing the measured parameters generally show some dispersion from the mean values. This is quantified in terms of measurement error which is the variation between measurements of the same quantity on the same test [181]. To quantify measurement error, the same test needs to be repeated several times. One of the common parameter used to quantify this error is standard deviation (SD). SD is a measurement of variability, or diversity, which illustrates the variation of ‘dispersion’ from the mean value. In this study, the SD value was calculated using equation (3-3):

$$SD = \left[\frac{1}{n} \sum_{i=1}^n (X_i - \bar{X})^2 \right]^{\frac{1}{2}} \quad (3-3)$$

Where SD is standard deviation, n is number of data, X_i is the measured data and \bar{X} is the mean value

To estimate the repeatability of measurement and the accuracy of the procedure the tests were repeated three times and the mean values have been obtained for the detailed analyses. The parameters that were investigated include brake specific fuel consumption, thermal efficiency, peak effective pressure and emission during the steady state and transient operation conditions. It was observed that the SD varied with the operation conditions and as such, the values were plotted on the perspective graph. The binary data corresponding to exhaust emissions, air flow rate, and in-cylinder pressures were collected by setting the data acquisition system to acquire 36 segments (sample points) in 40 Sec. The SD of the data obtained on emissions and in-cylinder pressure was calculated by using the 36 segments during the steady state operations as well. As the parameters of the transient conditions varied from one segment to the other, the SD of in-cylinder pressure and emissions was determined from the three sets of tests conducted at same operating conditions. The standard deviation in this study has been represented by \perp on the graph. The value of standard deviation and the size of the symbol are proportional. When the standard deviation value becomes smaller, the symbol may approach to dot symbol.

3.4 Summary on Chapter Three

Chapter three has focused on the description of the experimental facilities required for biodiesel characterisation, test engine’s characteristics and specifications and measuring instrumentation. The detail specification of measurement system, data acquisition system and application software have been discussed. In addition, test procedures for the physical

characterisation of biodiesel have been elaborated based on the European biodiesel test standards. Under the test procedures section, the methodology of biodiesel blending, the new steady and transient test procedures, water injection system and injection procedures have been discussed. The next chapter is focused on the numerical and experimental investigation of the biodiesel physical characterisation.

CHAPTER FOUR

4. BIODIESEL CHARACTERISATION

This Chapter outlines the effects of biodiesel fraction and temperature on the main fuel properties, such as density, viscosity and lower heating value based on the experimental values. It also includes new predicting models developed to predict the above properties [27],[64],[65],[68]. Most empirical correlations describing the density, viscosity and heating value of biodiesel include constants which vary with the type of biodiesel and percentage of blends. It is very important to have a simple, stable and reliable estimation method for density, viscosity and heating value as a function of biodiesel fraction and temperature. These relations will have immense use in the design of intake manifold and modelling and analysis of combustion, performance and emission. Furthermore, the properties of biodiesels affect the dynamic flow phenomena in the fuel pump, fuel pipe, fuel filter and injector spray [77]. Based on the above requirements, in this Chapter, the effect of temperature and biodiesel fraction on density and viscosity of biodiesel blend have been investigated in detail. In addition, the effects of biodiesel fraction, density and viscosity on the heating value of biodiesel have also been investigated. Finally, correlations have been developed to correlate the main physical parameters. The effects of density and viscosity of the biodiesel and its blends have also been considered on the fuel supply system, such as the fuel pump flow rate, fuel filter flow rate and sauter mean diameter (SMD).

4.1 Effect of Biodiesel Fraction and Temperature on Density

Density can be defined as the ratio of the mass of an object divided by its volume. The density of biodiesel has been measured in this study at various temperatures for different biodiesel blends. The density of the biodiesel has been measured by using hydrometer explained in section 3.1.2. Figure 4-1 presents the density variation of corn oil biodiesel, rapeseed oil biodiesel and waste oil biodiesel blends. Three of the biodiesels blends had similar density values, with a minimum value of 853kg/m^3 at 0% biodiesel fraction and maximum value of 880 kg/m^3 at 100% biodiesel fraction. The density of the blend increased with increase in the biodiesel volume fraction. Since three of the biodiesels and their blends had very similar density values, a common first degree regression equation was developed by taking the average slope and the interception point. The correlation is described by the equation (4-1)

$$\rho_{blend} = 0.2523X + 854.33 \quad (4-1)$$

Where ρ_{blend} is the density of diesel and biodiesel blends (kg/m^3), and X is the volume fraction of biodiesel at 15.6°C .

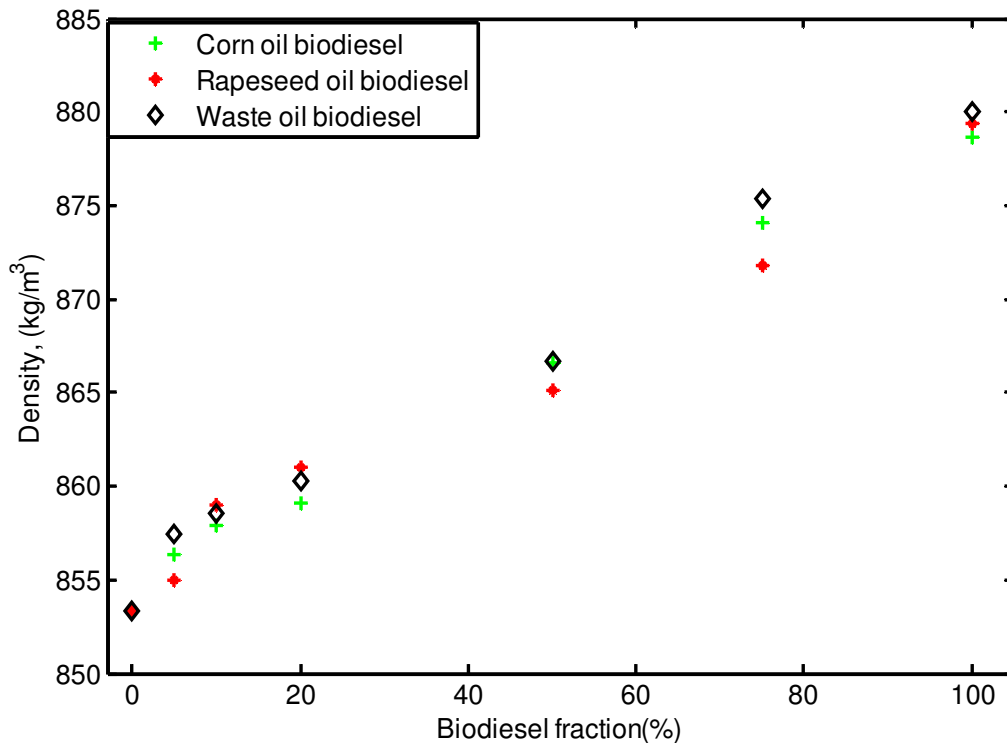


Figure 4-1 Variation of density of biodiesel with biodiesel fraction for different biodiesel source feeds

Table 4-1 presents density values of biodiesel corresponding to volume/mass method, the hydrometer method, mixing equation (2-2) and correlation equation (4-1) developed in the present study. The density values have been compared with each other and the errors have been calculated. The hydrometer and mass/volume methods, hydrometer method and mixing equation, and the hydrometer method and regression correlation showed maximum absolute errors of 0.60%, 0.50%, and 0.29%, respectively. The regression correlation and the experimental values showed R^2 of 0.9945. This suggests that if the densities of pure diesel and pure biodiesel are known, either equation (2-2) or equation (4-1) can be used to determine the density of biodiesel blend at any given blend percentage fraction with confidence. The comparison of the values obtained from the previous model and equation (4-1) which is presented in Table 4-1, validate that the new density predication model can used fairly to predict density of biodiesel blends.

Figure 4-2 shows the effect of temperature on the density of 100% biodiesel measured in the present study, and the estimated density by Tat and Gerpen correlation [28]. The temperature varied from 290K to 360K for 100% corn oil biodiesel, rapeseed and waste oil biodiesel. Three of the biodiesel fuels had very similar density values at a given temperature, and the density of the biodiesel decreased with an increase in temperature.

To generate the regression correlation, the average density of the biodiesel at a given temperature was taken and a linear-regression equation (4-2) was developed. The measured average biodiesel density and regression line had a maximum absolute error of 0.25% and R^2 of 0.9930. Similarly, the density of diesel as a function of temperature was experimentally determined and is described by equation (4-3). The empirical equation for density of diesel and the measured density values had a maximum absolute error of 0.15% and R^2 of 0.9962:

$$\rho_{biod} = -0.69T + 1075 \quad (4-2)$$

$$\rho_{diesel} = -0.657T + 1051 \quad (4-3)$$

Where ρ_{biod} is the density of biodiesel and ρ_{diesel} is the density of diesel and T is the temperature.

Table 4-1 Density of biodiesel blend by experimental methods, mixing equation and correlation equation at 15.6°C

Type of Biodiesel	Fraction of Biodiesel (%)	Density, by mass/volume	Density using hydrometer	Density using mixing equation (2-2)	Density using correlation equation (4-1)	Absolute percentage error between		
						Mass/volume and hydrometer methods	Mixing equation(2-2) and hydrometer methods	Correlation equation(4-1) and hydrometer methods
Corn oil biodiesel	0	853.36	855.00	853.36	854.43	0.1919	0.0000	0.1252
	5	856.39	860.00	854.68	855.70	0.3049	0.3164	0.0799
	10	857.94	860.00	855.99	856.97	0.2406	0.2268	0.1121
	20	859.10	860.00	858.62	859.52	0.0112	0.1719	0.0491
	50	866.61	865.00	866.50	867.15	0.1856	0.0120	0.0625
	75	874.10	875.00	873.08	873.51	0.1025	0.1177	0.0680
	100	879.65	885.00	879.65	879.87	0.6087	0.0000	0.0255
Rapeseed oil biodiesel	5	854.96	855.00	854.68	855.70	0.4608	0.5008	0.0870
	10	859.04	860.00	855.99	856.97	0.1115	0.3552	0.2407
	20	856.97	860.00	858.62	859.52	0.3536	0.1924	0.2973
	50	865.09	865.00	866.50	867.15	0.0102	0.1637	0.2384
	75	871.77	870.00	873.08	873.51	0.2028	0.1499	0.1998
	100	879.35	880.00	879.65	879.87	0.0739	0.0337	0.0591
Waste oil biodiesel	5	857.48	860.00	854.68	855.70	0.2944	0.3265	0.2069
	10	857.58	855.00	855.99	856.97	0.3008	0.1854	0.0707
	20	860.25	850.00	858.62	859.52	1.1911	0.1892	0.0846
	50	866.68	860.00	866.50	867.15	0.7710	0.0205	0.0540
	75	875.32	875.00	873.08	873.51	0.0366	0.2565	0.2068
	100	879.55	880.00	879.65	879.87	0.0512	0.0109	0.0364

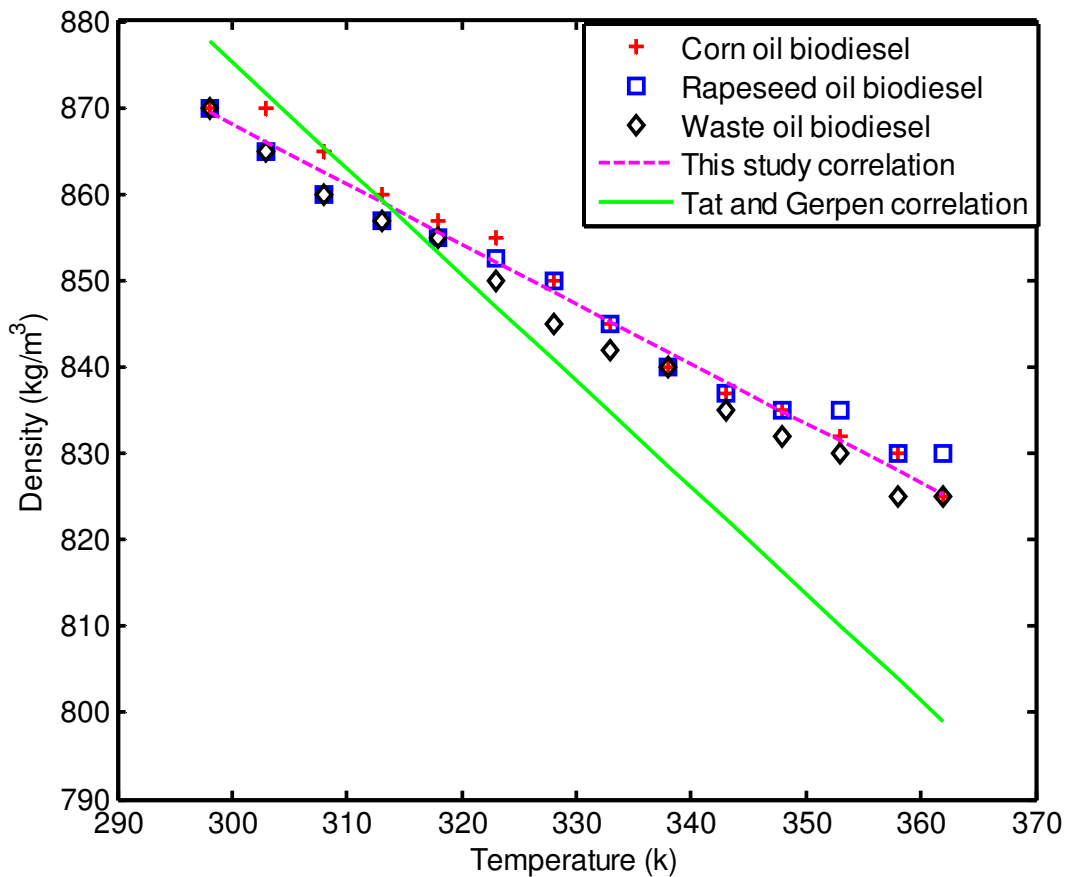


Figure 4-2 Variation of density of biodiesel with temperature for different biodiesel source feeds

These regression equations were compared with Tat and Gerpen's linear-regression equation (2-1), and a maximum absolute error of about 3.5% was obtained. This difference is due to the differences between the biodiesels used in this study and those used by Tat and Gerpen [56]. In Figure 4-2, it can be seen that for temperature range of 320 to 330K, the density of biodiesel was similar to that of the normal diesel density (850kg/m^3 - 860kg/m^3). This implies that had there been a system to pre-heat the biodiesel to within the temperature range of 320- 330K, the density of biodiesel could have been matched to the density of pure diesel. In the present study, equation (4-4) has been developed to estimate the density of various biodiesel blends at a given temperature. For this purpose, mixing equation (2-2) developed by Clements (Referenced in [28]) and the regression equations 4-2 and 4-3 of this study have been used. Equation 4-4 was developed to determine the density of a binary blend of biodiesel and diesel at a given temperature and blending fraction(X):

$$\rho_{mix} = (-0.033T + 24.4)X - 0.657T + 1051 \quad (4-4)$$

Where ρ_{mix} is density of the binary (kg/m^3), X is volume fraction of the biodiesel and T is the temperature (K).

The density, as obtained from experiments for the rapeseed oil biodiesel, was compared to the estimated value of biodiesel density using equation (4-4) and a maximum percentage error of 0.54% was observed. This implied that equation (4-4) could be used with confidence to estimate the density of the biodiesel blend at any temperature and biodiesel fraction.

4.2 Effect of Biodiesel Fraction and Temperature on Viscosity

Viscosity is one of the most important fuel parameters that affects operation of fuel filter, fuel pump and injection equipment. High viscosity leads to poorer atomisation of the fuel spray and less accurate operation of the fuel injectors [1]. It also forms carbon deposit and sticks on the fuel pump and fuel filter. To modify the fuel supply system components such as fuel filter, fuel pump and fuel injectors and/or the viscosity of biodiesel, understanding of the effects of biodiesel viscosity on system's response over a wide range of temperatures and biodiesel fractions is very important. Detailed studies have been conducted to estimate the viscosity of corn oil biodiesel, rapeseed oil biodiesel, and waste oil biodiesel blends at various temperatures. The viscosity of the biodiesel has been measured by Cannon-Fenske Viscometer tube (size B) apparatus. To measure the viscosity of the biodiesel blends, the official standard: EN ISO 3104:1996 which is explained in Appendix A, has been used. The effect of the biodiesel blends' fraction and temperature on the kinematic viscosity of biodiesel was investigated and corresponding models have been developed. The models have been compared with models published. Figure 4-3 shows the kinematic viscosity of corn oil biodiesel, rapeseed oil biodiesel, and waste oil biodiesel blends as function of biodiesel volume fractions as used in the present study.

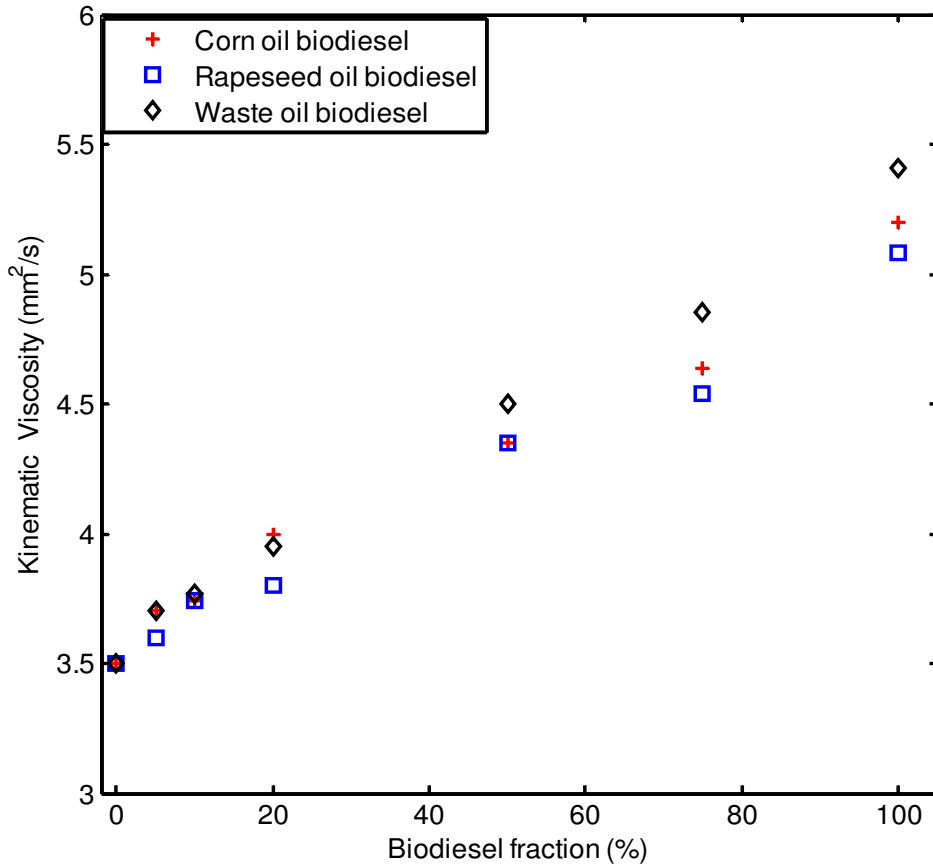


Figure 4-3 Variation of kinematic viscosity of biodiesel with biodiesel fraction for different biodiesel source feeds

The biodiesel kinematic viscosity increased with increasing biodiesel blend fraction for all blends. The rapeseed biodiesel had a higher kinematic viscosity compared to corn oil biodiesel and waste oil biodiesel blends. The experimental data were correlated by an empirical second degree correlation described as equation (4-5). The coefficients A , B , and C used in equation (4-5) are described in Table 4-2. This equation could be used to estimate the viscosity of biodiesel-diesel blend for a given biodiesel fraction:

$$\eta_{corr} = Ax^2 + Bx + C \quad (4-5)$$

Where η_{corr} is the kinematics viscosity (mm²/s), A , B , C are coefficients of the second degree equation and X is biodiesel fraction. Table 4-2 also presents the experimentally measured viscosity, the calculated viscosity by equation (2-4), the regression correlation values (4-5) and R^2 values, and the absolute error between the measured and calculated viscosities for the three biodiesel blends.

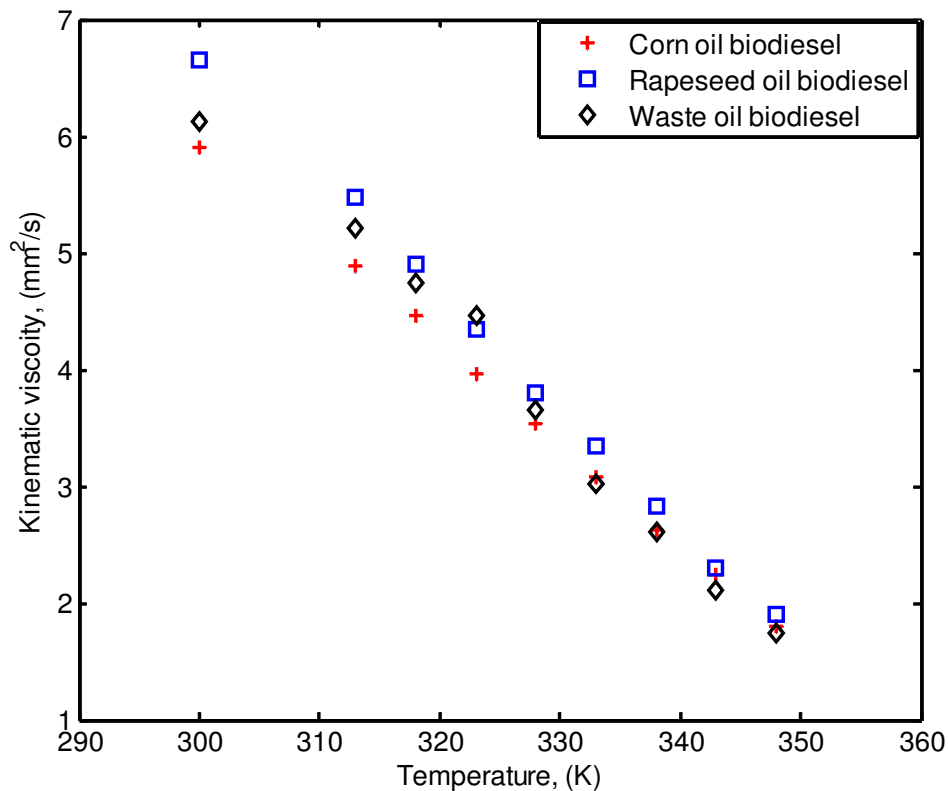


Figure 4-4 Variation of kinematic viscosity of biodiesel with temperature for different biodiesel sources feeds

The kinematic viscosity of the biodiesel as obtained in the present study varied within the range of 3.55 to 5.48mm²/s. The measured and regression correlations had a maximum absolute error of 0.299 and a maximum of R^2 value of 0.984. Both the Grun-Nissan correlation (equation (2-4)) and the empirical correlation proposed in this study were reasonably accurate in estimating the kinematic viscosity of the biodiesels. However, the regression coefficient variation with the type of biodiesel limited the use of correlation equation (4-5). Figure 4-4 shows the variation in kinematic viscosity of 100% corn oil, rapeseed biodiesel and waste oil biodiesel within a temperature range of 295K-360K. It can be seen that the kinematic viscosity of the biodiesel decreased with an increase in temperature.

The empirical correlation for the kinematic viscosity as a function of temperature is described by equation (4-6) and has been developed based on the experimental results; the developed equation had a R^2 value of 0.9999. Joshi et al. [68] and Tat & Gerpen [20] modified the Arrhens equation for the prediction of biodiesel viscosity at different temperatures. The viscosity values obtained from Joshi et al., Tat &

Gerpen's viscosity correlations, and the regression correlation developed in this study, are shown in Figure 4-5. All the curves follow a similar trend. The empirical correlation of the kinematic viscosity and temperature is described by equation (4-6) which has been developed from the experimental results obtained in the present study.

$$\ln(\eta) = -0.0219T + 9.12 \quad (4-6)$$

Where T is the temperature in K, and η is the kinematic viscosity in mm²/s

Furthermore, the density and kinematic viscosity of biodiesel were correlated and an equation was developed relating viscosity as function of density, as shown below in equation (4-7). This equation could be used to estimate kinematic viscosity of the biodiesel for a known density of biodiesel. The values from the predicting model and the experimental values had a maximum absolute error of 0.37:

$$\ln(\eta) = 0.0357\rho - 29.02 \quad (4-7)$$

Where is η the kinematic viscosity of the fuel biodiesel at a given temperature, and ρ is the density of the biodiesel at a given temperature.

In addition, an attempt had been made to develop a correlation to predict viscosity of a biodiesel blend at a given temperature. For this a new equation (4-8) had been developed by combining equations (4-2), (4-3) and (4-7)), in order to determine the viscosity of the blend at a given temperature and biodiesel fraction. The modified mixing equation has a maximum absolute error of 0.50:

$$\ln(\eta_{mix}) = (-0.0012T + 0.8456)X - 0.0234T + 8.64 \quad (4-8)$$

Where η_{mix} is the viscosity of the biodiesel, X is the volume fraction of the biodiesel and T is the temperature (K).

Table 4-2 Kinematic viscosity of biodiesel and its blends at 40°C.

Biodiesel	Blend (%)	Measured	A	B	C	R ²	Calculated kinematic viscosity		Absolute error between measured and	
							Regression correlation equation(4-5)	Grun-Nissan equation(2-4)	Regression correlation equation(4-5)	Grun-Nissan equation(2-4)
Corn oil biodiesel	0	3.50	8x10 ⁻⁶	0.0147	3.593	0.984	3.5930	3.5000	0.0930	0.0000
	5	3.80					3.6667	3.5590	0.1333	0.2410
	10	3.74					3.7408	3.6190	0.0008	0.1210
	20	3.72					3.8902	3.7421	0.1702	0.0221
	50	4.35					4.3480	4.1370	0.0020	0.2130
	75	4.54					4.7405	4.4978	0.2005	0.0422
	100	4.89					5.1430	4.8900	0.2530	0.0000
Rapeseed biodiesel	0	3.50	7*10 ⁻⁶	0.0143	3.537	0.987	3.5366	3.5000	0.0366	0.0000
	5	3.76					3.6083	3.5793	0.1517	0.1807
	10	3.90					3.6803	3.6605	0.2197	0.2395
	20	4.08					3.8254	3.8283	0.2546	0.2517
	50	4.47					4.2691	4.3795	0.2009	0.0905
	75	4.62					4.6485	4.8989	0.0285	0.2789
	100	5.48					5.0366	5.4800	0.4434	0.0000
Waste oil biodiesel	0	3.50	5x10 ⁻⁵	0.0129	3.597	0.992	3.5970	3.5000	0.0970	0.0000
	5	3.87					3.6628	3.5703	0.2073	0.2997
	10	3.77					3.7310	3.6420	0.0390	0.1280
	20	3.95					3.8750	3.7898	0.0750	0.1602
	50	4.30					4.3670	4.2702	0.0670	0.0298
	75	4.85					4.8458	4.7168	0.0042	0.1332
	100	5.21					5.3870	5.2100	0.1770	0.0000

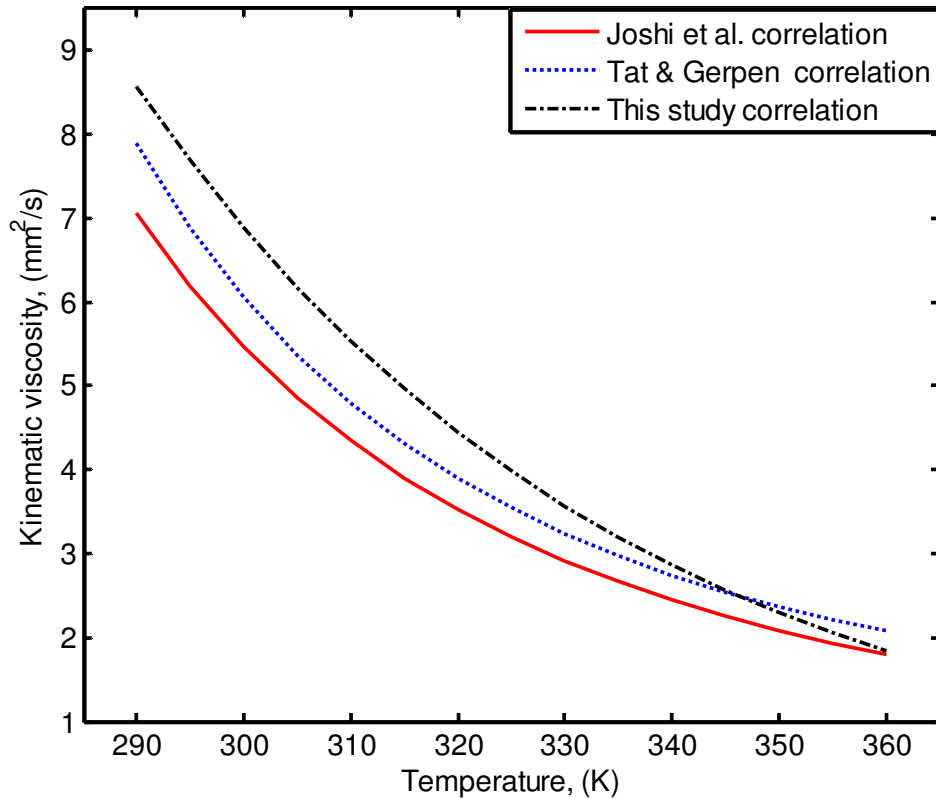


Figure 4-5 Variation of predicted kinematic viscosity of rapeseed biodiesel with temperature

The combination effect of temperature and biodiesel fraction on the kinematic viscosity of biodiesel is shown in Figure 4-6. It can be seen that when the biodiesel fraction increases and temperature decreases, the kinematic viscosity of the biodiesel increases.

The kinematic viscosity prediction models for biodiesel described by equations (4-6), (4-7) and (4-8) were used to determine numerically the kinematic viscosity at various temperatures, density and biodiesel fraction values. These models could be used in the design and investigation of fuel supply systems (fuel pump, fuel filter, fuel pipe, and injectors), as well as in predicting air-fuel mixing phenomena and combustion characteristics.

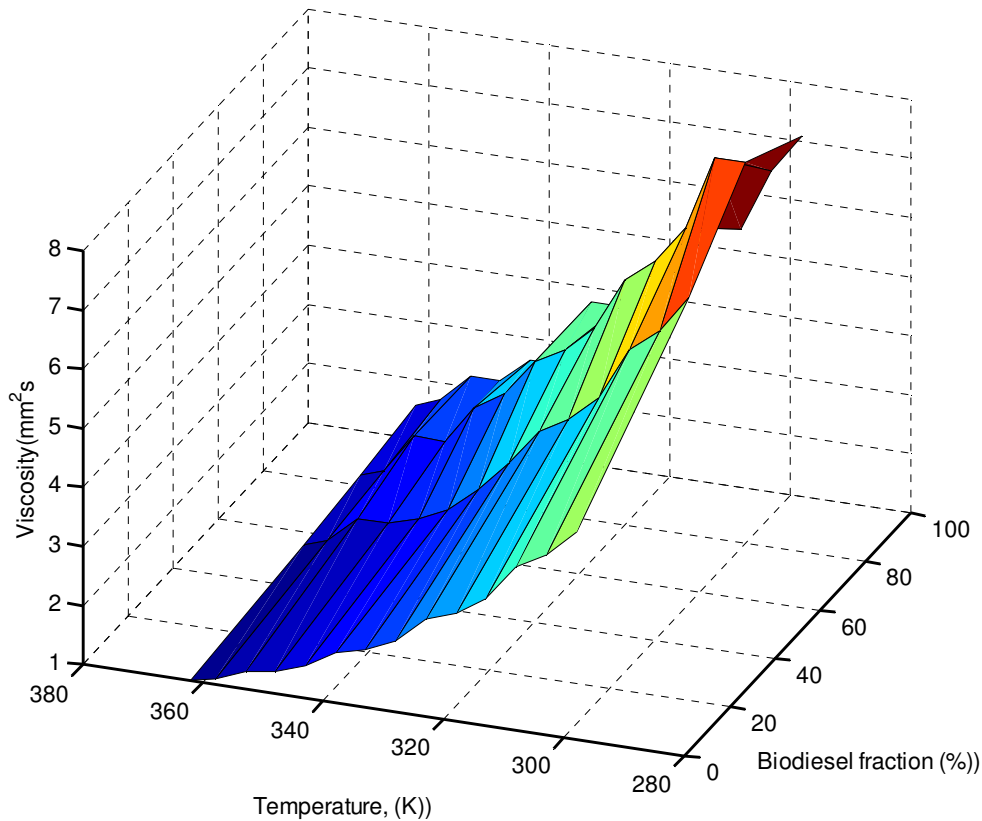


Figure 4-6 Variation of kinematic viscosity of biodiesel with temperature

4.3 Effect of Biodiesel Fraction on Lower Heating Value

Lower heating value is one of the most important parameters for the design of engine system and estimating the engine performance parameters such power torque, brake specific fuel consumption and thermal efficiency [71], [57], [62], [71]. The heating value of petroleum products is fairly standard. However, due to the variation of plants feed stock, growing climate conditions, soil type, plant health and production process, the biodiesel have been shown to have different lower heating values [20], [55]. In addition, for use in engine application, the neat biodiesel (100B) is blended with the petrol diesel. To understand the effects of the biodiesel fraction on the lower heating value, detailed numerical and experimental investigation is vital. Hence, in this section, the effects of biodiesel fraction, density and viscosity on lower heating value were investigated and predicting models were developed.

Using the procedure mentioned in Appendix A, the heating value of the biodiesel and its blends have been obtained experimentally. Three runs of benzoic acid were carried out and averaged values were generated for the energy equivalent of the bomb

calorimeter. Similarly, three replicates were run for each sample of the biodiesel and averaged values were used to calculate the heating values. The difference in LHV obtained from these tests did not exceed 0.45MJ/kg and hence its maximum deviation has been limited to 1.15%. The temperature change verses the time during the fuel combustion in the Oxygen Bomb Calorimeter is shown in Figure 4-7. It can be seen that the biodiesel combustion yielded lower temperature as compared to the diesel by 7.5%.

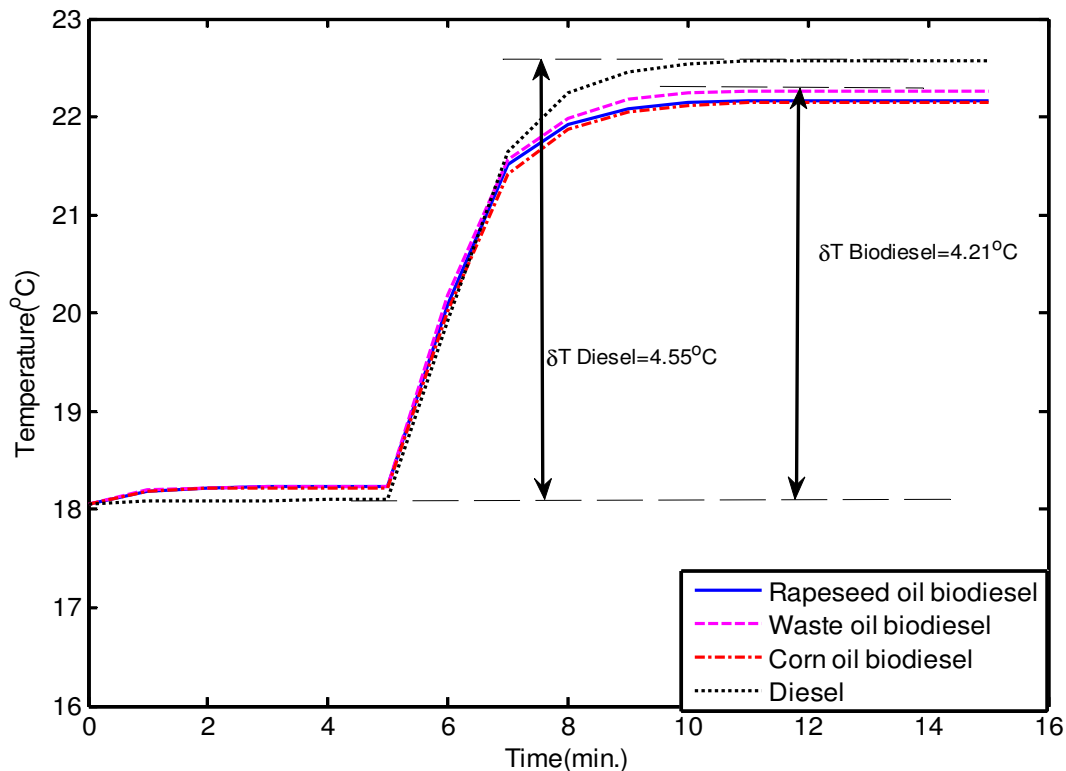


Figure 4-7 Temperature change in Bomb calorimeter for various biodiesel source feed.

The effects of the biodiesel volumetric blend fractions on heating value of the biodiesel blends are shown in Figure 4-8. From the figure it can be seen that as the biodiesel blend fractions increase, the lower heating values decrease. The rapeseed biodiesel, corn biodiesel and waste biodiesel resulted in lower heating values as compared to diesel by 9.96%, 10.19% and 9.67% respectively. The low heating value of the biodiesel could be explained on the basis that the 11% of the biodiesel molecular structure is occupied by oxygen molecules resulting in relatively lower number of carbon and hydrogen molecules.

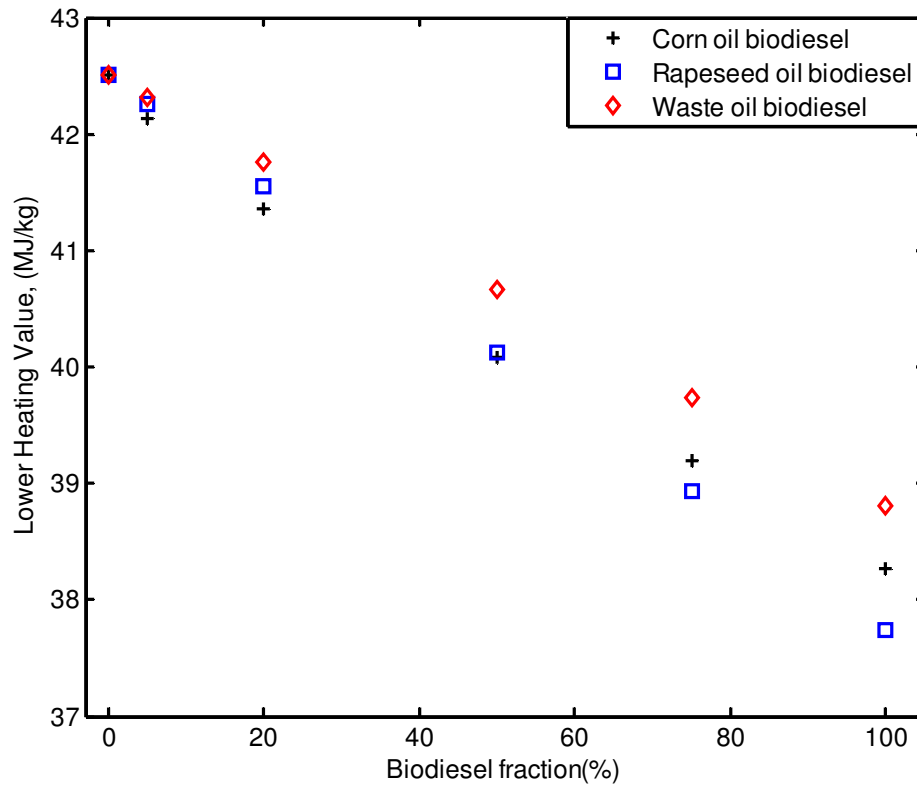


Figure 4-8 Variation of lower heating value of biodiesel with biodiesel fraction for different biodiesel source feeds

It is known that energy from the fuel results from the carbon and hydrogen molecules. The lower heating values of rapeseed oil, corn oil and waste oil biodiesel were shown to have a maximum difference of 1.48%. The lower heating values of the biodiesel were correlated with the biodiesel fraction, density and viscosity of the tested biodiesel. The correlation of lower heating value versus biodiesel fraction, lower heating value versus density and lower heating value versus kinematic viscosity are shown in equations (4-9), (4-10) and (4-11) respectively. The correlations resulted in R^2 values of 0.991, 0.981 and 0.988 for correlation 4-9, 4-10 and 4-11 respectively:

$$LHV = -0.041X + 42.32 \quad (4-9)$$

$$LHV = -0.167\rho + 42.32 \quad (4-10)$$

$$LHV = -2.27\mu + 50.84 \quad (4-11)$$

Where LHV is the lower heating value, X is biodiesel fraction, ρ is density of biodiesel and μ is kinematic viscosity

Demribus's [75] and Sadrameli *et al.*'s [63] have developed regression models which correlate density with lower heating value of neat biodiesel (100B). The measured and predicted lower heating values with percentage deviation values are presented in Table 4-3. It can be seen that the predictions of this study and measured values showed only a maximum error of 0.87%. However, the measured values deviate from the values obtained from Demirbas[75] and Sadrameli *et al.* [63] predictions by 6.82% and 5.93%, respectively. This higher deviation can be due to their model being developed only for neat biodiesel. However, this study considered neat biodiesel and different blends fraction.

Demribus's [75] also developed a correlation between the lower heating value and kinematic viscosity of neat biodiesel which is provided in Table 2-2. The values obtained from Demribus's [75] correlation, measured lower heating values and predicted lower heating values from the correlation developed in this study are presented in Table 4-4. It can be seen that the measured values are deviated by 1% and 10.31% from the values obtained from the correlation developed in this study and those from Demribus's [75]. It is also seen that the deviation of the values obtained from Demribus's [75] correlation as compared to the measured values decrease with increase of the biodiesel fraction. This indicates that the Demribus's [75] correlation only predicts the lower heating value for neat biodiesel. However, the correlation developed in this study results in acceptable percentage error in predicting the lower heating value for neat biodiesel and its blends.

Lower heating value is one of the most important parameters for estimating the design parameters and is vital input parameter for numerical simulation of combustion and estimating engine performances such as brake specific fuel consumption and thermal efficiency [71], [57], [62]. The new developed lower heating value models which correlate the heating values with biodiesel fraction, density, and kinematic viscosity will have significant application in investigation of combustion characteristics, engine performance and emission and in the development of new engines.

Table 4-3 Lower heating value prediction from the density of rapeseed oil biodiesel blends

Biodiesel fraction (%)	Density (kg/m ³)	Lower heating vale (MJ/Kg)				The measured percentage deviation (%)		
		Measured	This study correlation density	Demribus's [75] density correlation	Sadrameli et al.s' [63] density correlation	from this study correlation	from Demribus's [75] correlation	from Sadrameli et al.s' [63] correlation
0.00	853.36	42.50	42.39	41.87	42.97	0.27	1.49	-1.09
5.00	854.96	42.13	42.12	41.81	42.82	0.01	0.76	-1.64
20.00	860.97	41.36	41.12	41.58	42.26	0.60	-0.52	-2.15
50.00	865.09	40.08	40.43	41.42	41.87	-0.87	-3.34	-4.46
75.00	871.77	39.19	39.31	41.17	41.25	-0.32	-5.04	-5.25
100.00	879.35	38.27	38.05	40.88	40.54	0.57	-6.82	-5.93

Table 4-4 Lower heating value prediction from the viscosity of rapeseed oil biodiesel blends

Biodiesel fraction (%)	Viscosity(mm ² /s)	Lower heating vale (MJ/kg)			The measured percentage deviation (%)	
		Measured	by Viscosity correlation(this study)	by Demribus's [75] viscosity correlation	from this study correlation	from Demribus's [75] correlation
0.00	3.58	42.50	42.08	38.12	1.00	10.31
5.00	3.67	42.13	41.83	38.13	0.70	9.50
20.00	3.79	41.36	41.53	38.13	-0.39	7.82
50.00	4.28	40.08	40.29	38.16	-0.52	4.81
75.00	4.68	39.19	39.27	38.17	-0.21	2.59
100.00	5.13	38.27	38.12	38.20	0.40	0.19

4.4 Development of integrated Mathematical Models of Fuel Supply System

To evaluate the effects of density and viscosity of different biodiesel blends on the fuel supply system (fuel pump, fuel pipe, fuel filter and fuel injector), several key fuel supply parameters such as, head loss, flow rate and sauter mean diameter (SMD) have been predicted using well-accepted mathematical models for different fuel blends over a wide range of engine operating conditions. The characteristics of the compression ignition (CI) engine used in this prediction model are summarised in Table 3-1. The model has been used to determine the mass flow rate of fuel used to produce the required amount of power by the engine. The mass flow rate of fuel that needs to be injected for each cylinders and the power produced by the engine are calculated by the following equations [182]:

$$m_f = 360N_R P / (NQ_v n \eta \theta) \quad (4-12)$$

$$P = NP_1 V_1 n \left[q - \frac{(\beta^\gamma - 1)}{(\gamma - 1)} \right] \quad (4-13)$$

$$\eta = 1 - \frac{1}{\gamma \alpha^{(\gamma-1)}} \frac{(\beta^\gamma - 1)}{(\beta - 1)} \quad (4-14)$$

$$q = \frac{Q_v}{AR_g T_1} \quad (4-15)$$

Where m_f is the fuel mass rate of injection for each cylinder (kg/s), P is the power developed, n is the number of cylinders, η is the thermal efficiency calculated by equation (4-14), Q_v is the calorific value of fuel(J/kg), ρ is the density of fuel(kg/m³), N_R is the rotational speed of engine(rev/s), N is the number of cycles calculated by $N = N_R/2$ for 4-stroke engine (cycles per sec), θ is the crank angle duration for injection(degrees), V_1 is the volume at start of the compression process per cycle (m³), α is the compression ratio, β is the cut-off ratio in the diesel cycle (1.5), γ is the air specific heat ratio, q is the heat supply factor, A is the stoichiometric air fuel ratio, and, R_g is the gas constant of air (287J/kg.K), and T_1 is the ambient temperature.

One of the important fuel supply system components in the engine is a fuel filter. The main application of the fuel filter is to remove foreign matter of different sizes from the fuel as these could cause wear of the well polished materials. In addition, it filters any fraction of water left in the fuel to protect the equipment from corrosion. The filter flow characteristics

have been presented by Coulson and Richardsons [183] and modelled as described in equations (4-16) to (4-19). Equation (4-16) is the basic characteristic equation for filtration. By assuming constant pressure difference (ΔP), equation (4-16) can be modified to equation (4-18). Further Γ , v and A are assumed constants and fuel equation (4-19) was developed. Equation (4-19) shows the inverse relationships between fuel flow rate and the viscosity of the fuel in the filter media:

$$\frac{dV}{dt} = \frac{A^2(-\Delta P)}{\Gamma \eta v V} \quad (4-16)$$

$$\frac{V^2}{2} = \frac{A^2(-\Delta P)t}{\Gamma \eta v} \quad (4-17)$$

$$Q = \frac{C}{\sqrt{\eta t}} \quad (4-18)$$

$$C = \sqrt{\frac{2A^2(-\Delta P)}{\Gamma v}} \quad (4-19)$$

In the above equations, V (m^3) is the volume of filtrate which passes through the filter in time t (s), A (m^2) is the cross-sectional area of the filter cake, η (mm^2/s) is the kinematic viscosity of the filtrate and ΔP (pa) is the applied pressure difference, Γ (m^{-2}) is the filtration resistance constant, v is the volume of cake deposited by unit volume of filtrate, and C is filtration property constant given by equation(4-19)

The effect of viscosity on fuel flow through a pump was investigated by calculating the head loss that occurred in the pumping network. The head loss that occurs in pipes is dependent on the flow velocity, pipe length and diameter, and a friction factor based on the roughness of the pipe and the Reynolds number of the flow. In the simulation model, the frictional head loss in the section and head pipe was calculated by:

$$h_f = 2.4384(F_f)\left(\frac{L}{d_i}\right)\left(\frac{u^2}{2g}\right) \quad (4-20)$$

Where h_f is friction head loss, F_f is the dimension-less friction factor calculated by the equation $F_f = \frac{0.0396}{Re^{0.25}}$ for the turbulent flow, Re is Reynolds number, $\frac{L}{d_i}$ is the equivalent length to pipe diameter ratio, u is the velocity (m/s) and g is the gravitational acceleration (m/s^2).

The other important process which affects the performance of the engine system is the fuel-air mixing process in the engine cylinder. The penetration length, spray angle and sauter mean diameter (SMD) is the major parameters needed to quantify the efficiency of the mixing process. Since the viscosity and density of the fuel have less effect on the penetration length and the spray angle, the present work is focused only on the effect of biodiesel blending on the SMD. The SMD is the diameter of the model droplet, whose volume to surface area ratio is equal to the ratio of the sum of all droplet volumes (V) in the spray, to the sum of all droplet surface areas (A). There are different models to correlate the fuel properties and the injector characteristics with SMD. In this simulation, the model developed by Hiroyasu and Arai has been used [184]:

$$\frac{SMD}{D} = 0.38Re^{0.25}We_L^{-0.32} \left(\frac{\mu_l}{\mu_g}\right)^{0.37} \left(\frac{\rho_l}{\rho_g}\right)^{-0.47} \quad (4-21)$$

Where We_l is the Weber number given by $We_l = \frac{V^2 D \rho_l}{\sigma}$, Re is the Reynolds number given by $Re = \frac{u D \rho_l}{\mu_l}$, $V(m/s)$ is the velocity of jet, ρ_l (kg/m^3) is the density of the liquid, μ_l ($N.s/m^2$) is the dynamic viscosity of the liquid, D_n (m) is the nozzle hole diameter, ρ_g is the density of the gas, and μ_g is the dynamic viscosity of the gas ($N.s/m^2$), and σ is the surface tension at the liquid-gas interface (N/m).

4.5 Computational Procedures used for Models of Fuel Supply System

The effects of biodiesel density and viscosity on the fuel supply system have been simulated using the following input parameters and computational steps.

Input parameters: The input parameters used in fuel filter, fuel pump and sauter mean diameter simulation have been presented in Table 4-5. The input parameters have been obtained from the specification of the equipment and engine operating conditions.

Computational steps: To calculate the effects of biodiesel physical properties on the fuel filter, fuel pump and air-fuel mixing phenomena the following computational steps have been used:

Step 1: The mass flow rate of fuel (\dot{M}_f) has been calculated using equation 4-12. The input parameters in equation 4-12, such as the power, the thermal efficiency and

heat supply factor have been calculated using equations 4-13, 4-14 and 4-15 respectively.

Table 4-5 Input parameters for fuel supply system analysis

Parameters	Values
N_R : Rotational speed	1000 to 1800rpm
N : Number of cycles	500 to 900rpm
β : Cut-off ratio	1.5
γ : Air specific heat ratio	1.4
d_n : Injector nozzle diameter	0.16mm
N_h : Number of holes in the fuel injector	2
P_i : Ambient pressure	101.32kPa
T_i : Ambient temperature	293K
A : Filter cross-sectional area	0.05m
ΔP : Applied pressure difference	137kPa
Γ : Filtration resistance	$1.6 \times 10^{14} \text{m}^{-2}$
l/d : Equivalent length to pipe diameter ratio	250
μ_f : Dynamic viscosity of fuel	2.18Pa.s to 7.74×10^{-3} Pa.s
μ_g : Dynamic viscosity of gas	1.5×10^{-5} Pa.s
ρ_f : Density of fuel	853kg/m ³ to 879kg/m ³
ρ_g : Density of gas	1.21kg/m ³ to 4 kg/m ³
σ : Surface tension	0.03N.m

Step 2: The mean injection velocity (V_{in}) has been calculated from the fuel mass flow rate as per step 1 and injector geometry specified in Table 4-5

Step 3: The filtration constant (C), computed using equation 4-19 from filter parameters such as the filter area (A), applied pressure difference (ΔP), filtration resistance constant (Γ), volume of filter cake deposited by unit volume of filtrate (v). The fuel filter property has been presented in Table 4-5.

Step 4: The fuel flow rate has been calculated as a function of time and viscosity using equation 4-18.

Step 5: The velocity (u) has been computed from the pump geometry and engine operating conditions.

Step 6: The Reynolds number of the flow in the pump has been obtained using velocity calculated in step 5 and fuel physical properties presented in

Table 3-4 . Further, computation of the friction factor F_f from the Reynolds number by the relation discussed in equation 4-20 has been carried out.

Step 7: The friction head loss as function of viscosity and fuel flow rate has been obtained using equation 4-20 from the friction factor and fuel pump geometry which have been presented in Table 4-5.

Step 7: The Weber number and Reynolds number have been calculated using the

$$\text{equations: } We_l = \frac{V^2 D \rho_l}{\sigma} \text{ and } Re = \frac{u D \rho_l}{\mu_l}$$

Step 8: The sauter mean diameter (SMD) has been calculated using equation 4-21 from the parameters defined in step 7 and fluid properties which are given in Table 4-5.

Step 9: These predicted values obtained from the above have been compared with data available in this area.

Output parameters: The output parameters in fuel supply system model have shown the effects of density and viscosity of biodiesel on the fuel flow rate through filter(Q), the friction head loss of the pump(h_f) and sauter mean diameter(SMD). These effects have been quantified and are discussed below.

4.6 Effect of Density and Viscosity of Biodiesel on the Fuel Supply System Performance

This section describes the results obtained by using the mathematical models described in section 4.4 to quantify the effects of the biodiesel viscosity and density on the fuel filter; fuel pump and injection spray characteristics in the engine cylinder. The simulation results obtained from the model have been explained below. Figure 4-9 illustrates the variation of the fuel flow rate through the fuel filter as function of time for different values of kinematic viscosity representing various biodiesel blends. It can be seen that the fuel flow rate decreased with time in the fuel filter media.

This can be explained on the basis that at the start of filtration, the voids are active and the filtration rate is enhanced [183]. After a period of time, the numbers of active voids in the filter get reduced and the filtration rate became constant. Figure 4-10 also shows the effect of viscosity on the fuel flow rate through the fuel filter. It can be seen that when the

fuel viscosity increased, the fuel flow rate decreased. This could be attributed to a higher flow resistance encountered by highly viscous fluid. The fuel filter rate had direct effect on the fuel flow rate in the injector and hence the power produced by the engine. A higher viscosity meant a lower flow rate of fuel and lower engine power by the engine.

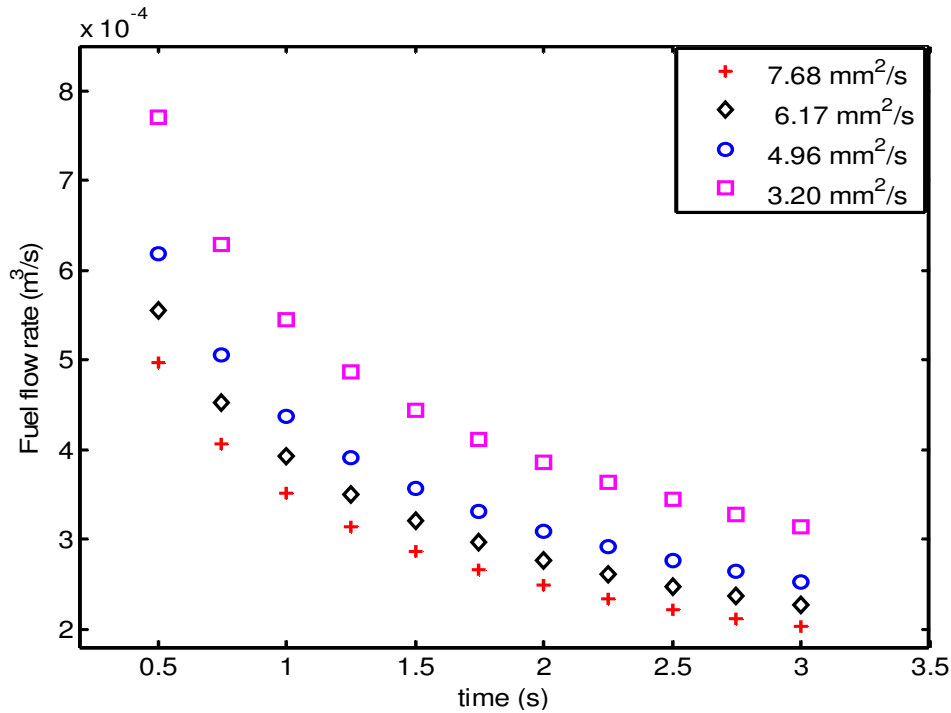


Figure 4-9 Flow rate of fuel through filter with time for different kinematic viscosity values

Figure 4-10 shows the fuel pump head loss versus the fuel flow rate of biodiesel and diesel fuel for different viscosity values. It can be seen that at a constant head, fuel with higher viscosity yielded a lower fuel flow rate than the fuel with a lower viscosity. A similar trend has been reported by Bannikov *et al.* [76]:

Figure 4-11 shows the relationship between the kinematic viscosity and sauter mean diameter (SMD) of fuel at different engine speeds. The SMD value of the fuel in combustion cylinder was determined by using a well-accepted model of Hiroyasu and Arai [184]. It can be seen that when the engine speed increased, the SMD of the fuel in the cylinder decreased.

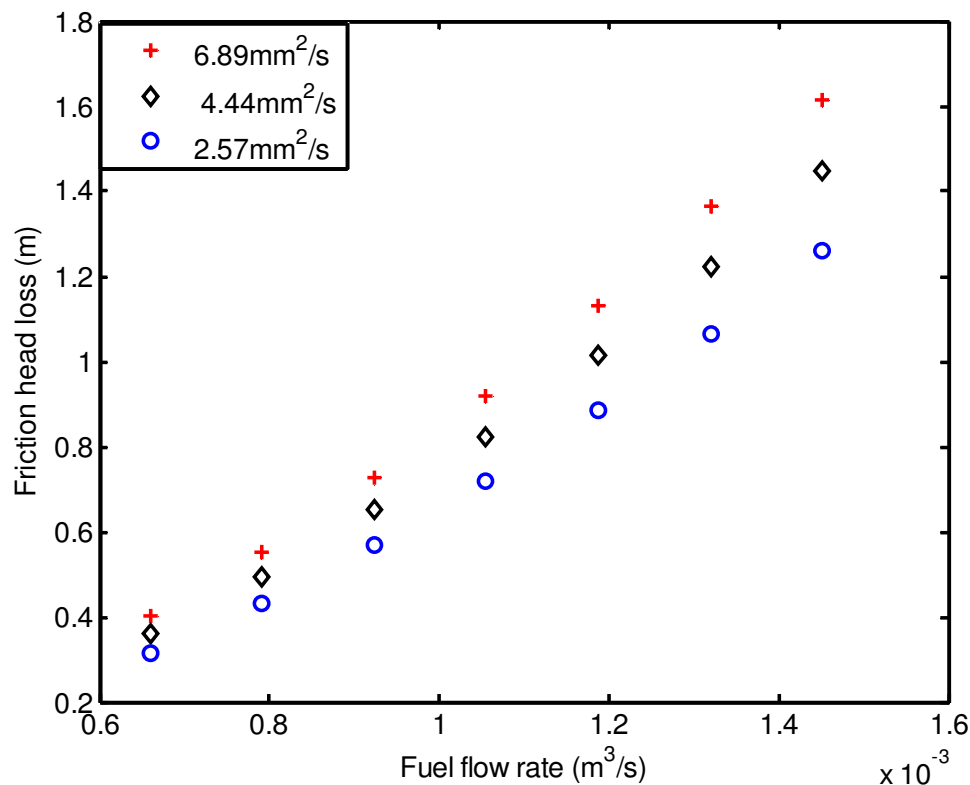


Figure 4-10 Variation of fuel pump head loss with fuel flow rate for various kinematic viscosity

The same trend had been reported by Hiroyasu [185]. It can also be seen that when the kinematic viscosity of the biodiesel increased, the SMD also increased proportionally. This could be explained on the basis that when the kinematic viscosity and surface tension of the fuel increased, the cohesion and the surface viscosity between fuel molecules increased [186]. As a result, the SMD of the fuel increased in the cylinder chamber. The increase in the SMD resulted in a reduced surface area of the fuel droplet. As a result, the tendency of evaporation of fuel decreased and this could have decreased the performance of the engine and increased the emissions. Geo *et al.* [78] compared the SMD corresponding to diesel, B5, B10, B20 and B100 of Jatropha oils blends. Their results showed that the SMD gradually increased with an increasing blend ratio of the biodiesel and the authors concluded that the kinematic viscosity was the major factor for this. The effect of kinematic viscosity of the biodiesel on the SMD has been reported by Geo *et al* and is shown in Figure 4-11. The reported values show the same trend with data as predicted in this study:

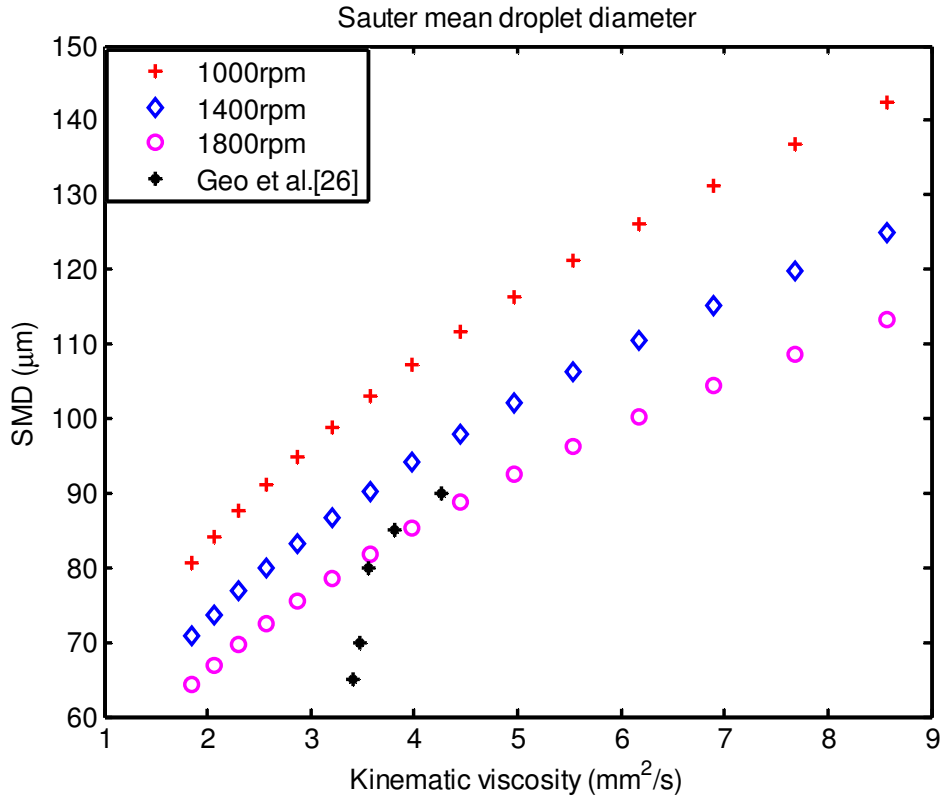


Figure 4-11 Variation of sauter mean diameter with kinematic viscosity using Hiroyasu and Arai Model [184]

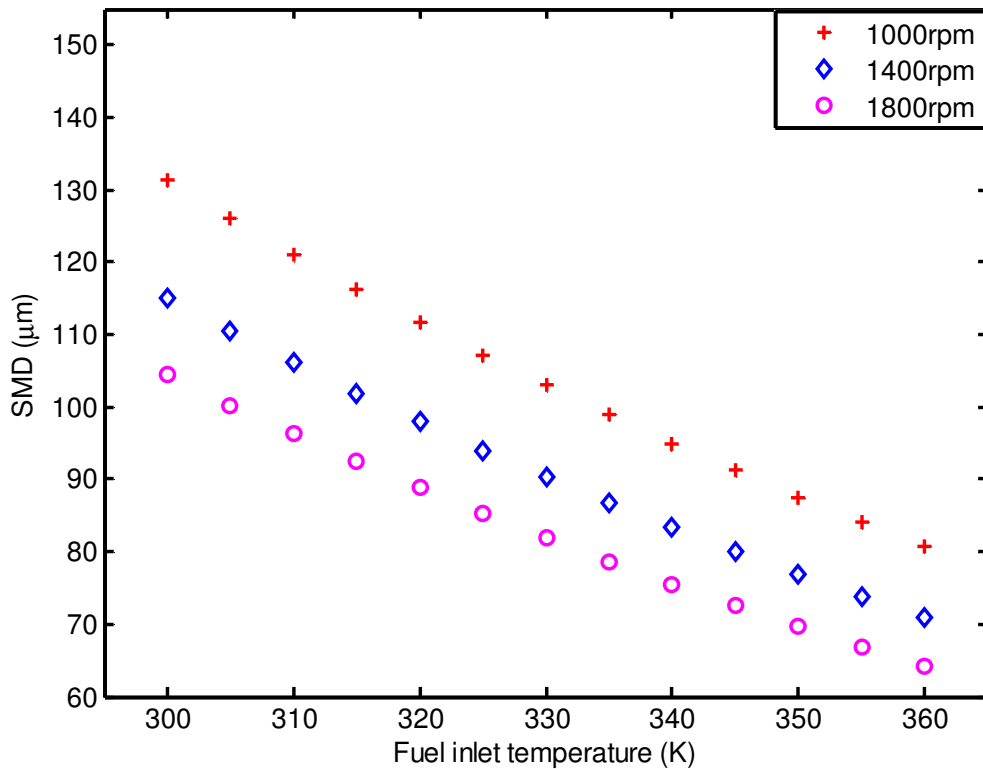


Figure 4-12 Variation of sauter mean diameters with temperature using Hiroyasu and Arai Model [184]

The same trend has been also reported by Park *et al.*[187] for a SMD variation for 20% ethanol blend biodiesel (BDE20) and 100% biodiesel (B100). Since BDE20 has lower kinematic viscosity than B100, the former has a lower SMD. Figure 4-12 illustrates the SMD of the biodiesel fuel versus injected fuel temperature for different engine speeds. It can be seen that the SMD of the biodiesel decreased with an increase in the injected fuel temperature. An explanation for this could be that when the temperature increased, the inter-molecular forces decreased. As a result, the SMD decreased in the engine cylinder. This facilitated the evaporation of the fuel and combustion rate in the engine cylinder.

4.7 Summary on Biodiesel Characterisation

In this chapter the effects of biodiesel fraction and temperature on the density, viscosity and LHV have been investigated. It has been noticed that the density and the viscosity of the biodiesel blends increase with increase of the biodiesel fraction. It is also seen that the density and viscosity of each blend decreases with increase in the temperature. The empirical equations to predict density, viscosity and LHV of the biodiesel and its blends as function of temperature have been developed. The empirical equations and the measured data are closely matched with acceptable error. This study models have been compared with previous models and the two models match closely. The comparison of the previous model and experimental results with new models which are presented from equation 4-1 to equation (4-11) validate that the new density prediction model can be used in prediction of density, viscosity and lower heating value of biodiesel blends.

In the second section numerical simulations have been carried out on fuel supply system using the characteristics of the biodiesel obtained from the experimental work. From numerical simulation it can be seen that the density and viscosity of the biodiesel affect the performance of the fuel supply system including the fuel pump, fuel filters and air-fuel mixing behaviour considerably. It has been seen that when the density and viscosity of the biodiesel increase the fuel pump head loss also increased and the flow rate of the fuel in filter reduced. A further noticeable effect was that the higher density and viscosity of biodiesel resulted in an increase in the sauter mean diameter of the spray droplet in combustion chamber. In next chapter the effects of the physical properties of biodiesel and its blends on the CI engine performance and emission have been investigated experimentally during steady state operations.

CHAPTER FIVE

5. PERFORMANCE AND EMISSION CHARACTERISTICS OF A CI ENGINE RUNNING WITH BIODIESEL BLENDS DURING STEADY STATE

The main aim of this chapter is to investigate the combustion, performance and emission characteristics of a compression ignition engine running on biodiesel and its blends during steady operating conditions. As per the previous review a lot of research has been carried out on the use of biodiesel in CI engines during steady state conditions. However, the researchers have not reported in detail the effects of biodiesel physical properties which have been discussed in Chapter four. In addition, to understand the transient combustion, performance and emission characteristics, the understanding of these characteristics during steady state operation are very important. Having these two objectives, the performance and emission characteristics of CI engine fuelled with different biodiesel blends have been investigated. Results are presented for all test conditions and attempts have been made to highlight the effects of different biodiesel physical properties and blends on the in-cylinder pressure, brake specific fuel consumption, thermal efficiency and emissions (CO₂, NO_x, CO, THC) during steady state operation. These effects have been discussed based on the experimental results obtained from the test CI engine. For each parameter, the effect of biodiesel content and its properties have been quantified.

5.1 In-Cylinder Pressure and Heat Release Rate of the CI Engine

The in-cylinder pressure measurement is considered to be a very valuable source of information during the development and calibration stages of the engine. The in-cylinder pressure signal can provide vital information such as peak pressure, P-V diagram, indicated mean effective pressure, fuel supply effective pressure, heat release rate, combustion duration, ignition delay and so on [188] [169]. Moreover, based on ideal gas and first law of thermodynamics it can be used in more complex calculations for example in air mass flow estimation, combustion diagnosis and NO_x prediction [188], [189]. In this section the P-V diagram, in-cylinder pressure variation with crank angle and the heat release rate variations for the test CI engine running with diesel and rapeseed biodiesel at 50B and 100B have been compared and discussed. The 50B blend has been used in this investigation to understand the effects of biodiesel blend on the combustion characteristics.

Figure 5-1 depicts the P-V diagram obtained from the measurements on the test compression ignition engine, which was obtained at an engine speed 1300 rpm and at 105, 210, 315 and 420Nm engine load conditions. The P-V diagram clearly shows the intake, compression, power and exhaust strokes. The results highlight that the power produced by the engine cylinder and calculated from the P-V diagram do not show any significant change for the different fuels, namely 50B, 100B and pure diesel at different engine loads of 105Nm, 210Nm, 315Nm and 420Nm. The maximum percentage difference between the power output of the CI engine running with diesel, 50B and 100B is less than 2% at 1300rpm and 210Nm. This indicates that the loss in power because of biodiesel's lower heating value is compensated by larger brake specific fuel consumption [9],[44],[94] .

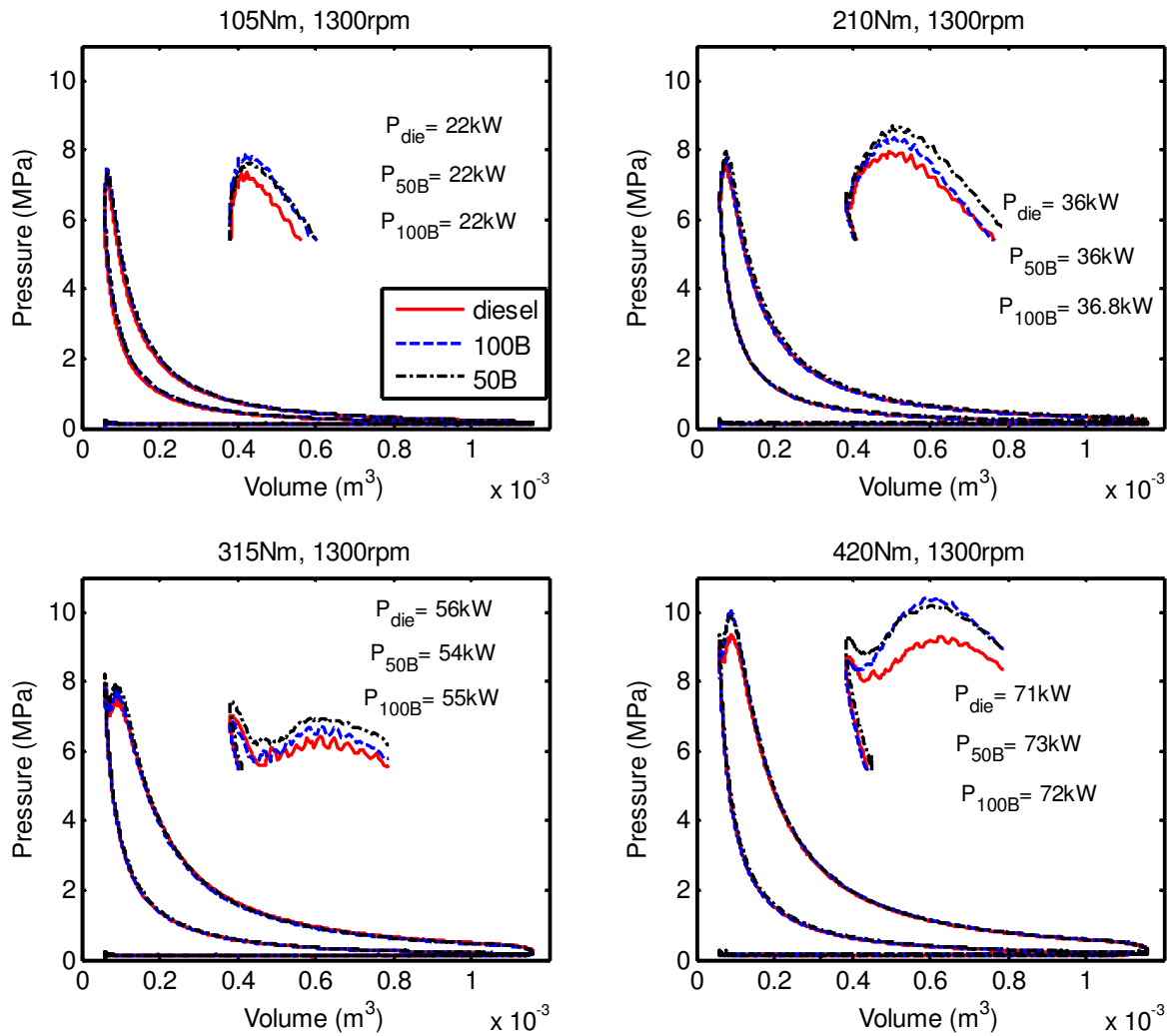


Figure 5-1 P-V diagrams for CI engine running with diesel and biodiesel blends at speed of 1300rpm and range of engine loads

Figure 5-2 shows the variation of in-cylinder pressure within the combustion chamber of the test CI engine with crank angle when running with 50B, 100B and normal diesel fuels at a speed of 1300 rpm and at different engine loads of 105Nm, 210Nm, 315Nm and 420Nm. The figure shows only part of combustion or power stroke section in stroke cycles. The figures depict that the peak cylinder pressure of the engine running with 50B and 100B is higher than the engine running with diesel by 4.5% and 3.4% at 420Nm respectively. For the rest of the load conditions, the difference is below 3%. The main reason for a higher in-cylinder pressure in the CI engine running with biodiesel is due to the advanced combustion process being initiated by the easy flow-ability of biodiesel and its other relevant physical properties such as viscosity, density and bulk modulus as claimed by Qi et al. [9].

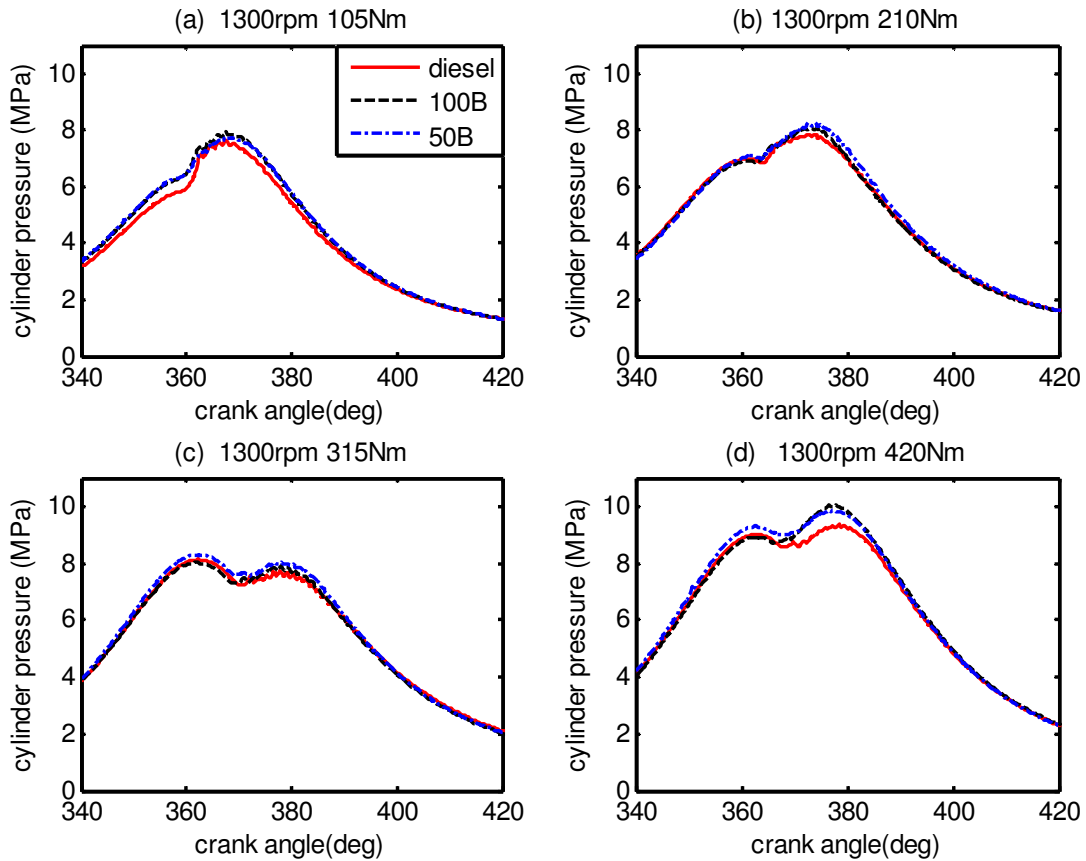


Figure 5-2 Variation of in-cylinder pressure with crank angel for CI engine running with 50B, 100B and diesel at engine speed of 1300rpm and range of engine loads

The cumulative effects of these properties result in a short ignition delay and advanced injection timing for biodiesel. Furthermore, due to the presence of oxygen molecules in biodiesel, the hydrocarbons have achieved complete combustion [121], [190], [125] resulting in a higher in-cylinder pressure. Similar trends have been reported by Qi *et al.*[9]. Gumus[83] however reported that the engine running with diesel resulted in higher in-cylinder pressure than that of biodiesel blends due to high viscosity and low volatility of the biodiesel which leads to poor atomization during the ignition delay period. Qi *et al.*[9] have argued that the higher viscosity and lower volatility can be compensated by the complex and rapid pre-flame chemical reactions at higher temperatures which result in cracking and creating of lighter biodiesel compounds. These compounds can result in earlier ignition.

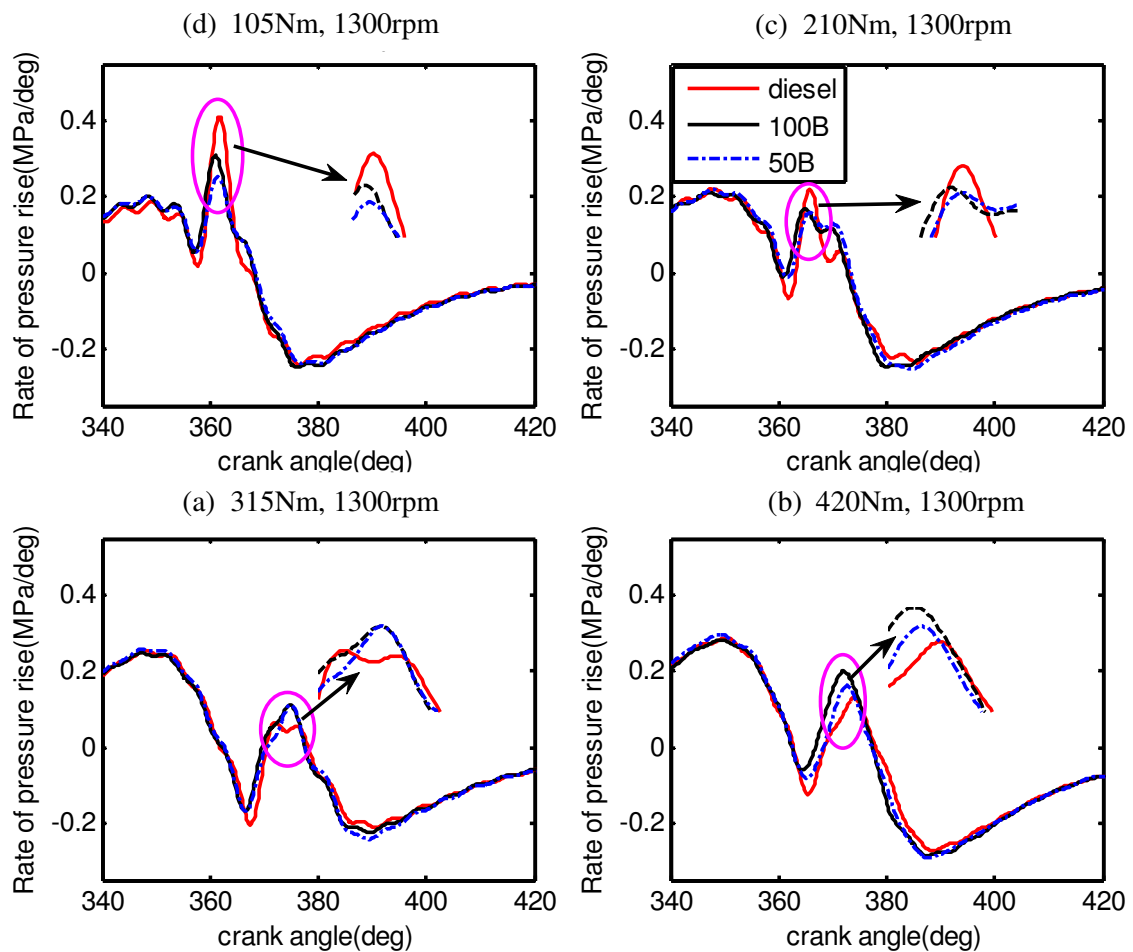


Figure 5-3 Variation of rate of in-cylinder pressure increase with crank angle for CI engine running with 50B, 100B and diesel at engine speed of 1300rpm and range of engine loads

The Variation in the rate of pressure rise with crank angle for diesel and biodiesel blends at different engine loads are shown in Figure 5-3. It can be seen that at a lower engine load the rate of pressure rise for diesel is slightly higher than for biodiesel. The reason is at this operating condition, a very small quantity of fuel is injected into the combustion chamber and combustion starts after TDC. However, the rate of pressure rise is higher for biodiesel at higher engine loads. This is due to the higher rate of heat release during premixed combustion phase as explained in the next section.

Heat release rate is one of the most important parameters to characterise the combustion process in compression ignition engine. Using the heat release rate diagram, it is possible to determine the ignition delay time, start of ignition and the peak heat release. The heat

release can be computed by using first law of thermodynamics and ideal gas laws as described in chapter two.

Figure 5-4 depicts that the heat release rates for a CI engine running on biodiesel blends and normal diesel, for a speed of 1300 rpm, and at different load values of 105Nm, 210Nm, 315Nm and 420Nm. The engine running with diesel and biodiesel blends shows the same combustion stages at all load conditions except the slight variation of the peak heat release rate and ignition delay. Because of the vaporization of the fuel accumulated during ignition delay, at the beginning the curve a negative heat release is observed and after combustion is initiated, the heat release values become positive [9].

As it is shown in Figure 5-6 the ignition of the biodiesel fuel has started earlier than the diesel fuel running with diesel fuel by 0.8deg, 1deg, 1.5deg and 1.2deg for 105Nm, 210Nm, 315Nm and 420Nm load conditions. Gumus[83] also reported that the start of ignition for biodiesel made of hazelnut kernel oil methyl ester was advanced by up to 1.65deg. The advanced start of ignition is attributed to the physical properties of the biodiesel such as higher bulk modulus[52], [77], [81],[191], [192], higher viscosity [34], [191], [193] and higher cetane number[102], [112]. Further it can be seen that at lower load conditions the test CI engine running on diesel has a higher peak heat release rate than the biodiesel by 4%. At higher load conditions the engine running on biodiesel blends have higher heat release rates than when running on diesel. This phenomenon is attributed to the presence of additional oxygen molecules in biodiesel fuel[9], [112], [128], [135], [131], which results in the air-mixed fuel in the cylinder burning completely and increasing the heat release rate.

The cumulative heat release is the other parameter, which shows the total heat released during the combustion stage. The cumulative heat values obtained from the experiments on engine running with diesel, 50B and 100B are shown in Figure 5-7. It can be seen that 50B resulted in higher cumulative heat release as compared to the diesel by 4%, 3%, 2.5% and 3.5% for different load values of 105Nm, 210Nm, 315Nm and 420Nm respectively. This is due to the dual effects of the complete combustion because of presence of the oxygen molecules in biodiesel and the higher heating value of 50% diesel as compared to 100B [83].

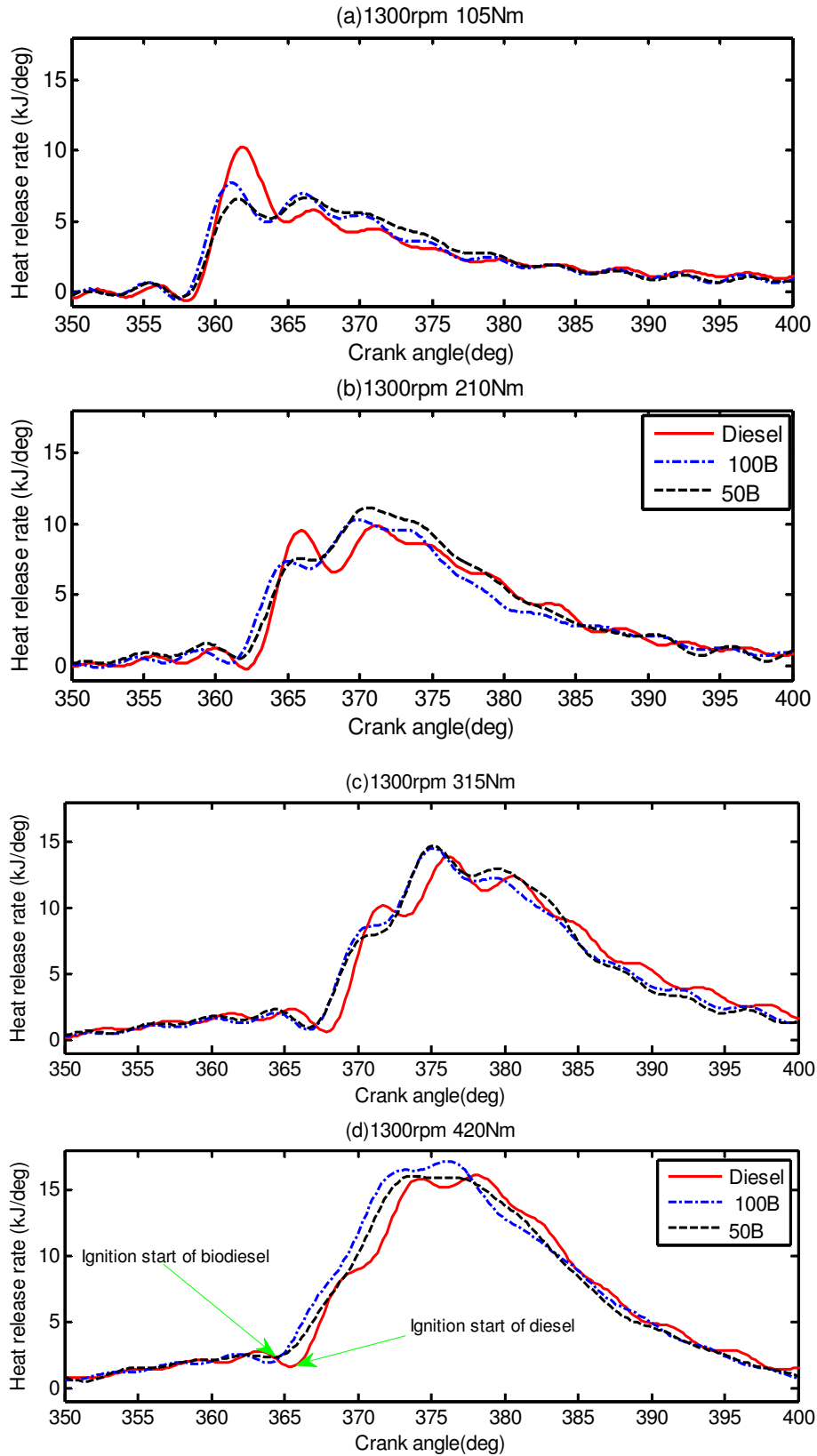


Figure 5-4 Variation of heat release rate with crank angle for CI engine running with 50B, 100B and diesel at engine speed of 1300rpm and range of engine loads.

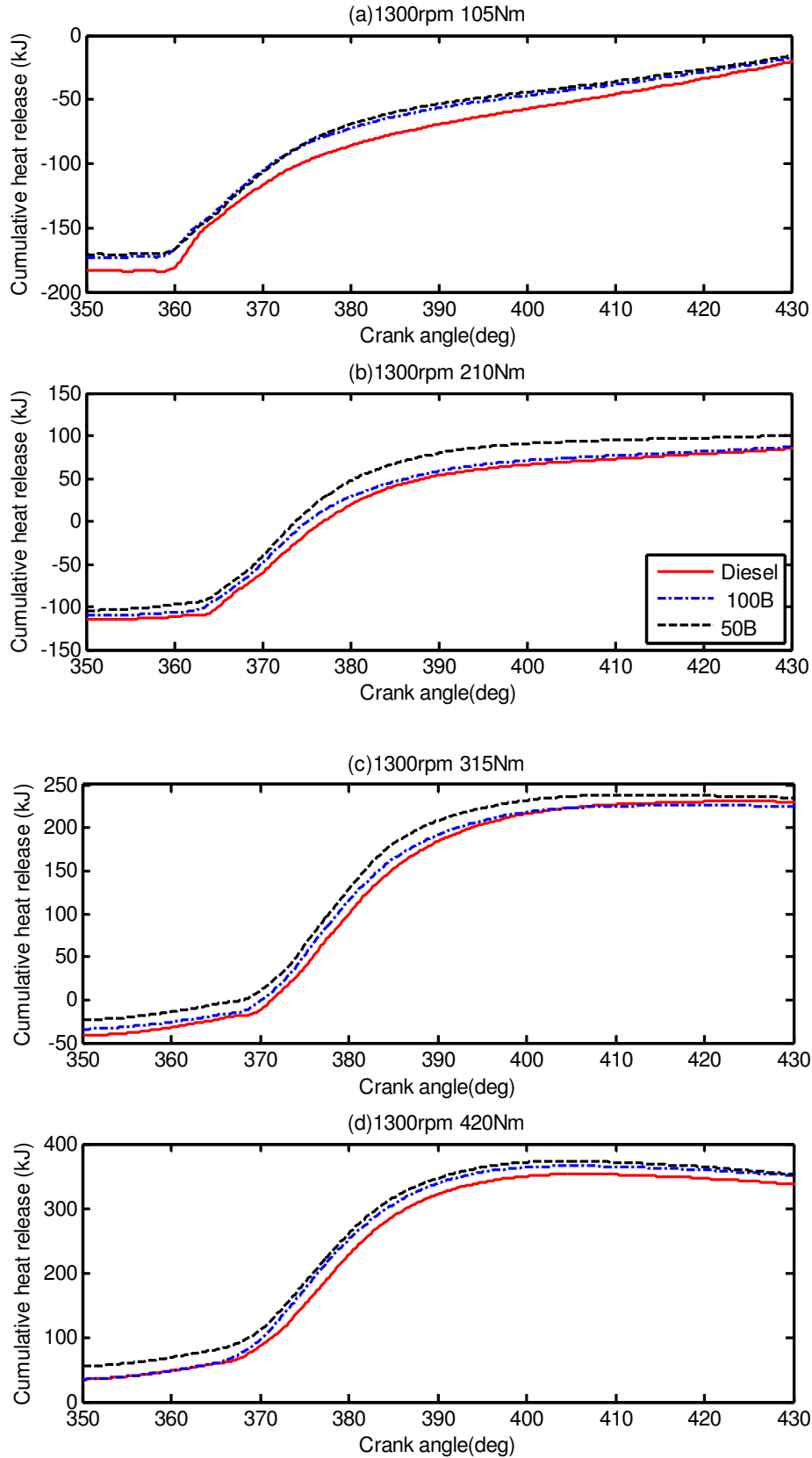


Figure 5-5 Variation of cumulative heat release rate with crank angle of CI engine running with 50B, 100B and diesel at engine speed of 1300rpm and range of engine loads

5.2 Performance Characteristics of the Test CI Engine Running with Biodiesel Blends during Steady State Operating Condition

In this section the engine performance characteristics have been evaluated based on experimental observations using different operating parameters. The common parameters used to evaluate engine performance are: the peak in-cylinder pressure, brake specific fuel consumption and the thermal efficiency. In the following, the effects of the feed stock, blend fractions, density, viscosity and heating value of the biodiesel have been investigated on the engine's in-cylinder pressure, brake specific fuel consumption and thermal efficiency as well as exhaust emissions (CO₂, NO_x, CO, THC and O₂).

5.2.1 Effects of Biodiesel Feedstock Sources on the Engine Performance Parameters

The overall scope of feedstock sources for biodiesel production becomes much broader over time. The most common biodiesel sources are edible oil such as rapeseed oil, corn oil, palm oil, and soybean oil [194]. In this study, two categories of biodiesel were investigated: biodiesel from 'virgin' vegetable (rapeseed oil (ROB) and corn oil biodiesel (COB) oil, and waste cooked oil (waste oil biodiesel (WOB)). The aim of this investigation was to establish whether biodiesel source has any effect on performance obtained from a biodiesel. The peak in-cylinder pressure, brake specific fuel consumption and thermal efficiency behaviour of the three biodiesels are presented here.

The peak in-cylinder pressure of a CI engine running on diesel, ROB, COB and WOB, at a load of 420Nm and over a wide range of engine speeds, is shown in Figure 5-6(a). It can be seen that the in-cylinder pressure increased slightly with increasing engine speed. This is due to an increase in air/fuel ratio with engine speed increment. Figure 5-6(b) shows the in-cylinder pressure deviation observed for the data on ROB, COB and WOB from the data on diesel. It can be observed that the peak in-cylinder pressure corresponding to COB and ROB are higher than normal diesel by 1.3%. The engine running with the ROB and COB did not show any significant difference in peak in-cylinder pressure values. However, the engine running on WOB showed an inconsistent variation in in-cylinder pressure across the range of engine speeds.

Figure 5-7 shows the variation in the brake specific fuel consumption (BSFC) of the engine running on ROB, WOB, COB and normal diesel against engine speeds at two different loads

of 105Nm and 420Nm. The BSFC has been estimated from the brake power output of the engine and the mass flow rate of the fuel. At both load conditions, the BSFC has been seen to be higher at lower engine speeds. It then decreases with engine speed to a minimum value, eventually increasing again with engine speed.

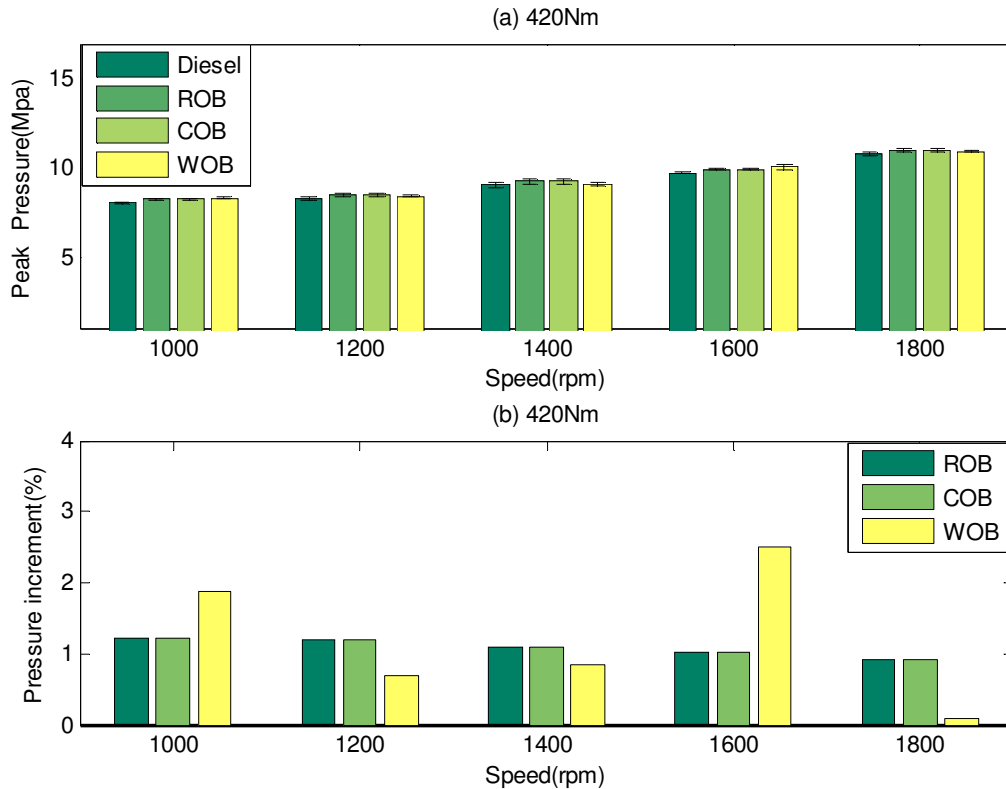


Figure 5-6 Variation of peak in-cylinder pressure with engine speed for CI engine running with ROB, COB, WOB and diesel at load of 420Nm

This can be explained on the basis that, at low speeds, heat loss from the combustion chambers walls is proportionately greater and combustion efficiency is poorer, resulting in higher fuel consumption for the power produced. At higher speeds, the friction power increases at a rapid rate, resulting in a slower increase in power than in fuel consumption with a consequent increase in BSFC [195]. Pal *et al.* [99] and Hazar [121] also reported similar trends for BSFC and engine speed dependence. At a lower load (105Nm), the engine achieved its minimum BSFC between 1000-1200rpm. However, at the maximum load (420Nm), the engine reached its minimum BSFC between 1200-1400 rpm for all fuel types.

Figure 5-7 also depicts the comparison of the engine's BSFC when fuelled with biodiesels and normal diesel. It can be seen that the BSFC of the biodiesel was higher than the diesel by up to 15% at lower engine load and up to 7% at the higher engine load. Lapuerta *et al.*[44]

have also reported that, the BSFC of the engine running with neat biodiesel was higher than that of engine running with diesel by up to 18%. The increment of BSFC of the biodiesel compared to diesel is mainly due to the low heating value of the biodiesel as claimed by previous authors [34], [88], [89], [92-94] and discovered by the author in this study. Some authors have also explained the increase in the BSFC in relation to the higher density and viscosity of the biodiesel [32], [97], [98], [100]. In the lower heating value analysis, the heating value of the biodiesel was lower than the diesel by 11.1%. The BSFC of the engine running on ROB, COB and WOB did not show any significant differences in BSFC values. The maximum difference in BSFC values corresponding to ROB, COB and WOB was limited to 1.25% for an engine speed of 1900rpm and load of 105Nm.

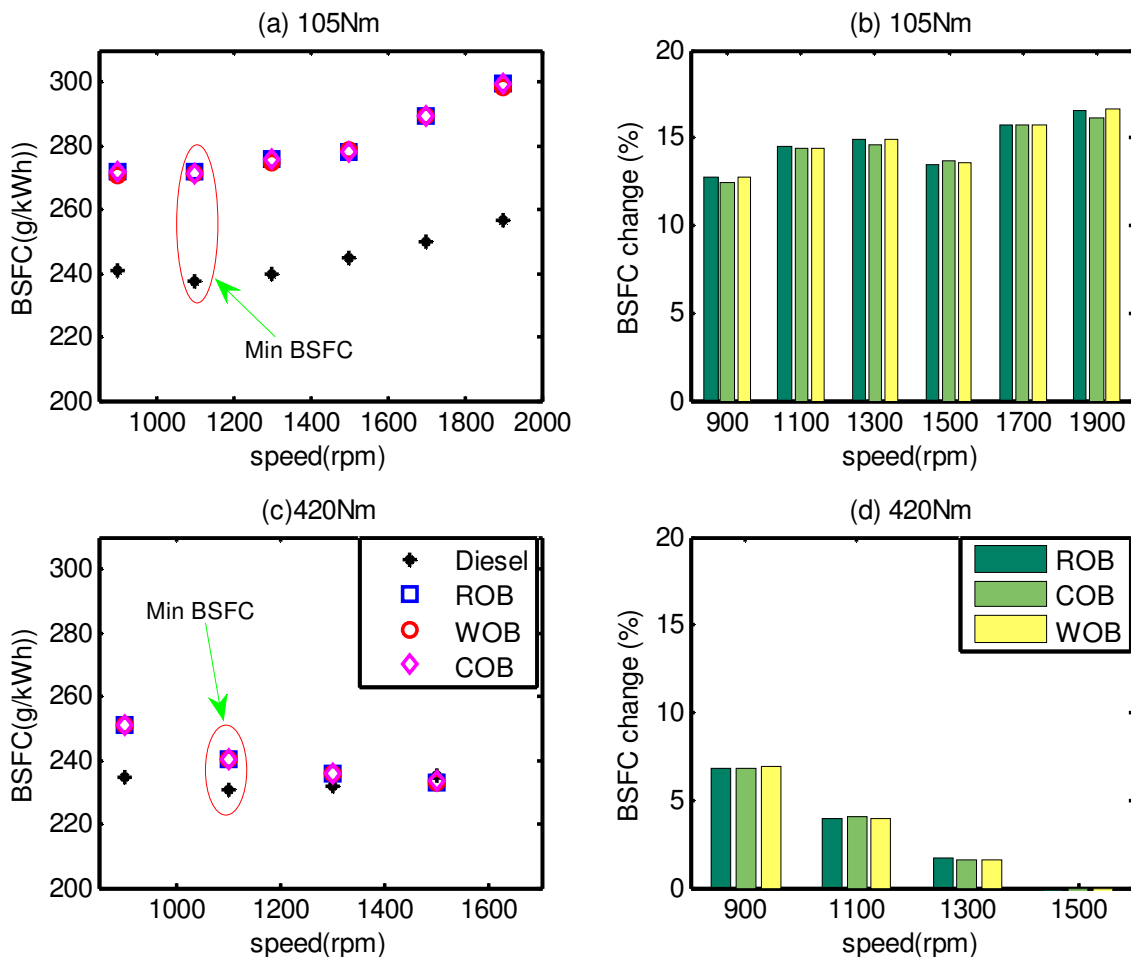


Figure 5-7 Variation of brake specific fuel consumption (BSFC) with engine speed of CI engine running with ROB, COB, WOB and diesel at load of 105Nm and 420Nm

Furthermore, the thermal efficiency of the engine has been computed from the BSFC and heating values of the COB, ROB, WOB and diesel using equation (5-1), for different engine speeds at two load conditions (105Nm and 420Nm). The result is presented in Figure 5-8:

$$\eta = \frac{3600}{BSFC \times LHV} \times 100 \quad (5-1)$$

Where η is the thermal efficiency (%), $BSFC$ is brake specific fuel consumption (g/kWh) of the biodiesel and LHV is lower heating value (kJ/kg) of the biodiesel.

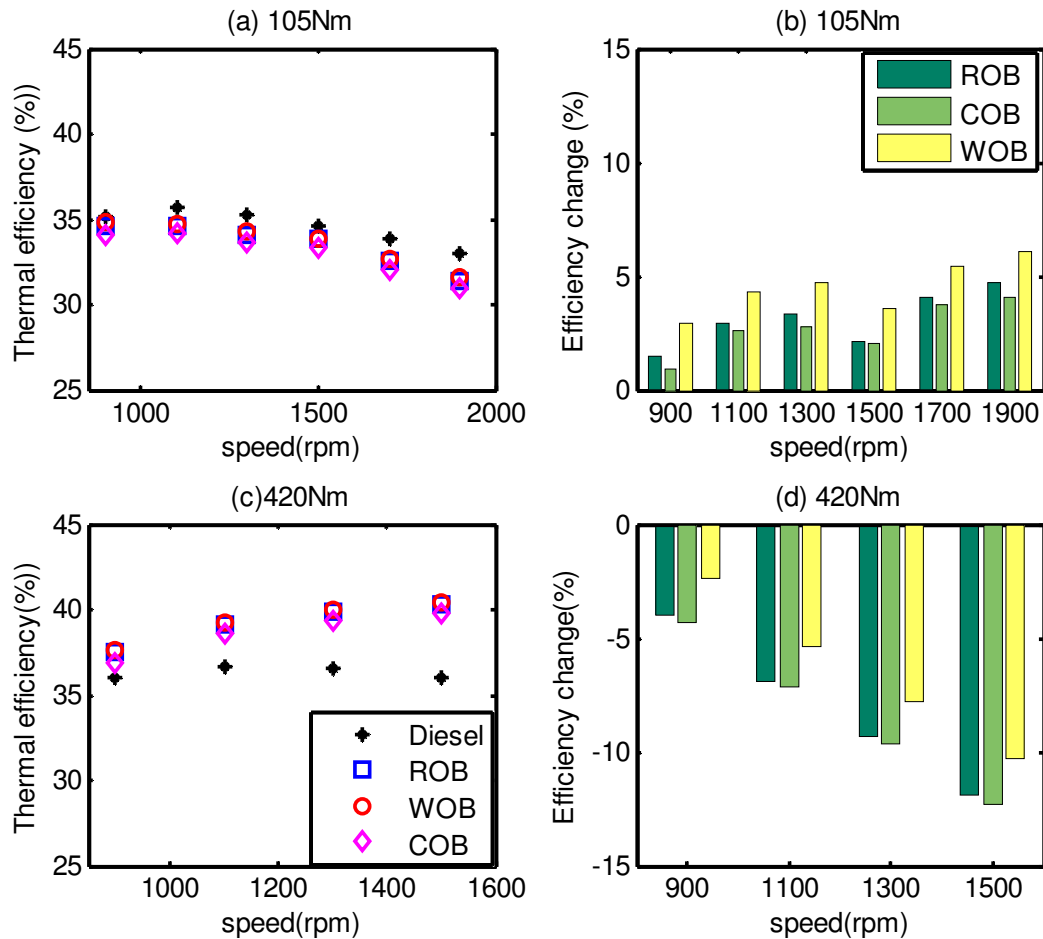


Figure 5-8 Variation of thermal efficiency with speed for CI engine running with ROB, COB, WOB and diesel at load of 420Nm

Since the brake thermal efficiency is inversely proportional to BSFC, the trends observed are opposite to that obtained for BSFC of the fuel. It can be observed from Figure 5-8(b), that at low loads, the engine brake thermal efficiency when using diesel is higher than the brake thermal efficiency when using biodiesel by approximately 5%. However, at the maximum engine load, the engine fuelled with biodiesel achieves higher thermal efficiency than the engine fuelled with diesel, with maximum increment of 12.3%. As per Lapuerta *et al* [44] review, 80% of the authors reported that engines fuelled with diesel and biodiesel resulted in

the same thermal efficiency. Our work has however shown that the trends are mixed and depend on engine operating conditions.

The brake thermal efficiency of the test engine when running with ROB and COB showed insignificant differences in thermal efficiency values at both lower and higher engine loads. However, the brake thermal efficiency of WOB has been seen to be higher than the ROB and COB by 1.51% and 1.9% at 105Nm, respectively. At the maximum load, the brake thermal efficiency of the WOB was lower than the ROB and COB by 1.69% and 1.86%, respectively. Graboski *et al.* [123] also tested a large number of methyl esters from different feedstock's and reported that neither the oil origin, the length of the carbon chain, nor the number of the double bonds provided significant differences in thermal efficiency.

As it is mentioned in chapter 4, the three biodiesels were produced by the same transesterification process. In this study, the biodiesel source was varied by source location (soil type and climate variation). The biodiesel production processes, however, were controlled and identical. As discussed in chapter 4 the three biodiesels have almost similar density, viscosity and heating values with differences limited to 5%. It can be concluded from the study that the biodiesel feedstock does not have significant impact on the performance of the biodiesel.

5.2.2 Effects of Biodiesel Feed Sources on the Engine Emission Parameters

One of the benefits of using biodiesel as alternative fuel is its capability of reducing the pollutant emission to the environment. In this section the emission characteristics of the test CI engine running with diesel, ROB, COB and WOB have been investigated. The main exhaust emission analysed in the present investigation are carbon dioxide (CO₂), carbon monoxide (CO), nitrogen oxides (NO_x), total hydrocarbon (THC) and oxygen(O₂). The CO₂ emission values of the CI engine running on ROB, COB, WOB and diesel fuel at a 420Nm load and at a range of engine speeds are shown in Figure 5-9(a). The ROB, COB, WOB and diesel resulted in maximum CO₂ emissions of 4.85%, 4.74%, 4.80% and 6%, respectively. As seen in Figure 5-9(b), the CI engine running on biodiesel emitted lower CO₂ than when running on diesel by 17%. Comparing the three biodiesels ROB, COB and WOB, it can be seen that each fuel emitted almost equal amounts of CO₂. Similar results have been reported earlier [44], [30], [32], [91]. However, some others have reported that the engine fuelled by biodiesel fuels emit higher CO₂ [91], [94], [96], [196]. Some investigations in the past have also shown same value of CO₂ emission [98], [111].

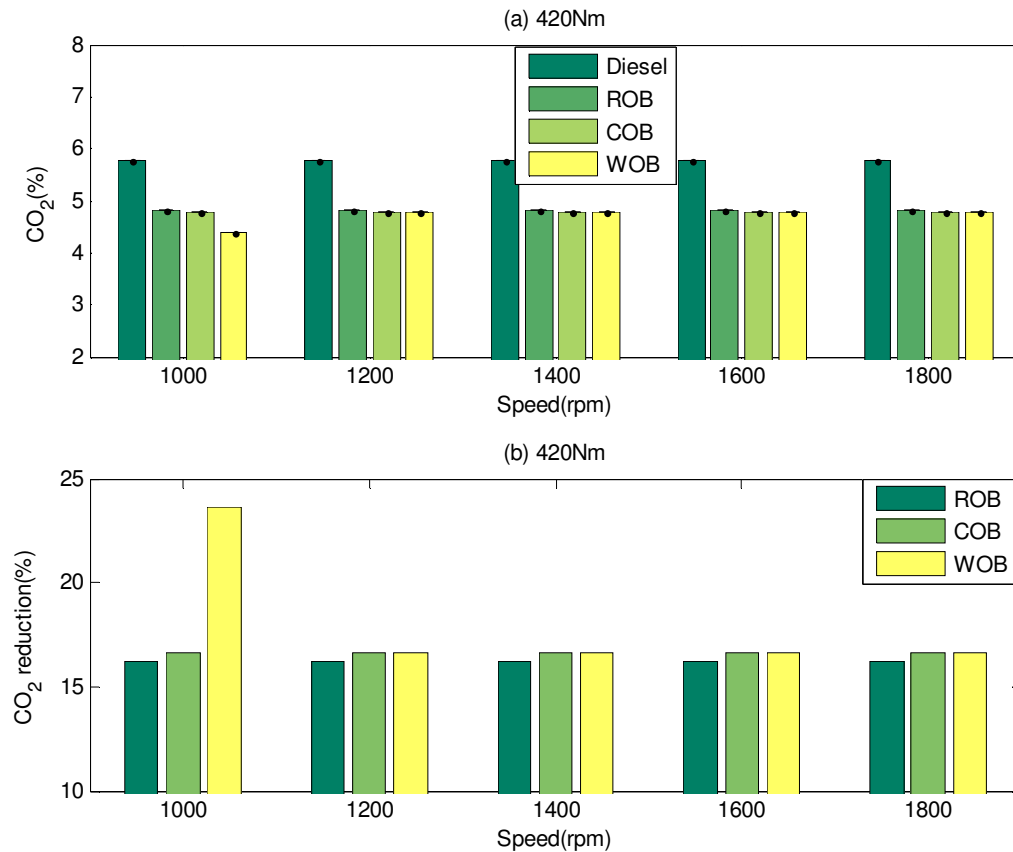


Figure 5-9 Variation of CO₂ emission of CI engine running with ROB, COB, WOB and diesel at load of 420Nm

Figure 5-10 (a) depicts the NO_x emissions of the test CI engine running on the ROB, COB, WOB and diesel. The corresponding maximum engine emission values were observed to be 1350ppm, 1355ppm, 1340ppm and 1040ppm, respectively, at a load of 420Nm over the engine speed range of 1000-1800 rpm. From Figure 5-10, it is apparent that the NO_x emissions increased with increase in the engine speed. This can be primarily due to an increase in volumetric efficiency and gas flow motion within the engine cylinder under higher engine speeds and higher load operating conditions, which led to a faster mixing between fuel and air and hence shorter ignition delay [50],[97]. The ROB, COB and WOB resulted in higher NO_x emissions than the normal diesel by up to 27%, as shown in Figure 5-10(b). This phenomenon is due to the resulting advanced injection because of influence of physical properties of biodiesel, such as viscosity, density, compressibility and sound velocity [44], [77], [89], [91]. Some researchers argue that the main cause of NO_x increase with biodiesel use is the increased cetane number [89], [130] which leads to an advanced combustion by shortening the ignition delay and the higher availability of oxygen [44], [91], [130], which in turn promotes NO_x formation. However, when comparing the NO_x emission of ROB, COB

and WOB, no significant differences in the NO_x emission are apparent. The standard deviations values have been indicated with the mean value of the NO_x emission for each condition. The maximum standard deviation was computed to be 15ppm at 1800rpm.

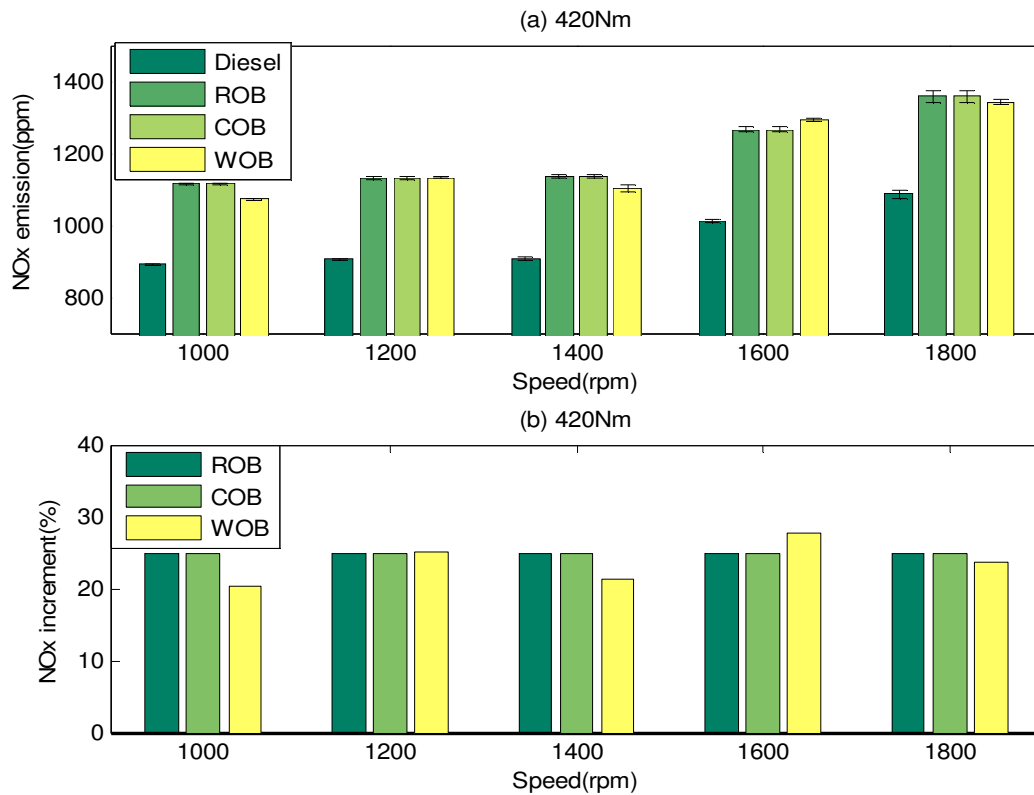


Figure 5-10 Variation of NO_x emission with engine speed for CI engine running with ROB, COB, WOB and diesel at load of 420Nm and range of engine speeds

The histogram shown in Figure 5-11(a) depicts the THC emission of CI engine running with ROB, COB, WOB and diesel at a load of 420Nm over a speed range of 1000-1800 rpm. From the figure, it can be seen that the THC emission decreased with an increase in engine speed. This may be due to better air-fuel mixing process and/or the increased fuel/air ratio at higher engine speeds [111], [9], [122]. The two 'virgin' biodiesels i.e. ROB and COB did not show any significant differences in THC emission values. However, the engine running on these two biodiesel has a reduced THC emission value by 28%, as compared to the neat diesel, as shown in Figure 5-11(b). The WOB use also reduced the THC; however the reduction was only about 5% as compared to diesel. The standard deviations of the measurements are indicated along with the mean value of the THC emission for each condition in the figure. The maximum standard deviation has been computed to be 2ppm at 1800rpm.

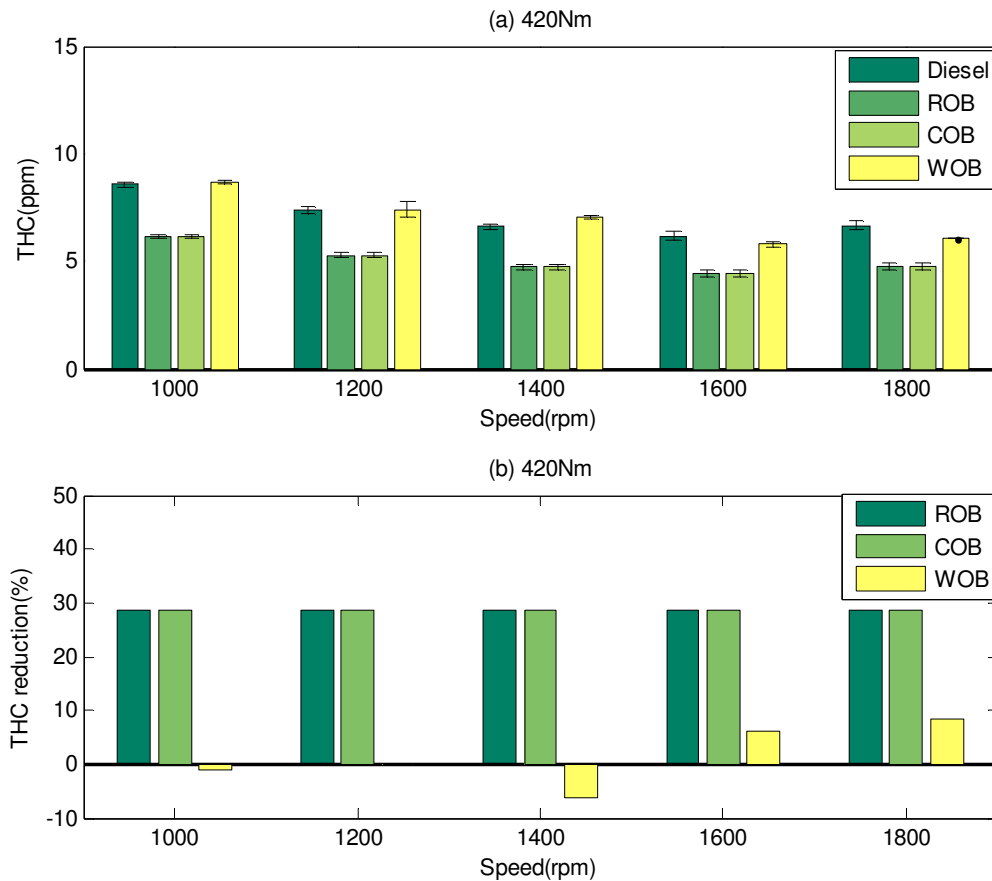


Figure 5-11 Variation of THC emission with engine speed for CI engine running with ROB, COB, WOB and diesel at load of 420Nm

Figure 5-12(a) presents the CO emission for the engine running with ROB, COB, WOB and diesel at a load of 420Nm over an engine speed range of 1000-1800 rpm. In Figure 5-12, a clear trend can be seen that CO emission decreases with increasing engine speeds. This is because when the engine speed increases, the air-fuel mixing process may become more intensive and a higher fuel/air equivalence may have resulted in enhancing the conversion of CO to CO₂ [9],[111], [122]. The CO emission of the neat biodiesel was lower than that of the diesel by 28%, as indicated in Figure 5-12(b). However, comparing ROB, COB and WOB, the three neat biodiesels did not show any significant differences in CO emission. The standard deviations of the measurements are indicated with the mean value of the CO emission for each condition, having a maximum standard deviation of 3.5ppm.

The above discussion has clearly indicated the biodiesel source does not affect the engine performance and as long as physical properties are similar we can expect same performance and emission characteristics from the engine. The next section is therefore focussed on investigation with one of the biodiesel used (ROB) for detailed analysis and in this

investigation the fuel properties have been varied by blending diesel with biodiesel in different proportions.

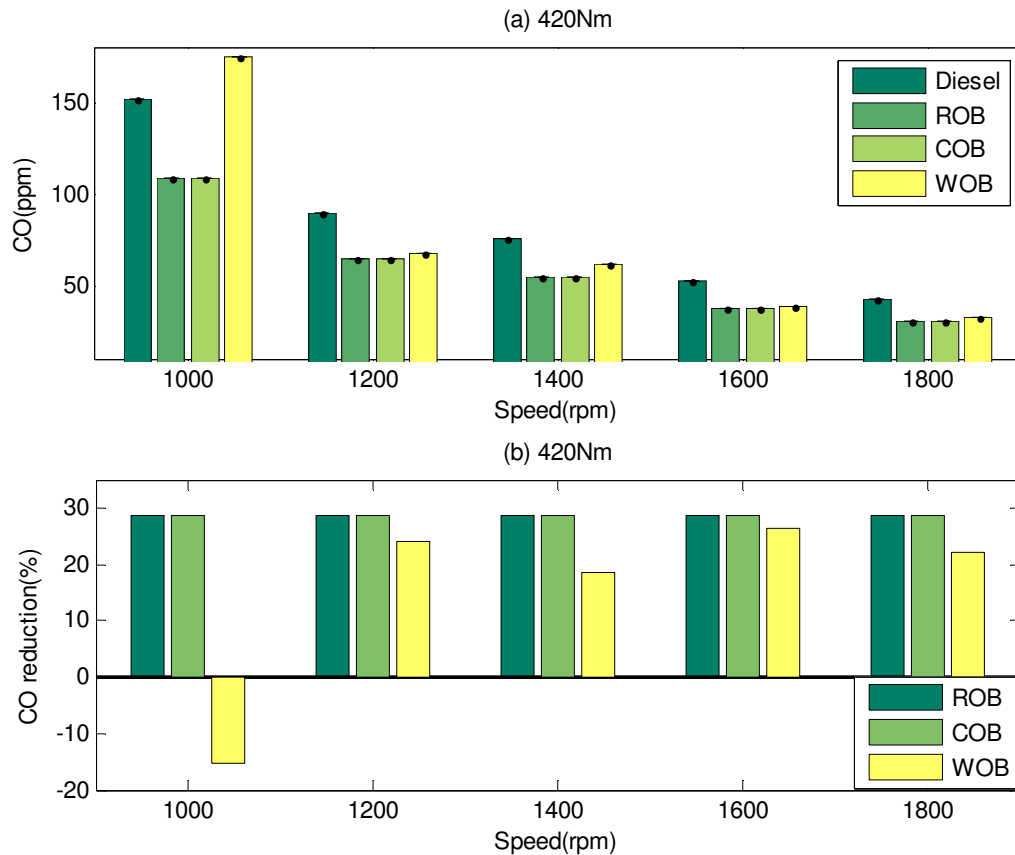


Figure 5-12 Variation of CO emission with speed for CI engine running with ROB, COB, WOB and diesel at a load of 420Nm

5.2.3 Effects of Biodiesel Blend Fraction on Engine Performance Parameters

Currently, biodiesel is used as a fuel in different proportions (as neat biodiesel (100B) and different blends). In this study, diesel, 10B, 20B, 50B and 100B blends have been used for analysis. Considering the wide application of ROB biodiesel in European countries, detailed investigation has been carried out on the performance and emission characteristics of the test CI engine running with various ROB blends. The blends were prepared from rapeseed biodiesel and diesel as per procedure mentioned in the section 6.1. The in-cylinder pressure, brake specific fuel consumption and thermal efficiency of the CI engine have been evaluated when running with different biodiesel blends at various operating conditions.

Figure 5-13 presents the peak in-cylinder pressure of the CI engine fuelled with the biodiesel blends at 420Nm over a wide range of engine speeds. It can be seen that the peak in-cylinder pressure increases consistently with increasing engine speeds. The peak in-cylinder pressure

also increased with increasing biodiesel fraction. The neat biodiesel resulted in a maximum in-cylinder pressure (14% more than diesel).

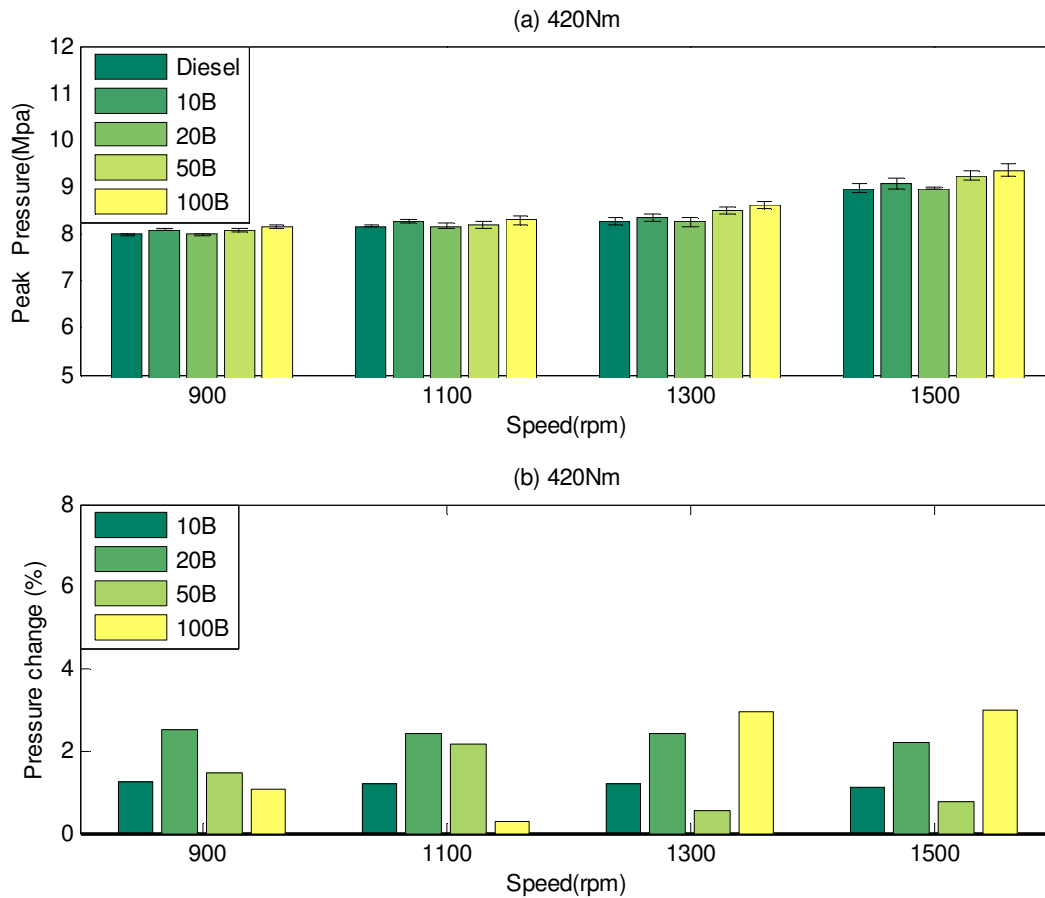


Figure 5-13 Variation of in-cylinder pressure with speed of CI engine running with biodiesel blends at load of 420Nm

Figure 5-14 shows the BSFC obtained for different biodiesel blends over a range of engine speeds and at two engine loads of 105Nm and 420Nm. It can be clearly seen that at lower engine speeds, the BSFC is higher which then decreases to a minimum point, and increases again with the engine speeds (see Figure 5-14(a)). The effects of engine speed on BSFC have been discussed in detail in section 5.2.1.

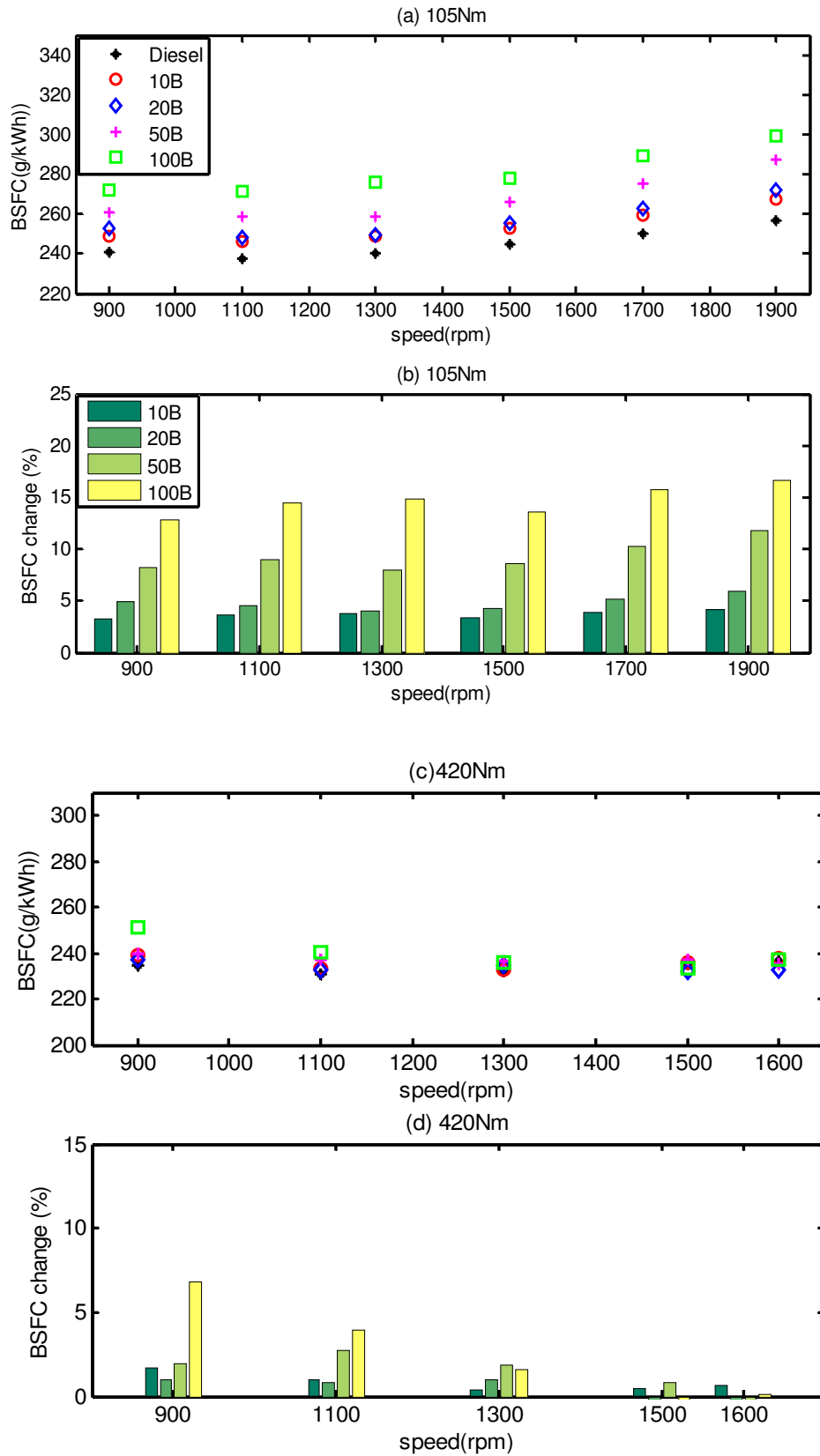


Figure 5-14(a,c) Variation of BSFC with engine speed for different biodiesel blends at 105Nm and 420Nm (b,d) Variation of BSFC increment with engine speed for biodiesel blends at load of 105 and 420Nm

Figure 5-14(b) depicts that when the biodiesel blend percentages increase, the BSFC values also increase. The BSFC of the engine fuelled with 10B, 20B, 50B and 100B blends increased by 2.5%, 5%, 10% and 15% respectively, at a load of 105Nm as compared to BSFC when fuelled with Diesel only. However, at a higher load (420Nm), the difference between the BSFC of biodiesel blends and diesel narrowed, as depicted in Figure 5-14(c-d), which shows a maximum BSFC increment of 5%. Previous research have also reported similar trends [9], [32], [93], [100-102], [130], [9].

The effects of the engine load on the biodiesel blends' BSFC values are shown in Figure 5-15. It can be seen that the engine running at a lower load (105Nm) resulted in higher BSFC by corresponding amounts of 15%, 12% and 16% than the values observed at 210Nm, 315Nm and 420Nm load conditions at 1500 rpm engine speed.

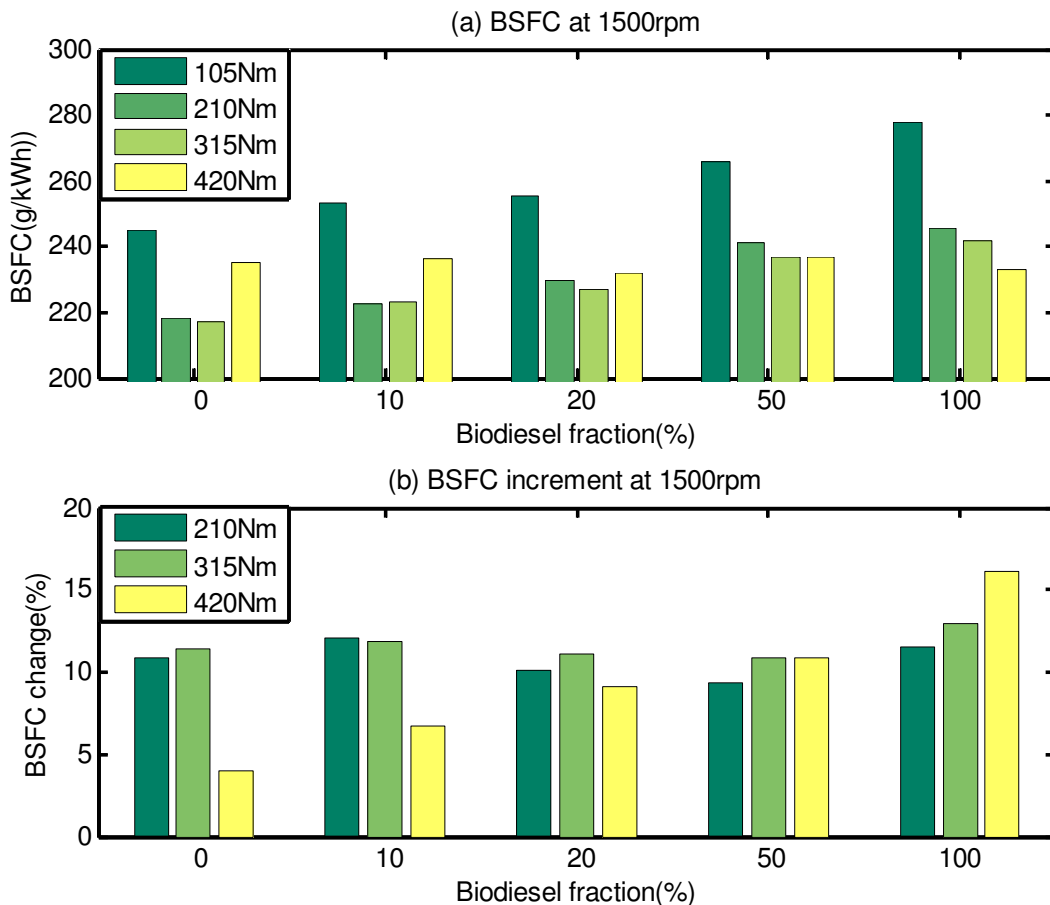


Figure 5-15 (a) Variation of BSFC with biodiesel fraction at engine speed of 1500rpm and various engine loads (b) Variation of BSFC percentage increment with biodiesel fraction at engine speed of 1500rpm and at various engine loads

It is also seen that the BSFC of the engine at a low load (105Nm) increased linearly with increase in the biodiesel fraction values. In general, it can be seen that at lower loads, the BSFC of the CI engine is higher and then decreases before increasing again very slowly. Similar trends in BSFC were reported by Gumus and Kasifoglu[95] for all blends investigated (B10, B20, B50, B100 and diesel) at different load conditions. One of the explanations for a decreasing BSFC with an increase in load is because of a higher increase in brake power, as compared to fuel consumption [91].

5.2.4 Effects of Biodiesel Blend Fraction on Engine Emissions Parameters

Experimental emission results obtained from the tests on CI engine fuelled with rapeseed biodiesel blends running at a range of engine speeds and at 420Nm load are shown in Figure 5-16 to Figure 5-19. The higher load was selected for emissions investigation due to its sensitivity for emissions. Both the real values of the emissions and the percentage change of the emission over a wide range of conditions are reported.

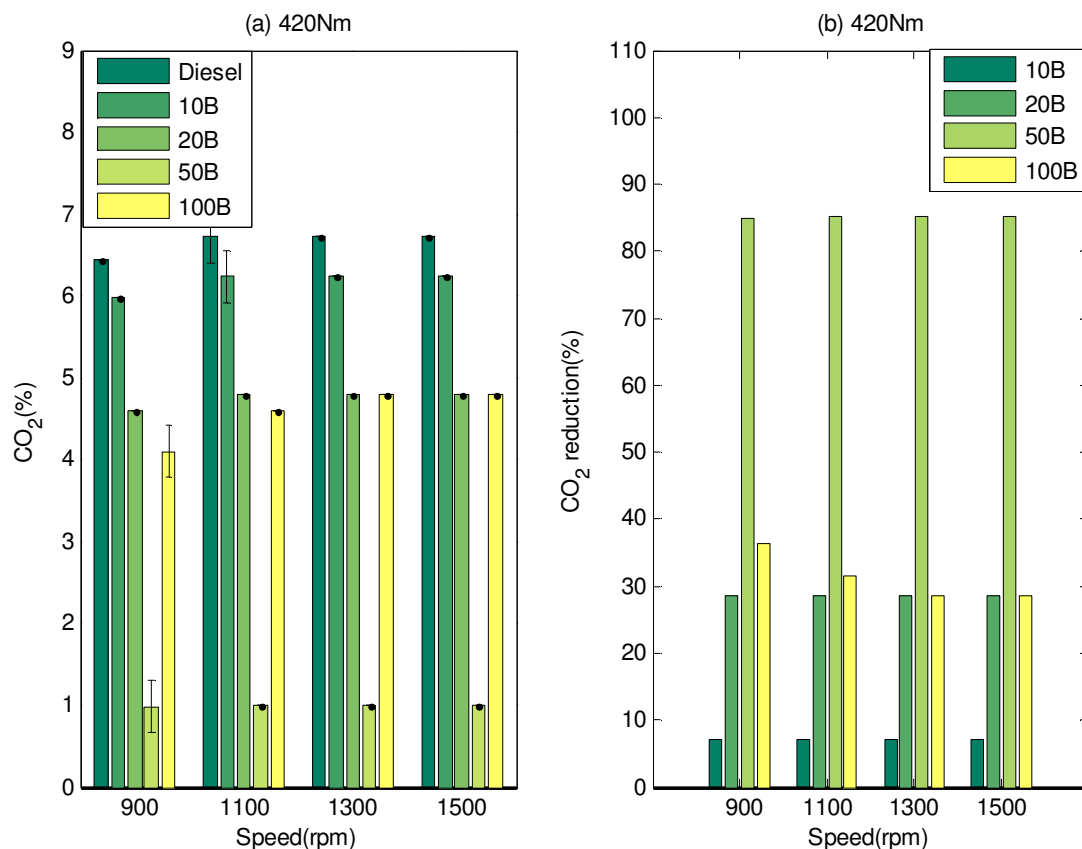


Figure 5-16 (a) Variation of CO₂ emissions with engine speed for CI engine running with biodiesel blends at load of 420Nm (b) Variation of CO₂ emissions percentage reduction with engine speed for CI engine running with biodiesel blends at load of 420Nm

Figure 5-16(a) provides the CO₂ emissions of CI engines over a range of engine speeds. It can be seen that the CO₂ emission reduced significantly with increase in the engine speeds. The CI engine's CO₂ emissions corresponding to neat diesel as well as various biodiesel blends (10B, 20B, 50B and 100B) have been compared and their percentage reductions in CO₂ emission are shown in Figure 5-16(b). The histogram shows that the CI engine's CO₂ emission reduced by 7%, 27%, 85% and 35% corresponding to 10B, 20B, 50B and 100B as compared to diesel value respectively.

The engines fuelled by 50B resulted in the maximum CO₂ emission among the different blends used. Previous researchers recommended optimum biodiesel blends of 20% and 40%. The engine fuelled with biodiesel emitted lower CO₂ emission than diesel due to the lower carbon to hydrogen ratio [50], [91]. The carbon content of biodiesel was 77%, whilst for diesel it was 87% as can be seen in Table 3-4.

Figure 5-17(a) compares the NO_x emissions from the test CI engine fuelled with diesel, 10B, 20B, 50B and 100B, at a load of 420Nm over a wide range of engine speeds. It can be seen that the NO_x emission increases with an increase in engine speed as discussed in section 5.6.2. It can further be seen that a higher percentage of biodiesel blend emits higher values of NO_x emissions, as shown in Figure 5-17(b).

The use of biodiesel blend 10B increased the NO_x emission by 10%, whilst the neat biodiesel increased the emission value by up to 32% at 1100rpm both as compared to the emission resulting from the use of diesel. Other researchers have also reported that NO_x emission has been increased by 35% [37], [71] if biodiesel is used as fuel as compared to diesel. The main reasons for higher NO_x emissions with increase in biodiesel content could be due to the advance injection and advance combustion, as a result of its higher viscosity [44], [77], [89], [91], higher oxygen content which enhances NO_x formation [44], [91], [130] and a higher cetane number which shortens ignition delay and advances the combustion [89][130].

The THC emission of the test CI engine running on diesel and biodiesel blends at various engine speeds and at 420Nm load is depicted in Figure 5-18(a). It can be noticed that at lower engine speeds (900rpm and 1100rpm), the diesel and rapeseed biodiesel blends did not show clear differences between the emission levels. However, at higher engine speeds, the biodiesel blends emitted lower THC emission as compared to diesel as shown in Figure 5-18.

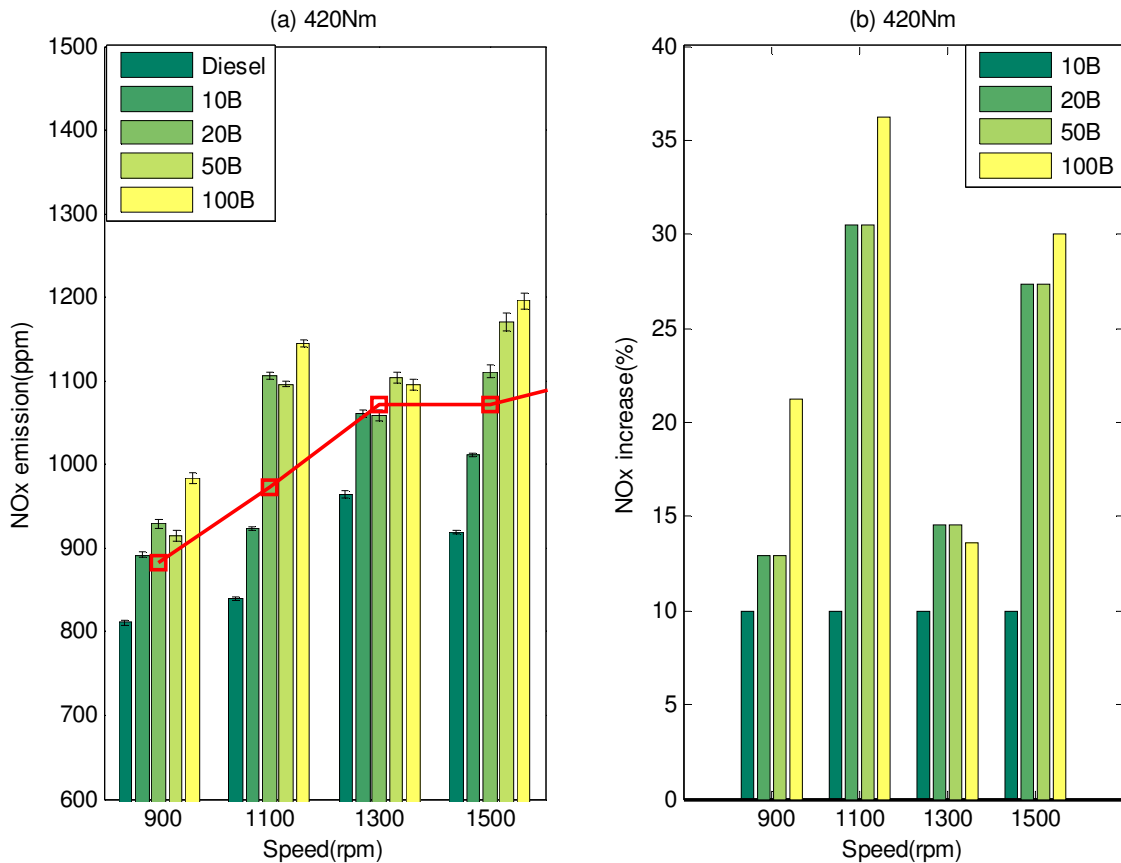


Figure 5-17 Variation of NOx emissions with engine speed for CI engine running with biodiesel blends at load of 420Nm (b) Variation of NOx emissions percentage reduction with engine speed for CI engine running with biodiesel blends at load of 420Nm

The THC reduction reached to 45% at 1300rpm engine speed for 100B. Previous researchers have also reported that the engine fuelled with biodiesel could reduce the THC by 67% [30], [197], [128], [134], [135]. The reduction of the THC in CI engines running on biodiesel can be explained on the basis of lower content of carbon to hydrogen ratio than the normal diesel and presence of up to 11% oxygen in its molecular structure.

The CO emission characteristics of the CI engine fuelled by the diesel and rapeseed biodiesel blends at the maximum engine load and at various speed conditions are shown in Figure 5-19. All the fuels used produced a higher amount of CO emissions at lower speeds and emitted less CO emissions at higher engine speeds. The effect of engine speed on CO emission is discussed in section 5.6.2.

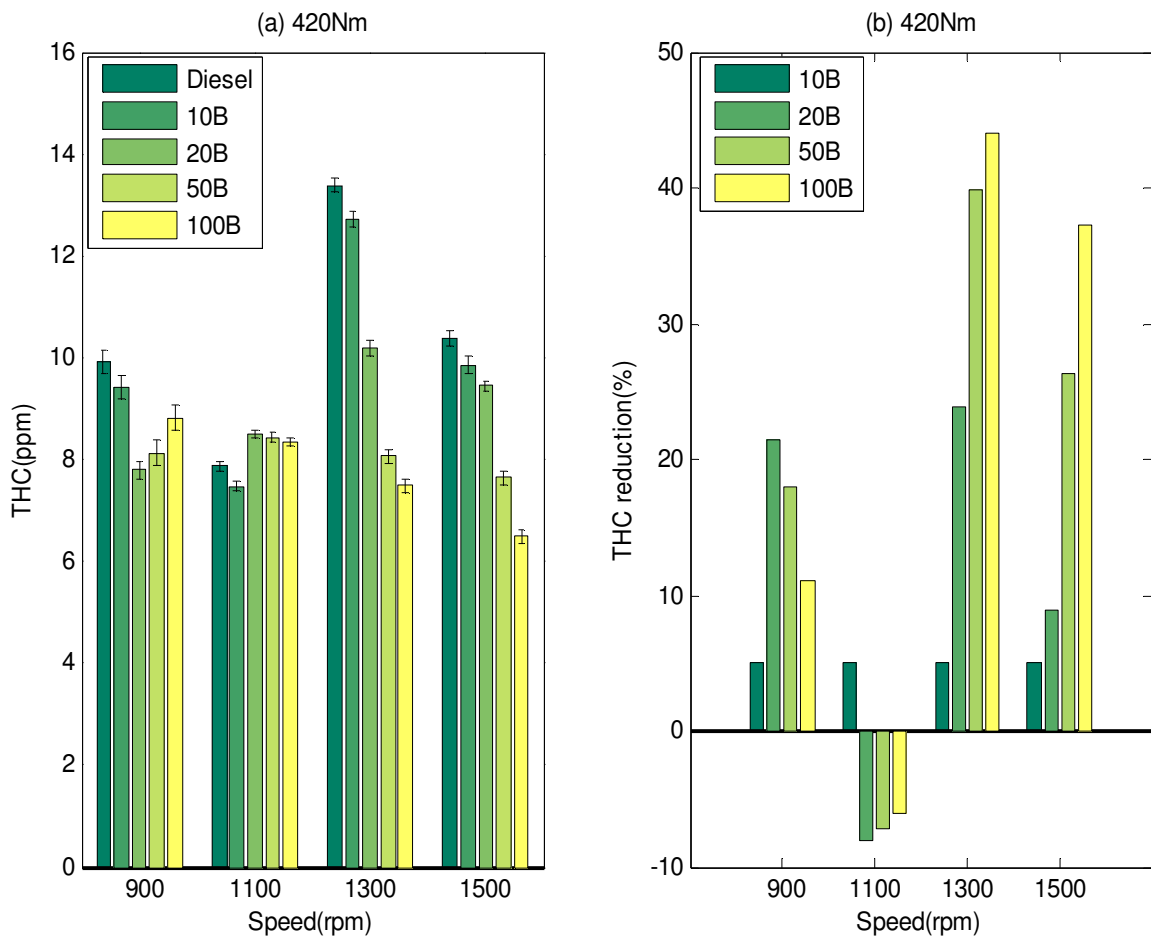


Figure 5-18 Variation of NOx emissions with engine speed for CI engine running with biodiesel blends at load of 420Nm (b) Variation of NOx emissions percentage reduction with engine speed for CI engine running with biodiesel blends at load of 420Nm

With increase in the biodiesel contents, the CO emission levels decreased on average by up to 65%. Krahl *et al.* [134] and Raheman and Phadatre [101] reported that the engine running on biodiesel reduced the CO emission by 50% and 73-94%, respectively. The main reason for reduction of CO emission is the availability of oxygen in the biodiesel for better combustion. The extra oxygen in the biodiesel promotes complete combustion of fuel and thus results in the reduction of CO emissions [9], [60], [97], [100], [110], [111], [121], [9], [131].

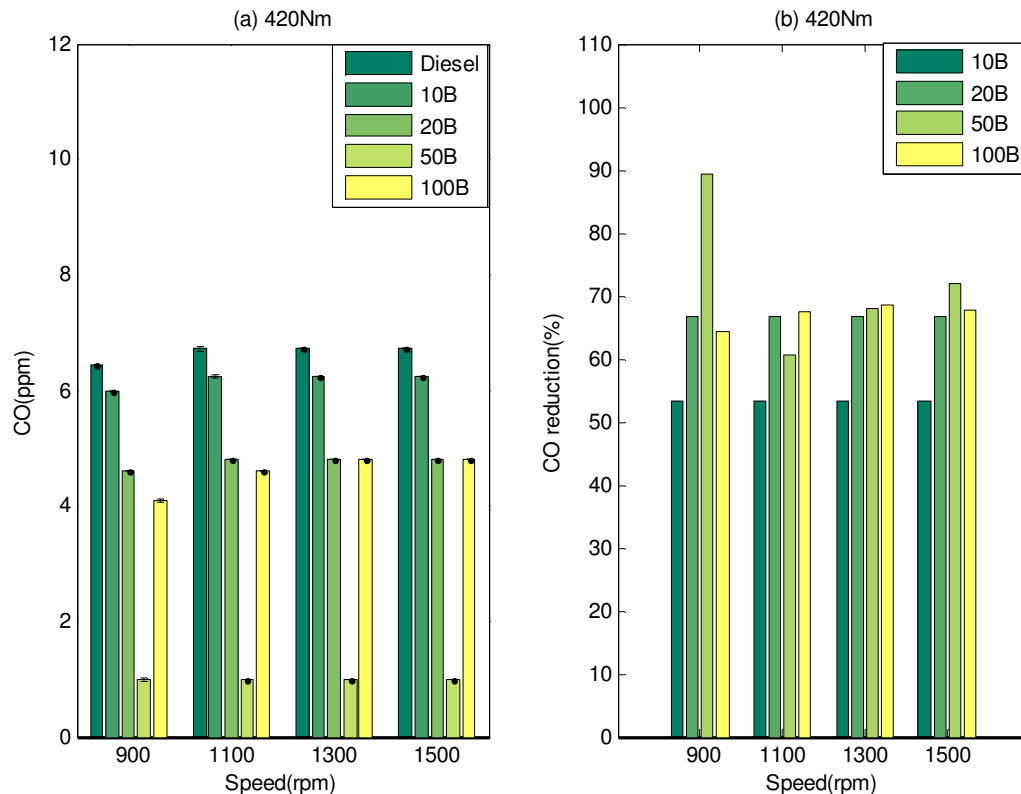


Figure 5-19 Variation of CO emissions with engine speed for CI engine running with biodiesel blends at load of 420Nm (b) Variation of CO emissions percentage reduction with engine speed for CI engine running with biodiesel blends at load of 420Nm

5.2.5 Effects of Physical Properties of Biodiesel on Engine Performance Parameters

The physical properties of a fuel such as density, viscosity and lower heating value affect the engine performance and emission characteristics. The effects of the fuel density on the BSFC of the CI engine running at 900 rpm and 1500rpm are presented in Figure 5-20. For easy comparison, tests have been conducted at same load and speed conditions.

It was noticed, that increasing the fuel density increased the BSFC at all the load conditions investigated. This can be due to the fuel meter delivering fuel on a volumetric basis and the density being higher for biodiesel than for diesel resulting in fuel injection pump discharging more biodiesel mass as compared to that of diesel mass [9], [131], [167].

This causes higher fuel consumption for almost the same power output. It is also seen that at load conditions of 105Nm and 210Nm, the engine running at 1500rpm resulted in a higher BSFC by approximately 5% and 3%, than at a speed of 900rpm respectively. At higher

engine loads i.e. 315Nm and 420Nm, the engine running at a speed of 1500 rpm resulted in a lower BSFC by approximately 3% and 6%, than the engine running at a speed of 900 rpm. The effect of engine speed on BSFC has been discussed in section 5.2.1.

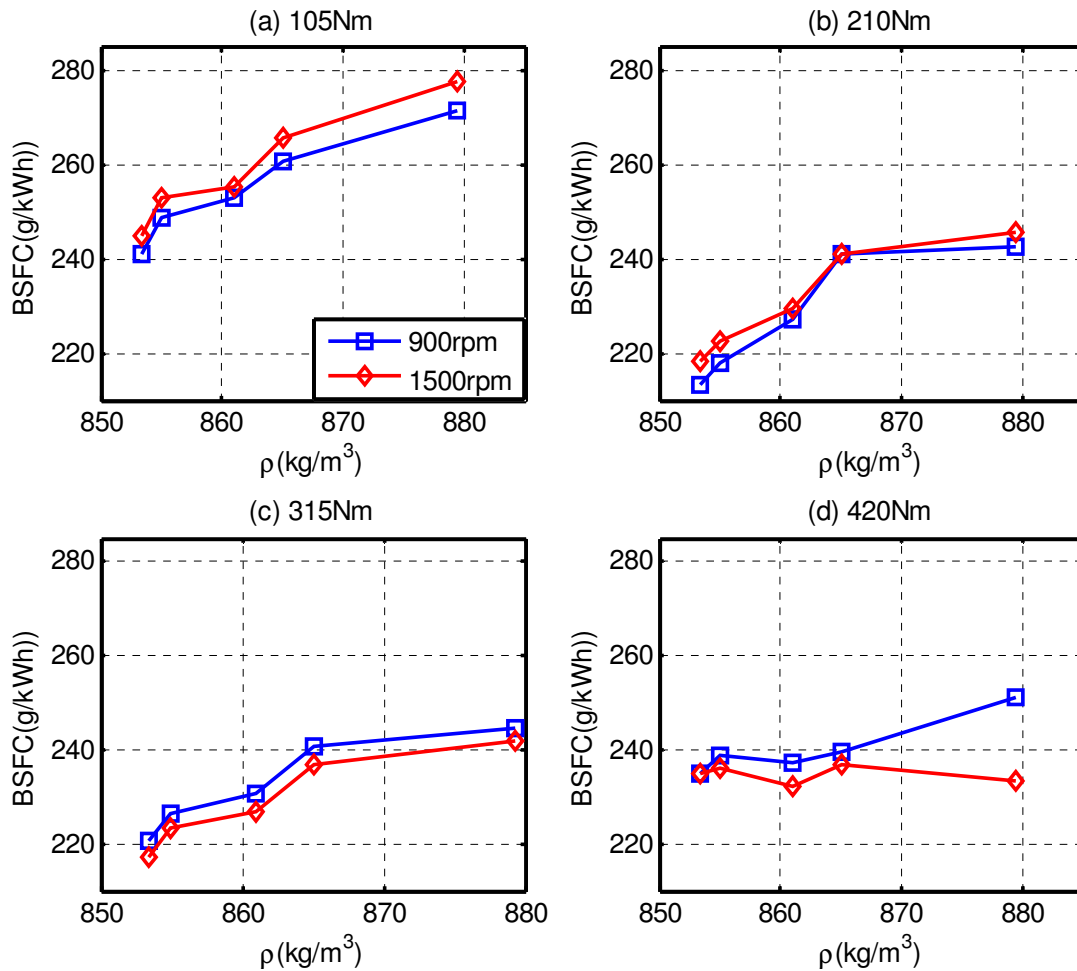


Figure 5-20 Variation of BSFC with density of biodiesel at engine speed of 900rpm and 1500rpm and various engine loads

Figure 5-21 presents the effects of the kinematic viscosity of the fuels on the BSFC in the test CI engine at operating speeds of 900 rpm and 1500 rpm and at various engine loads. It can be seen that when the kinematic viscosity of fuel increases the BSFC also increases. The effects of viscosity on the BSFC of the test engine can be explained on the basis that as the fuel viscosity increases, the fuel injection atomisation is affected and this leads to poor combustion and lower power for the same volume of fuel [97], [131]. Some authors argue that the higher viscosity of biodiesel enhances the fuel spray penetration and improves air-fuel mixing [91]. The effect of lower heating values of the fuels used on CI engines' BSFC at various engine loads and at speeds 900 rpm and 1500 rpm are shown in Figure 5-22.

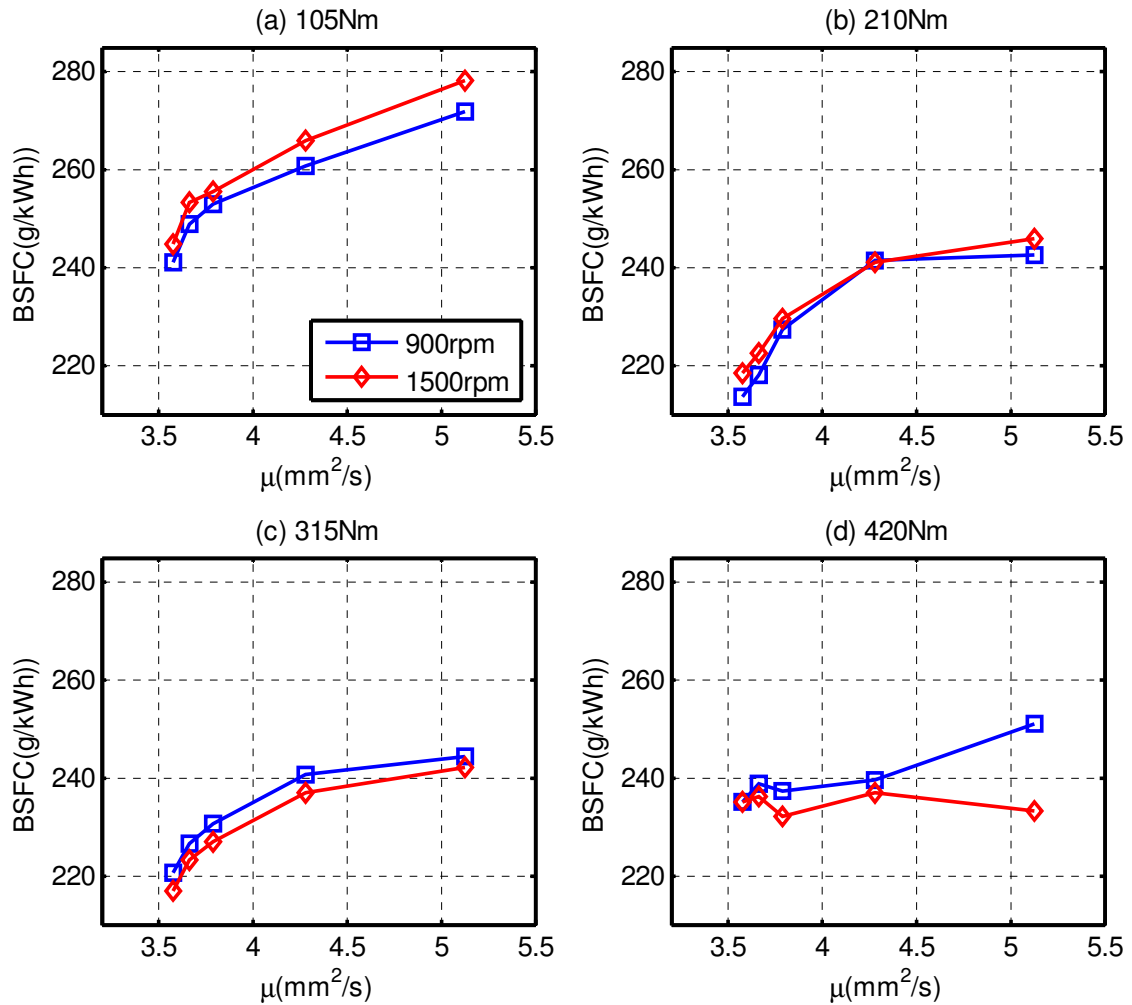


Figure 5-21 Variation of BSFC with viscosity of biodiesel at engine speed of 900rpm and 1500rpm and various engine loads

It can be seen that at all operating conditions, as the lower heating value increases the BSFC decreases. Biodiesel's heating value is lower than diesel by about 11.09% as discussed in section 4.3. The BSFC of biodiesel is found to be higher than diesel by 15% and 7% at lower load and higher load conditions, respectively.

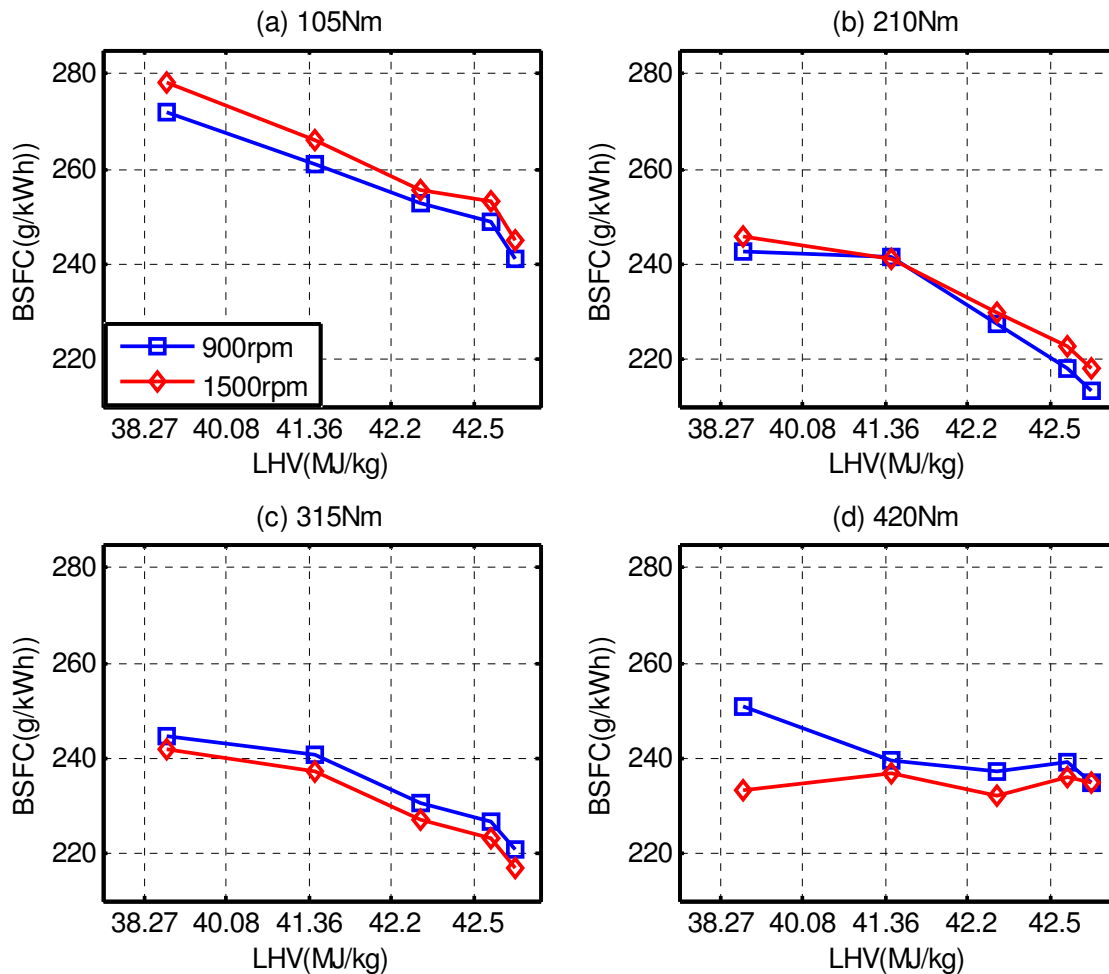


Figure 5-22 Variation of BSFC with density of biodiesel at engine speed of 900rpm and 1500rpm and various engine loads

5.3 Summary on the Performance and Emission characteristics of the test CI engine during Steady State Operation

The effects of biodiesel blend fraction values and physical properties on the CI engine's in-cylinder pressure, brake specific fuel consumption, thermal efficiency and exhaust emissions (CO_2 , NO_x , CO , THC and O_2) have been investigated in detail for steady state operation conditions. The main summary drawn from the analysed data are as given below.

1. In this study three biodiesel feed stocks have been used: ROB, COB and WOB. It has been seen that the feed stock sources do not result in any significant differences in the engine performance and emission characteristics.
2. The peak cylinder pressure of the engine running with biodiesel blends is slightly higher than the engine running with diesel. The main reason for a higher in-cylinder

pressure in the CI engine running with biodiesel could be due to the advanced combustion process being initiated by the easy flow-ability of biodiesel and its other relevant physical properties such as viscosity, density and bulk modulus.

3. The results highlight that the power produced by the engine as calculated from the P-V diagram does not show any significant change with the diesel and biodiesel blends. This indicates that the offset of biodiesel lower heating value is compensated by higher mass flow rate.
4. The engine running with diesel and biodiesel blends show the same combustion stages at all load conditions except for the slight variation in peak heat release rate and ignition delay. When using biodiesel, the ignition is seen to be advanced when compared to diesel fuel by crank angles of 0.8° , 1° , 1.5° and 1.2° for load values of 105Nm, 210Nm, 315Nm and 420Nm respectively.
5. It was noticed that when the density and viscosity of biodiesel is increased an increase in BSFC of CI engine is observed at all load conditions investigated.
6. The use of biodiesel has been seen to increase the brake specific fuel consumption of the CI engine due to its low heating value, higher density and viscosity. However, this trend is seen to weaken as the proportion of biodiesel reduces in the blend.
7. The emission analyses of the CI engine running with biodiesel highlights a significant reduction in CO₂, CO and THC emission. It is also found that when the biodiesel content increases a further reduction in emissions is observed. This emission reduction is a result of the oxygen content in biodiesel and the low carbon hydrogen ratio.
8. For all biodiesel contents and operating conditions the NO_x emission increases during use in a CI engine. This increase is mainly due to the higher oxygen content present in biodiesel and the advanced injection characteristics.

After extensive investigations into the steady state operating characteristics, the transient state operating behaviours have been investigated in next chapter which is mainly focused on the performance and emission characteristics of CI engine running with biodiesel.

CHAPTER SIX

6. PERFORMANCE AND EMISSION CHARACTERISTICS OF THE TEST CI ENGINE DURING TRANSIENT OPERATION

The main aim of this chapter is to investigate the combustion, performance and emission characteristics of a compression ignition engine running on biodiesel and its blends during transient operating conditions. As per the previous review a lot of research has been carried out on the use of biodiesel in CI engines during steady state conditions as discussed in Chapter five. However, the performance and emission characteristics of CI engines running with biodiesel during transient operations have not been investigated extensively. Results are presented for all test conditions and attempts have been made to highlight the effects of different biodiesel blends on the in-cylinder pressure, fuel consumption rate and emissions (CO_2 , NO_x , CO , THC) during transient state operation. These effects have been discussed based on the experimental results obtained from the test CI engine. Detailed analyses on the effects of biodiesel blends on emission of CI engine during both positive and negative transient operations have been carried out. In addition a transient emission prediction model has been developed from the data obtained from steady and transient state CI engine operations.

6.1 Performance Characteristics during Transient Operation

To understand the effects of biodiesel blends on the CI engine performance during transient operation, the fuel consumption rate, exhaust temperature and in-cylinder pressure have been investigated. Since the fuel consumption rate data is more sensitive than the BSFC, the former has been selected to analyse the effects of biodiesel blends on engine performance. Exhaust gas temperature represents the temperature of the fuel mixture after combustion in the engine cylinder. It can be measured at exhaust manifold. Due to its high sensitivity for dynamic phenomena and its accessibility for measurement, the exhaust gas temperature has been used in detection of combustion anomalies [198][199], in the design of exhaust gas recirculation (EGR) [147], [200], [143], [155], prediction of emission models [201]. Due to this, the exhaust temperature has been selected as parameter to investigate the performance the engine running with biodiesel during a transient condition. Furthermore to get more in-depth information about combustion process in-cylinder pressure values have also been monitored.

6.1.1 Fuel Consumption Rate

The fuel flow rate has been measured by FMS-1000 gravimetric fuel measurement system during both steady and transient conditions. The variations of the fuel flow rate with the operating conditions have been reported here. Figure 6-1 shows the variation of fuel flow rate of diesel and biodiesel blends during the speed transient of 1000 to 1500rpm and 1500 to 1000rpm at 420Nm load. It can be clearly seen that the fuel flow rate increases by 35% during the acceleration of the engine from 1000 to 1500 rpm and the fuel flow rate decreases by 33% during the deceleration of the engine from 1500 to 1000 rpm. The fuel flow rate increment with acceleration can be explained on the basis that when the engine speed increases the cylinder charging rate increases as a consequent fuel flow rate increases [50], [195].

In addition, during acceleration the friction horsepower increases because of a drop in the mechanical efficiency to maintain a fixed torque output, leading to an increase in the fuel consumption rate [202]. Figure 6-1(c-d) depicts that the fuel consumption of the engine running with 100B is higher than that of diesel by 16% during the acceleration and 14% during the deceleration transient operations respectively. This has occurred due to the effect of lower heating value of the biodiesel which is lower than the diesel by 11%. Previous researchers have also reported similar trends [9], [32], [93], [100-102], [130] in fuel consumption based on discrete engine speed tests.

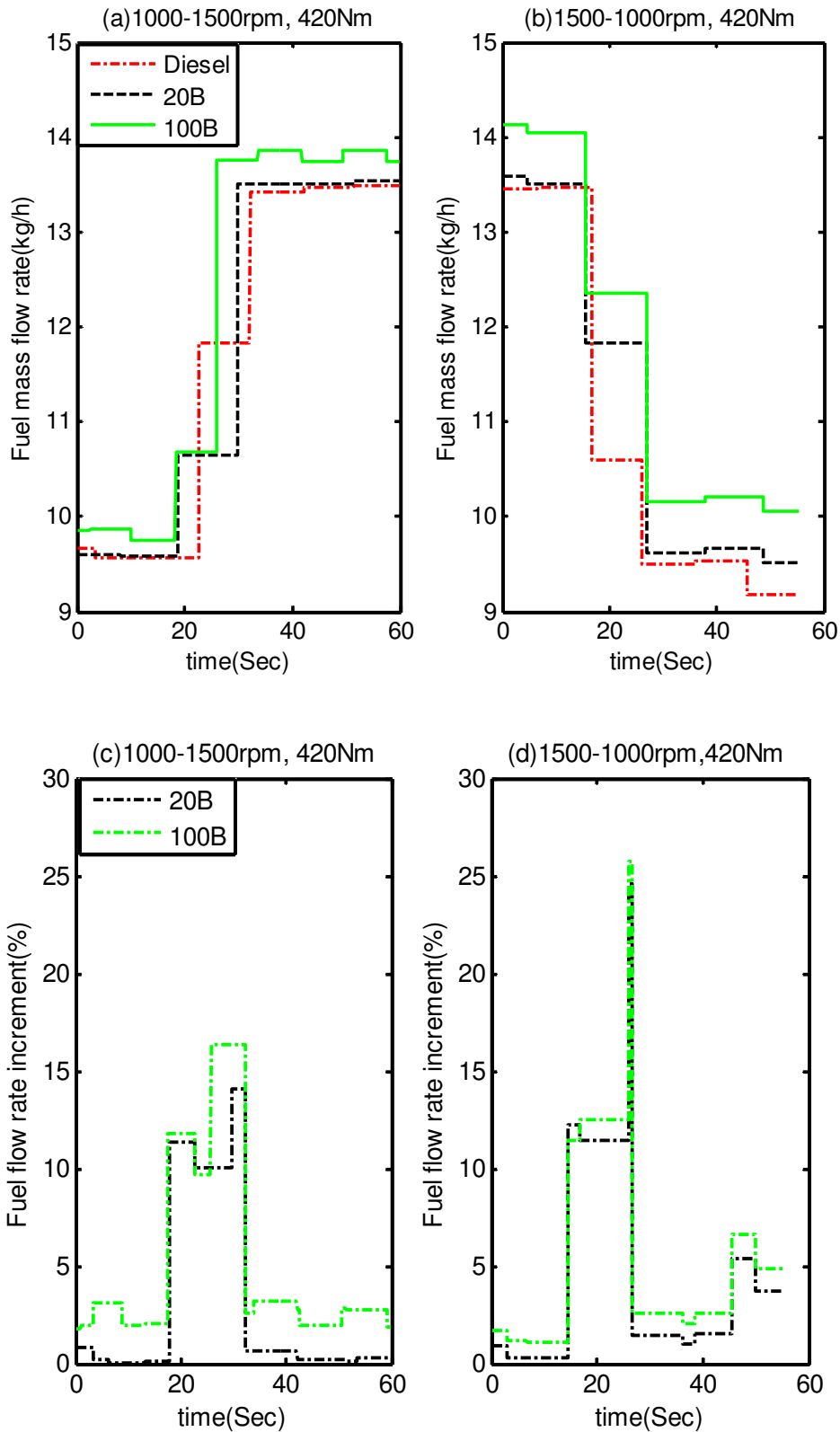


Figure 6-1 (a) Variation of Fuel flow rate with time for CI running with biodiesel during speed transient at 420Nm (b) Variation of Fuel flow rate percentage increment with time by using biodiesels blends during speed transient at 420Nm

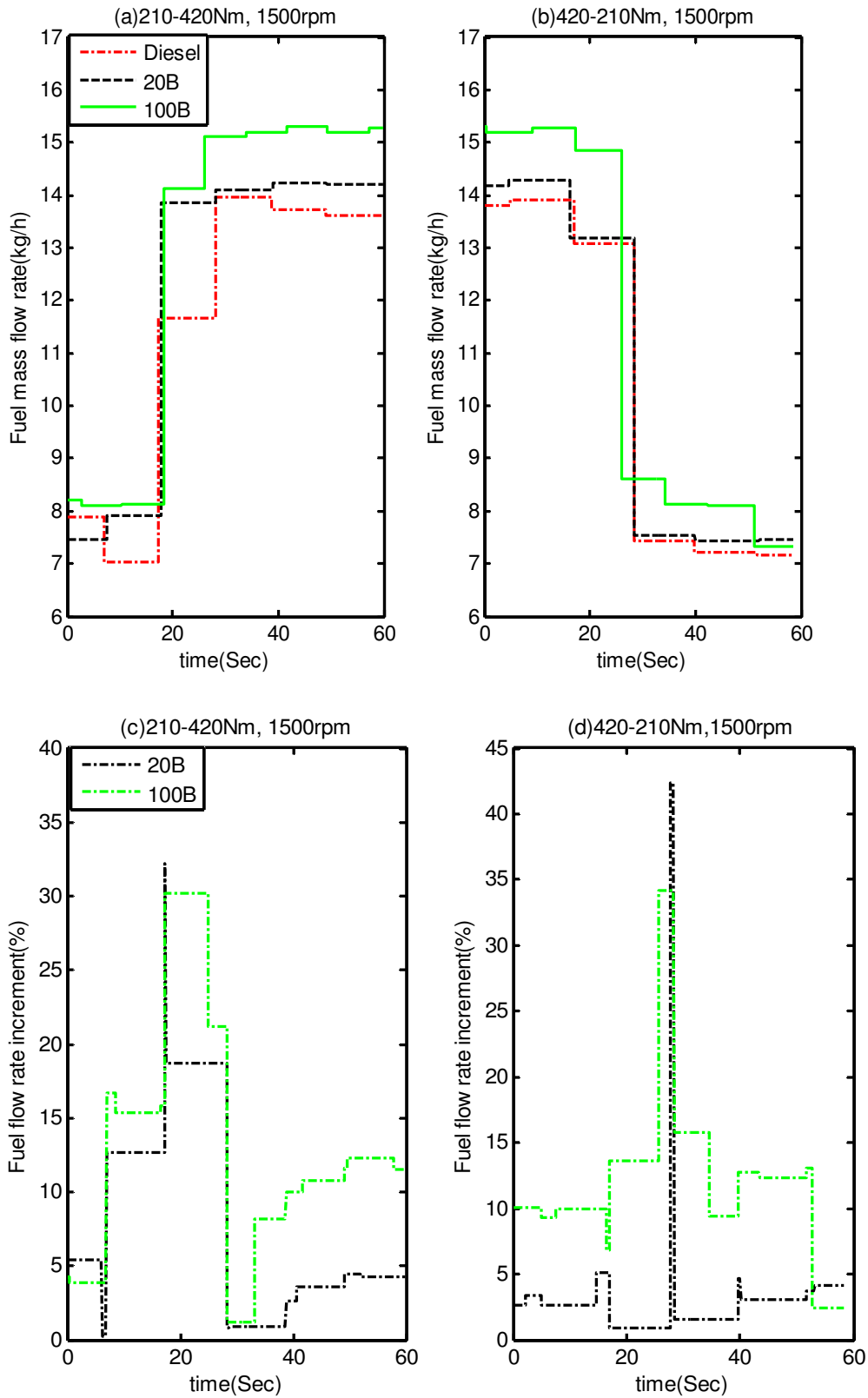


Figure 6-2 (a) Variation of Fuel flow rate with time for CI running with biodiesel during torque transition at 420Nm (b) Variation of Fuel flow rate percentage increment with time by using biodiesel blends during torque transition at 420Nm

The effects of the torque transient operation on fuel consumption rate for the engine running with diesel and two blends 20B and 100B are presented in Figure 6-2. The fuel consumption rate increases by 31% during the positive torque transition of 210-420Nm at 1500rpm. Similarly, the fuel consumption rate decreases by 34% during the negative torque conditions of 420-210Nm. This is due to the increase in the fuel injection to attain the required higher total energy output at a given engine speed. Comparing the fuel consumption rates of CI engine running with the biodiesel blends and diesel, it can be seen in Figure 6-2(c-d) that the engine running with the former resulted in higher fuel consumption rate by 17% and 15% for both positive and negative torque operations respectively.

6.1.1.1 Exhaust Gas Temperature

The exhaust gas temperature values obtained from the test engine running with diesel, 20B and 100B during speed transient of 1000-1500rpm and 1500-1000rpm and at a load of 420Nm are depicted in Figure 6-3. It can be seen that the exhaust gas temperatures of the diesel and biodiesel blends do not show any significant difference for both acceleration and deceleration transient conditions. In both the conditions, the maximum difference between the exhaust gas temperature of the engine running with diesel and biodiesel blends is limited to 2%. The exhaust temperature increases from 600K to 710K during the acceleration operation and decreases from 710K to 630K during the deceleration transient operations. This reason behind this can be explained as when the engine accelerate from 1000rpm to 1500rpm, the amount of fuel injected to the cylinder also increases in order to maintain a constant engine torque output. As a result, the heat release rate and the exhaust gas temperature increases from burning of the fuels [50]. During the deceleration from 1500-1000rpm, the reverse phenomenon occurs in the cylinder.

The effects of the torque transition operation on exhaust gas temperature for the engine running with diesel, 20B and 100B are presented in Figure 6-4. The exhaust temperature increases from 570K to 670K during the positive torque transient of 210-420Nm at a speed of 1500rpm (see Figure 6-4(a)). Similarly, the exhaust gas temperature decreases during negative torque conditions of 420-210Nm. This is due to the increase in the fuel injection to attain the required higher total energy input.

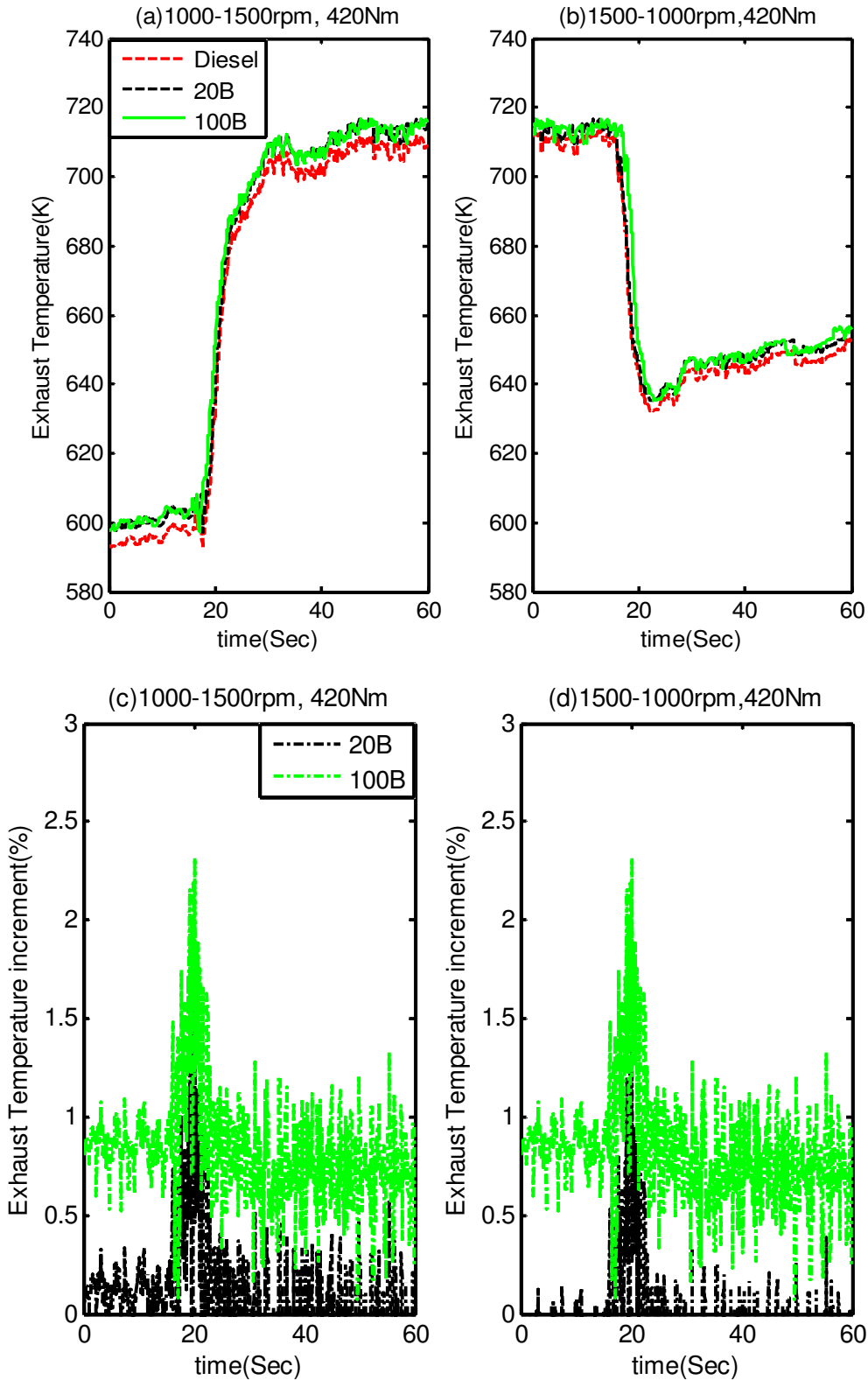


Figure 6-3 (a) Variation of exhaust temperature with time for CI engine running with biodiesel during speed transient at 420Nm (b) Variation of exhaust temperature percentage increment with time by using biodiesel blends during speed transient at 420Nm

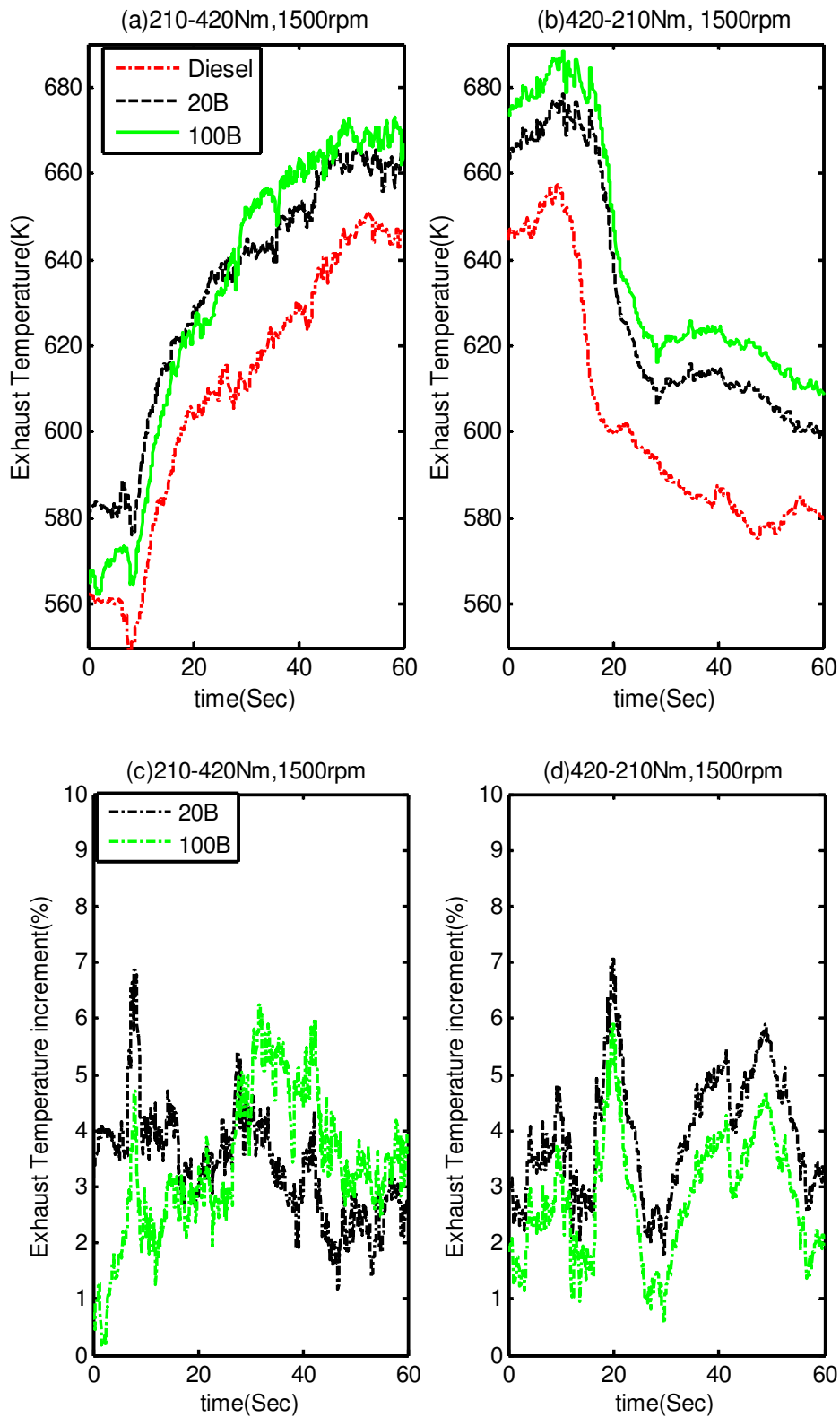


Figure 6-4 (a) Variation of exhaust temperature with time for CI running with biodiesel during torque transition at 420Nm (b) Variation of exhaust temperature percentage increment with time by using biodiesel blends during torque transition at 420Nm

Comparing the exhaust temperature of engine running with the biodiesel blends and diesel, it can be seen in (Figure 6-4) that the engine running with the former resulted in higher exhaust gas temperature by 7% for both positive and negative torque operations. In addition, the exhaust temperature increases with increasing the biodiesel fraction in the blends. This can be explained on the basis that as biodiesel have 11% oxygen in its molecular structure, the oxygen molecule enhances the complete combustion of fuel in the cylinder. As a result the in-cylinder temperature increases and consequently the exhaust temperature increases [44], [91].

6.1.1.2 In-cylinder Pressure

One of the most valuable sources of combustion information during the development and calibration stages of the engine is obtained from the in-cylinder pressure. The in-cylinder pressure signal can provide vital information such as peak pressure, P-V diagram, indicated mean effective pressure, injector pressure, heat release rate, combustion duration, ignition delay and so on [188] [169]. In this section the in-cylinder pressure and its dependence on the fuel type have been discussed in detail. The peak in-cylinder pressure corresponding to four operating conditions i.e. the speed acceleration from 1000-1500rpm, the speed deceleration from 1500-100rpm, the positive torque transition from 210-420Nm and the negative torque transition from 420-210Nm are shown in Figure 6-5 to 6-6. Figure 6-5 shows the in-cylinder peak pressure within the CI engine fuelled by diesel, 20B and 100B fuels at a load of 420Nm and during speed transients of 1000-1500rpm.

As it can be seen in Figure 6-5(a), the CI engine fuelled with 100B and 20B resulted in a higher peak in cylinder pressure than the diesel by 15% and 7%, respectively in the transient sections of the operation.

This phenomenon is due to the complete combustion of the carbon molecules to yield the maximum torque. The main cause for the higher peak in-cylinder pressure of CI engine running with biodiesel is the advanced combustion process initiated by easy flow-ability of biodiesel derived from the physical properties of biodiesel. In addition, due to the presence of oxygen molecules in biodiesel, the hydrocarbon receives complete combustion. The in-cylinder pressure changes almost uniformly with respect to time in

the pre-transient steady operation, as shown in Figure 6-5(b). However, due to the effect of the transient operation, during the post-transient operation in-cylinder pressure rate shows some irregularities. During the transient section, the in-cylinder peak pressure attained its peak rate in the middle of the time span of the transient operation.

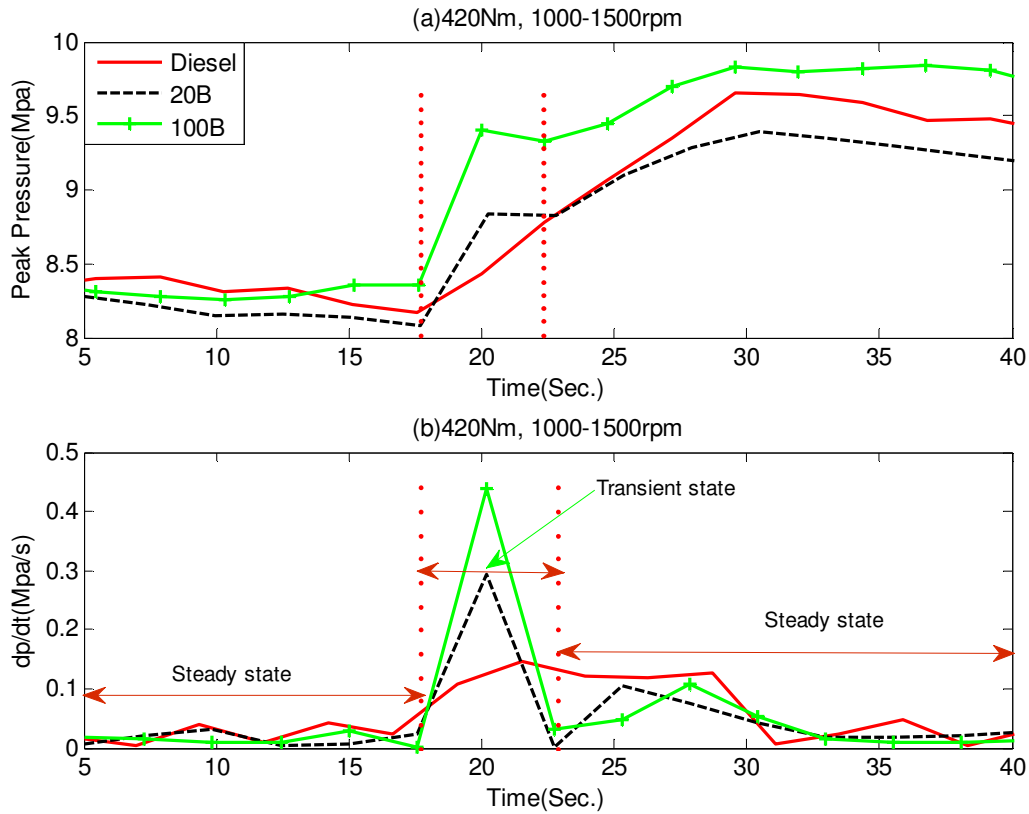


Figure 6-5 (a) Variation of in-cylinder peak pressure with time for CI engines running with different fuels during speed positive transient (b) Variation of rate of change in-cylinder peak pressure with time for CI engines running with different fuels during negative speed transient

Figure 6-6 shows the in-cylinder peak pressure within the CI engine fuelled by diesel, 20B and 100B at a load of 420Nm and a deceleration transient of 1500-1000rpm. Similar to the acceleration transient condition, the CI engine fuelled with 100B resulted in a higher peak in cylinder pressure than the diesel by 5% during the transient section of the operation. The in-cylinder pressure rate changed almost uniformly during pre-transient and post-transient steady state operations, as shown in Figure 6-6(b). In the transient section, the engine running with biodiesel blends showed higher in-cylinder peak pressure rates than diesel.

The effects of positive torque transition from 210Nm to 420Nm on the in-cylinder peak pressure when fuelled with diesel, 20B and 100B fuels at 1500rpm, is shown in Figure 6-7(a). In the pre-transient section, the diesel followed by 100B, resulted in a higher peak in-cylinder pressure (higher by 9%). However, in the post-transient operation, the engine fuelled by 100B and 20B showed higher in-cylinder pressures than the engine fuelled by diesel by 12% and 6%, respectively. Comparing the in-cylinder pressure rates during the transient section, the 100B resulted in a higher rate than the diesel and 20B by 45%, as shown in Figure 6-7(b).

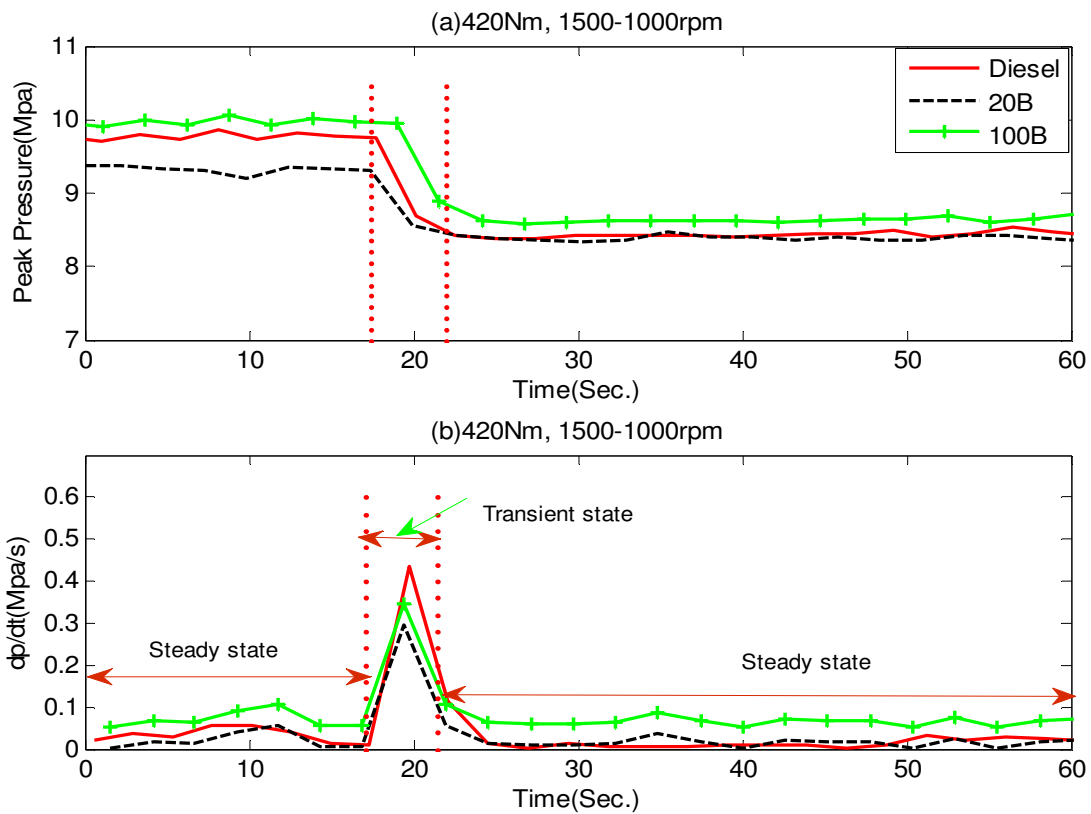


Figure 6-6 (a) Variation of In-cylinder peak pressure with time for CI engines running with different fuels during negative speed transient (b) Variation of rate of change in-cylinder peak pressure with time for CI engines running with different fuels during negative speed transient

Figure 6-8 shows the in-cylinder peak pressure when fuelled by diesel, 20B and 100B fuels at a speed of 1500rpm, and during a deceleration torque transient of 420-210Nm. Similar to the acceleration torque transient, the CI engine fuelled with 100B resulted in a higher peak in cylinder pressure than the diesel by 8% in the pre-transient steady section of the operation. However, in post-transient operation, the engine fuelled by the diesel had higher in-cylinder pressure than the engine fuelled by 100B. In the transient section, both 20B and 100B resulted

in higher in-cylinder peak pressures. The in-cylinder pressure rate changed irregularly in the three sections. In the transient section, the rate change of the peak in-cylinder pressure was lower than that of the diesel.

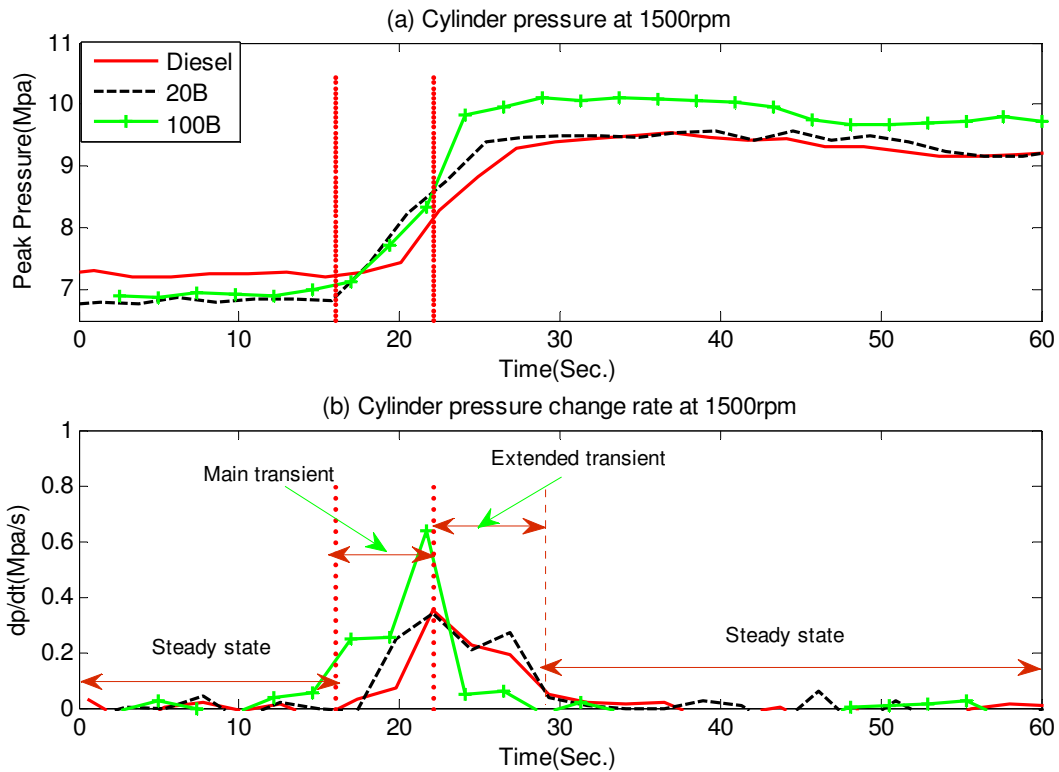


Figure 6-7 (a) Variation of In-cylinder peak pressure with time for CI engines running with different fuels during torque positive transient (b) Variation of rate of change in-cylinder peak pressure with time for CI engines running with different fuels during negative torque transient.

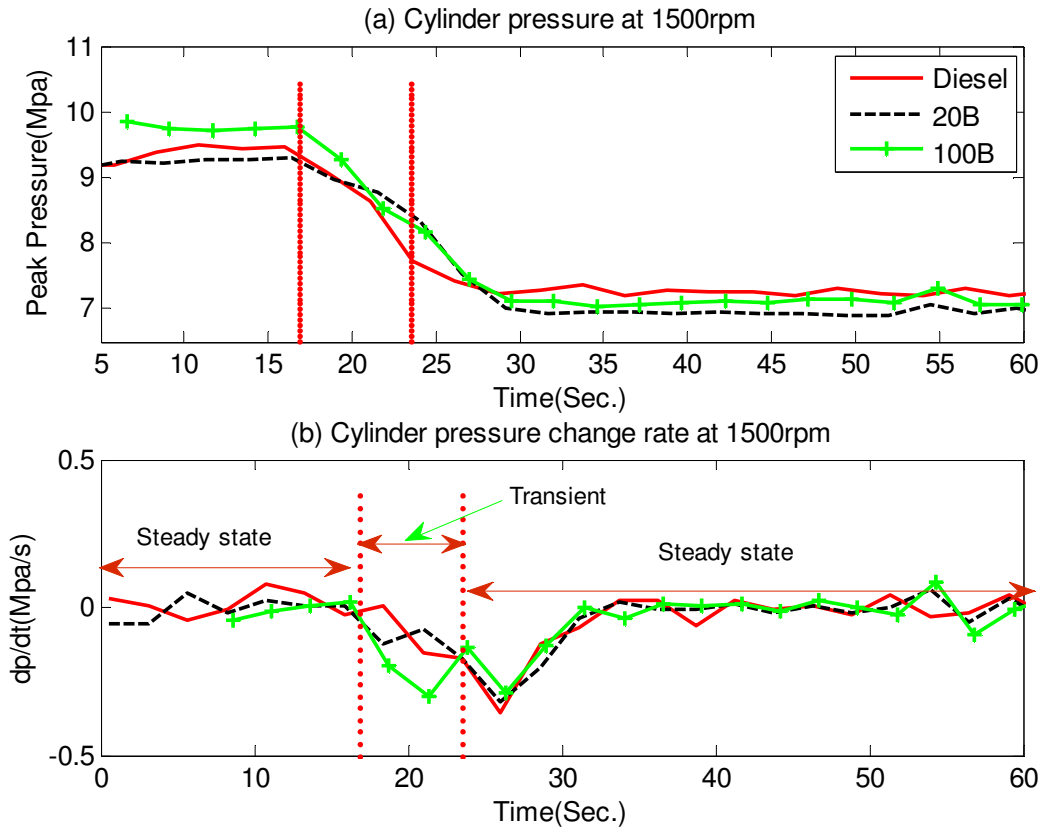


Figure 6-8 (a) Variation of in-cylinder peak pressure with time for CI engines running with different fuels during negative torque transient (b) Variation of rate of change in-cylinder peak pressure with time for CI engines running with different fuels during negative torque transient.

6.1.2 Emission Characteristics of CI Engine during Transient Operation

In this section the detailed investigation on the emission characteristics of CI engine running with diesel and biodiesel blends have been investigated. The analysis has been carried out for four transient operation conditions namely acceleration, deceleration, negative torque transition and positive torque transition. The analyses have been carried out in three stages. Firstly the measured engine emissions characteristics for different operation condition have been compared and secondly the emission release changing rates have been computed. Finally, the amount by which emission reduced when using a range of biodiesel blends has been computed. Furthermore, a new transient emission prediction model has been developed which has been validated against the measured values. The major emissions considered in the analysis are CO₂, NO_x, CO and THC. Even though, O₂ is not considered as an emission, to understand the combustion phenomena and the link

between exhaust gas emissions with O₂, the O₂ release characteristics of the transient operation have also been investigated.

6.1.2.1 The Carbon -dioxide (CO₂) Emission

Figure 6-9 shows the emission of CO₂ from the CI engine fuelled with diesel, 20B and 100B at a speed transient of 1000rpm to 1500rpm and at a load of 420Nm. It can be seen that the CO₂ emission at 1000rpm was higher than that at 1500rpm by 25%, 35%, and 5% for diesel, 20B and 100B fuels respectively which decreased during the acceleration stage. This can be explained on the basis that at higher engine speeds, the fuel/air equivalence ratio of the entering mix into the cylinder increased. To yield the maximum speed, the amount of fuel needed to burn completely in the cylinder increases, as result the CO₂ emission production increases. The CO₂ emission rate for the speed acceleration is depicted in Figure 6-9(b).

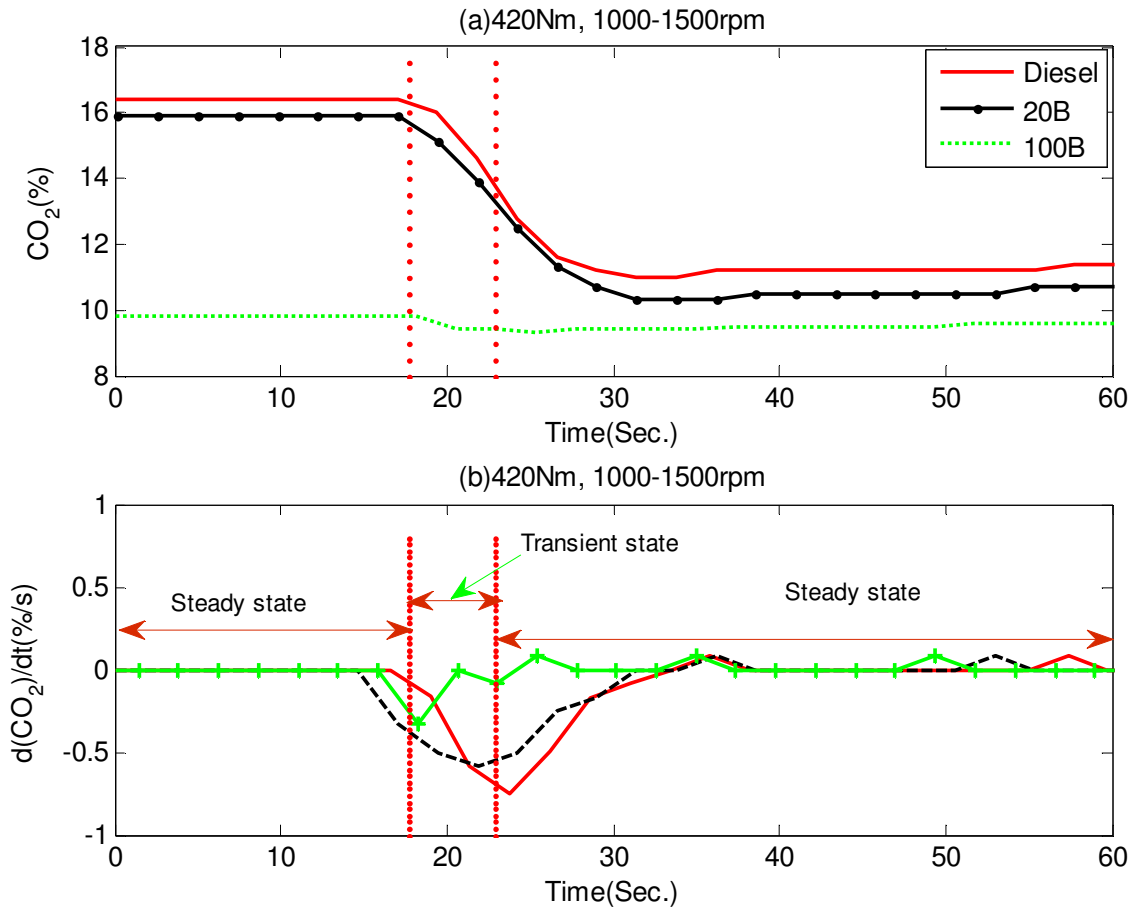


Figure 6-9 (a) Variation of CO₂ emission of CI engines with time for running with different fuels during positive speed transient (b) Variation of rate of change CO₂ emission with time for CI engines running with different fuels during positive speed transient

The emission rates corresponding to the diesel, 20B and 100B were observed to be irregular. The engine fuelled with diesel showed the highest change rate, i.e. 0.8%/s.

The transient effects on the CO₂ emission continued after the transient operation stopped for about 13 seconds. The effect of the engine deceleration from 1500-1000rpm on CO₂ is shown in Figure 6-10. During the deceleration operation, the CO₂ emission increased when the engine speed decreased from 1500-1000rpm. It can be seen in Figure 6-10(b) that the emission rate change attained its maximum value after 1.5 seconds of the start of the transient time span. The CO₂ change rate reached a stable values 13 seconds after the transient finished. Comparing the CO₂ emission change rate, for acceleration (Figure 6-9(b)) and deceleration (Figure 6-10(b)) it can be concluded that the former attained the stable condition earlier than the latter by 3seconds.

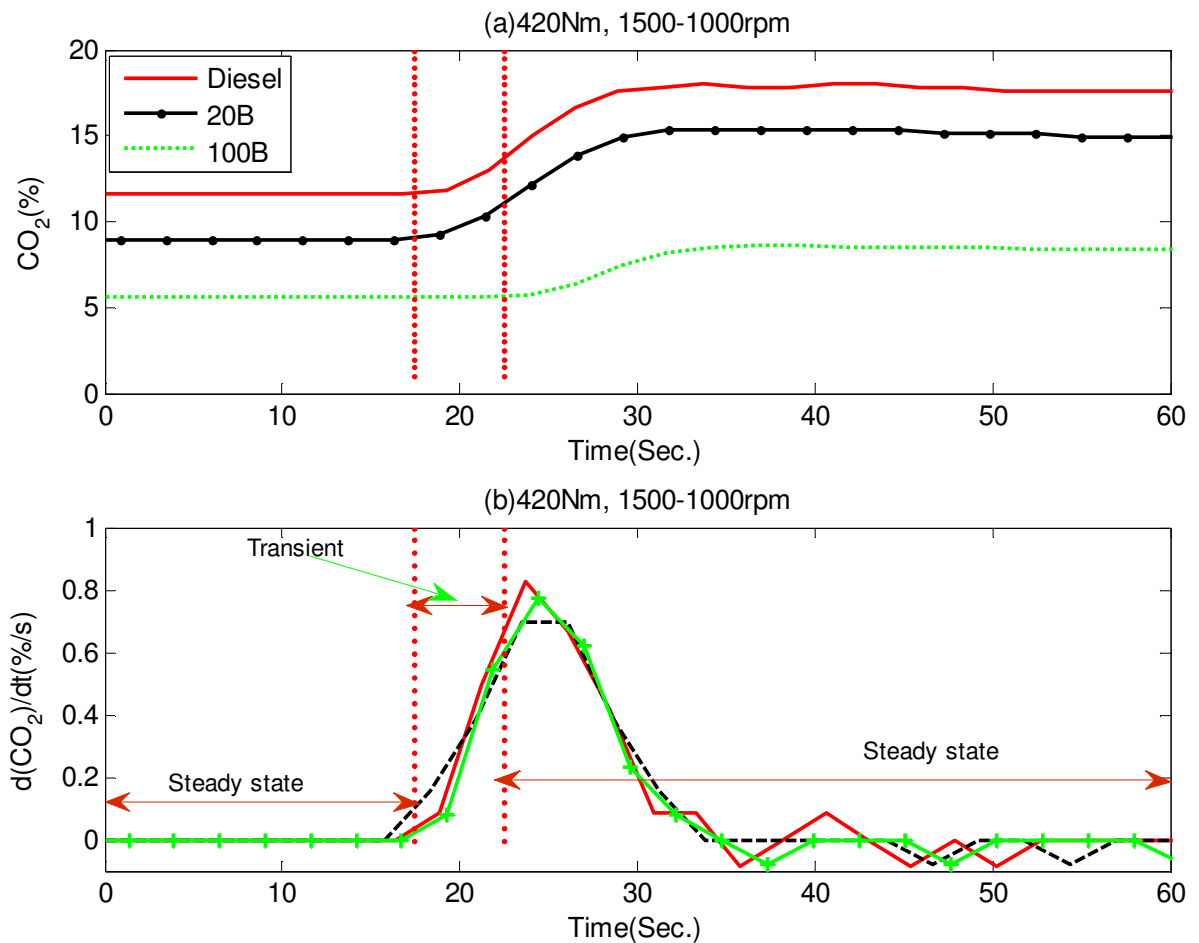


Figure 6-10 (a) Variation of CO₂ emission of CI engines with time for running with different fuels during negative speed transient (b) Variation of rate of change CO₂ emission with time for CI engines running with different fuels during negative speed transient

The effects of the torque transitions on the operational parameters of the engine fuelled with diesel, 20B and 100B at 1500rpm are presented in Figure 6-11 and Figure 6-12. As seen in Figure 6-11(a), the CO₂ emission increased during torque increase from 210-420Nm. Similarly, during the negative transition transient condition (Figure 6-12(b)), the CO₂ emission decreased during the torque decrease from 420-210Nm. In both conditions, the engine with the higher torque emitted higher CO₂ emissions. This can be explained on the basis that at the maximum engine load, the fuel/air equivalence ratio entering to the cylinder increased. To yield the maximum torque, the fuel needed to burn completely in the cylinder in order to produce higher CO₂ emissions. As shown in Figure 6-11(b) and Figure 6-12(b), the rates of CO₂ emissions are 0.35%/s and 0.30%/s, respectively. The emission rates for the diesel, 20B and 100B were observed to be irregular. During both the acceleration and deceleration transient, the engine running on 100B resulted in higher CO₂ emissions.

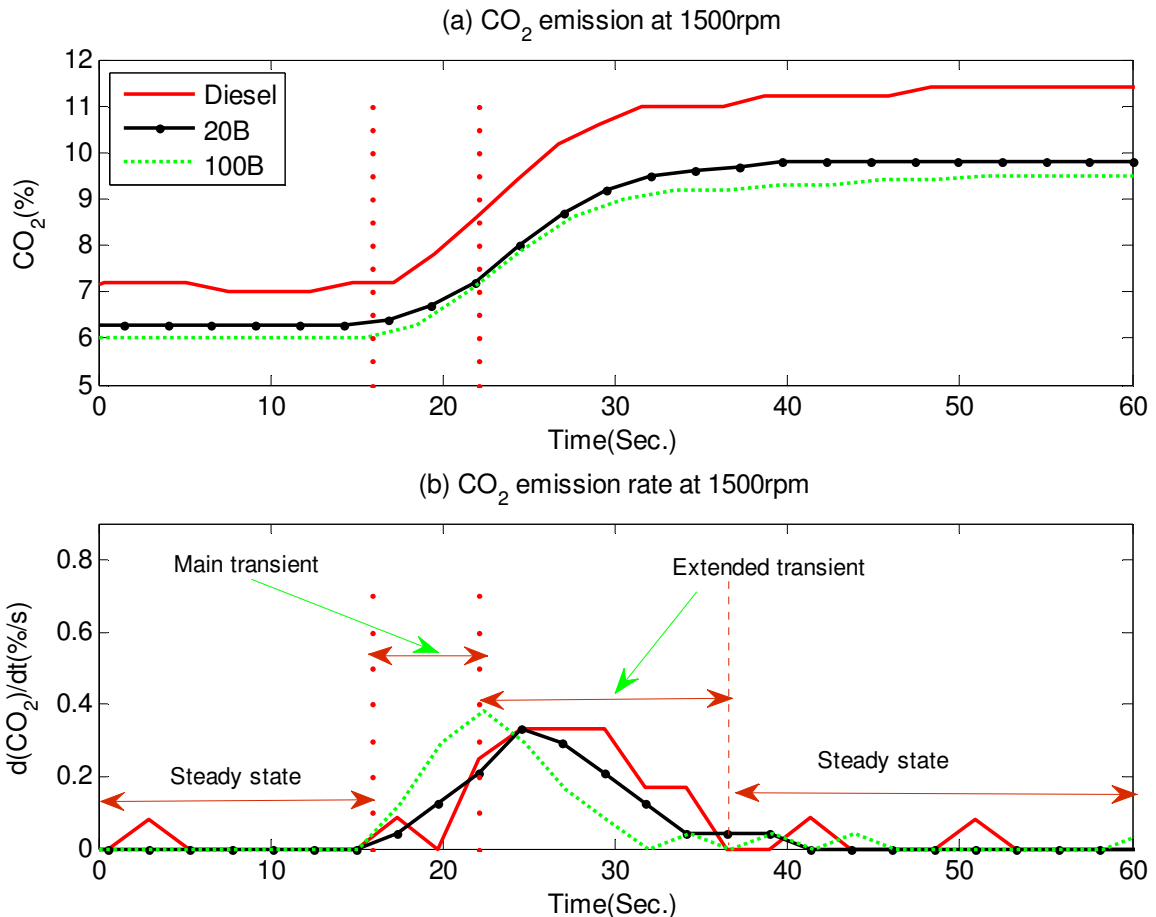


Figure 6-11 (a) Variation of CO₂ emission of CI engines with time for running with different fuels during positive torque transient (b) Variation of rate of change CO₂ emission with time for CI engines running with different fuels during positive torque transient.

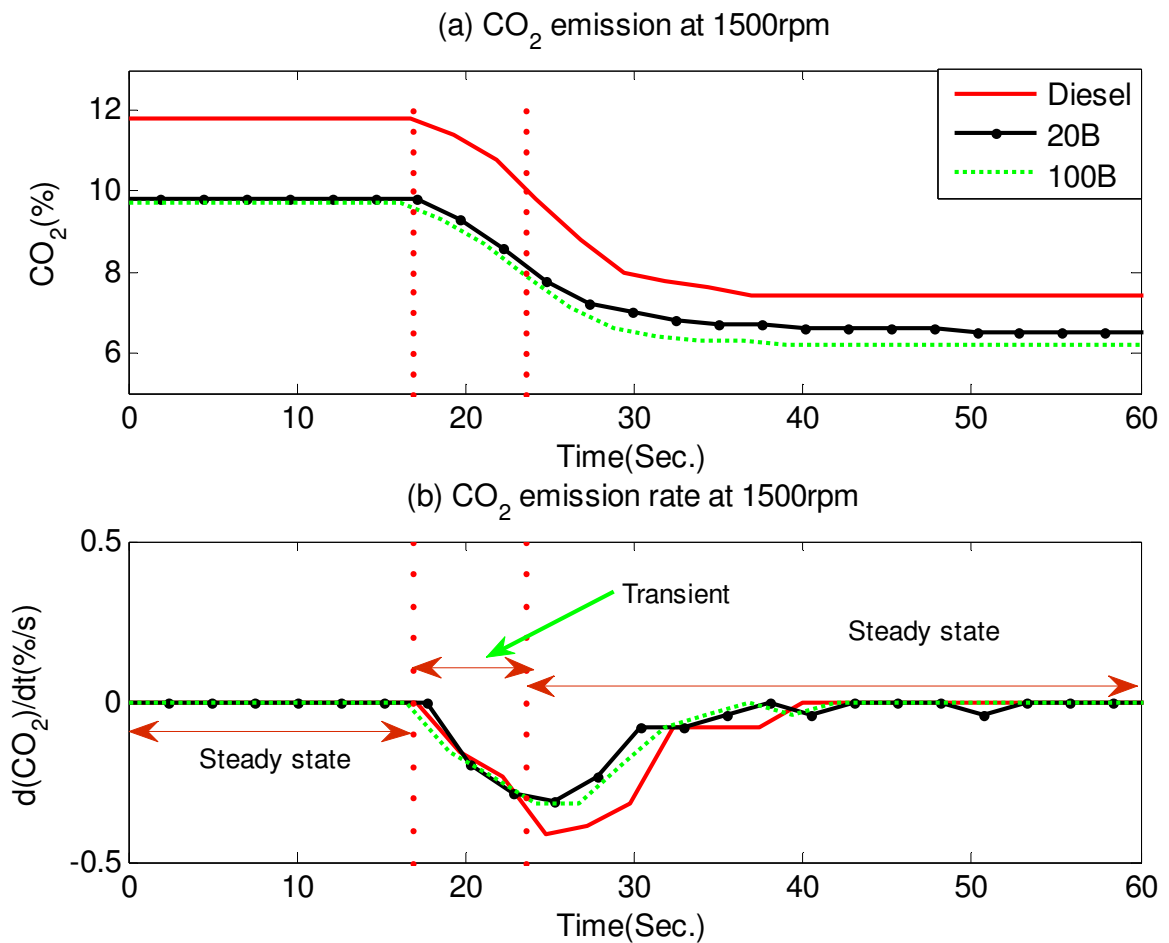


Figure 6-12 (a) Variation of CO₂ emission of CI engines with time for running with different fuels during positive torque transient (b) Variation of rate of change CO₂ emission with time for CI engines running with different fuels during positive torque transient

Under all the four transient operation conditions i.e. 1000-1500rpm, 1500-1000rpm, 210-420Nm and 420Nm-210Nm, the 20B and 100B fuels resulted in lower CO₂ emission values than the diesel fuel during both steady and transient operations, as shown in Figure 6-13 and Figure 6-14. Figure 6-13 shows the CO₂ emission variation achieved by fuelling the CI engine with biodiesel blends during acceleration and deceleration at a load of 420Nm. During the acceleration operation, 20B and B100 reduced the CO₂ emission by 53% and 122%, as shown in Figure 6-13. Similarly, during the deceleration operation, the CO₂ emission from the engine fuelled with 20B and 100B was reduced by 50% and 107%, respectively. In both operation conditions, the maximum reduction was achieved during the transient operation. During the pre-transient and post-transient steady operations CO₂ emission reduction was fairly constant.

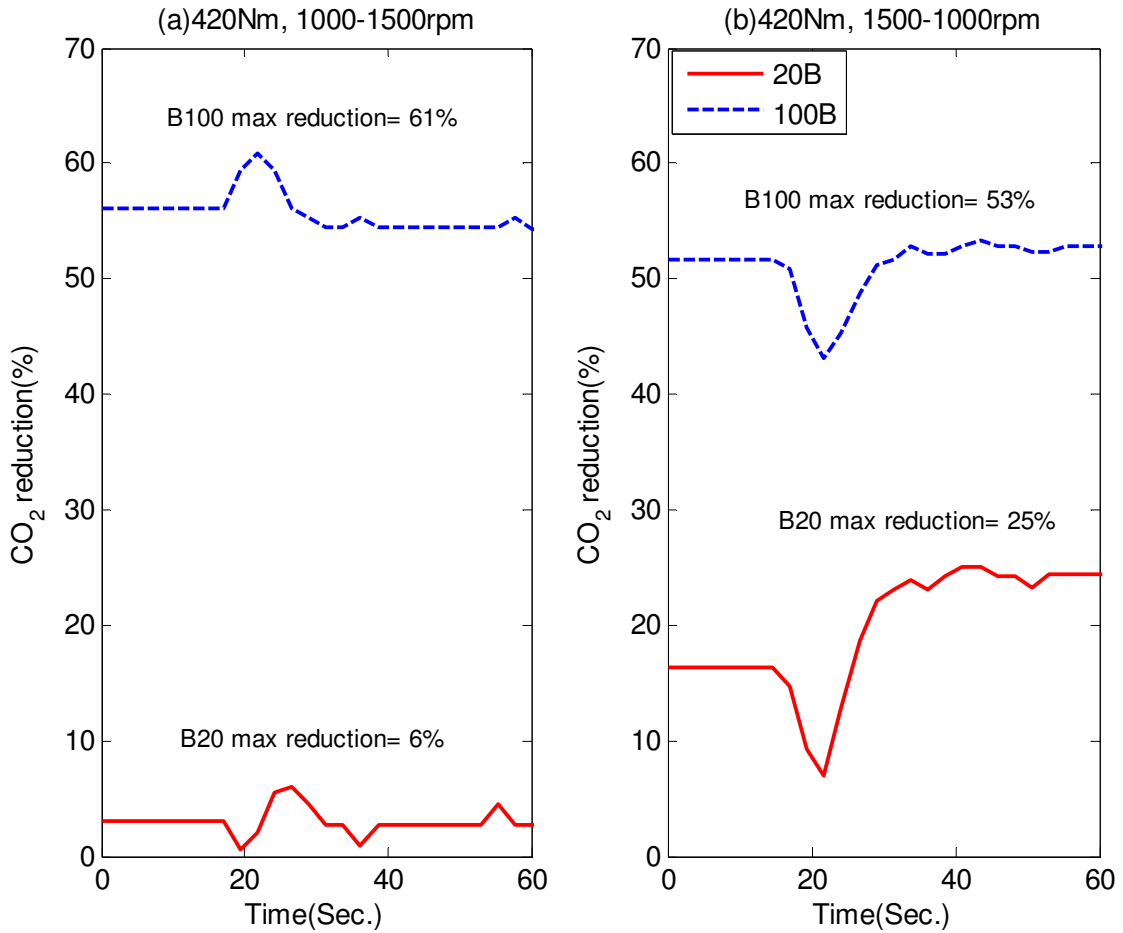


Figure 6-13 Variation of CO₂ emission percentage reduction of CI engine with time by using different biodiesel blends during speed transient condition

Figure 6-14 depicts the CI engine's CO₂ emission reduction values during the torque transient operation. The positive torque transition resulted in inconsistent CO₂ emission reduction values as shown in Figure 6-14(a). The CO₂ emission was found to reduce by up to 16% and 19% when the engine was fuelled with 20B and 100B. During the negative torque transition, the CO₂ emission reduced by 17% and 18% when the engine was fuelled with 20B and 100B as compared to diesel respectively.

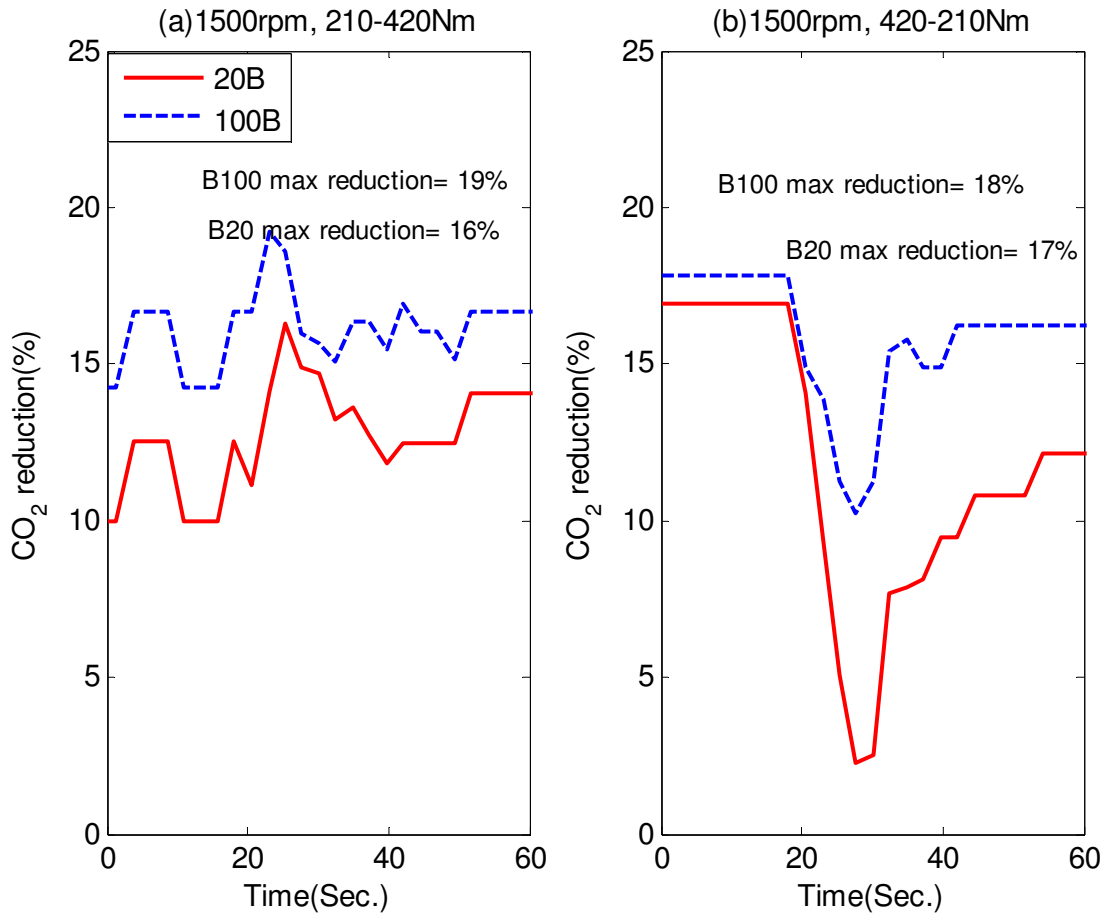


Figure 6-14 Variation of CO₂ emission percentage reduction of CI engine with time by using different biodiesel blends during torque transient condition

Among all operation conditions, the speed transient (1000-1500rpm) reduced the CO₂ emission by maximum amount. The primary reason for this result can be that biodiesel has a lower number of carbon molecules than diesel fuel (i.e. biodiesel: 77% and diesel: 87%, as described in Table 3-4. The combustion of the biodiesel with air resulted in lower CO₂ emission than diesel.

6.1.2.2 The NO_x Emission

The effects of biodiesel blends on the NO_x emission from a CI engine fuelled with diesel, 20B and 100B, at a speed transient of 1000-1500rpm and a load of 420Nm, is presented in Figure 6-15. It can be seen that the NO_x emission during pre-transient operation resulted in fairly constant emission values. However, at post-transient stage, the NO_x emission registered increases with time. This can be explained on the basis that at higher engine speeds, the fuel/air equivalence ratio entering into the cylinder increased. During high torque and speed operation, the fuel needed to burn completely in the cylinder that resulted in higher NO_x

emissions. The NO_x emission rates for the speed acceleration are depicted in Figure 6-15(b). The emission rate of the diesel, 20B and 100B at both pre-transient and post-transient process were fairly uniform as expected. The NO_x emission rate change for engine operation with Biodiesel was lower than both 20B and diesel. The engine fuelled with diesel showed the highest change rate, i.e. 16ppm/s.

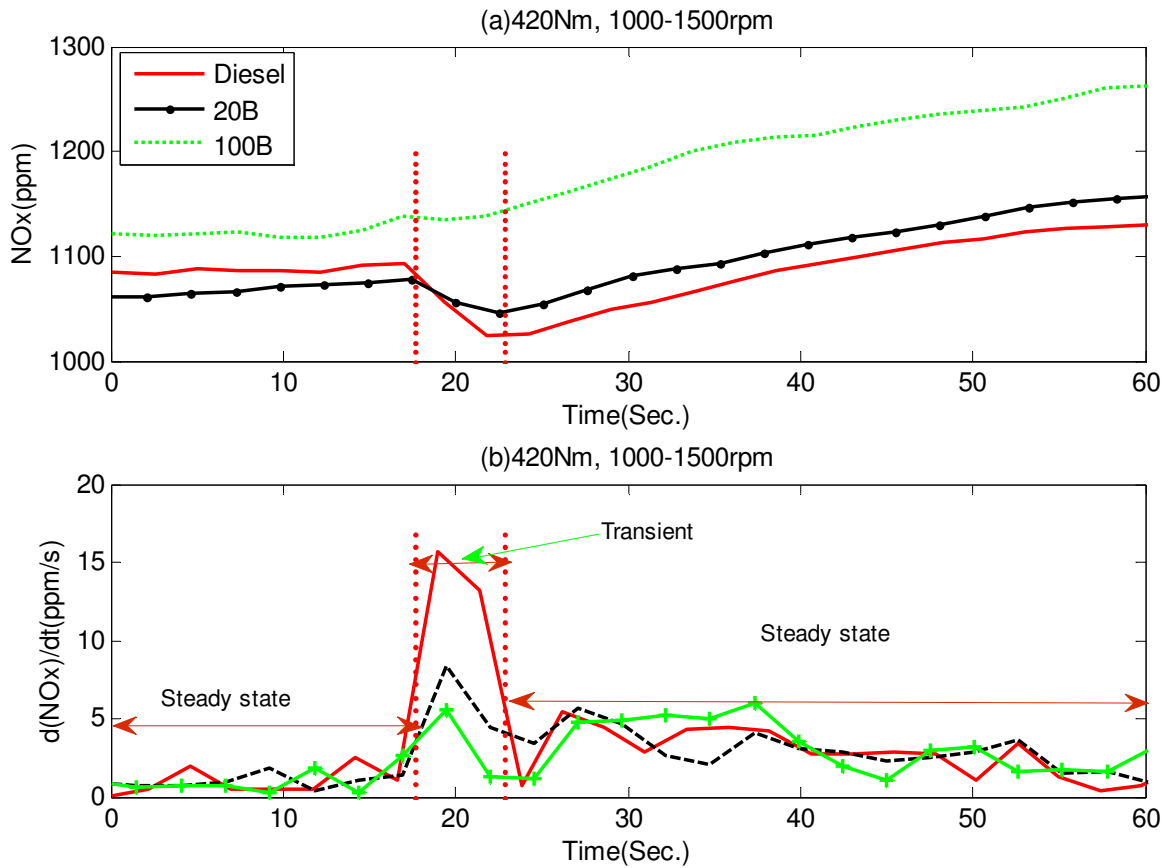


Figure 6-15 (a) Variation of NO_x emission of CI engines with time for running with different fuels during positive speed transient (b) Variation of rate of change NO_x emission with time for CI engines running with different fuels during positive speed transient

The effect of the engine deceleration on NO_x emission during 1500-1000rpm transient is shown in Figure 6-16. The CI engine's NO_x emission increased with a decrease in engine speed from 1500 to 1000rpm. As seen in Figure 6-16(b), the emission rate change was near zero during the pre-transient and post-transient operations. The maximum NO_x emission rate was attained three seconds after the scheduled transient. Comparing the acceleration and deceleration NO_x emission change rates, the former emission rate was higher during the same time span. In both cases, the engine fuelled by 100B resulted in higher NO_x emissions.

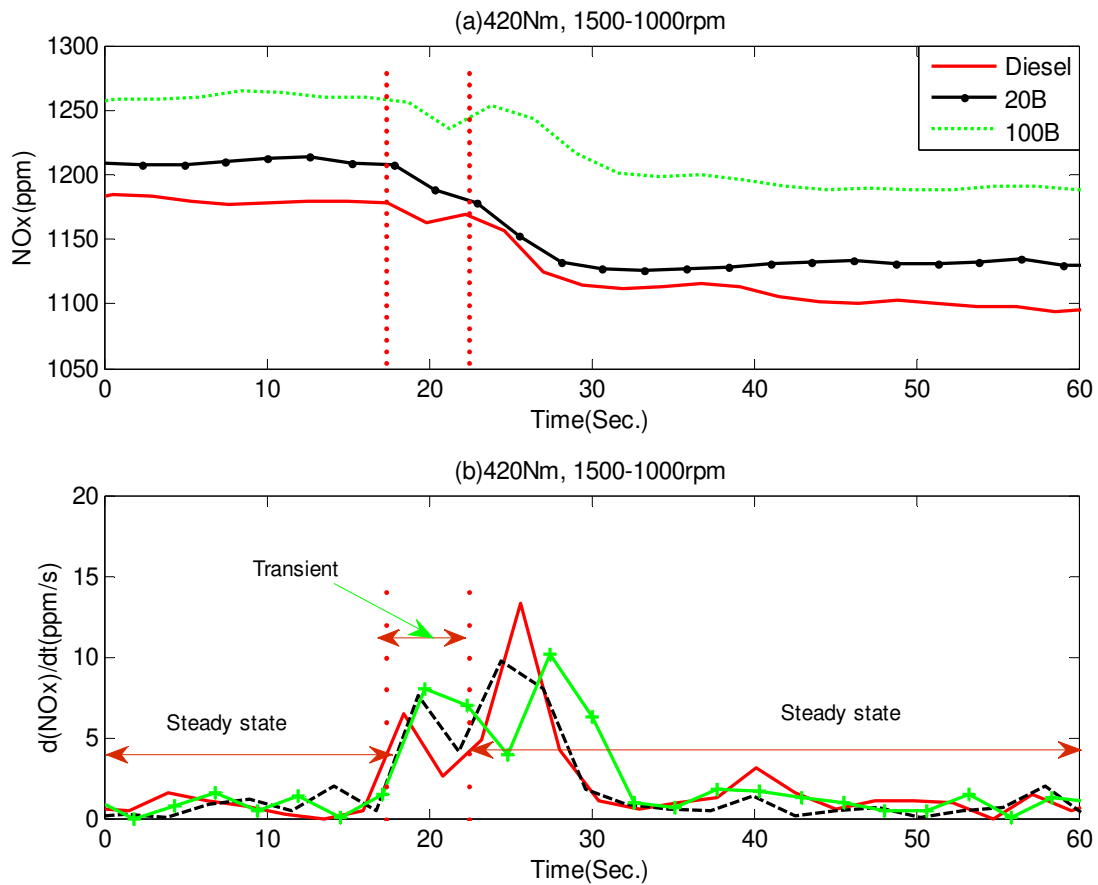


Figure 6-16 (a) Variation of NOx emission of CI engines with time for running with different fuels during negative speed transient (b) Variation of rate of change NOx emission with time for CI engines running with different fuels during negative speed transient

The NOx emission values from the CI engine fuelled by diesel, 20B and 100B at 1500rpm during the torque transitions are presented in Figure 6-17 and Figure 6-18. As it can be seen in Figure 6-17(a), the NOx emission increased steeply with increase in torque from 210 to 420Nm. Similarly, during the negative torque transition condition, the NOx emission decreased during the torque change from 420 to 210Nm, as shown Figure 6-18 (a). In both conditions, the engine with the higher torque emitted higher NOx emission. This can be explained on the basis that at the maximum engine load, the fuel/air equivalence ratio entering into the cylinder increased. The rate change of the NOx emission is shown in Figure 6-17(b) and Figure 6-18(b). In both conditions, the 100B resulted in a higher rate of change in NOx emission, with maximum rate value of 95%

and 92% for the positive torque and negative torque transient, respectively. The pre-transient and post-transient of NOx emission rates were almost zero for both positive and negative torque transition. The transition effects on the NOx emission continued for 10 seconds after the assigned transition time.

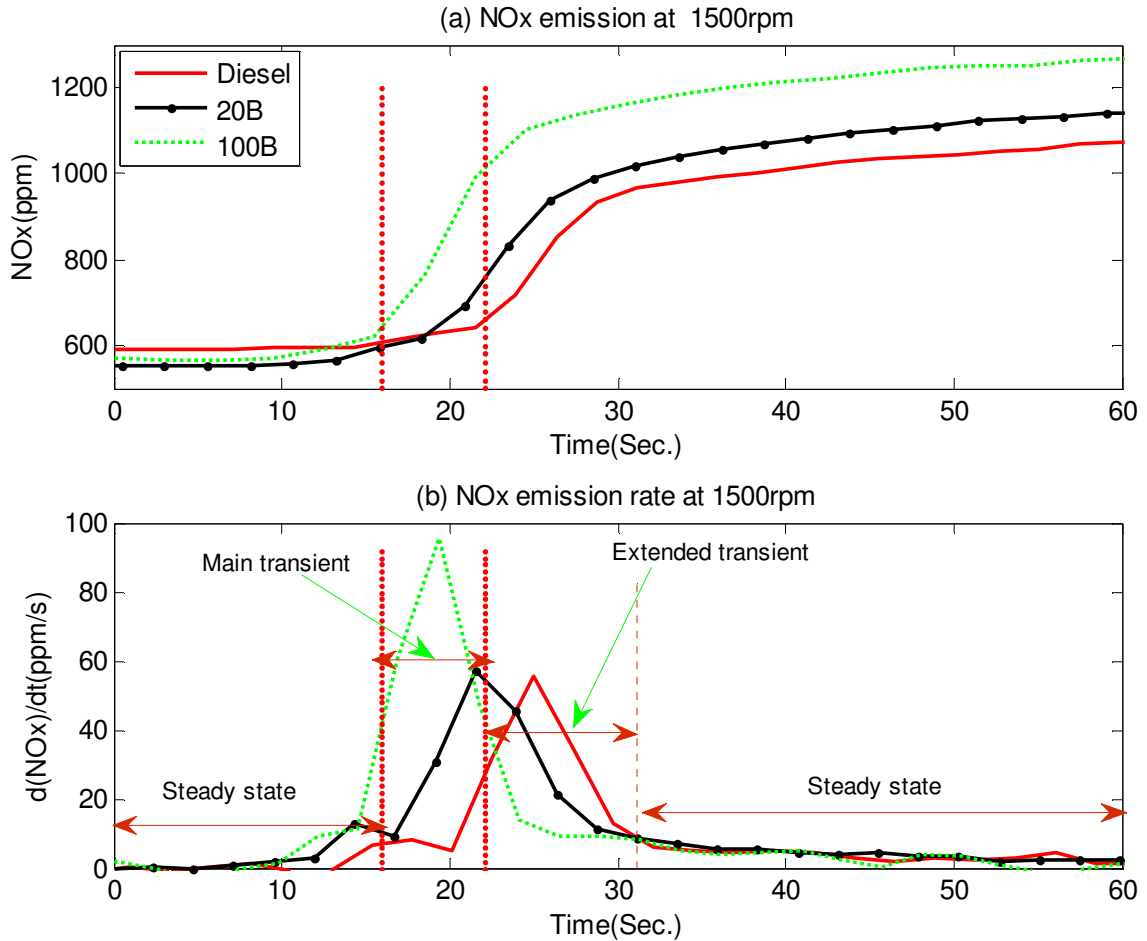


Figure 6-17 (a) Variation of NOx emission of CI engines with time for running with different fuels during positive torque transient (b) Variation of rate of change NOx emission with time for CI engines running with different fuels during positive torque transient

Figure 6-19 depicts the NOx emission increment of the CI engine fuelled by 20B and 100B, during 1000-1500rpm acceleration and 1500-1000rpm deceleration at 420Nm. The NOx emission of the engine fuelled with 20B and 100B, increased by up to 3% and 16%, respectively as compared to engine running with diesel. Similarly, the deceleration operation also increased the NOx emission by up to 4% and 8% for 20B and 100B biodiesel blends respectively.

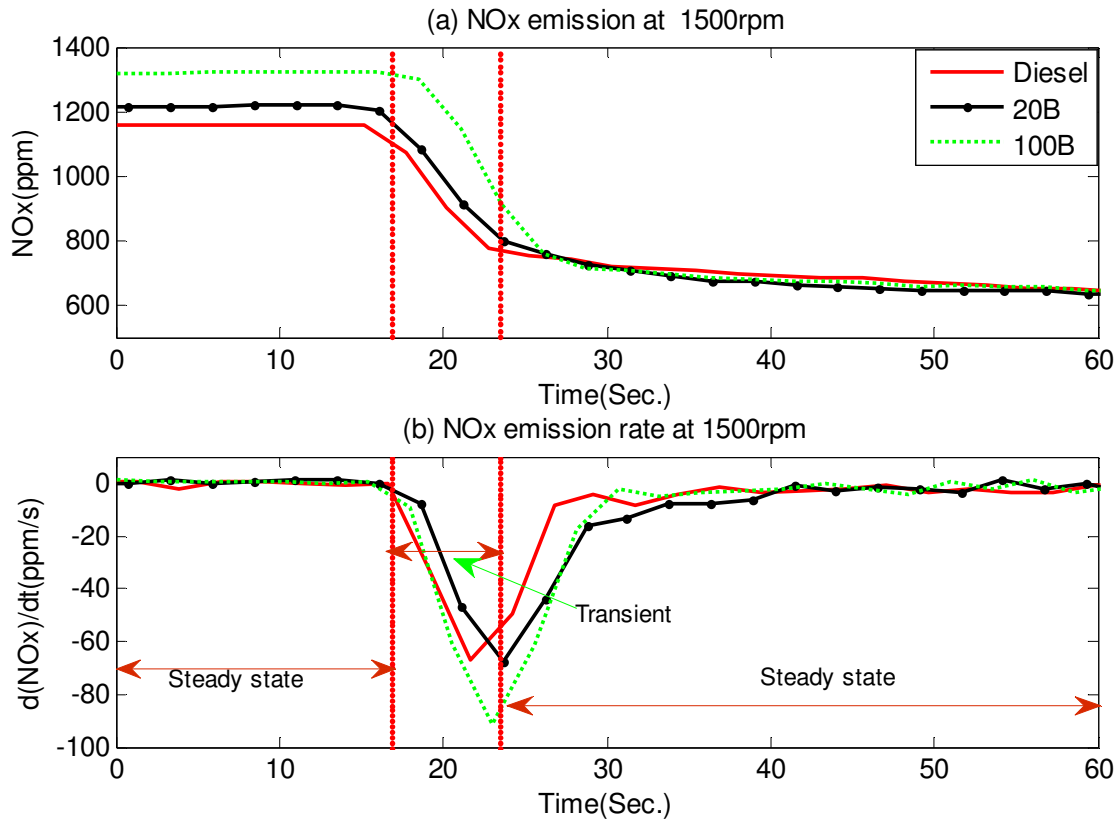


Figure 6-18 (a) Variation of NOx emission of CI engines with time for running with different fuels during negative torque transient (b) Variation of rate of change NOx emission with time for CI engines running with different fuels during negative torque transient

Figure 6-19(a) shows that the NOx emission increases steeply during the 1000-1500rpm transient. This can be explained on the basis that as the engine speed increased the in-cylinder temperature increased and as a result the NOx emission also increased. Although during the deceleration operation the engine speed decreased, the in-cylinder temperature decreased slowly due to the heat transfer phenomena, which results in slow reduction in NOx values. The effect of the torque transient on the NOx emission of the engine running on biodiesel at 1500rpm is shown in Figure 6-20. The NOx emission of the CI engine running on 20B and 100B increased by up to 8% and 20% respectively during the positive torque transient from 210-420Nm, as shown in Figure 6-20(a). Similarly, the NOx emission of the engine is increased by up to 20% and 27%, for 20B and 100B respectively. The main reason for higher NOx emission of biodiesel is due to the advanced combustion process initiated by the physical properties of biodiesel (viscosity, density, compressibility, sound velocity). When biodiesel is injected, the pressure rise produced by the pump is quicker as a consequence of its lower compressibility (higher

bulk modulus) and propagates more quickly towards the injectors. In effect, the cylinder gas gets richer by fuel producing higher peak temperature which enhances the formation NO_x

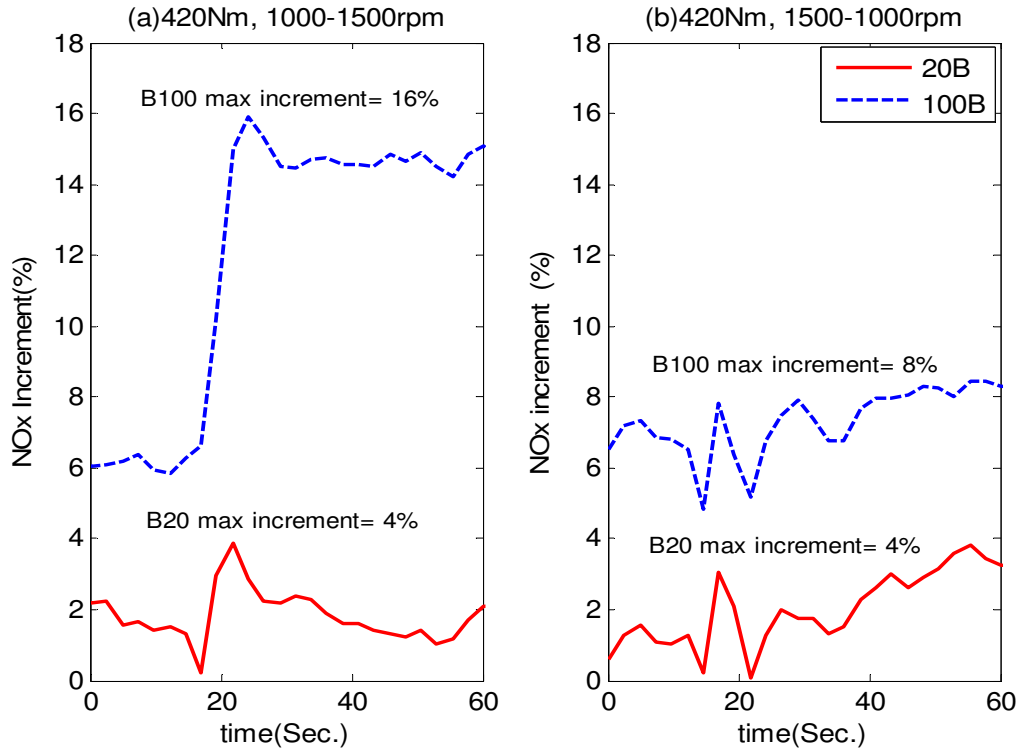


Figure 6-19 Variation of NO_x emission percentage reduction of CI engine with time by using different biodiesel blends during speed transient condition

6.1.2.3 The CO Emission

Figure 6-20 shows the CI engine's CO emission at a load of 420Nm and acceleration from 1000rpm to 1500rpm. It can be seen that the CI engine emits higher CO emission during the lower engine speeds. This can be explained on the basis that at lower engine speeds, the gas temperature within cylinder was lower, which prevented the CO components to be effectively converted to CO₂. The CO and CO₂ emission values showed opposing trends, as shown in Figure 6-9(a) and Figure 6-20(a). At higher engine speeds, the air/fuel equivalence ratios increased, resulting in increase in the in-cylinder gas temperatures, which in turn lead to increase in the kinetic reaction rate from CO to CO₂. This leads to lower CO emissions. The emission rate change of CO is depicted in Figure 6-20(b).

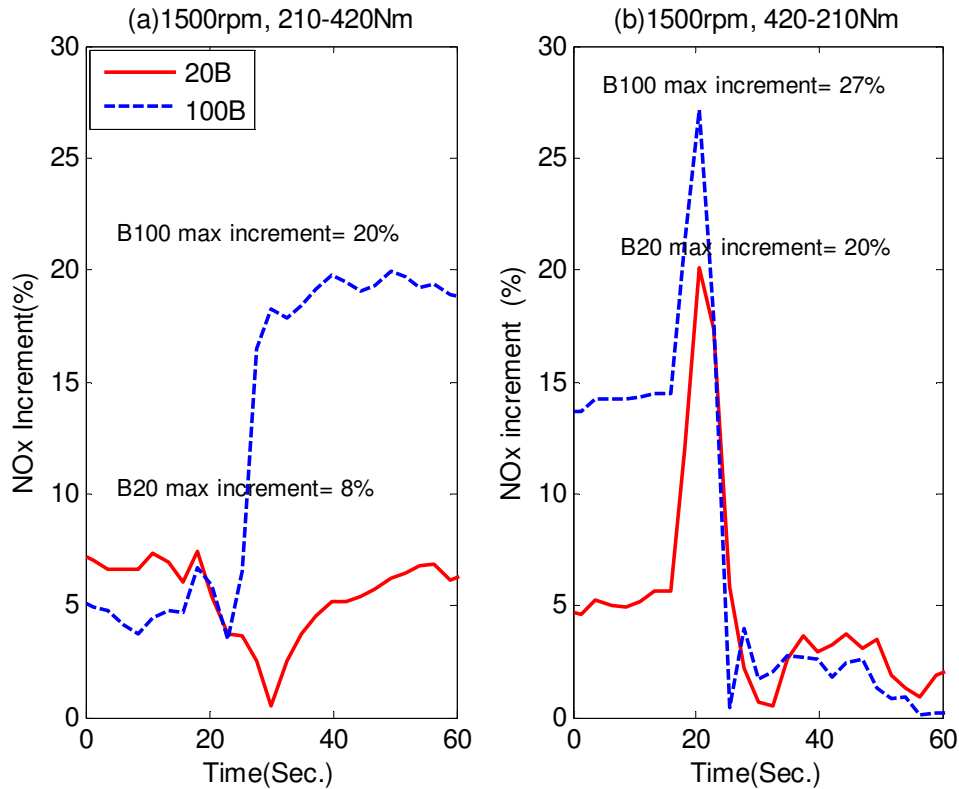


Figure 6-20 Variation of NOx emission percentage reduction of CI engine with time by using different biodiesel blends during torque transient condition

It can be seen that use of 20B resulted in the highest emission rate, followed by diesel in the transient stage. The effects of the transient operation were extended to the post-transient steady CO emission behaviour. As seen in the Figure 6-20 the CO emission rate change extended for more than 16 seconds after the time span of the transient operation. The pre-transient and post-transient CO emission rate change was near zero; this indicates that in both operations the CO emission was constant.

The CI engine's CO emission during deceleration from 1500rpm-1000rpm is shown in Figure 6-22. It can be seen that the CI engine's CO emission increased steeply with engine acceleration. However, the main effects of the transient operation on the CO emission appeared after the transient range. As seen in Figure 6-22(b), the transient effects extended for 18 seconds after the transient time span. The diesel and 20B resulted in a maximum CO emission rate of 110ppm/s.

The effects of the torque transition operations on the CO emission of the test engine fuelled with diesel, 20B and 100B at a speed of 1500rpm, are shown in Figure 6-23 and

Figure 6-24. As it can be seen in Figure 6-23(a) and Figure 6-24(a), the torque transient did not show any significant effects on the CO emission for both positive transient and negative transient operations. In both cases, the emission rate varied between 0-3ppm/s, as indicated in Figure 6-23(b) and Figure 6-24(b), respectively. The maximum CO emission rate was 3ppm/s during positive and negative transients.

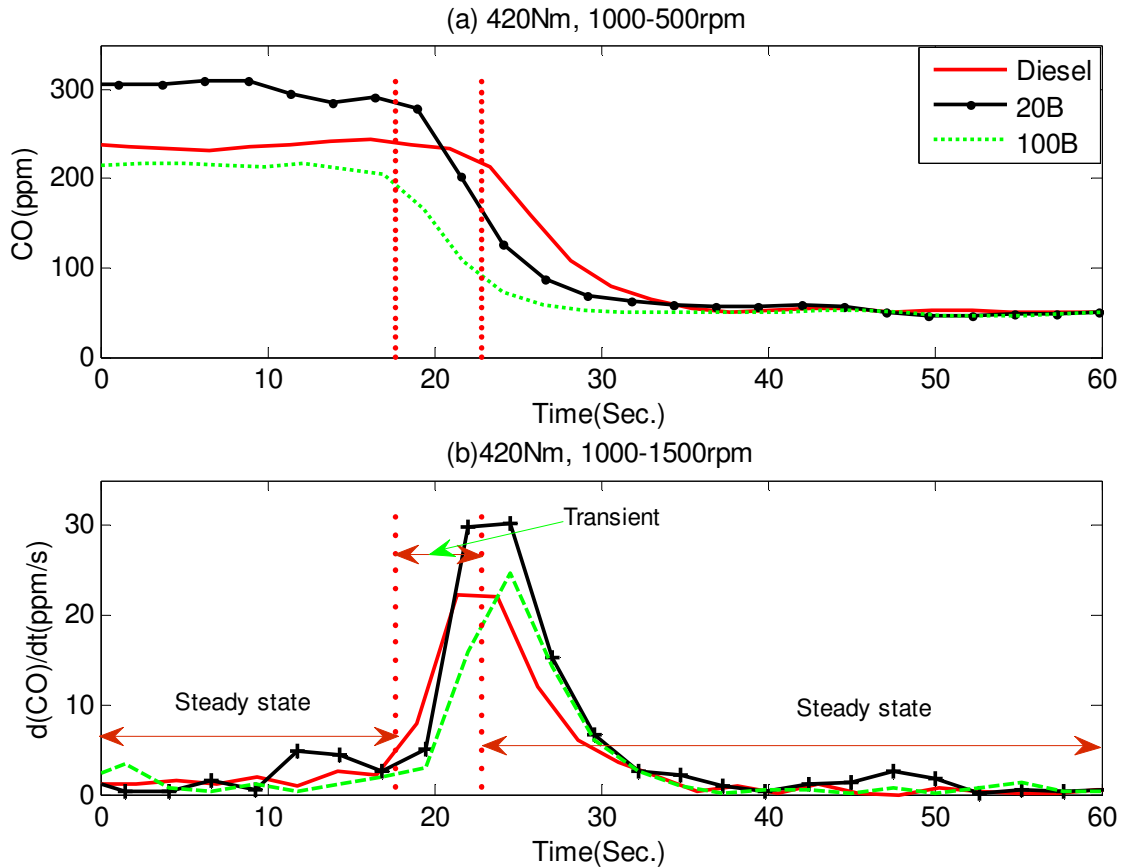


Figure 6-21 (a) Variation of CO emission of CI engines with time for running with different fuels during positive speed transient (b) Variation of rate of change CO emission with time for CI engines running with different fuels during positive speed transient

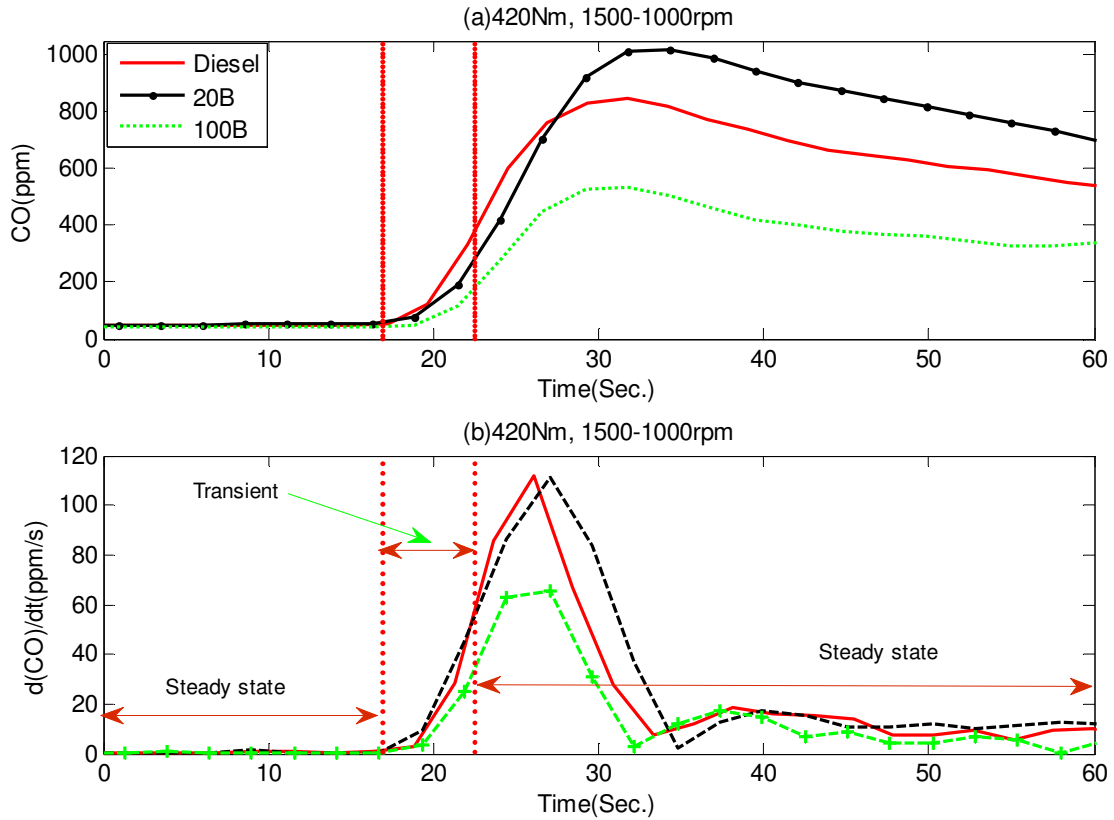


Figure 6-22 (a) Variation of CO emission of CI engines with time for running with different fuels during negative speed transient (b) Variation of rate of change CO emission with time for CI engines running with different fuels during negative speed transient

The effects of biodiesel blends on a CI engine's CO emission during the speed transient and torque transition conditions are shown in Figure 6-25 and 6-26. During the former condition, the engine fuelled with 20B and 100B reduced the CO emission by up to 39 and 45%, respectively. The deceleration operation showed peak values of 122% and 124% for 20B and 100B. The effect of the biodiesel blends on the CO emission of the engine running on biodiesel at an engine speed of 1500rpm during torque transient is shown in Figure 6-26. The CO emission of the CI engine running on 20B and 100B decreased by 22% and 24% for positive torque transition, and 18% and 22% for negative torque transition, respectively, as shown in Figure 6-26.

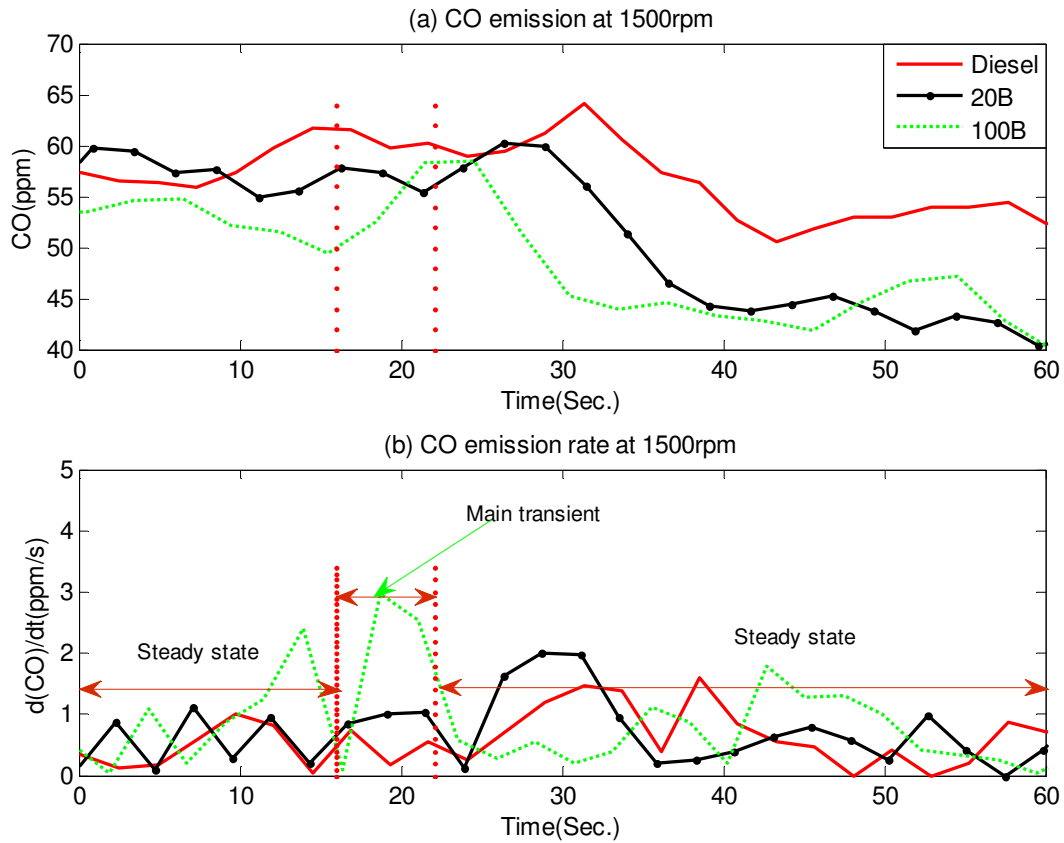


Figure 6-23 (a) Variation of CO emission of CI engines with time for running with different fuels during positive torque transient (b) Variation of rate of change CO emission with time for CI engines running with different fuels during positive torque transient

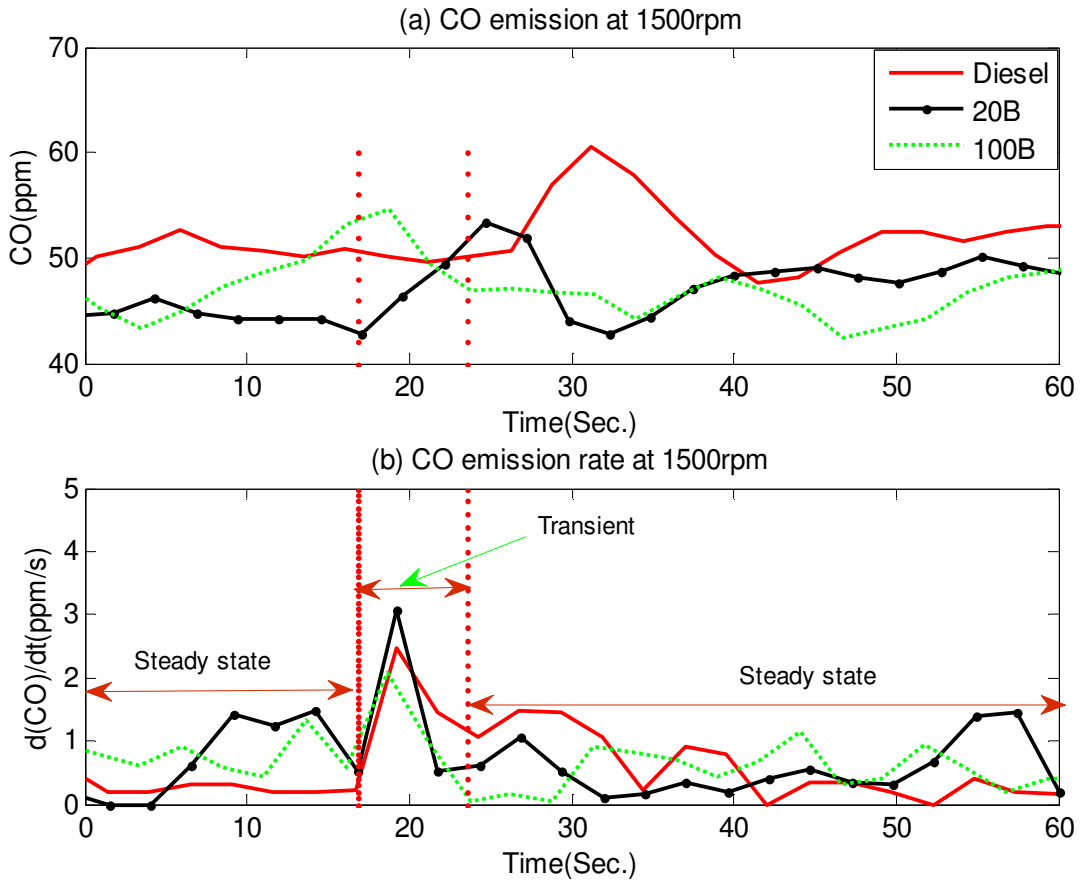


Figure 6-24 (a) Variation of CO emission of CI engines with time for running with different fuels during negative torque transient (b) Variation of rate of change CO emission with time for CI engines with different fuels during negative torque transient

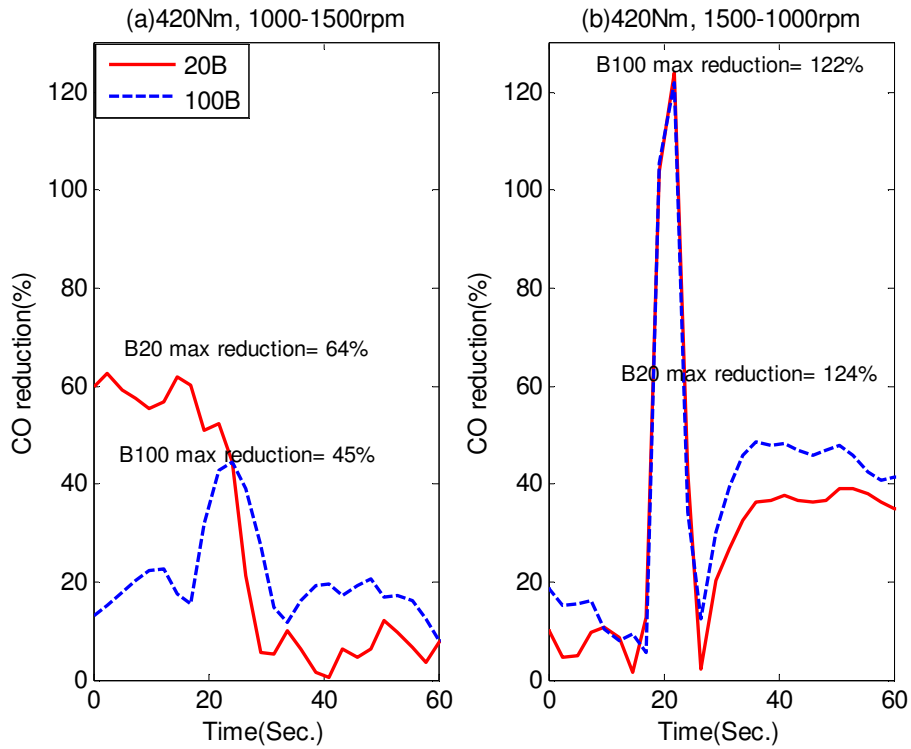


Figure 6-25 Variation of CO emission percentage reduction of CI engine with time by using different biodiesel blends during speed transient condition

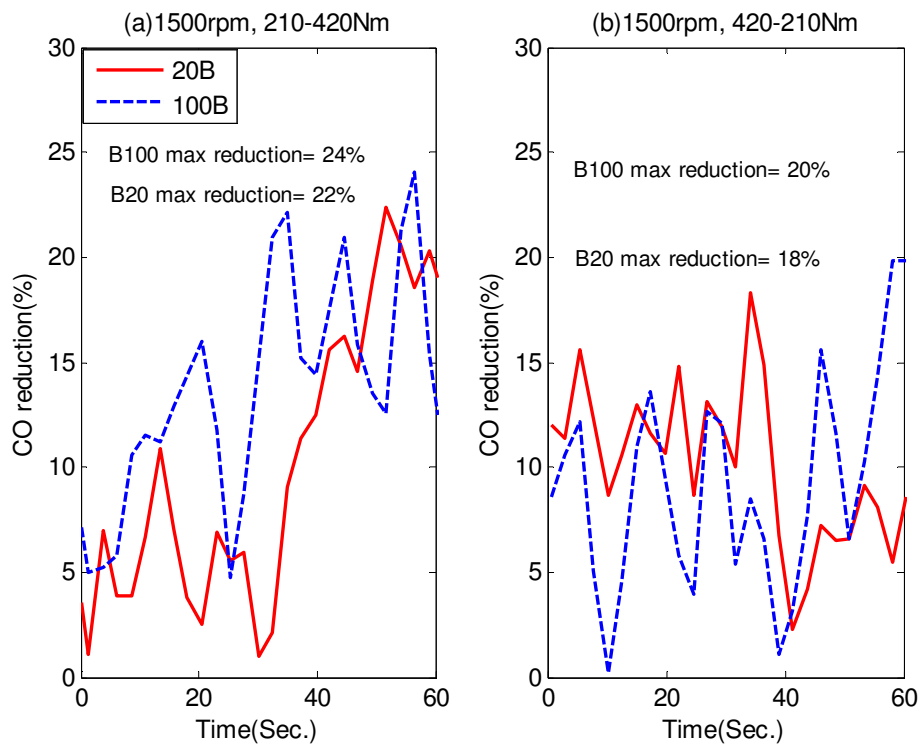


Figure 6-26 Variation of CO emission percentage reduction of CI engine with time by using different biodiesel blends during torque transient condition

6.1.2.4 The THC emission

Figure 6-27(a) shows the total hydrocarbon (THC) emission of the CI engine fuelled with 20B and 100B at a load of 420Nm and a speed transient from 1000rpm-1500rpm. The THC emission decreased during engine acceleration from 1000rpm-1500rpm. The THC emission rate of the CI engine running with 100B was higher than the diesel and 20B in the transient section, as presented in Figure 6-27(b). It can be seen that the THC emission rate change at the pre-transient and post-transient stages was below 0.1%/s. The transient operation has not affected significantly the post-transient steady operations. The effects of the acceleration operation on the THC emission of the CI engine are depicted in Figure 6-28(a). It can be seen that with decreases in engine speeds from 1500rpm-1000rpm, the THC emission increased steeply. The engine fuelled with diesel produced the highest THC emission rate, followed by 20B, as shown in Figure 6-28(b).

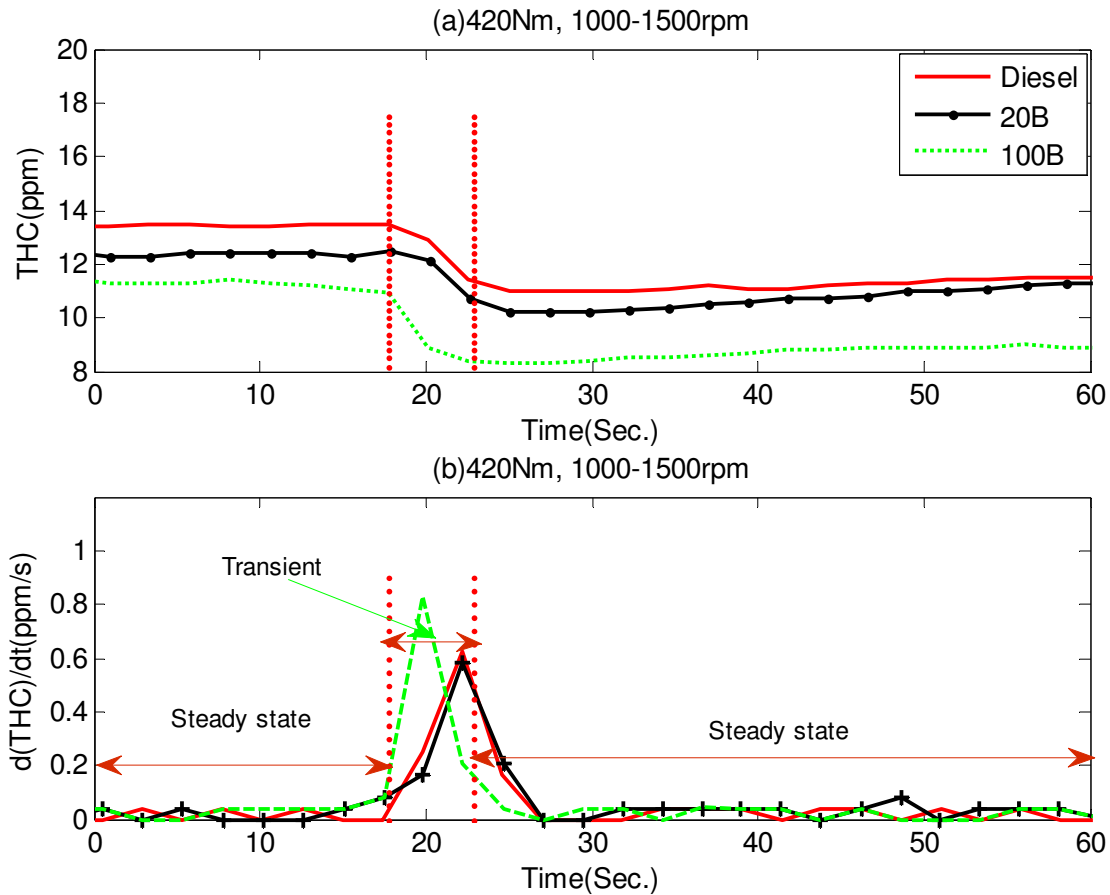


Figure 6-27 (a) Variation of THC emission of CI engines with time for running with different fuels during positive speed transient (b) Variation of rate of change CO emission with time for CI engines running with different fuels during positive speed transient.

The pre-transient and post-transient THC emission rates were almost zero. Similar to the acceleration operation, the transient operation resulted in minimal effects on the next steady operation.

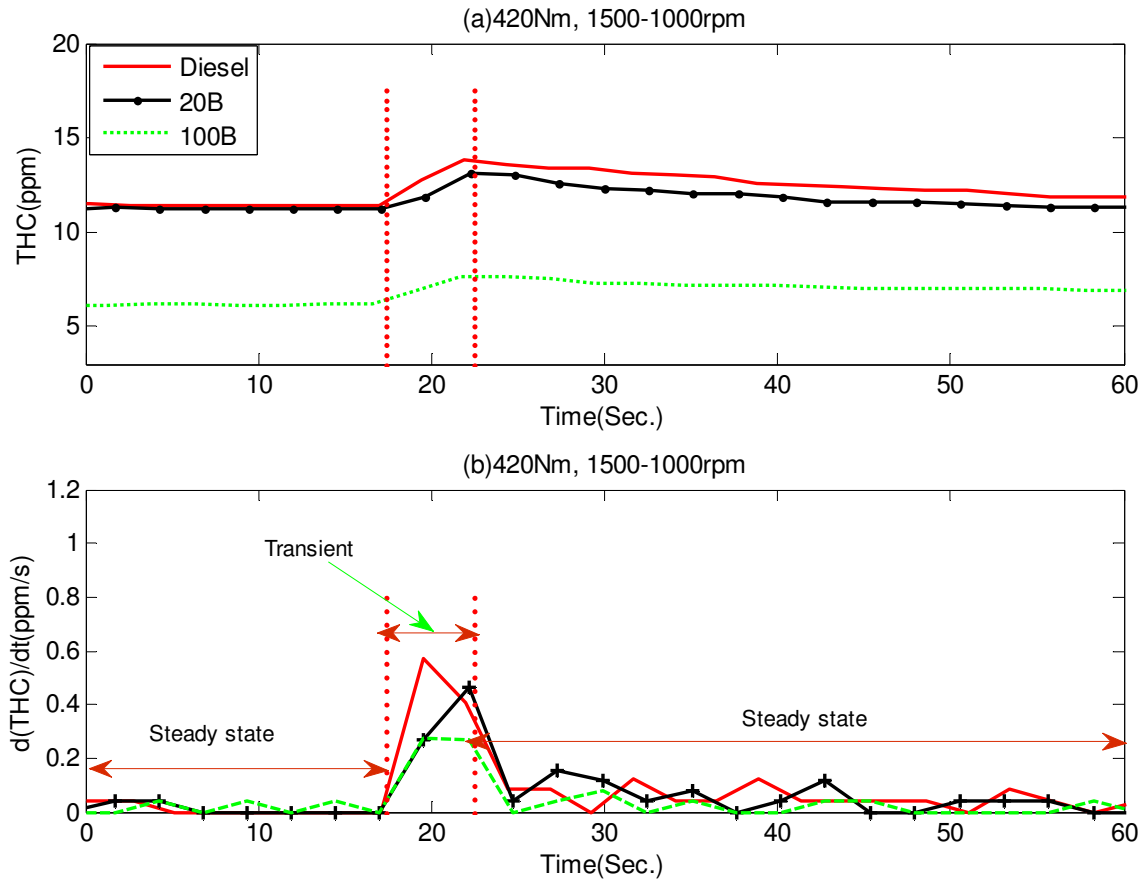


Figure 6-28 (a) Variation of THC emission of CI engines with time for running with different fuels during negative speed transient (b) Variation of rate of change CO emission with time for CI engines running with different fuels during negative speed transient.

The effects of the torque transition operations on THC emission for the engine fuelled by diesel, 20B and 100B at 1500rpm are presented in Figure 6-29 and Figure 6-30. As seen in Figure 6-29(a), the THC decreased with increasing torque from 210-420Nm for all fuels. The emission rates during the positive torque and negative torque transition operations varied between -0.5 and 0.5ppm/s, as shown in Figure 6-29(b) and Figure 6-30(b). In both instances, the THC emission rate of the engine fuelled with 100B tended to zero.

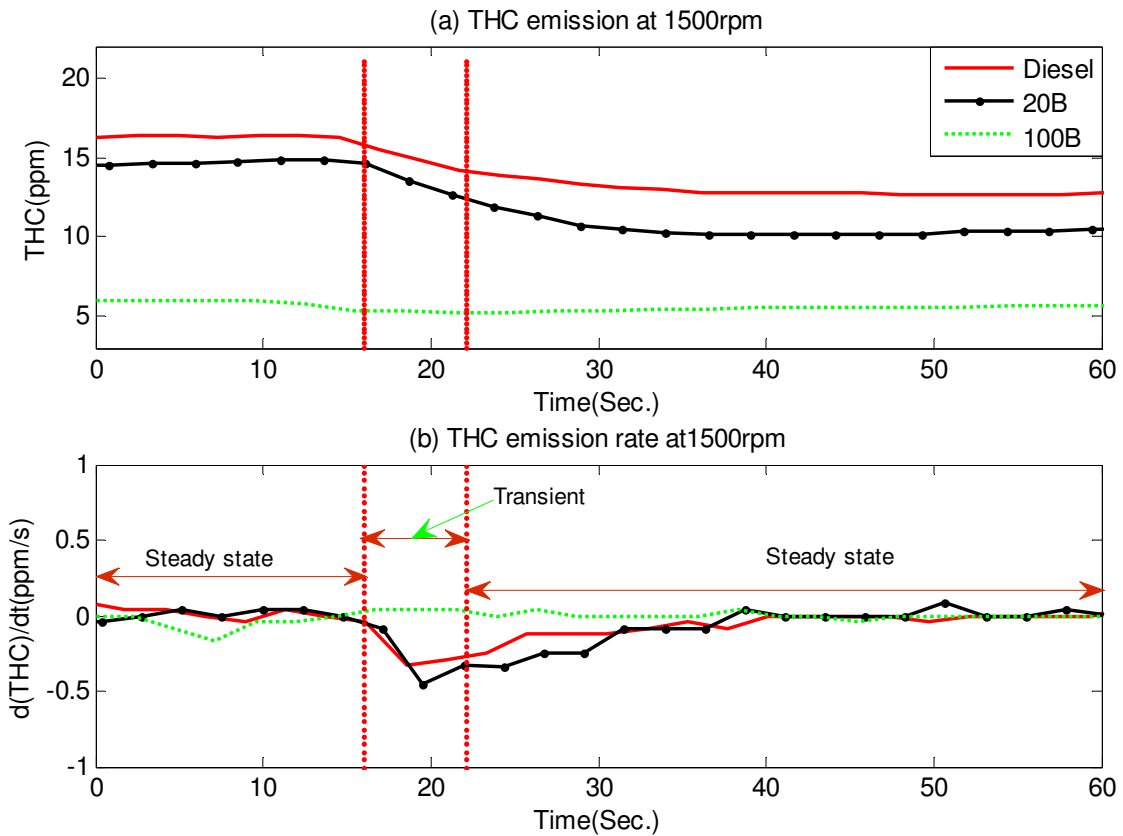


Figure 6-29 (a) Variation of THC emission of CI engines with time for running with different fuels during positive torque transient (b) Variation of rate of change CO emission with time for CI engines running with different fuels during positive torque transient.

The reduction in THC emission when using biodiesel blends for the speed transients is shown in Figure 6-31. In addition, biodiesel has higher cetane number which reduces the combustion delay by up to 33% and 45%, and 9% and 48% when fuelling the CI engine with 20B and 100B. Similarly, during the torque transition operation, the THC was reduced by up to 21% and 63% and 28% and 66% when using biodiesel blends of 20B and 100B, respectively as it is depicted in Figure 6-32. The reduction of the THC is due to the biodiesel having 11% oxygen in its chemical composition. The presence of oxygen: a) reduces the number of carbon and hydrogen molecules which enter the cylinder; b) the oxygen molecule present in biodiesel guarantees the complete combustion

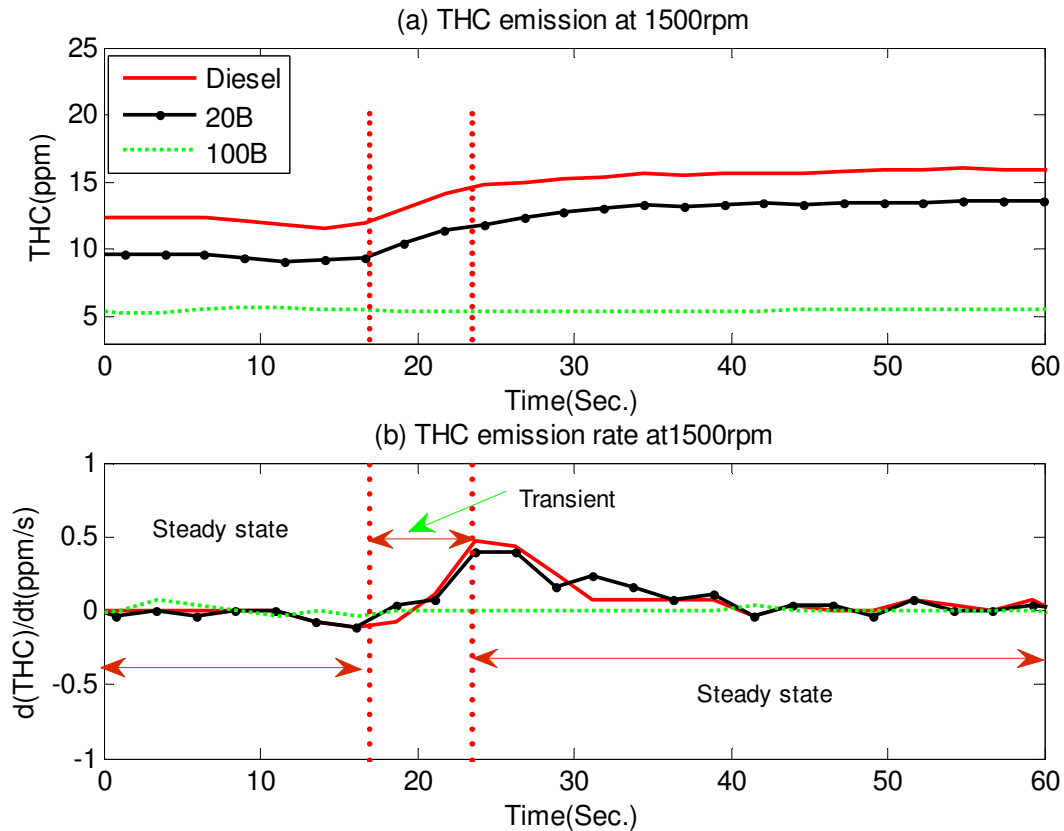


Figure 6-30 (a) Variation of THC emission of CI engines with time for running with different fuels during negative torque transient (b) Variation of rate of change CO emission with time for CI engines running with different fuels during negative speed transient.

The effects of biodiesel blends on engine emissions are presented in Table 6-1. It can be seen that the biodiesel and its blends result in lower CO_2 , CO and THC emission during all the transient operations. However, the use of biodiesel as a fuel in the test CI engine increases the NOx emission during the speed transient and the torque transition. The effects of transient operation on emission variation have not been limited to the transient operation period. The emissions experience transient conditions far beyond the regulated speed and torque transient condition as summarised in Table 6-2. The post transient emission time of NOx and CO is relatively higher than the other emissions. The higher extended time of NOx emission after the transient operation can be explained from the direct relation between NOx emission and the thermal nature of the combustion in the cylinder. After the instant transient operations, the conditions within the cylinder change. These changes can take a long time to reach steady conditions due to the slow stability of heat transfer inside the cylinder through convection and conduction processes.

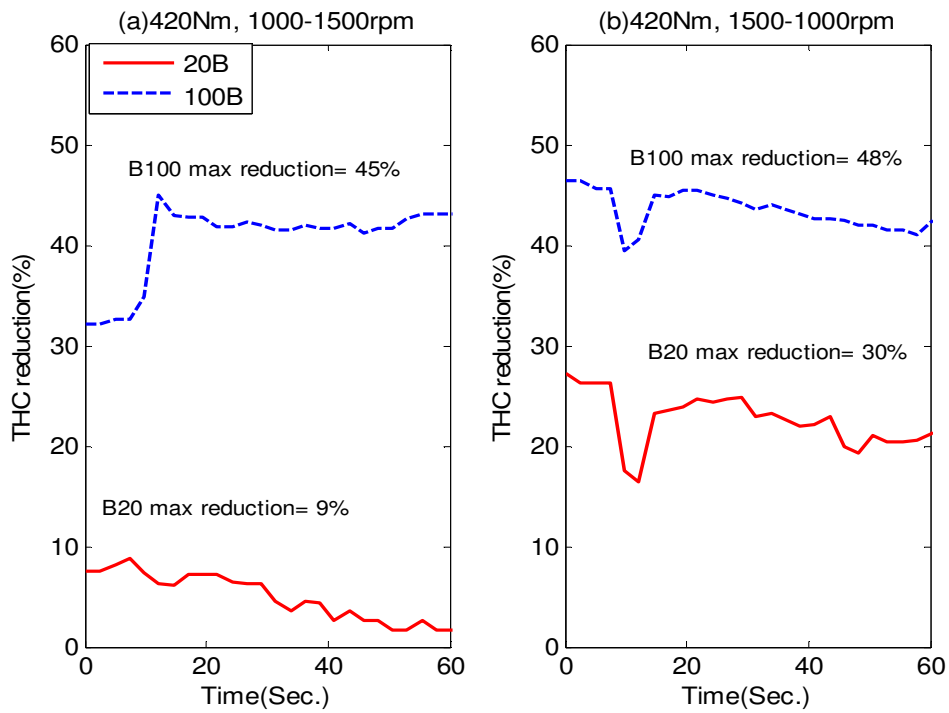


Figure 6-31 THC emission percentage reduction of CI engine by using different biodiesel blends during speed transient condition

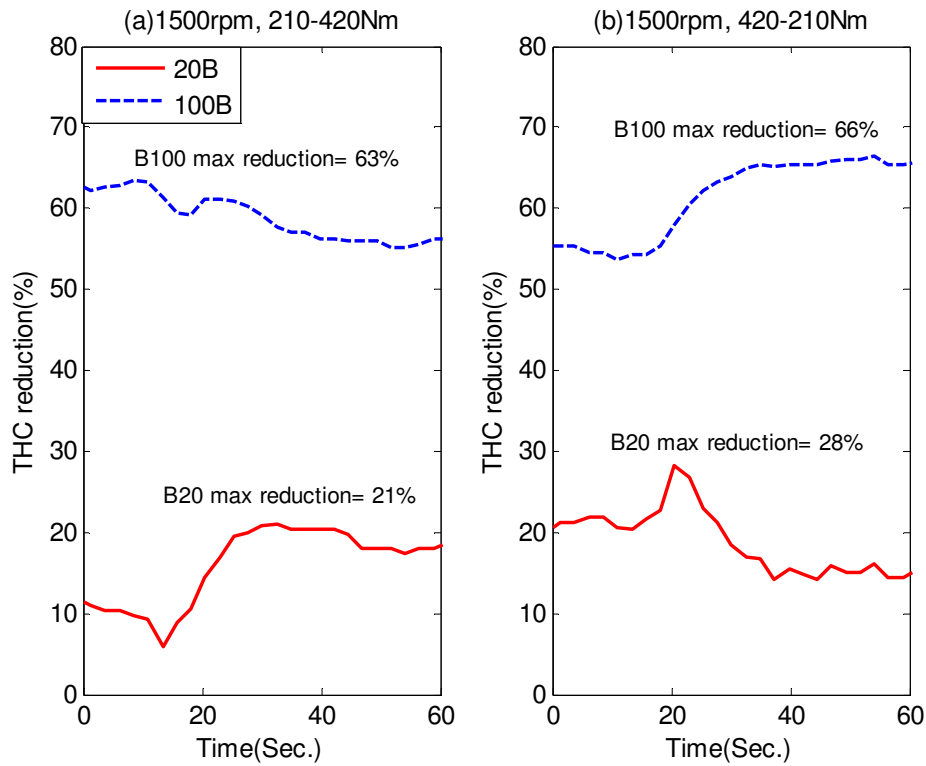


Figure 6-32 THC emission percentage reduction of CI engine during torque transition condition

Table 6-1 Summary of the maximum emission reduction when using biodiesel blends as compared with diesel during transient operations

Operating Condition	Maximum CO ₂ emission reduction(%) by		Maximum NOx emission increment(%) by		Maximum CO emission reduction(%) by		Maximum THC emission reduction (%) by	
	20B	100B	20B	100B	20B	100B	20B	100B
1000 – 1500rpm	36	61	3	16	64	45	9	45
1500 - 1000rpm	25	53	4	8	124	122	30	48
210 - 420Nm	16	19	8	20	22	24	21	63
420 – 210Nm	17	8	20	27	18	20	28	66

Table 6-2 The effects of transient operation on of the post- transient operation

Operating Condition	Post transient CO ₂ emission extended time (sec.)	Post transient NOx emission extended time(sec.)	Post transient CO emission extended time(sec.)	Post transient THC emission extended time(sec)
1000 – 1500rpm	13	30	13	6
1500 - 1000rpm	14	16	20	6
210 - 420Nm	14	30	23	12
420 – 210Nm	18	3	23	15

6.2 Effects of Engine Parameters on Transient Emissions

In the previous section the effects of biodiesel blends on the emission behaviour as well as the nature of emission after transient phenomena have been discussed extensively. In this section for better understanding of the dependence of various types of emissions on engine operating parameters following cross plots have been developed. Figure 6-33(a) shows the variation of CO₂ emission with respect to engine speed when running with diesel fuel during a positive speed transient for various engine torques. It can be seen that for a given torque value, with increase in engine speed CO₂ emission decreases. At a given speed, however, with increasing torque CO₂ emission shows increasing trend. Similar trends are seen for engine running with neat biodiesel (Figure 6-33 (c)). The trend seems to change when engine runs with biodiesel blend (Figure 6-33 (b)). In this case, maximum CO₂ emission is noticed for 315Nm torque.

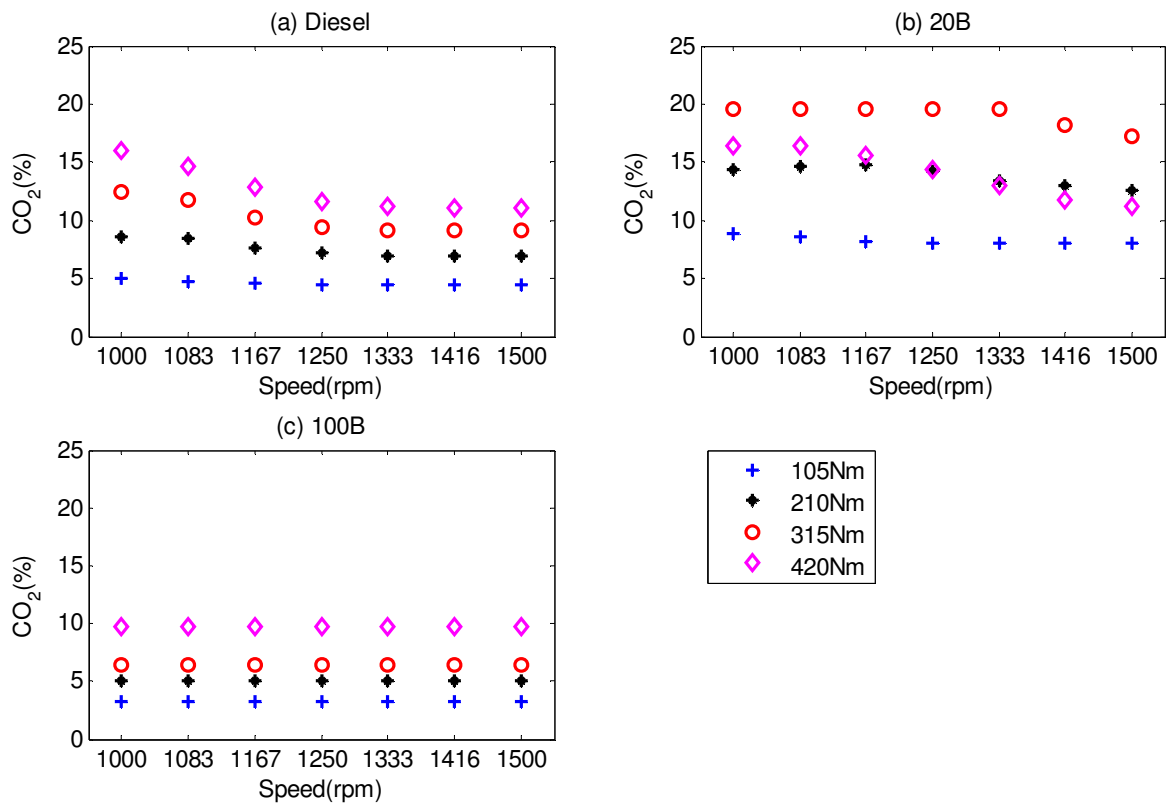


Figure 6-33 CO₂ emission of CI engine running with various fuels during speed transient of 1000-1500rpm at range of engine loads

The variation of CO₂ emission with respect to the engine speed when running with diesel fuel during a negative speed transient for various engine torques is depicted in Figure 6-34. It can be seen that for a given torque value with decrease in the engine speed from

1500 to 1000rpm the CO₂ emission increases. At a given speed however with increasing torque, CO₂ emission shows increasing trend. Similar trends are seen for engine running with neat biodiesel (Figure 6-34 (c)). The trends seem to change when engine runs with biodiesel blend as shown in Figure 6-34(b). In this case, maximum CO₂ emission is noticed for 315Nm torque where as at the highest torque of 420 Nm, CO₂ emission is lower than that at 315 Nm. Furthermore, it can be seen that the CO₂ emission values during the positive and negative transient conditions are comparable at various engine loads.

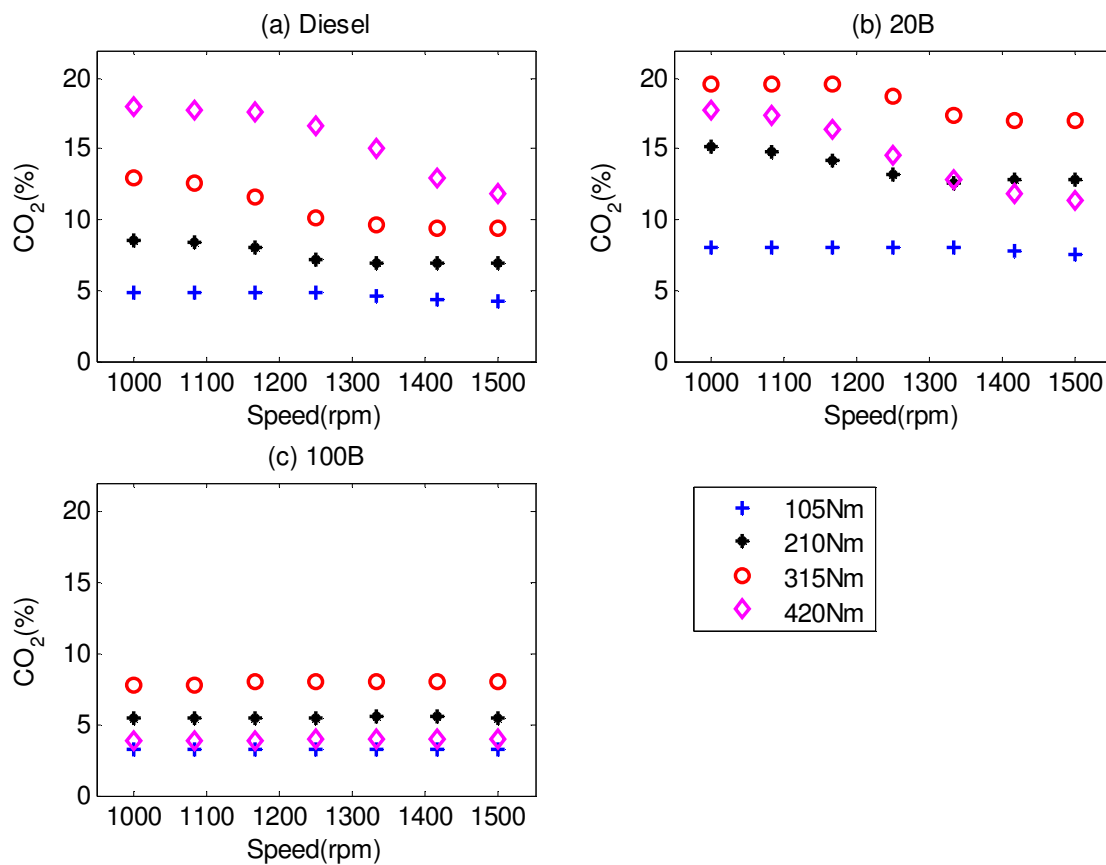


Figure 6-34 CO₂ emission of CI engine running with various fuels during speed transient of 1500-1000rpm at range of engine loads

Figure 6-35(a) shows the variation of CO₂ emission with respect to the engine torque when running with diesel fuel during a positive torque transient for various engine speeds. It can be seen that for a given speed value with increase in engine torque CO₂ emission increases. At a given torque, however, with increasing speed CO₂ emission shows decreasing trend. This phenomenon has been also seen during speed transient conditions. The trends seem to change when engine runs with neat biodiesel (Figure

6-35(b)). Similar trends are seen for engine running with biodiesel blend (Figure 6-35(c)). In this case, maximum CO₂ emission is noticed for 1250rpm speed where as at the highest speed of 1500rpm CO₂ emission is lower than that at 1250rpm.

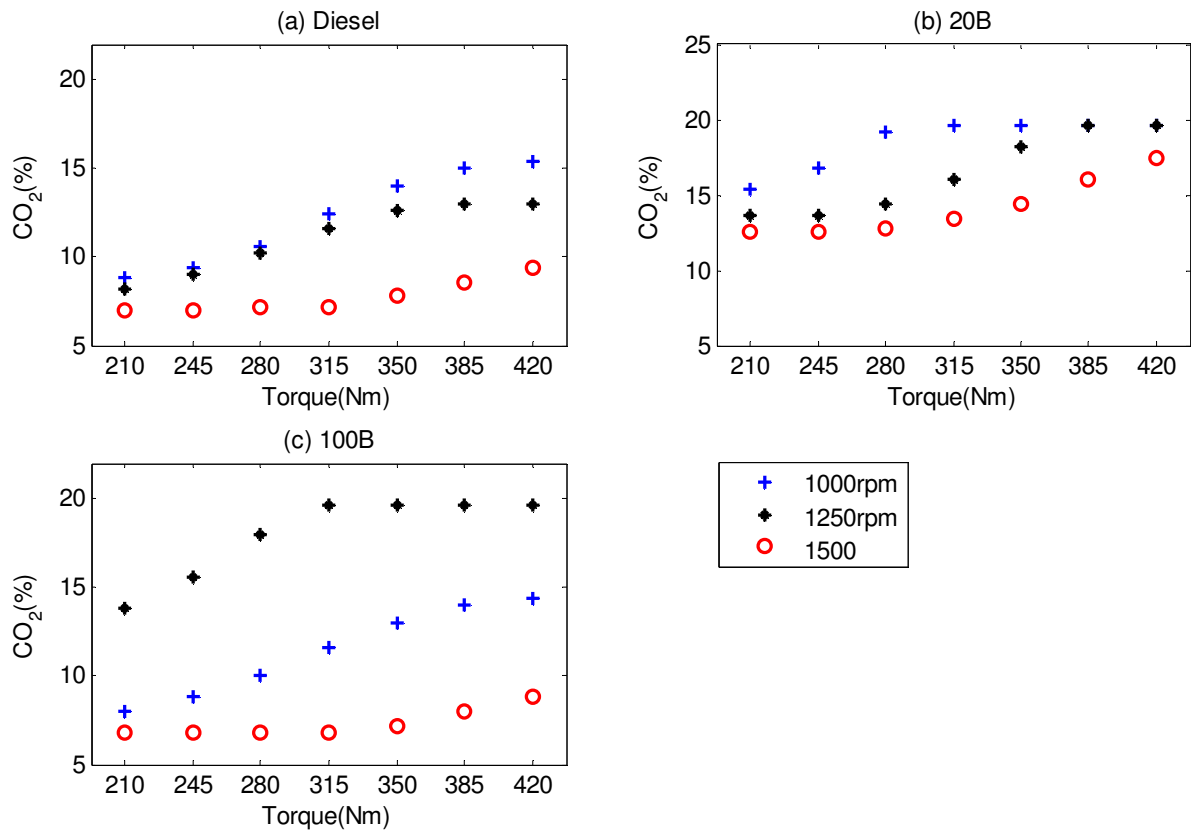


Figure 6-35 CO₂ emission of CI engine running with various fuels during torque transition of 210Nm to 420Nm and at range of engine speeds

Figure 6-36(a) shows the variation of CO₂ emission with respect to the engine torque when running with diesel fuel during a negative torque transient for various engine speeds. It can be seen that for a given speed value with decrease in engine torque CO₂ emission decreases. At a given torque, however, with increasing speed CO₂ emission shows decreasing trend. Similar trends are seen for engine running with biodiesel blends (Figure 6-36(b)). The trends seem to change when engine runs with neat biodiesel (Figure 6-36(c)). In this case, CO₂ emission increases dramatically for a speed for 1250 rpm speed.

Figure 6-37(a) shows the variation of NO_x emission with respect to the engine speed when running with diesel fuel during a positive speed transient for various engine

torques. It can be seen that for a given torque value with increase in engine speed NOx emission increases in low speed range with almost no change in the high speed range.

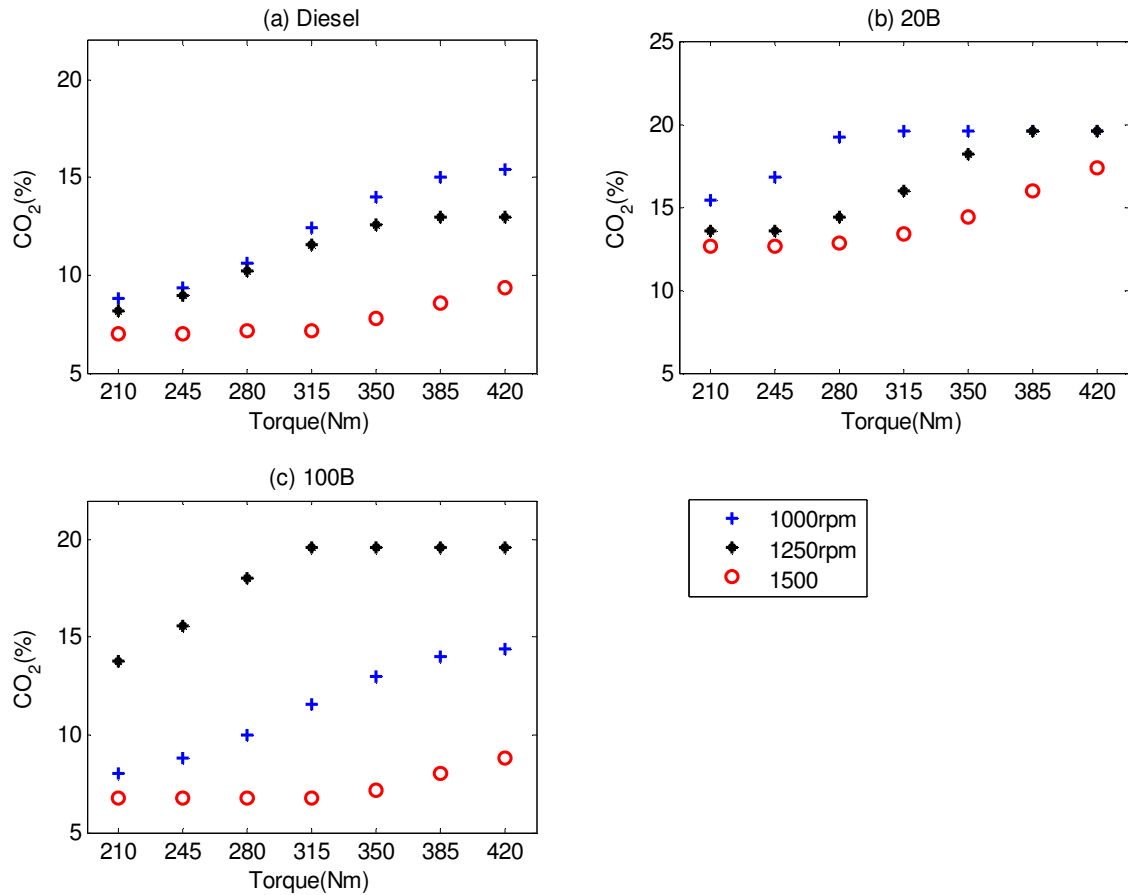


Figure 6-36 CO₂ emission of CI engine running with various fuels during torque transition of 420Nm to 210Nm and at various engine speeds

At a given speed, however, with increasing torque, NOx emission shows increasing trend. Almost similar trends are seen for engine running with biodiesel blends with almost no effect of speed on NOx emission over the entire speed range (Figure 6-37(c)). The trends seem to change when engine runs with biodiesel blend (Figure 6-37(b)). In this case, in the mid torque range NOx emission decreases with increasing speed.

The variation of NOx emission with respect to engine speed when running with diesel fuel during a negative speed transient for various engine torques has been depicted in Figure 6-38(a). It can be seen that for a given torque value with decrease in the engine speed from 1500 to 1000rpm, NOx emission increases slightly at lower speeds. At a given speed, however, with increasing torque, NOx emission shows increasing trend. The

NO_x emission at 420Nm shows almost constant values over the entire range of engine speeds. Almost similar trends are seen for engine running with biodiesel blend (Figure 6-38(b)). The engine running with neat biodiesel (100B) shows almost no effect of speed on NO_x emission over the entire speed range (Figure 6-38(c)).

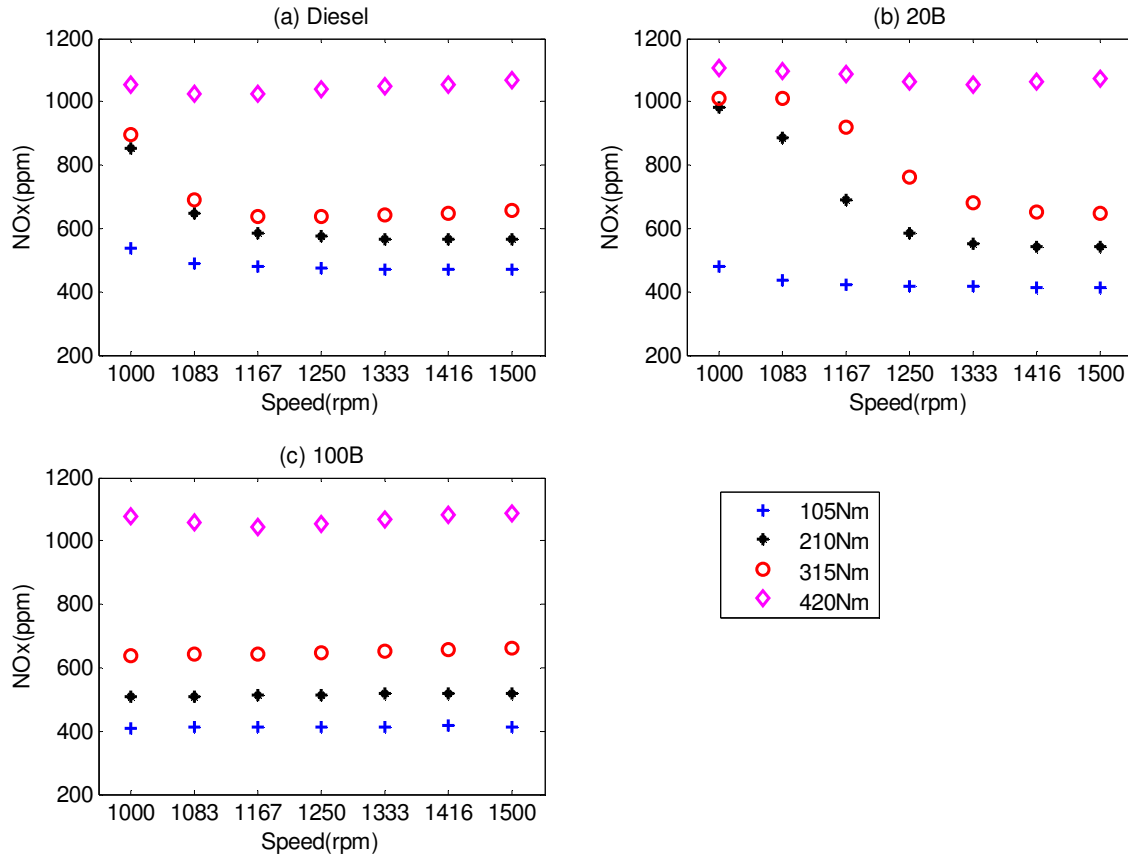


Figure 6-37 NO_x emission of CI engine running with various fuels during speed transient of 1000-1500rpm at range of engine loads

Figure 6-39(a) shows variation in the NO_x emission with respect to engine speed when running with diesel fuel during a negative speed transient for various engine torque values. It can be seen that for a given torque value with decrease in engine speed NO_x emission increases. At a given speed with increasing torque NO_x emission shows increasing trend. Almost similar trends are seen for engine running with biodiesel blends (Figure 6-39(b)) and neat biodiesel (Figure 6-39(c)).

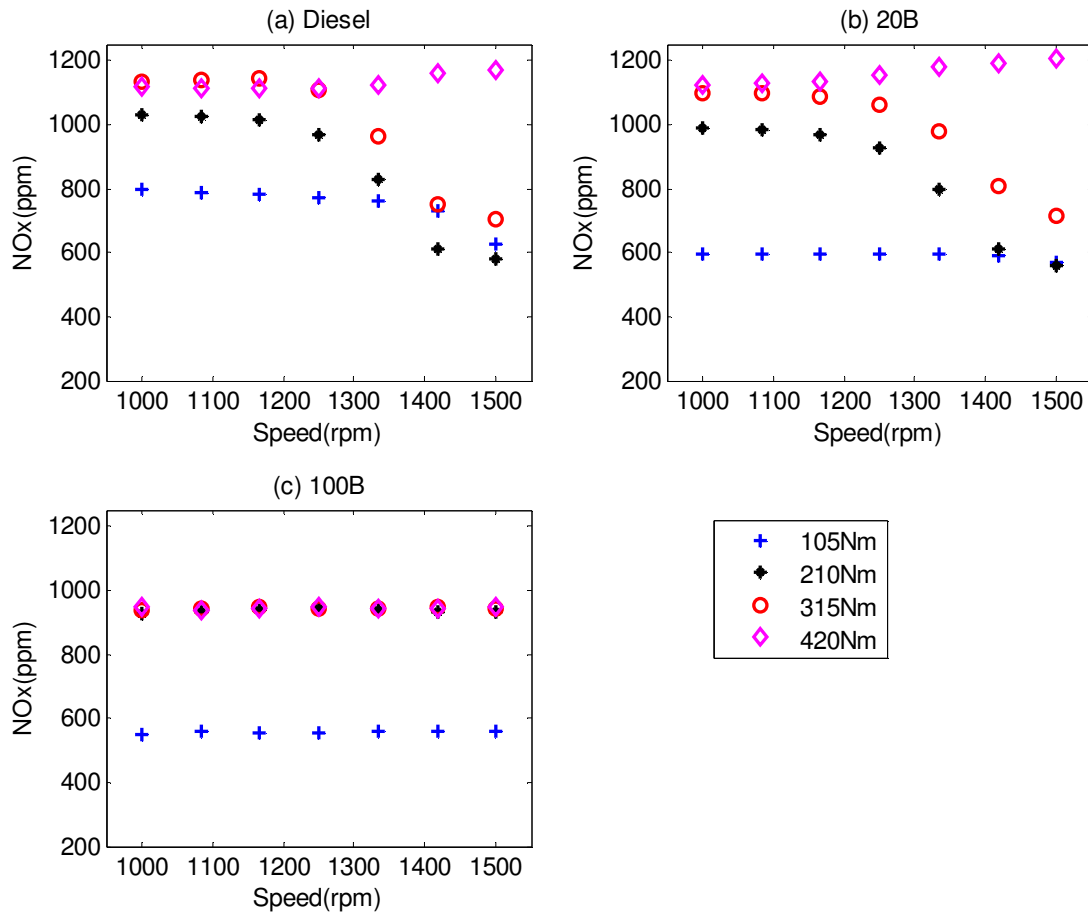


Figure 6-38 Variation of the NOx emission with respect to the engine speed for the test engine operating with different fuels during a negative speed transient of 1500 rpm to 1000 rpm at different engine torques.

Figure 6-40(a) shows variation in the NOx emission with respect to engine torque when running with diesel fuel during a positive torque transient for various engine speeds. It can be seen that for a given speed value with increase in engine torque NOx emission increases at higher speeds. At a given torque however with increasing speed NOx emission shows decreasing trend. Almost similar trends are seen for engine running with neat biodiesel (Figure 6-40(b)) and biodiesel blend (Figure 6-40(c)).

Figure 6-40(a) shows the variation in NOx emission with respect to the engine torque when running with diesel fuel during a negative torque transient for various engine speeds. It can be seen that for a given speed value with decrease in engine torque NOx emission decreases. At a given torque however with increasing speed NOx emission shows decreasing trend. Almost similar trends are seen for engine running biodiesel

blend(Figure 6-40(b)). For engine running with biodiesel NO_x emission is almost independent of the torque but is a strong function of the speed (Figure 6-40(c)).

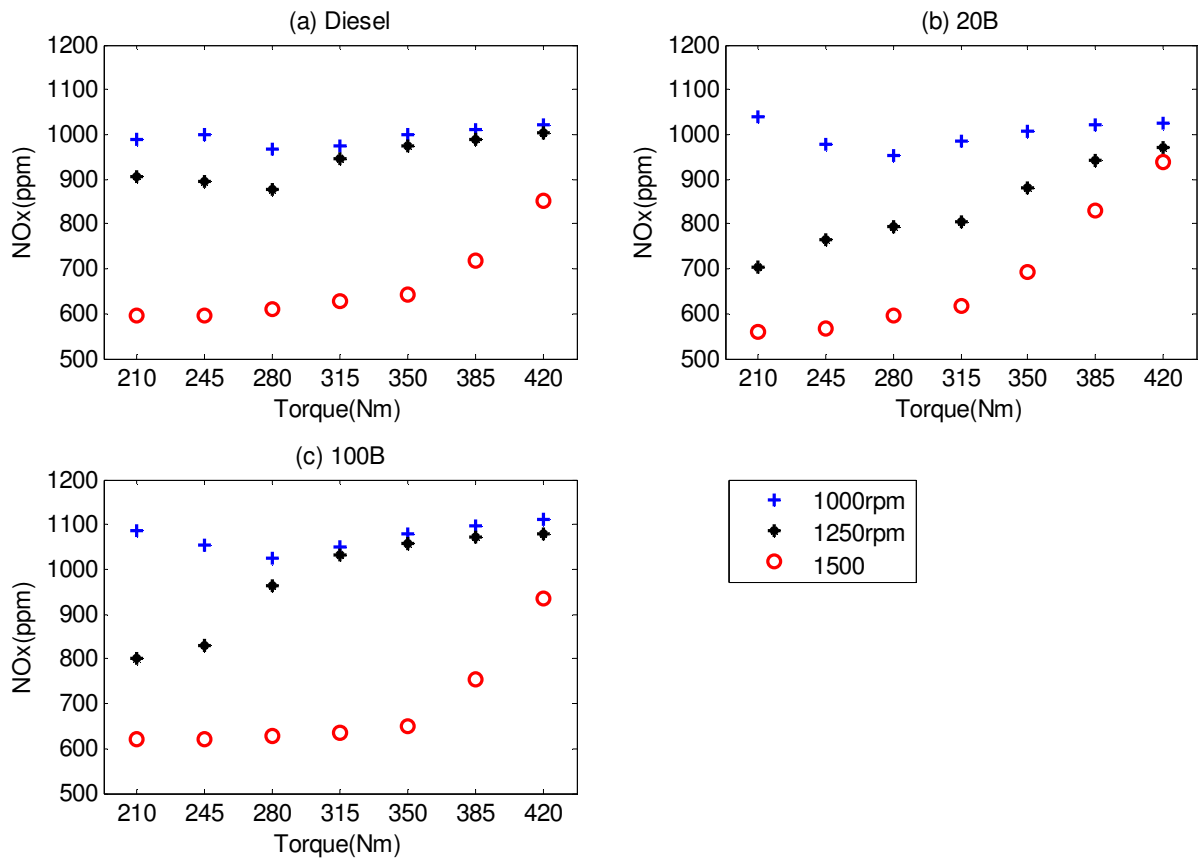


Figure 6-39 NO_x emission of CI engine running with various fuels during torque transition of 210Nm to 420Nm and at various engine speeds

Figure 6-41(a) shows the variation of THC emission with respect to the engine speed when running with diesel fuel during a positive speed transient for various engine torques. It can be seen that for a given torque value with increase in engine speed THC emission remains constant. This trend was observed for all the torque values. The effect of torque on THC emission was quite pronounced. It can be clearly seen that at lower torque values the THC emission has been higher and for highest torque used in the present investigation the THC emission has been lowest. Similar trends were seen for neat biodiesel Figure 6-41(a) and biodiesel blends (Figure 6-41(a)).

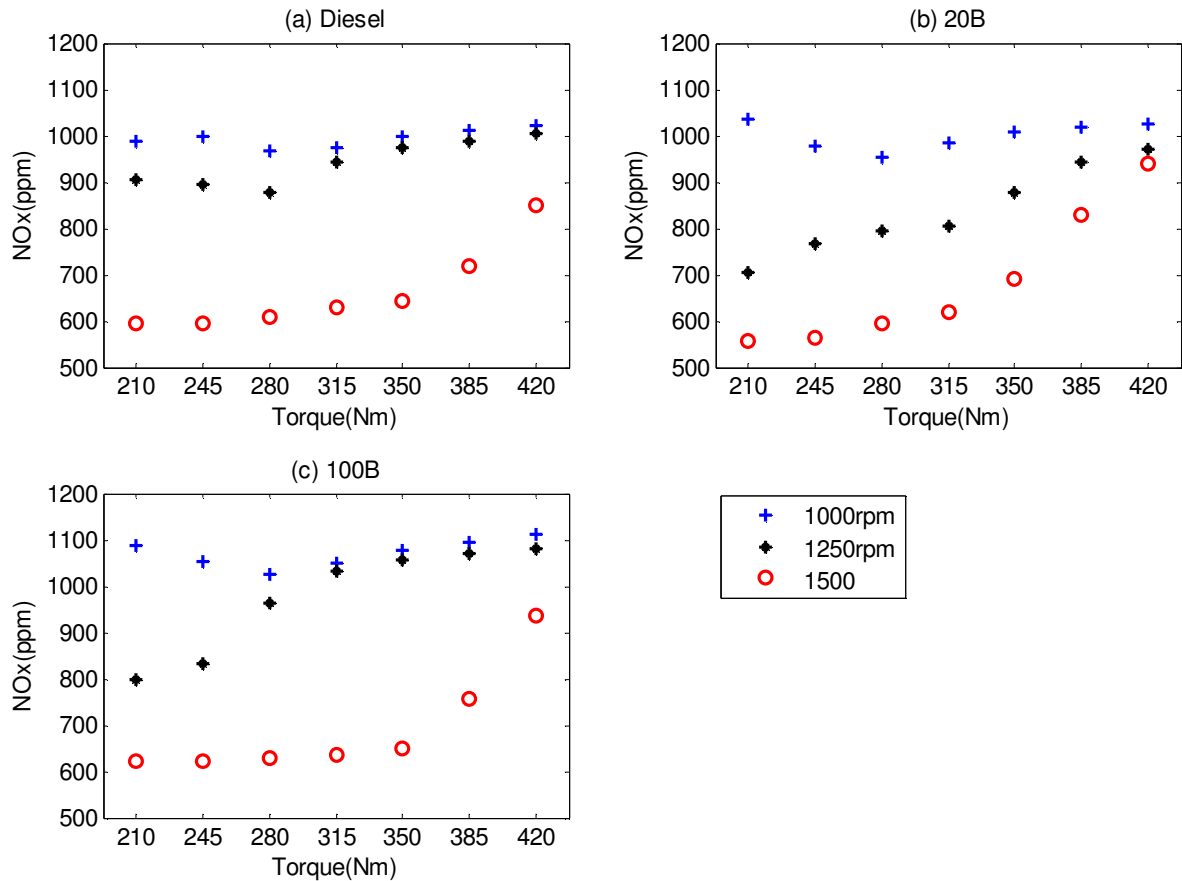


Figure 6-40 NOx emission of CI engine running with various fuels during torque transition of 420Nm to 210Nm and at various engine speeds

The variation in THC emission with respect to the engine speed when running with diesel fuel during a negative speed transient for various engine torques are shown in Figure 6-42. It can be seen that for a given torque value with decrease in engine speed THC emission shows only slight changes. This trend was observed for all the torque values. The effect of torque on THC emission was quite pronounced. It can be clearly seen that the THC emission decreases with increasing loads from 105Nm to 315Nm. However, at the maximum torque THC emission shows inconsistent trends. Similar trends have been observed for biodiesel blends (Figure 6-42(b)) and biodiesel (Figure 6-42(c)).

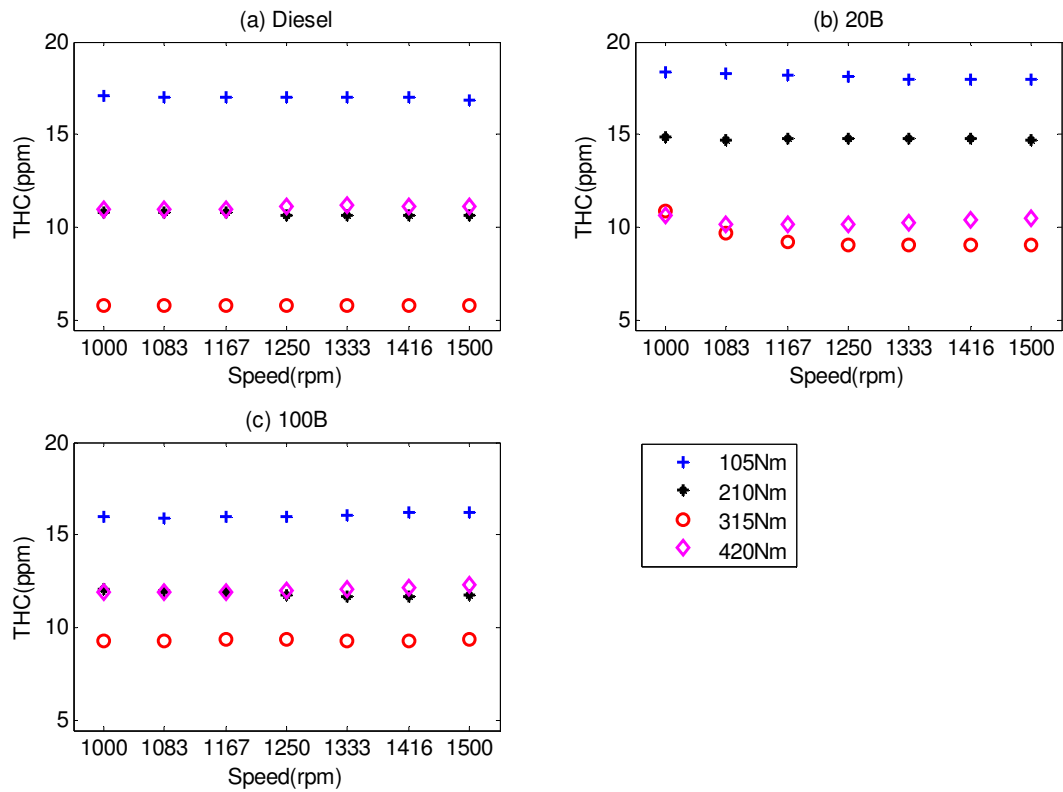


Figure 6-41 THC emission of CI engine running with various fuels during speed transient of 1000-1500rpm at range of engine loads

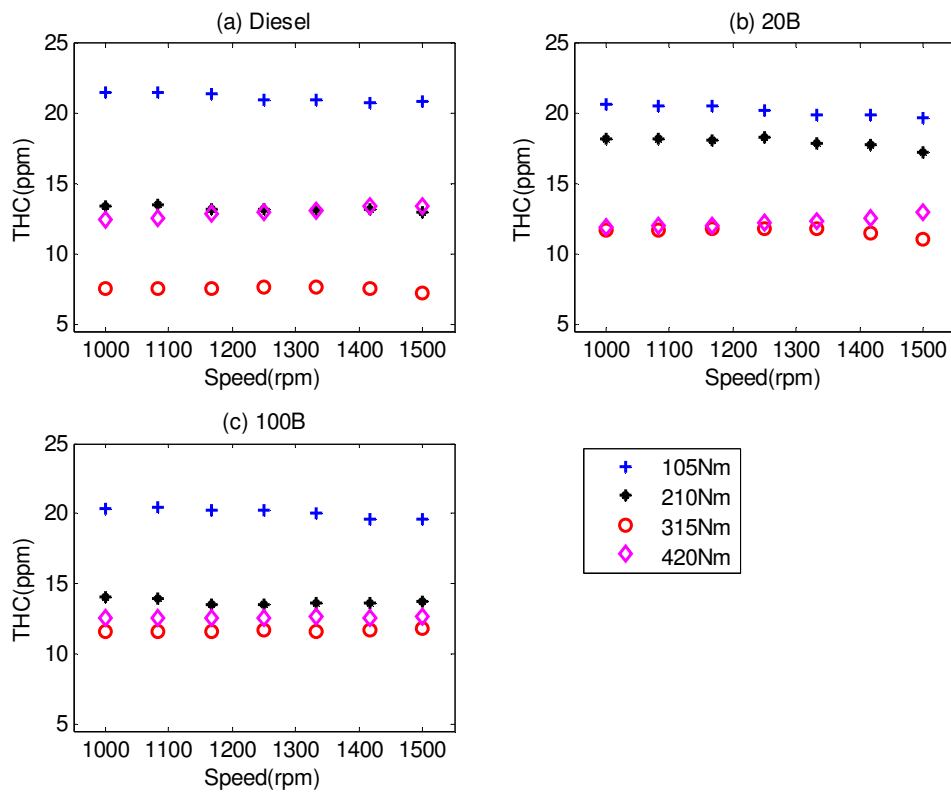


Figure 6-42 THC emission of CI engine running with various fuels during speed transient of 1500-1000rpm at range of engine loads

Figure 6-43(a) shows variation in the THC emission with respect to the engine torque when running with diesel fuel during a positive torque transient for various engine speeds. It can be seen that for a given speed value with increase in engine torque THC emission decreases, the decrease being more prominent at higher torque values. At a given torque however with increasing speed NOx emission shows decreasing trend. Almost similar trends are seen for engine running with biodiesel blends (Figure 6-43(b)) and neat biodiesel (Figure 6-43(c)) although not at the same rate as for diesel.

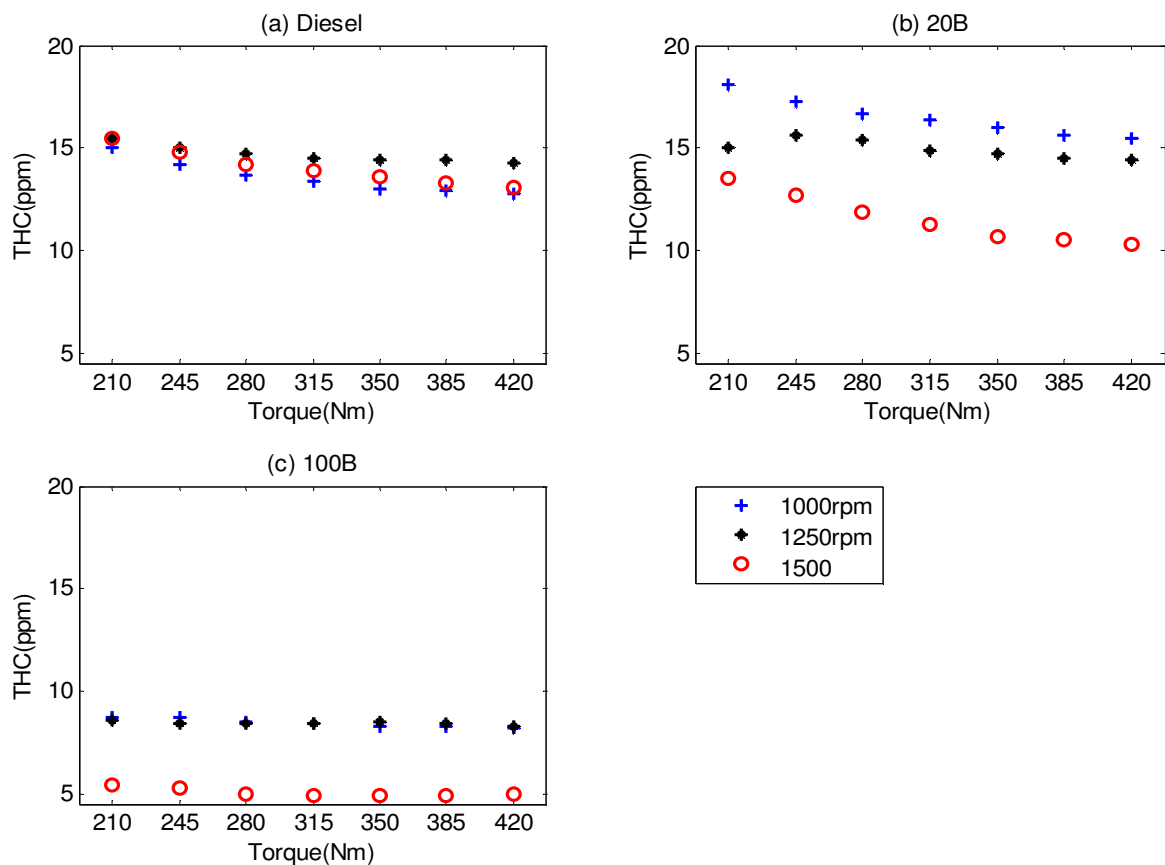


Figure 6-43 THC emission of CI engine running with various fuels during torque transition of 210Nm to 420Nm and at various engine speeds

Figure 6-44(a) shows variation in THC emission with respect to engine torque when running with diesel fuel during a negative torque transient for various engine speeds. It can be seen that for a given speed value with decrease in engine torque THC emission increases. At a given torque however with increasing speed NOx emission shows mixed trend with higher emission in the mid-speed range. Almost similar trends are seen for engine running biodiesel blend (Figure 6-44(a)) as far as THC and torque relationship is

concerned and effect of speed is now more systematic with higher THC emission at lower speed and lower emission at higher speed.

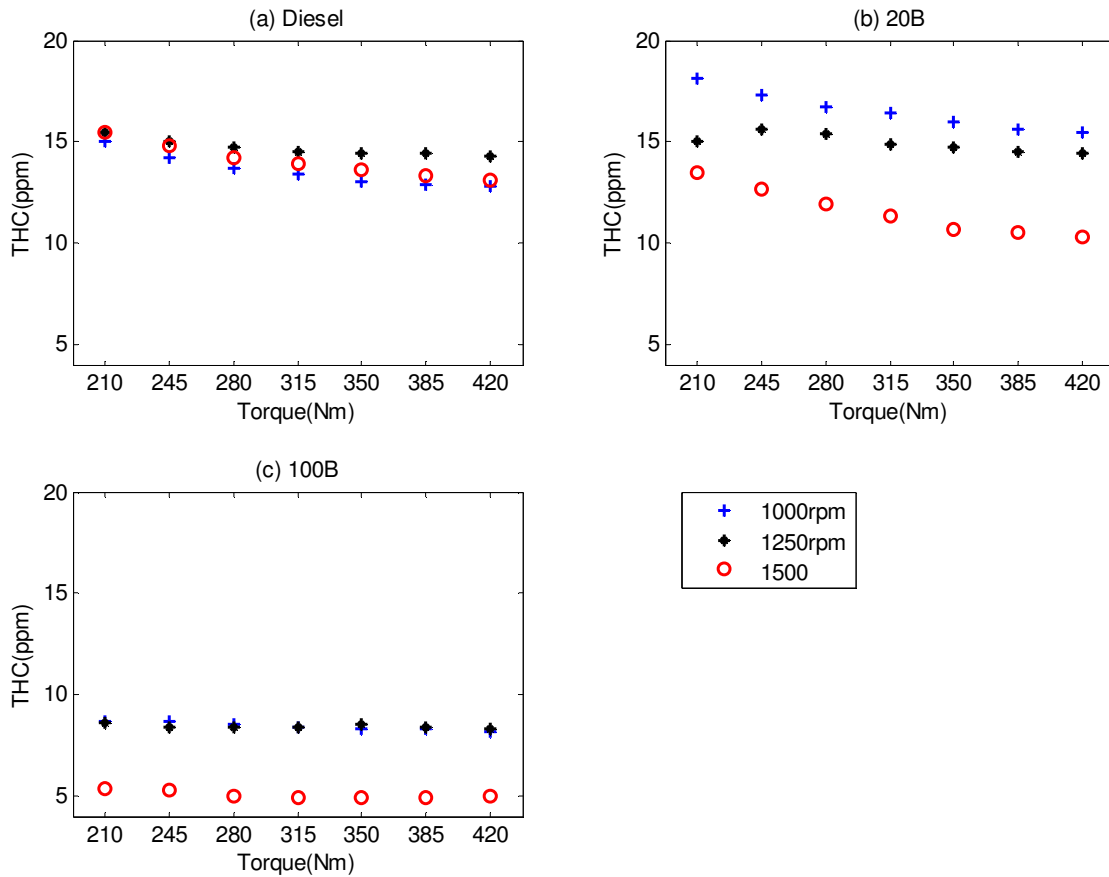


Figure 6-44 THC emission of CI engine running with various fuels during torque transition of 420Nm to 210Nm and at various engine speeds

Figure 6-45(a) shows variation of the CO emission with respect to the engine speed when running with diesel fuel during a positive speed transient for various engine torques. It can be seen that for a given torque value with increase in engine speed the CO emission remains constant for all except the highest torque value. For the highest torque, CO emission decreases initially with increasing torque before becoming independent. Similar trends have been seen for biodiesel blends (Figure 6-45(b)) and neat biodiesel (Figure 6-45(c)).

Figure 6-46(a) shows variation of the CO emission with respect to the engine speed when running with diesel fuel during a negative speed transient for various engine torques. It can be seen that for a given torque value with decrease in engine speeds from 1500 to

1000rpm, CO emission remains constant for all except the highest torque value. For the highest torque, CO emission increases with decrease in engine speeds. Similar trends have been seen for biodiesel blends (20B)(Figure 6-46(b)) and neat biodiesel(100B)(Figure 6-46(c)). However, the engine running with neat biodiesel (100B) shows unique characteristics at maximum load values.

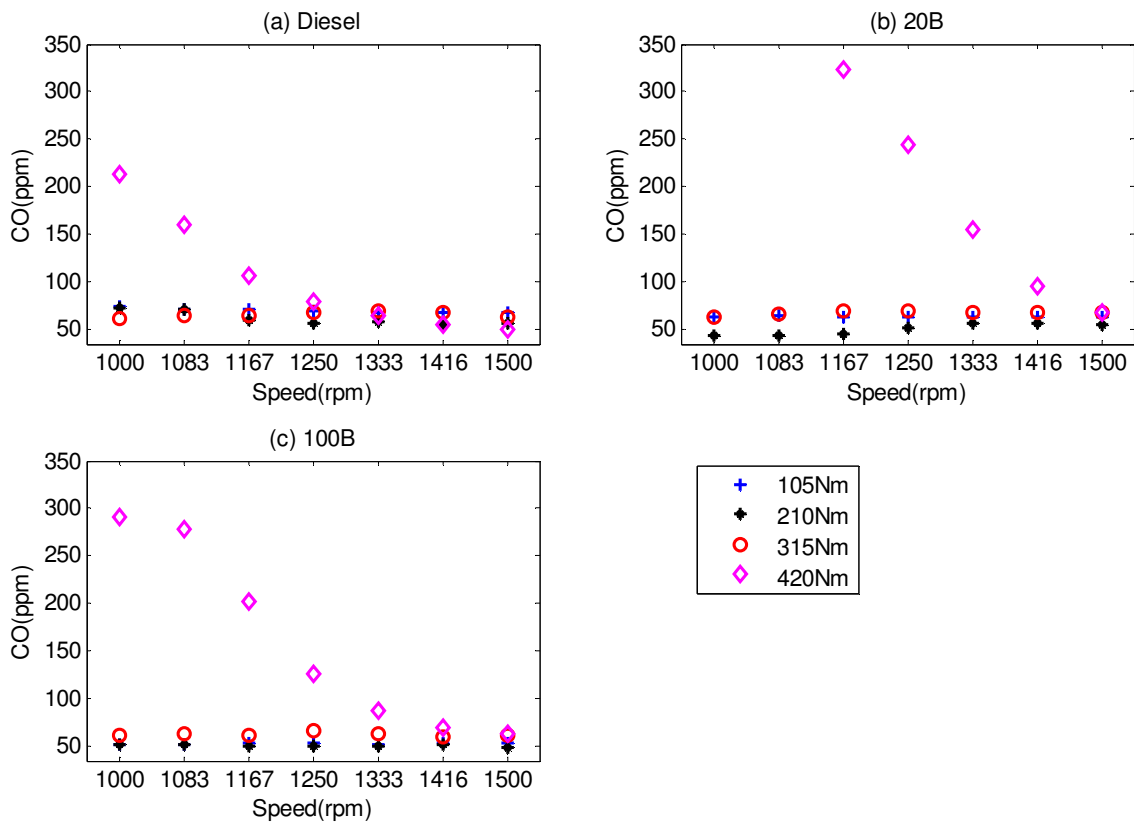


Figure 6-45 CO emission of CI engine running with various fuels during speed transient of 1000-1500rpm at range of engine loads

Figure 6-47 shows the variation in CO emission with respect to the engine torque when running with diesel fuel during a positive torque transient for various engine speeds. It can be seen that for a given speed value with increase in engine torque CO emission remains largely constant. Only for lowest engine speed with increase in torque CO emission increases. Almost similar trends are seen for engine running with biodiesel blends (Figure 6-47(b)) and neat biodiesel (Figure 6-47(c)).

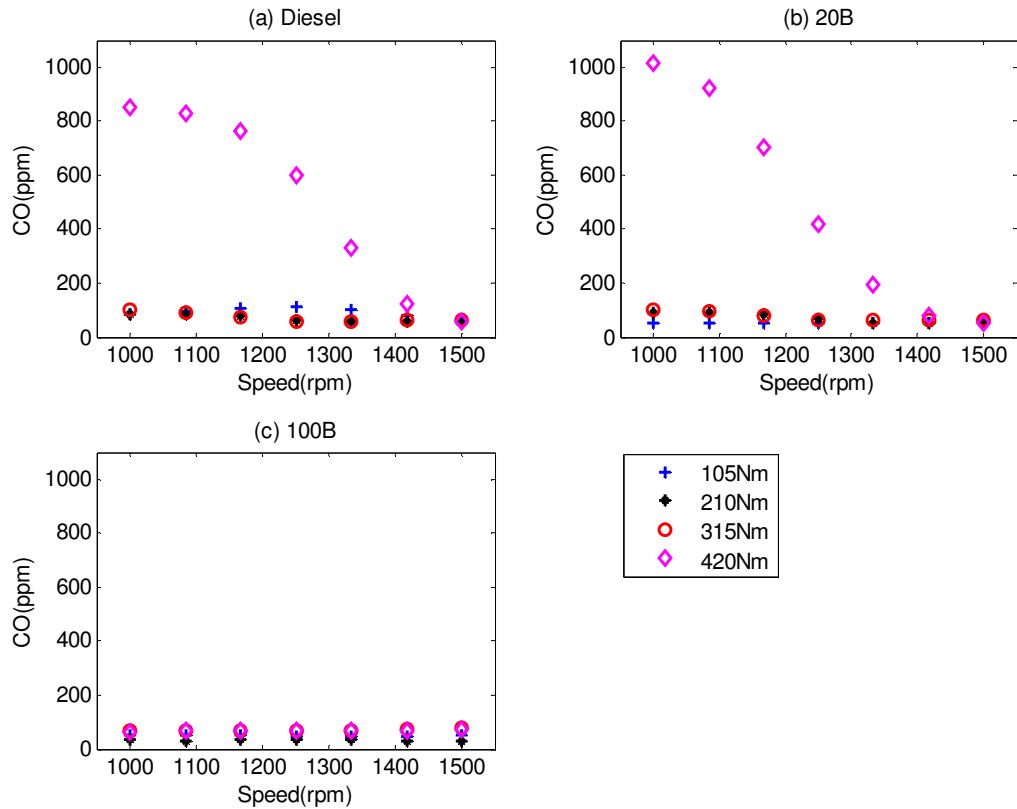


Figure 6-46 CO emission of CI engine running with various fuels during speed transient of 1500-1000rpm at range of engine loads

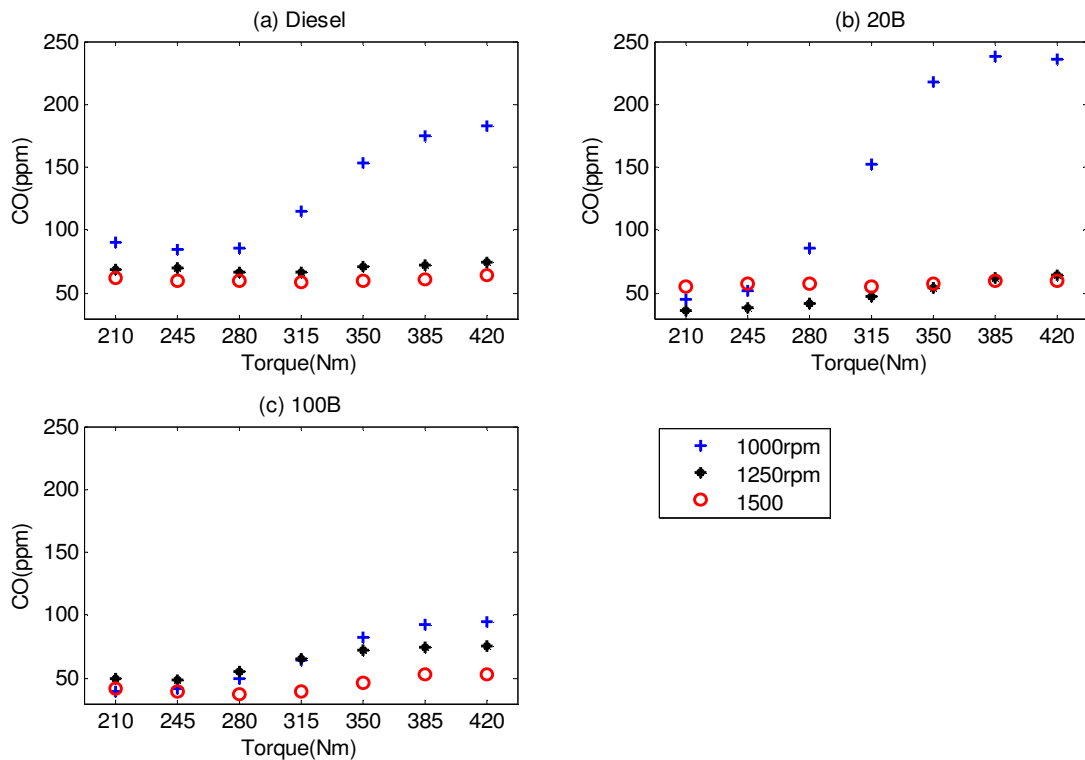


Figure 6-47 CO emission of CI engine running with various fuels during torque transition of 210Nm to 420Nm and at various engine speeds

Figure 6-48(a) shows variation in the CO emission with respect to the engine torque when running with diesel fuel during a negative torque transient for various engine speeds. It can be seen that for a given speed value with increase in engine torque CO emission remains largely constant except for the lowest speed tests. Only for lowest speeds with decrease in torque CO emission decreases significantly before attaining a constant value. Almost similar trends are seen for engine running with biodiesel blends (Figure 6-48(b)) and neat biodiesel (Figure 6-48(c)).

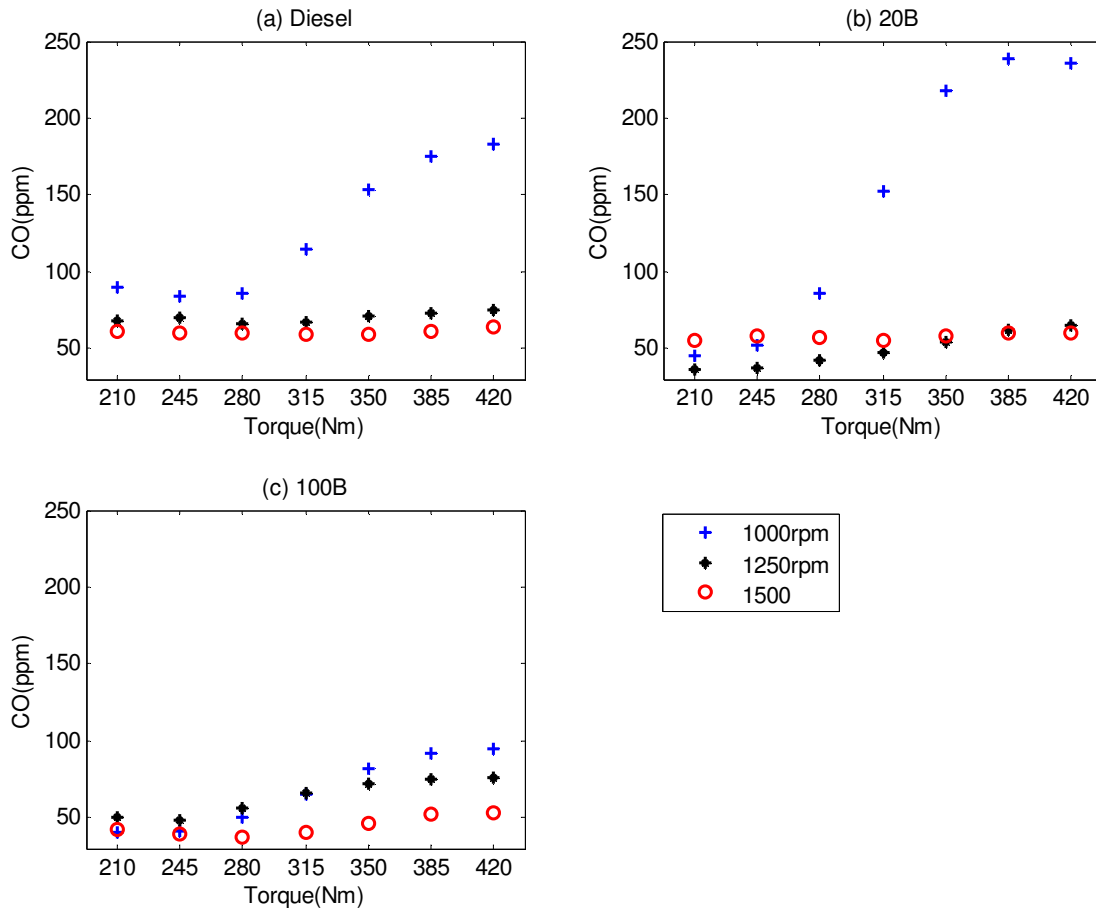


Figure 6-48 CO emission of CI engine running with various fuels during torque transition of 420Nm to 210Nm and at various engine speeds

6.3 Quantitative Dependence of Emissions on Engine Operating Parameters

Previous section has clearly identified that emissions vary with engine speed and torque during a transient. To establish quantitative interdependence amongst different variables multiple regression analysis has been carried out. A predictive model of the following form has been chosen to establish this effect.

$$Em = C_1 + C_2N + C_3T + C_4NT + C_5N^2 + C_6T^2 \quad (6-1)$$

Where Em is the emission from the engine, N is the engine speed, T is the engine torque and $C_{i,s}$ are coefficients for the predictive model. For the purpose of the development all the data corresponding to speed and torque transients (both positive and negative) have been combined. The table shown below gives the coefficients for different types of emission.

To establish accuracy of predictions the predicted values of different emissions have been compared against the measured values and shown in the Figure 6-49 to Figure 6-52 for three different fuels.

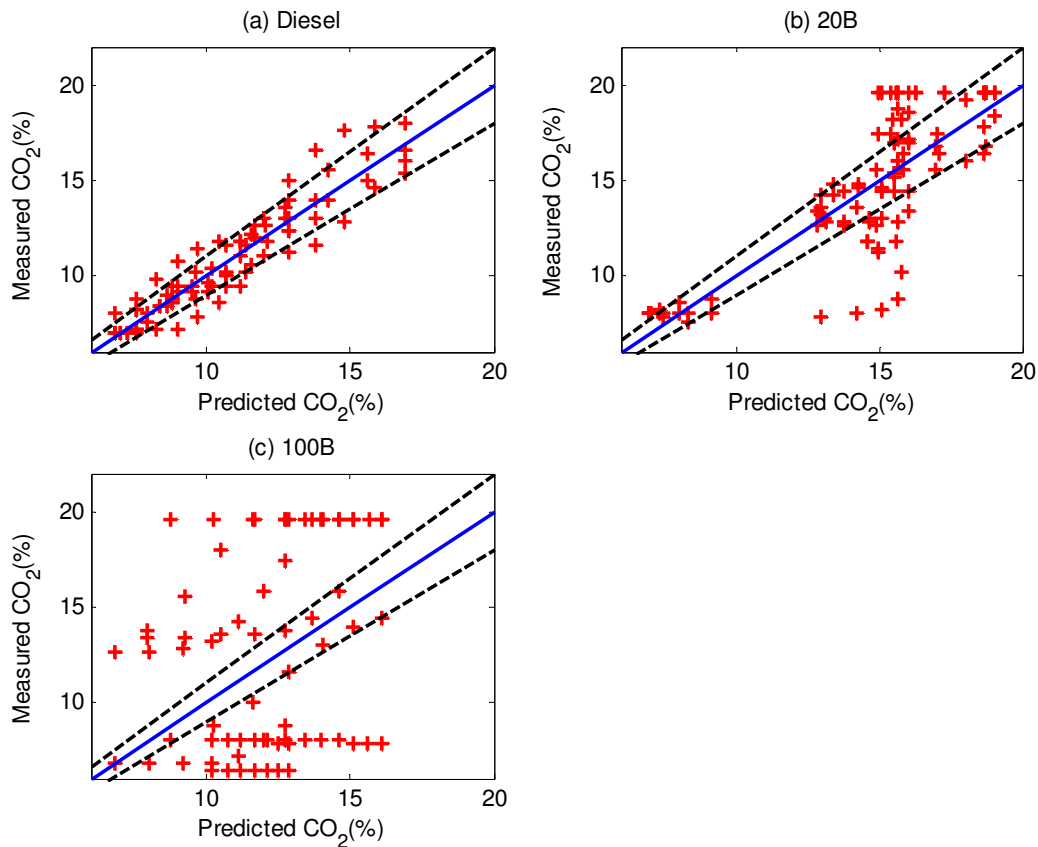


Figure 6-49 Accuracy of prediction models for CO₂ emission estimation

Table 6-3 Emission predicting models coefficients of CI engine running with diesel and biodiesel blends

Emission	Fuel	Predicting models coefficients					
		C ₁	C ₂	C ₃	C ₄	C ₅	C ₆
CO ₂	Diesel	3.61	-0.0070	0.0739	-0.000036	0.0000042	0.0000008
	B20	40.77	-0.0691	0.1258	-0.000018	0.0000277	-0.0001477
	B100	-3.82	0.0040	0.0719	-0.000013	-0.0000021	-0.0000381
NO _x	Diesel	1166.79	-0.2066	-0.5213	0.001229	-0.0002440	0.0006013
	B20	1257.55	-0.7018	0.8151	0.001193	-0.0000488	-0.0010946
	B100	583.07	-0.3636	3.9243	-0.000598	0.0000505	-0.0032304
THC	Diesel	62.89	-0.0535	-0.1245	0.000005	0.0000211	0.0001813
	B20	40.01	-0.0219	-0.0437	-0.000013	0.0000077	0.0000678
	B100	5.77	0.0415	-0.1205	-0.000006	-0.0000178	0.0001961
CO	Diesel	-234.28	0.3345	0.9456	-0.002245	0.0000360	0.0043628
	B20	-379.75	0.4040	1.5041	-0.002840	0.0000698	0.0049651
	B100	155.73	-0.2767	0.5873	-0.000820	0.0001721	0.0011742

Figure 6-49(a) shows the accuracy of prediction for CO₂ emission when diesel is used as a fuel. It can be seen that the measured and predicted values match reasonably well and most of the data is within 10% error band. The matching is not so good for biodiesel and biodiesel blend (Figure 6-49 (b and c)) indicating that the coefficients used in the equations are complex functions of other variables.

Figure 6-50(a) shows the accuracy of prediction for NO_x emission when diesel is used as a fuel. It can be seen that the measured and predicted values match reasonably well and most of the data is within 20% error band. The same trend is seen for biodiesel and the biodiesel blend used in this study (Figure 6-50(b and c)). All the figures shown above depict same level of scatter. The scatter is limited within 20% error band indicating that the coefficients used in the equations are functions of other variables and more experiments need to be conducted to make these equations more accurate.

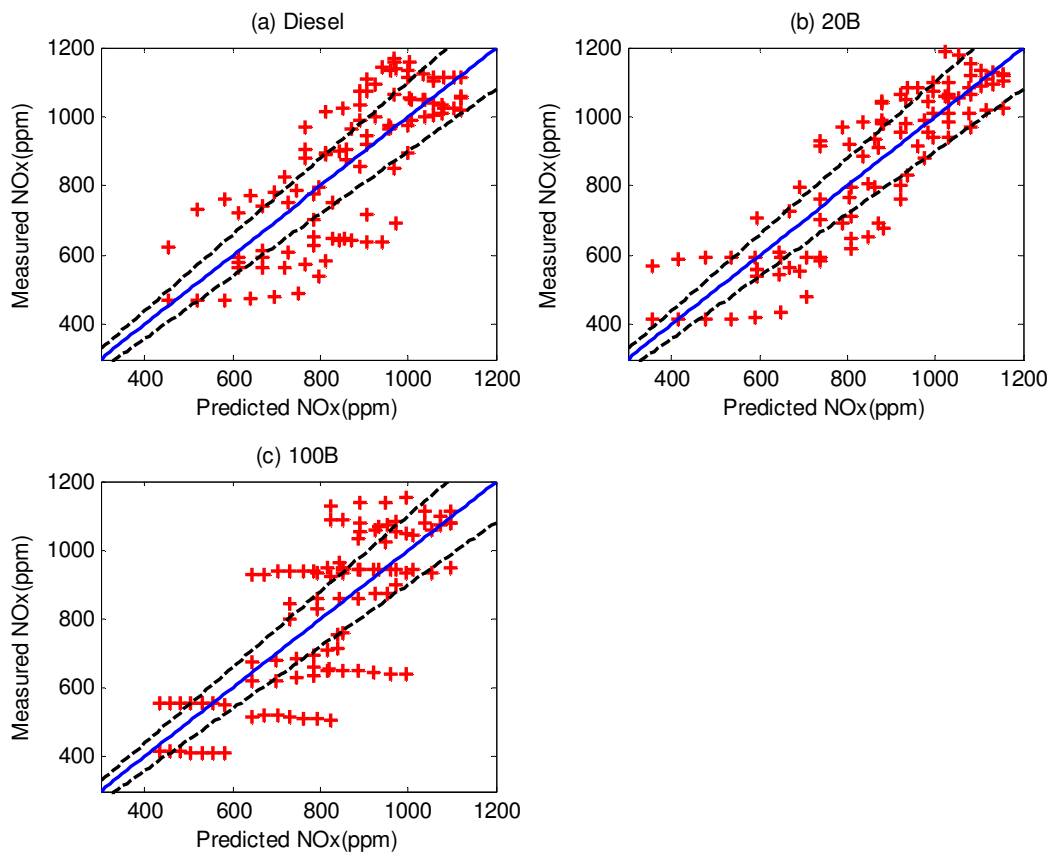


Figure 6-50 Accuracy of prediction models for NO_x emission estimation

Figure 6-51(a) shows the accuracy of prediction for THC emission when diesel is used as a fuel. It can be seen that the measured and predicted values match reasonably well and

most of the data is within 20% error band. The same trend is seen for biodiesel and the biodiesel blend used in this study (Figure 6-51(b and c)). All the figures shown above depict almost same level of scatter. The scatter is limited within 20% error band indicating that the coefficients used in the equations are functions of other variables and more experiments need to be conducted to make these equations more accurate.

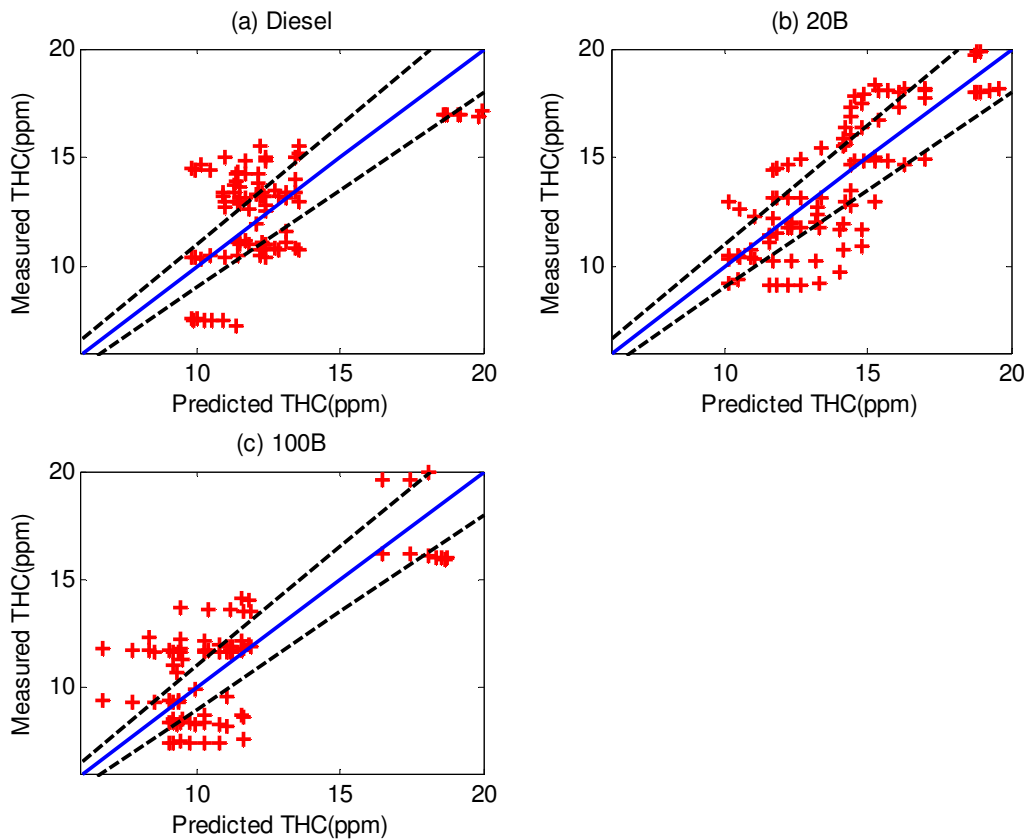


Figure 6-51 Accuracy of prediction models for THC emission estimation

Figure 6-52(a) shows the accuracy of prediction for CO emission when diesel is used as a fuel. It can be seen that the measured and predicted values do not match favourably indicating very rough correlation. This indicates that there are some other variables that need to be considered to make these predictions better. The same trend is seen for biodiesel and the biodiesel blend used in this study (Figure 6-52(b and c)). All the figures shown above depict almost same level of scatter. The scatter is limited within 40% error band indicating that the coefficients used in the equations are functions of other variables and more experiments need to be conducted to make these equations more accurate. The above comparisons have indicated that the equations developed show reasonable

dependence of emissions with engine operating parameters during transients. These equations can further be modified to improve accuracy of predictions.

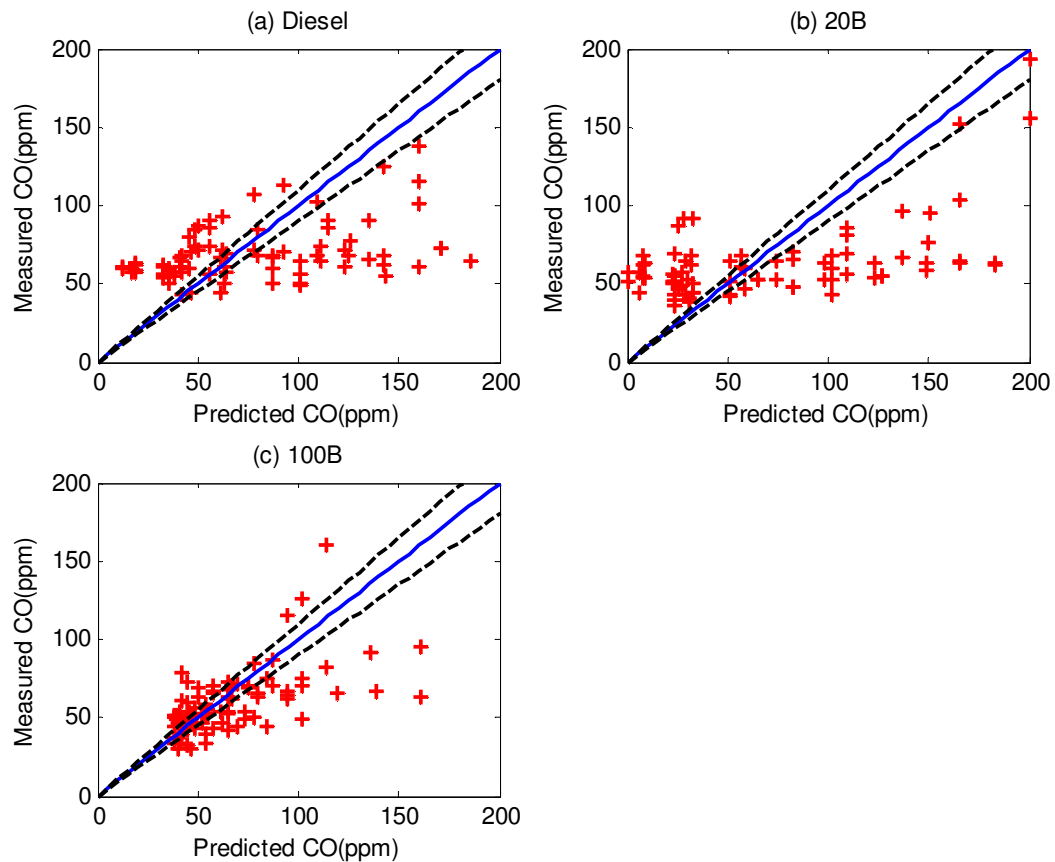


Figure 6-52 Accuracy of prediction models for CO emission estimation

6.4 Summary on the Performance and Emission Characteristics of the Test CI Engine during Transient Operation

The work presented here contributes to the knowledge on the performance and emission characteristics of the engines running with biodiesel during transient operations. The data has been analysed to compare the fuel flow rate, exhaust gas temperature, in-cylinder pressure and the engine emission (CO_2 , NO_x , CO and THC). The following conclusions can be drawn from the results obtained from both performance and emission studies during transient operation.

1. The analysis conducted on the fuel flow rate shows that the fuel consumption of the engine running with 100B is higher than that of diesel by 16% and 14% for the

acceleration and deceleration transient operations respectively. These values increased to 17% and 15% for positive and negative torque transition operations.

2. In acceleration and deceleration conditions, the maximum difference between the exhaust temperature of engine running with diesel and biodiesel blends is less than 2%. During torque transition operations, the engine running with biodiesel has higher exhaust gas temperature than that of running with diesel by 7%.
3. Most of current online emission techniques being used are usually developed at specific engine working conditions under steady state conditions of operation. However, a typical diesel engine can work under different ambient conditions, loads, and other dynamic features reflecting a transient nature of operation. These operating conditions have wide ranging effects on performance and emission characteristics of the engines.
4. Transient emission predicting models have been developed using the available emission data for various biodiesel blends and transient operation conditions. The models presented in equation (6-1) can be used for the prediction of emission during transient operation within acceptable error values. The equations given above (5-4) relate emissions with speed and torque.

The next chapter has focused on the development of NO_x prediction using the online measurement of in-cylinder pressure and air mass flow rate.

CHAPTER SEVEN

7. PREDICTION OF NO_x EMISSION FROM THE TEST CI ENGINE BASED ON THE IN-CYLINDER PRESSURE MEASUREMENT

As it has been discussed in both Chapter five and Chapter six one of the drawback of biodiesel application in CI engine is its higher NO_x emission. To manage the NO_x emission it is very important that to have an accurate measurement system at both steady and transient conditions. This chapter is focused on the development of a novel method for prediction of NO_x from the experimentally measured cylinder pressure for on-line monitoring. The in-cylinder pressure and temperature curves have investigated for different engine operation conditions based on the experimental measurements. The NO_x emissions of CI engine running with biodiesel and diesel have been predicted using the in-cylinder pressure and air mass flow rate. The model is validated by the experimental measured NO_x emission values. This chapter have the following sections: NO_x prediction model development, computational procedures for NO_x prediction, parametric investigation on in-cylinder pressure and in-cylinder temperature and validation for NO_x prediction model.

7.1 NO_x Prediction Model Development

Internal combustion engines release NO_x, which is one of the most toxic emissions for the public and the environment. Currently, there is a stringent emission law for NO_x gas emission. NO_x can only be monitored through state-of-the-art measuring techniques. Chapter two has clearly highlighted that NO_x emission is biggest stumbling block in large scale uptake of biodiesel; furthermore it is still a big problem for diesel engines. As it is discussed in section 2.5 in detail, the available methods such as heated chemiluminescent detector (HCLD), engine map and artificial neural network (ANN) system, are limited either only for steady state operations or limited for only some engine operations. Therefore, it is important to develop an online NO_x emission which can be used universally for all operating conditions. NO_x emission in CI engines is largely a thermal phenomenon and thus cylinder pressure and air flow rate can be used to make an accurate online quantitative prediction of NO_x emission in real-time. In-cylinder pressure measurement has been chosen parameters for this purpose due to its well established relationship with in-cylinder temperature either with ideal gas law or thermodynamic equations [203]. Further, this relationship would be integrated with easily measurable engine dynamics data, for example, vibration and acoustic emission, to enable prediction of NO_x emission with ease.

The approach used to predict NO_x emissions involves use of the in-cylinder pressure to obtain the in-cylinder temperature, and then use the in-cylinder temperature to obtain the NO_x emission from the CI engine. NO_x formation is a thermal mechanism, which occurs in the post-flame burned gases, which is modelled by the extended Zeldovich mechanism, described by equations (2-14 to 2-16). These equations include the reactants, products and rate constants. In order to drive the rate of change of NO concentration in equation (2-17), it was assumed that the concentration of the N is minor in comparison to the concentrations of the other species, so that the rate of change in N can be set equal to zero. The rate constants for equation (2-17) have been measured and critically evaluated in numerous studies [137], [196], [142], [143], [140]. The reaction rates used in this NO_x model are given in Table 2-4. In Table 2-4, the (-) sign indicate the backward reaction. The [N₂] and [O₂] concentrations were determined at ambient condition of the atmospheric air. In order to predict the thermal NO_x emission from the in-cylinder temperature, the ideal-gas equation of state, described by equation (7-1), has been used.

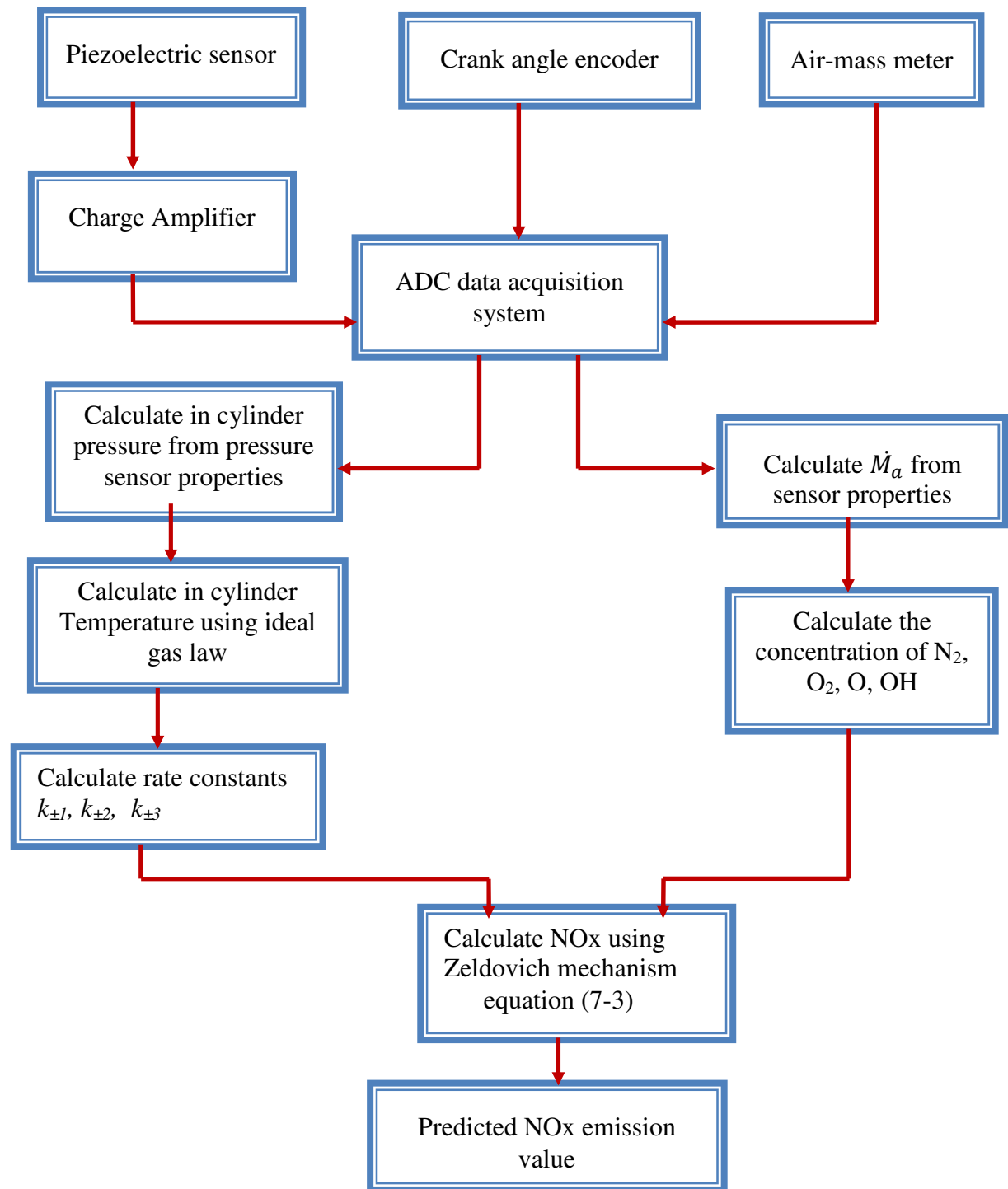


Figure 7-1 Flow chart for NOx prediction from in-cylinder pressure

The flow chart of the NOx prediction from the in-cylinder pressure and air flow rate is shown in Figure 7-1. As Figure 7-1 shows the in-cylinder pressure and the air flow rate were measured by using the procedure highlighted in section 3.2.3.1 and 3.2.2.3 respectively.

The in-cylinder temperature has been estimated from the ideal gas law stated in equation (7-1)

$$T(\theta) = \frac{P(\theta).V(\theta)}{Ma(\theta)Rg} \quad (7-1)$$

Where, $T(\theta)$ is the instantaneous in-cylinder temperature(K) at crank-angle θ , $P(\theta)$ is the instantaneous in-cylinder pressure(Pa) at crank-angle θ , $Ma(\theta)$ is the instantaneous mass in cylinder at crank-angle θ (kg) and Rg is gas constant (J/kgK).

$$V(\theta) = \frac{V_d}{\gamma-1} + \frac{V_d}{2} [R + 1 - \cos\theta - (R^2 - \sin^2\theta)^{-1/2}] \quad (7-2)$$

Where $V(\theta)$ is the instantaneous cylinder volume (m³) at crank-angle θ , V_d is displacement volume given (m³), R is the ratio of connecting rod length to crank angle and r_c is compression ratio.

The NOx emission formation and emission rate have been discussed in detail in section 2-4. In this section general NOx emission rate (equation 7-3), rate constants (Table 7-1), O estimation (equation 7-4 and 7-5) and OH estimation (equation 7-6) has been repeated for clarity in modelling of NOx emission prediction.

$$\frac{dNO}{dt} = 2k_1[O][N_2] \frac{\left(1 - \frac{k_{-1}k_{-2}[NO]^2}{k_1[N_2]k_2O_2}\right)}{\left(1 + \frac{k_{-1}[NO]}{k_2[O_2] + k_3[OH]}\right)} \quad \text{gmol}/(\text{m}^3 \text{ s}) \quad (7-3)$$

Table 7-1 Rate constants for thermal NOx formation [140]

Rate constants	Values [(m ³ /(gmol s))]
k_1	$1.8 \times 10^8 e^{-38370/T}$
k_{-1}	$3.8 \times 10^7 e^{-425/T}$
k_2	$1.8 \times 10^4 T e^{-4680/T}$
k_{-2}	$3.8 \times 10^3 T e^{-20820/T}$
k_3	$7.1 \times 10^8 e^{-450/T}$
k_{-3}	$1.7 \times 10^8 e^{-24560/T}$

Where k_1 , k_2 , and k_3 are the rate constants for the forward reactions as given in Table 7-1.

$$[O] = 3.97 \times 10^5 T^{-1/2} [O_2]^{1/2} e^{-31090/T} \quad \text{gmol/m}^3 \quad (7-4)$$

$$[O] = 36.64 T^{1/2} [O_2]^{1/2} e^{-27123/T} \quad \text{gmol/m}^3 \quad (7-5)$$

$$[OH] = 2.129 \times 10^2 T^{-0.57} e^{-4595/T} [O_2]^{1/2} [H_2O]^{1/2} \quad \text{gmol/m}^3 \quad (7-6)$$

7.2 Computational Procedures for NOx Prediction from in-cylinder Pressure

To predict the NOx emission using the in-cylinder pressure and air flow rate the following input parameters and computational procedures have been used.

The Input parameters: The input parameters used in the NOx prediction are engine geometry, gas constant (R_g), air percentage composition, air-mass flow rate and in-cylinder pressure.

Computational steps: The NOx emission can be predicted from in-cylinder pressure and in-cylinder temperature values. The steps used in these computations are outlined below.

Step 1: The air flow rate and in-cylinder pressure data have been acquired by ADC as described in Figure 7-1.

Step 2: The air mass flow rate and in-cylinder pressure have been calculated from the air-flow meter readings and pressure sensor calibration coefficients.

Step 3: The instantaneous cylinder volume has been calculated from engine geometry described in Table 3-1 and instantaneous crank angle.

Step 4: The N_2 and O_2 concentration have been computed from the air composition and air flow rate. The percentage air composition for O_2 and N_2 are 20.9% and 79% respectively.

Step 5: The O concentration has been computed using the maximum value obtained from equations 6-4 and 6-5. OH concentration has been calculated from equation 4-8.

Step 6: The in-cylinder temperature has been computed from air-flow rate, air-gas constant, in-cylinder volume and in-cylinder pressure using ideal gas law which is described in equation 7-1.

Step 7: The NOx formation reaction constants have been computed from the N_2 , O_2 , O and OH concentration which have been obtained in steps 4 and 5 using rate constant equations presented in Table 7-1.

Step 8: The NO_x emission has been computed from the in-cylinder temperature calculated in step 6 and NO_x reactions rate constants obtained in Step 7 using the extended Zeldovich mechanism which is described by equation 7-3.

Output parameters: The output parameters from NO_x prediction models are in-cylinder temperature and NO_x emission. In the following section the measured in-cylinder pressure measured and in cylinder temperature characteristics simulated during combustion have been described with a view to understanding the NO_x emission relationship with in-cylinder pressure. Finally, the predicted NO_x emission values have been compared with measured NO_x emission data for both diesel and biodiesel fuel.

7.3 Parametric investigations (In-cylinder temperature and NO_x)

The diesel combustion flame temperature values, which have been calculated from the instantaneous in-cylinder pressure, cylinder volume and air flow rate, are depicted in Figure 7-2 for different engine speeds and loads ranges. The mathematical relation between the in-cylinder temperature and in-cylinder pressure has been discussed in section 7.1. It can be seen, in Figure 7-2(a), that when the load increases, the in-cylinder temperature also increases. Similarly, when the engine speed increases, the in-cylinder pressure also increases, as it is shown in Figure 7-2(b). It can be concluded from the above that when the engine speed and load increase, the in-cylinder pressure increases. Even though, the cylinder volume and cylinder pressure are inversely proportional, since the change in the magnitude of the in-cylinder pressure is higher, its effect dominates the in-cylinder temperature values. Similar trends have been seen for CI engine running with biodiesel (Figure 7-3).

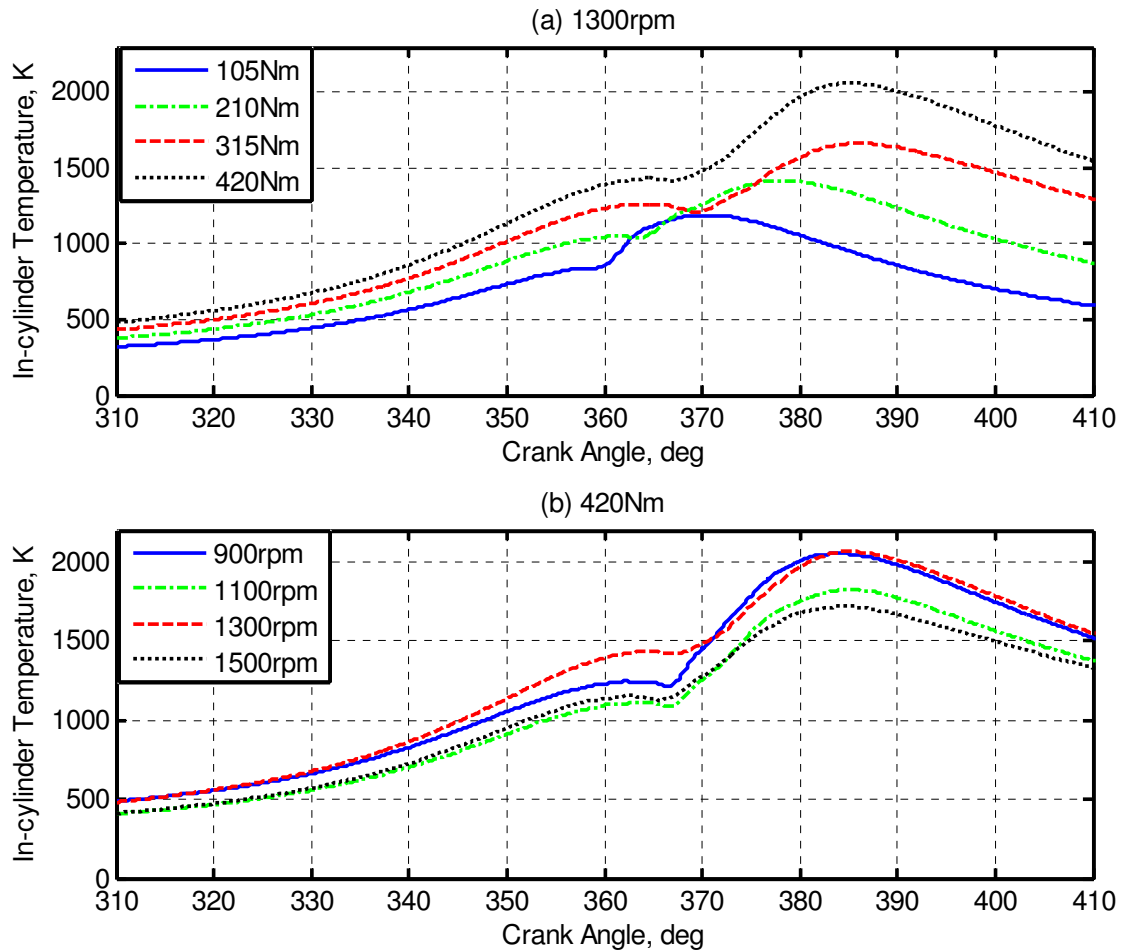


Figure 7-2 In-cylinder temperature versus crank angle of CI engine running with diesel during: (a) engine speeds of 1300 rpm and various loads (b) engine loads of 420Nm and at various engine speeds.

Figure 7-4 shows the in-cylinder temperature for biodiesel and diesel fuel at different operating conditions. The result shows that the flame temperature, corresponding to biodiesel operation, is higher than the diesel operation. The higher temperature of the biodiesel is caused due to the availability of additional oxygen molecule as mentioned earlier. As it will be discussed later, this is the main cause for the higher emission of NO_x. On the contrary, Monyem et al [191] reported that for both constant-volume combustion and constant-pressure combustion, the flame temperature for biodiesel is slightly below that for diesel fuel.

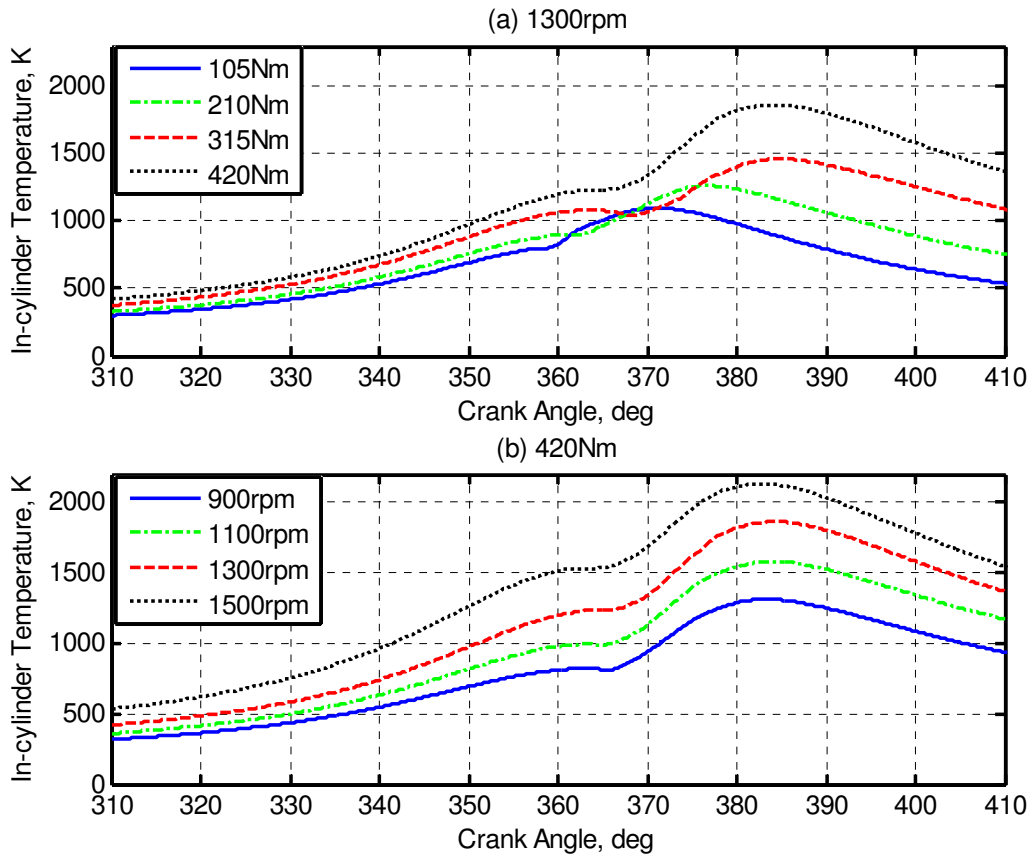


Figure 7-3 In-cylinder temperature versus crank angle of CI engine running with biodiesel(100B) during: (a) engine speeds of 1300 rpm and various loads (b) engine loads of 420Nm and at various engine speeds.

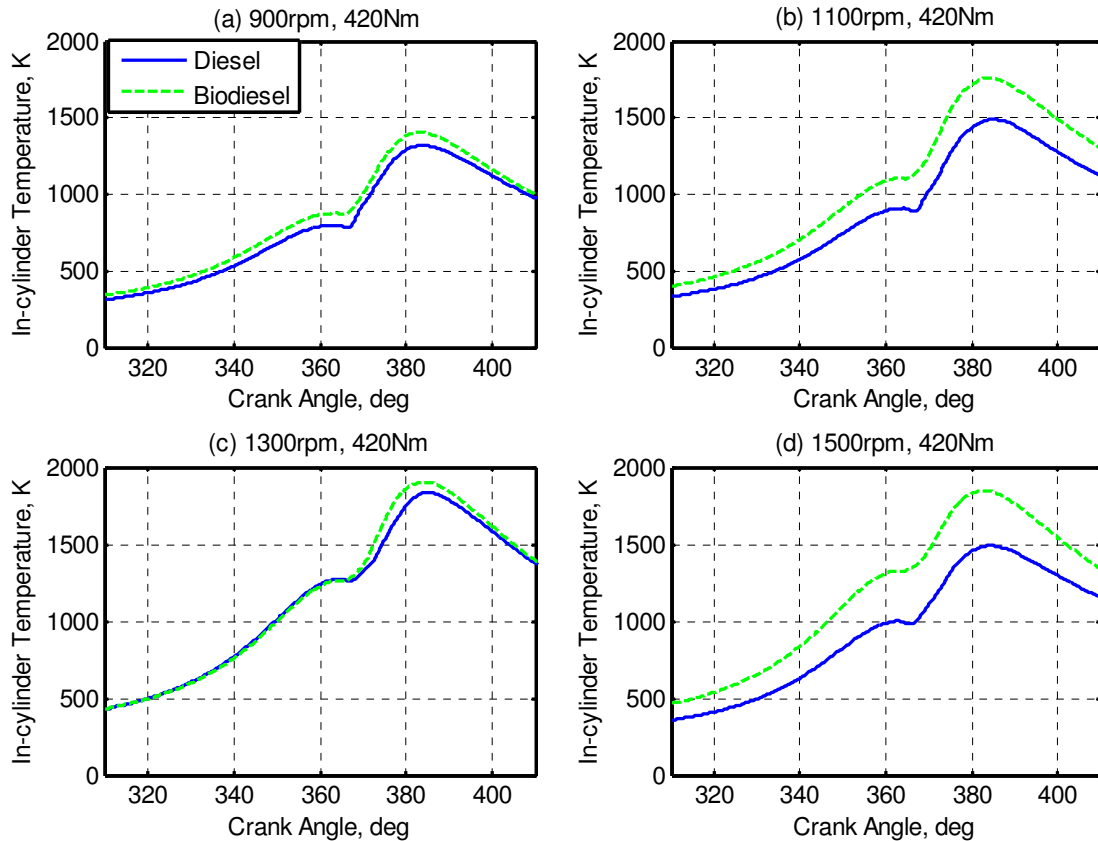


Figure 7-4 In-cylinder temperature versus crank angle of CI engine running with diesel and biodiesel for engine loads of 420Nm and range of speeds

The predicted NO_x emission corresponding to the biodiesel operation at a various loads and various engine speeds are shown in Figure 7-5. The NO_x emissions were found to decrease with an increase in the engine speed at lower engine loads (Figure 7-5(a, b)), while the emission increases with engine speed at higher loads (Figure 7-5(c,d)). This can be explained on the basis that at lower loads and lower speeds, the volumetric efficiency and gas flow motion within the engine cylinder are decreased. These lead to slower mixing between air and fuel and increase the ignition delay [179]. As a result the nitrogen and oxygen molecule resident time is increased. This causes higher NO_x emission at lower engine speeds and lower loads. At higher engine speed and load, the opposite phenomenon happens.

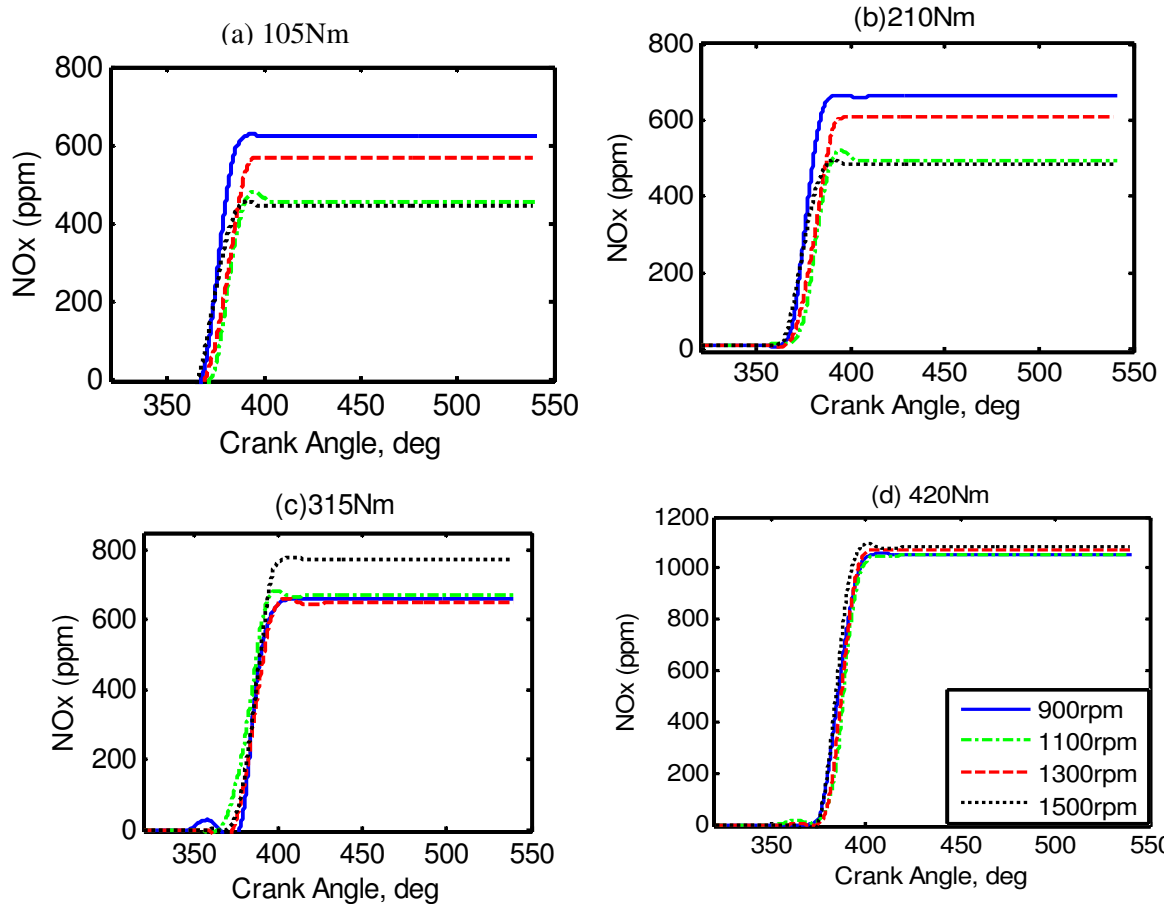


Figure 7-5 Variation of predicted NOx emission with crank angle of CI engine running with biodiesel at various loads and range of engine speeds

Figure 7-6 shows the predicted value of nitrogen oxides (NOx) emission for engine running with biodiesel and diesel at various loads and engine speeds. It can be seen that the NOx emission, when the engine running with biodiesel, is higher than when it runs with diesel. The main reason for higher emission with biodiesel is the advanced combustion process initiated because of the physical properties of biodiesel (viscosity, density, compressibility, sound velocity) [204], [132]. When biodiesel is injected, the pressure rise produced by the pump is higher as a consequence of its lower compressibility (higher bulk modulus) and fuel propagates quickly towards the injectors. As a result, the cylinder gas becomes rich fairly quickly by fuel and reaches its peak temperature which speeds up the formation of NOx. Similar trend have been seen in Figure 7-7 for the engine running at 315Nm.

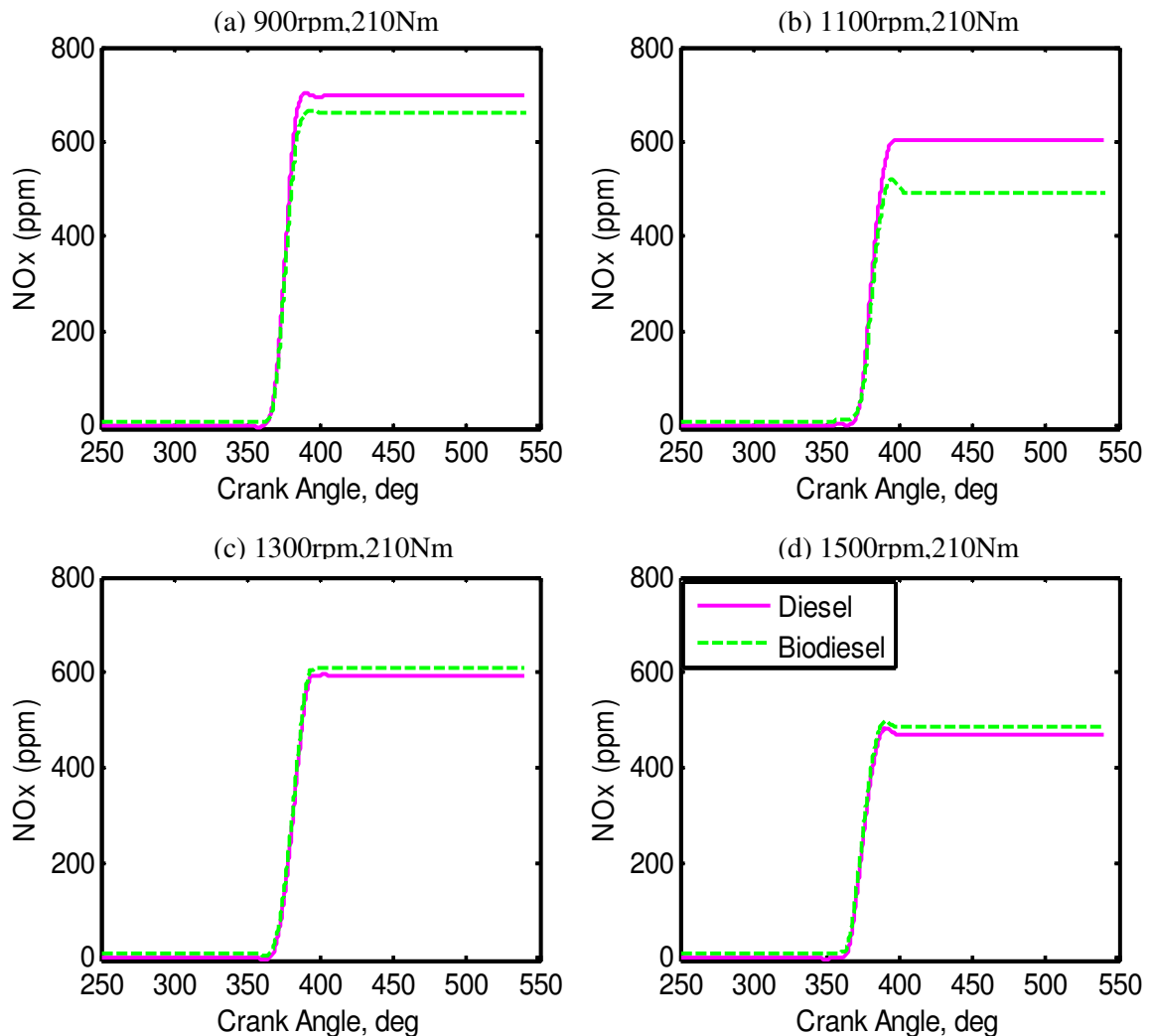


Figure 7-6 Variation of predicted NO_x emission with crank angle of CI engine running with biodiesel and diesel at engine load of 210Nm and various engine speeds.

7.4 Validation of the NO_x Prediction Model

To investigate the accuracy of the NO_x prediction model from the cylinder pressure, the measured and the predicted value of NO_x emission of CI engine running with both diesel and biodiesel are presented in Table 7-2 and Table 7-3. It can be seen from the tables that the new NO_x developed model can predict NO_x emission for all engine operating conditions and fuel types.

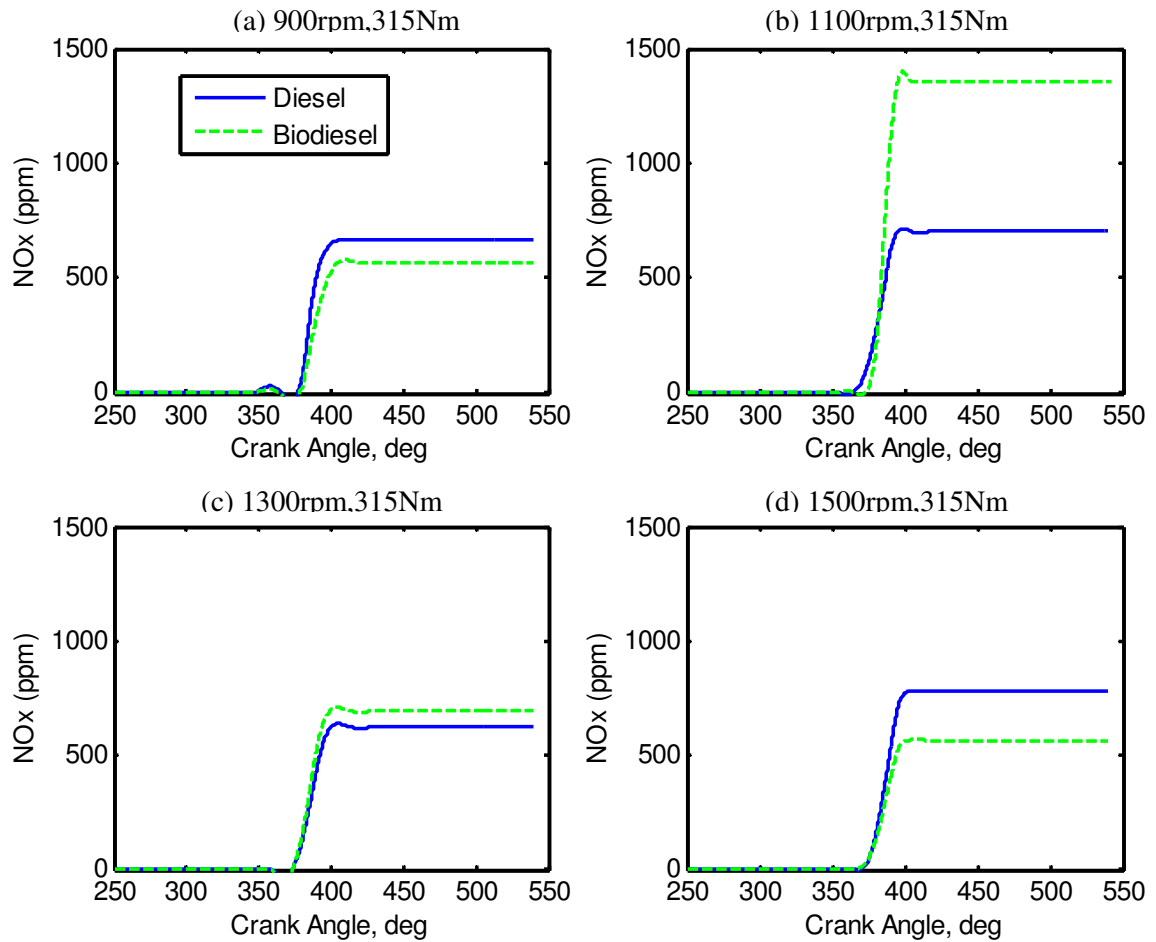


Figure 7-7 Variation of predicted NO_x emission with crank angle of CI engine running with biodiesel and diesel at engine load of 315Nm and various engine speeds

Table 7-2 Measured and Predicted NOx emission values of CI engine running with biodiesel (100B)

Speed (rpm)	NOx emission(ppm) at 105Nm			NOx emission(ppm) at 210Nm			NOx emission at 315Nm			NOx emission(ppm) at 420Nm		
	Measured (ppm)	Predicted (ppm)	Error (%)	Measured (ppm)	Predicted (ppm)	Error (%)	Measured (ppm)	Predicted (ppm)	Error (%)	Measured (ppm)	Predicted (ppm)	Error (%)
900	538	456	15.24	854	702	17.79	896	666	25.66	1056	1057	0.13
1100	478	435	9.07	583	604	3.64	638	712	11.62	1025	1053	2.69
1300	471	476	1	566	594	4.89	644	635	1.38	1049	1072	2.18
1500	469	474	1.15	565	481	14.85	655	781	19.24	1066	1095	2.7

Table 7-3 Measured and Predicted NOx emission values of CI engine running with biodiesel (100B)

Speed (rpm)	NOx emission(ppm) at 105Nm			NOx emission(ppm) 210Nm			NOx emission(ppm) 315Nm			NOx emission(ppm) 420Nm		
	Measured (ppm)	Predicted (ppm)	Error (%)	Measured (ppm)	Predicted (ppm)	Error (%)	Measured (ppm)	Predicted (ppm)	Error (%)	Measured (ppm)	Predicted (ppm)	Error (%)
900	480	477	0.67	981	656	33.14	1011	675	33.26	1105	1057	4.33
1100	423	438	3.62	692	511	26.11	918	682	25.71	1087	1053	3.1
1300	417	483	15.91	554	598	7.98	680	676	0.6	1055	1072	1.65
1500	414	462	11.54	542	486	10.32	649	794	22.4	1072	1095	2.14

7.5 Summary on NO_x Prediction from In-cylinder Pressure

In this chapter a model for predicting NO_x emission has been developed which uses experimentally measured in-cylinder pressure as an input. Furthermore, the dependence of NO_x formation on the in-cylinder temperature has been investigated based on the model developed. The efficacy of using the in-cylinder pressure to predict the NO_x emission has also been investigated for a compression ignition (CI) engine running with different fuels including biodiesel. The temperature of the cylinder is predicted using the cylinder pressure by ideal-gas state equation. Using the predicted temperature the NO_x emission is then calculated based the Zeldovich extended mechanism. The measured and prediction results of NO_x emission are compared and it has been shown that the deviation of the values obtained from the model from the measured emission values with diesel and biodiesel are in acceptable error. The prediction model paves the way for real-time NO_x emission estimation for engine transient study and on-line diagnosis. This model can be used during the design stage of engine to meet the emission standards requirements especially during transient operations. To become fully functional for road vehicles, it needs further integration to link the in cylinder temperature with engine dynamics such as engine vibration or acoustic emission. This can be achieved through correlating the in-cylinder temperature with vibration or acoustic by using the in-cylinder pressure.

The next chapter focuses on the effect of water injection on the engine performance and emission behaviour especially NO_x when the engine fuelled by biodiesel.

CHAPTER EIGHT

8. MANAGEMENT OF NO_x EMISSIONS FROM A CI ENGINE OPERATING WITH BIODIESEL USING A WATER INJECTION SYSTEM

Chapter eight provides the experimental results as well as analysis and discussion on the effects of water injection in a CI engine running with biodiesel. Although the engine fuelled with biodiesel provide comparable performances and better emissions of CO₂, CO and THC as compared to an engine running with diesel fuel, the experimental results in Chapter five and Chapter six indicated that the engine running with biodiesel emitted more NO_x emission than the engine running with diesel by up to 30% at maximum load condition. As discussed in section 2.2.2, NO_x and PM emissions are major toxic emissions which are being regulated with emission regulations and these regulations are becoming increasingly more stringent [50], [145]. Therefore the main objective of this chapter is to investigate the effects of water injection on the NO_x emission characteristics of the engine when it runs with biodiesel. This development can be used to manage NO_x emission coming out of CI engines running with Biodiesel. The test apparatus and the procedures have been discussed in Chapter three. This Chapter has focused on the effects of water injection on in-cylinder pressure, heat release rate, brake specific fuel consumption, thermal efficiency and emission of NO_x and CO when the CI engine is fuelled with biodiesel blends.

8.1 Effects of Water Injection on NOx and CO Emissions

The effects of water injection on NOx emissions from a CI engine running with biodiesel have been investigated experimentally. To understand the effects of water injection on other exhaust emissions, the CO emission characteristics has been also discussed in detail. CO emission has been selected due to its sensitivity with water injection as per previous reports on the application of water injection with diesel fuel [60], [96], [100], [109-111], [121], [122]. The NOx emission from the CI engine running on 100% biodiesel at loads of 105Nm, 201Nm, 315Nm and 420Nm over range of engine speeds and at different water injection rates (0kg/h, 1.8kg/h, 3kg/h) are depicted in Figure 8-1. At all operating conditions, NOx emissions have been found to decrease with an increase in engine speeds. This can be explained on the basis that at higher engine speeds, the volumetric efficiency and gas flow within the combustion cylinders were found to increase.

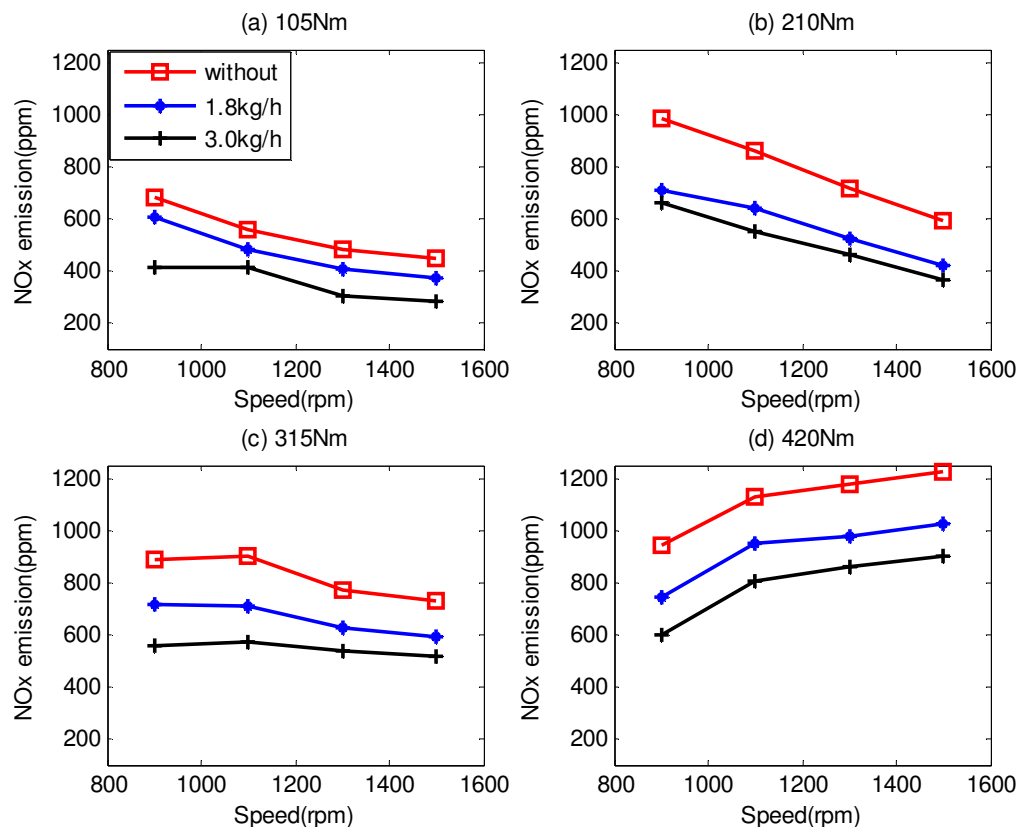


Figure 8-1 NOx emission values of CI engine running with biodiesel(100B) and water at range of engine speeds and engine loads

This in turn led to a faster mixing of air and fuel which resulted in the minimisation of the ignition delay [49]. This reduction of ignition delay minimised the reaction time of free

nitrogen and oxygen gas in the combustion cylinder, which is the main mechanism of NOx formation. Figure 8-1 clearly depicts that as the water flow rate increases, the NOx emission reduces proportionally.

As it can be seen in Figure 8-2 the water injection into the intake manifold reduces the NOx exhaust emission by around 20% and 40%, at 1.8kg/h and 3kg/h water injection rates, respectively. This phenomenon can be explained on the basis that when the water-air mixture is injected into the combustion chamber, some of the heat is absorbed by the water during the process of water vaporisation.

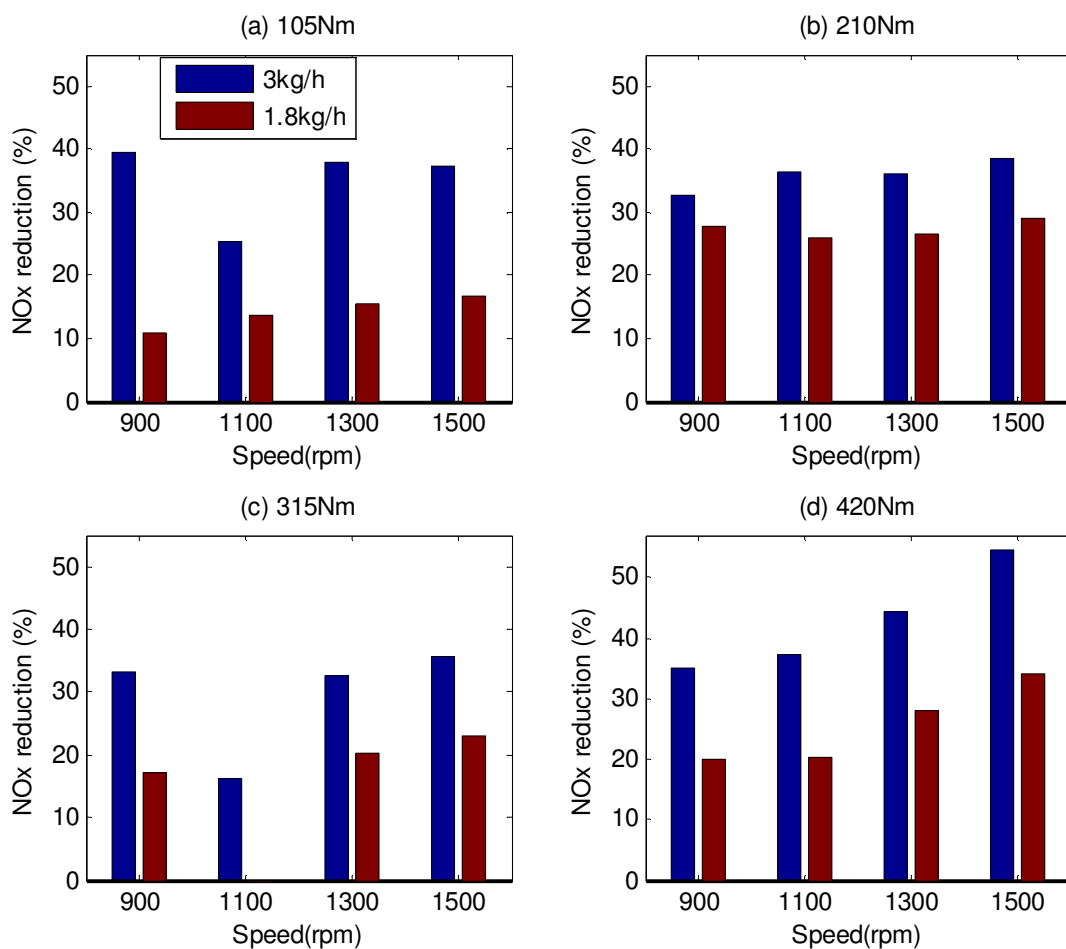


Figure 8-2 Reduction of NOx emission from CI engine running with biodiesel(100B) due to the effects of water injection at range of engine speeds and engine loads

This process reduces the peak flame temperature of the combustion chamber and negatively impacts on the formation of nitrogen oxides (NOx) [157-159]. In addition, the water injection into cylinder chamber changes the thermo-physical properties of water and consequently affects the heat transfer coefficient of the gas mixture, thereby facilitating heat

loss through the cylinder walls. Furthermore, Figure 8-2 depicts that the effects of water flow rates vary with the engine load conditions. It can be seen that when the water flow rate increases from 1.8kg/h to 3.0kg/h(66%), the NOx percentage reduction change by 58.37%, 23.75%, 40.87% and 40.67% for engine loads of 105Nm, 210Nm, 315Nm and 420Nm respectively.

Figure 8-3 shows the effect of water injection on CO emissions at various engine speeds and at engine loads of 105Nm, 210Nm, 315Nm and 420Nm. It can also be seen that when the engine speed and load increases, the CO emission decreases. A reason for this could be that at higher engine speeds, the air/fuel equivalence ratio increases and this increases the in-cylinder gas temperature leading to an increase in the kinetic reaction rate from CO to CO₂. Furthermore, Figure 8-3 depicts that at higher water flow rate (3kg/h), the CO emission increases during all operating conditions. However, the 1.8kg/h water injection results in insignificant CO emission over the range of engine speeds and loads. As it can be seen in Figure 8-4 the CO emission is higher at lower engine speeds by up to 57%. This value reduces to 25% for intermediate and higher engine speeds.

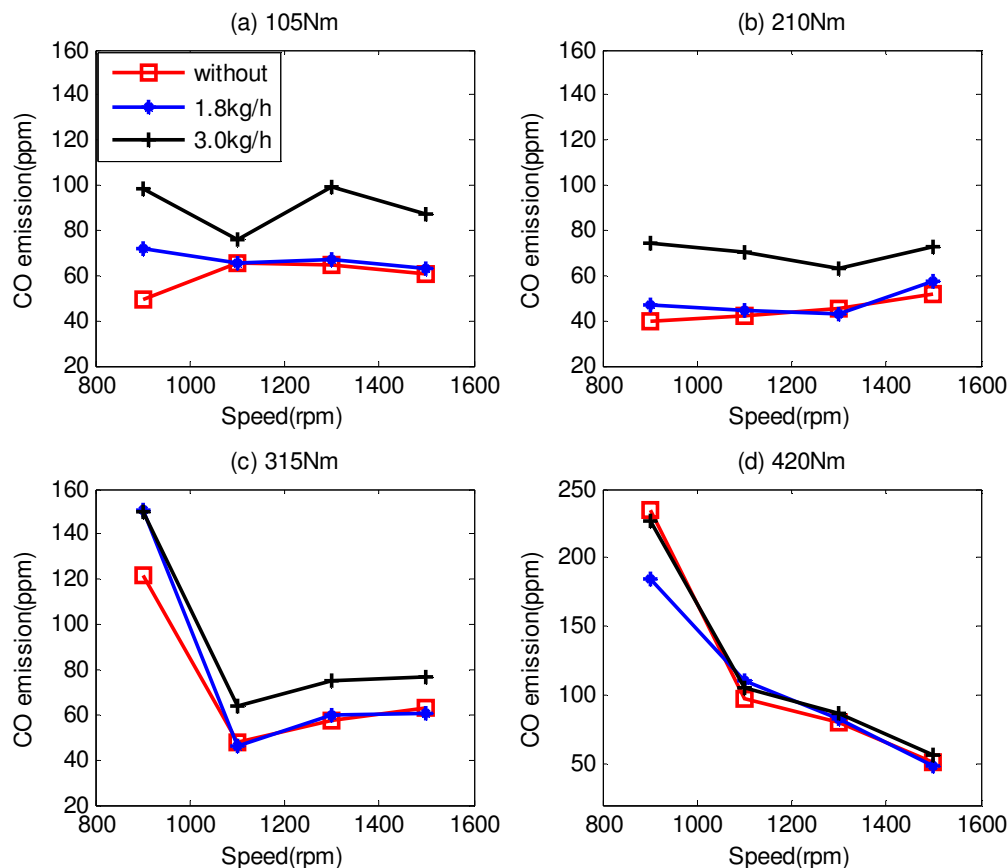


Figure 8-3 CO emission values from CI engine running with biodiesel(100B) and water at range of engine speeds and engine loads.

There are two main reasons for the increase in CO emission during water injection to the CI engine. First, the reduction of the pre-combustion temperature due to water injection slows the chemical conversion of the CO to CO₂. Second, the solid carbon reaction at high temperature with water vapour enhances the formation of CO and H₂O in the cylinder.

Even though the water injection increases the CO emission, considering the stringent NOx emission laws in EU VI, water injection can prove to be a viable technology for NOx reduction. For both Euro IV (2005) and Euro VI (2014) the CO emission standards are 0.5g/Km for passenger cars. However, the NOx emission standards of Euro IV (2005) and Euro VI (2014) are 0.25g/km and 0.08g/km.

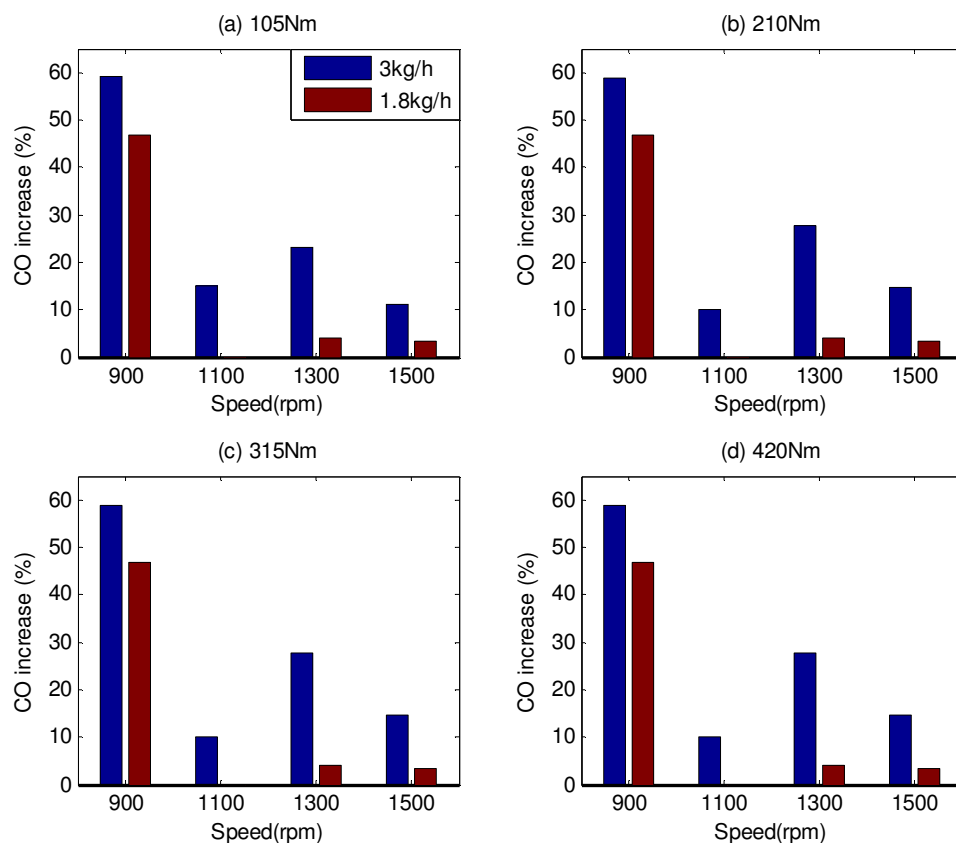


Figure 8-4 Percentage increase in CO emission from CI engine running with biodiesel(100B) due to the effects of water injection at range of engine speeds and engine loads

To manage the NOx emission of engine fuelled with biodiesel and the stringent NOx emissions in 2014, new technologies like water injection system development are required.

The CO emission increment during the water injection can be managed by finding the optimum emission values of CO and NOx.

8.2 Water Injection Effects on Cylinder Pressure and Heat Release Rate

The injection of water in diesel engines mainly affects the combustion characteristics such as the air-fuel-water mixing phenomenon, the ignition delay, the cylinder pressure and the heating release rate. Understanding of combustion characteristics specifically the in-cylinder pressure and heat release rate can benefit the design of the engine combustion chamber and its thermal analysis. In this section the effects of water injection on in-cylinder pressure, heat release rate and cumulative heat release rate have been covered. The variation of in-cylinder pressure with cylinder volume for an engine speed of 1300rpm, at loads of 105Nm, 210Nm, 315Nm and 420Nm, corresponding to different water injection rates (0kg/h, 1.8kg/h and 3kg/h) into the intake manifold is depicted in Figure 8-5.

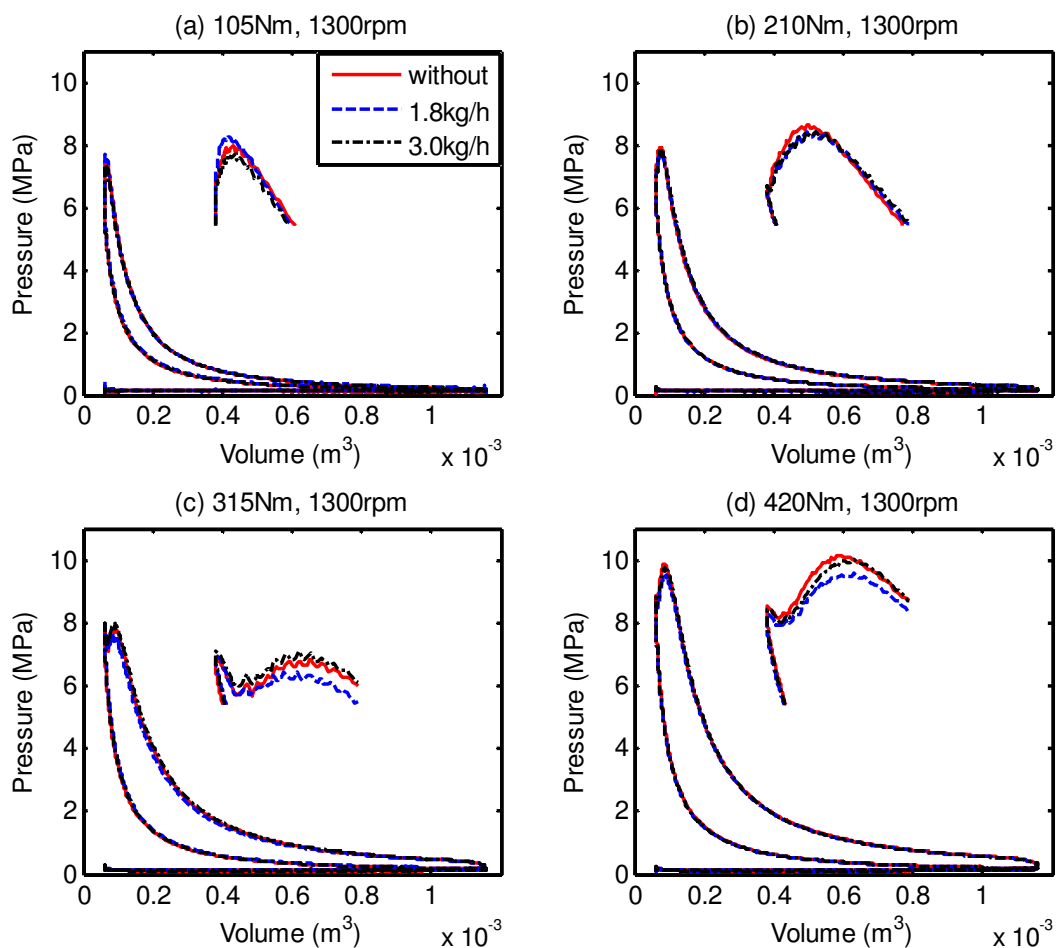


Figure 8-5 P-V diagram of CI engine running with biodiesel(100B) and water at an engine speed of 1300rpm at various engine loads

The results show that the P-V diagrams obtained are fairly similar and follow typical characteristics under different operating conditions. Effects of water shows only marginal effects on peak pressure values within the cylinder. This suggests that the work done by the engine, calculated from the P-V diagrams, is largely unaffected by the water injection. The work done which is calculated from the P-V diagram shows less than 2% change in work output due to the water injection.

Figure 8-6 and Figure 8-7 show the variations of in-cylinder pressure with crank angle under different operating conditions for the engine running with biodiesel at different water injection rates (0kg/h, 1.8kg/h, 3kg/h), for engine speeds of 900rpm, 1100rpm, 1300rpm and 1500rpm, at different engine loads of 105Nm, 210Nm, 315Nm and 420Nm. In both these figures, it can be seen that the peak cylinder pressures had only minor differences in magnitude for different water flow rates at a given operating conditions.

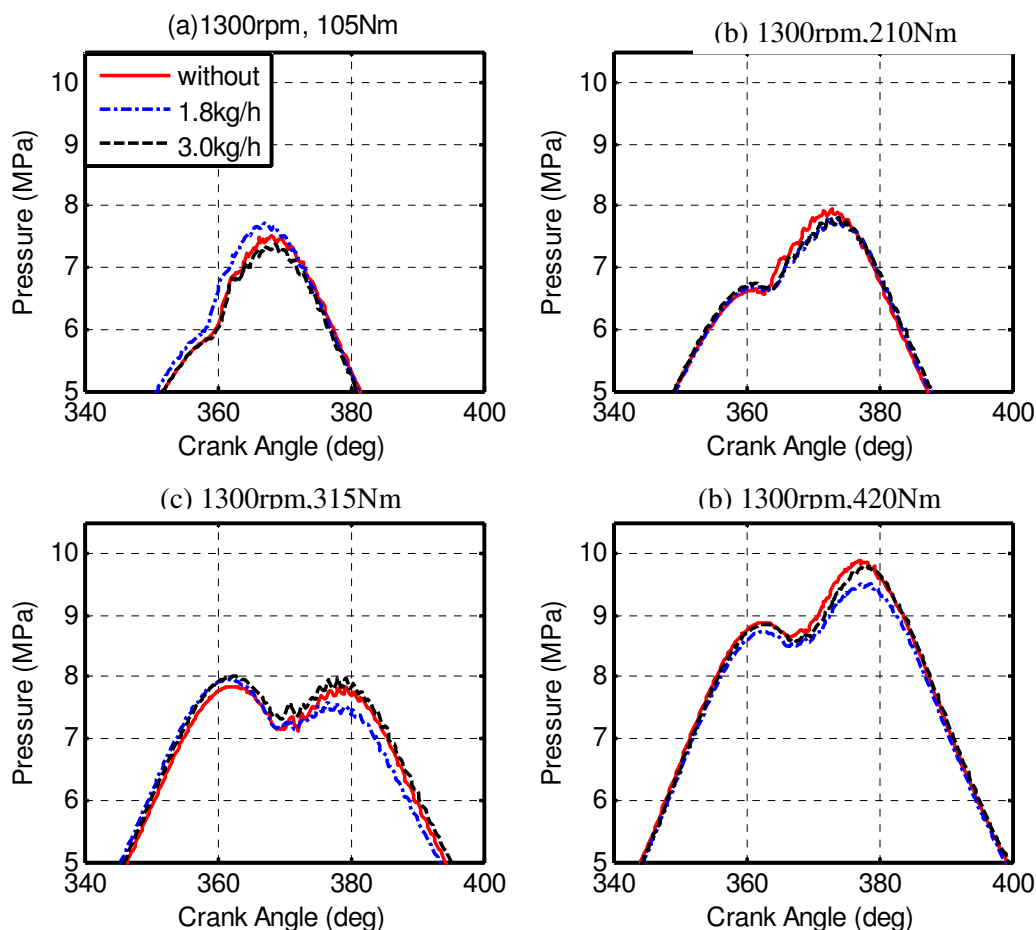


Figure 8-6 In-Cylinder pressure versus crank angle of CI engine running with biodiesel(100B) and water at engine speed of 1300rpm and various engine loads

This result indicates that water injection into the intake manifold does not affect the peak flame temperature considerably during the combustion at a given operating condition (speed and load). Instead, water injection has reduced the premixed combustion flame temperature at which high concentrations of nitrogen and oxygen react to form oxides of nitrogen [190].

The main cause for temperature reduction in premixed combustion is due to the absorption of heat by water to form vapour, water cooling effects due to evaporation of water from combustion chamber surfaces, increase in heat capacity and specific heat capacity due to higher trapped mass, combustion delay due to increase in ignition delay and decrease in the chemical reactions rates due to the inert ‘chemical’ water [115], [152]. As a result, the NOx emission during the premixed combustion is reduced. However, it can be seen that with the change of operating conditions, the pressure variation profile changed substantially. For example, when the engine load has increased from 105Nm to 210Nm, the peak in-cylinder pressure has also increased from 8MPa to 9.5MPa.

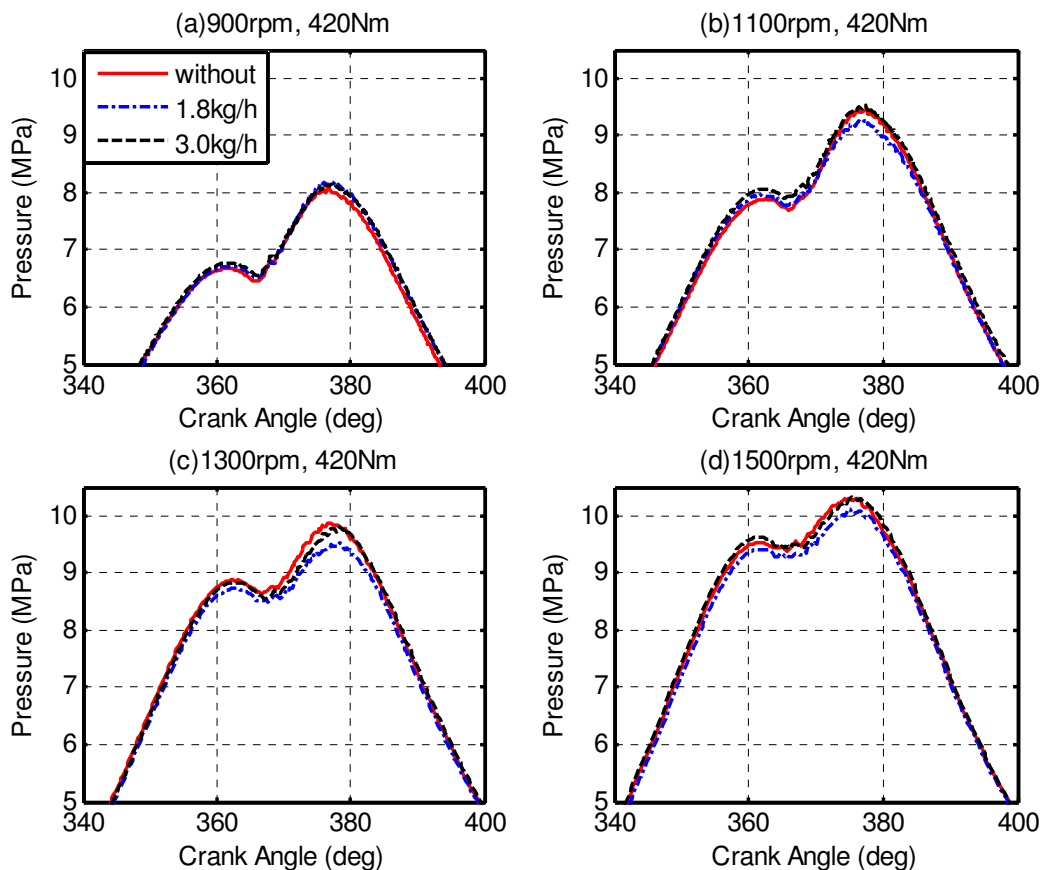


Figure 8-7 In-Cylinder pressure versus crank angle of CI engine running with biodiesel(100B) and water at loads 420Nm and various engine speeds

Figure 8-8 illustrates the rate of heat release (ROHR) for the CI engine used in the present investigation running with biodiesel with water injection at speeds of 900 rpm and 1300 rpm, and at two different loads of 210 Nm and 420 Nm. At lower engine speeds and lower engine loads, since the vaporised fuel accumulated during ignition delay [190], at the beginning, negative heat release rates were observed as shown in Figure 8-8(a) and Figure 8-8(b). However, at higher engine speed (1300rpm), the heat release rate started with a positive ROHR due to the higher fuel-air mixing phenomena (Figure 8-8(c) and Figure 8-8(d)). In Figure 8-8, it can also be seen that the maximum heat release rate of combustion with water injection is higher than without water. This is due to the ignition delay and accumulation of fuel in the combustion chamber at the time of combustion resulting in higher ROHR [115]. Furthermore, it can be seen from the figures that the main effect of water injection on combustion is to increase the ignition delay. This observation is in agreement with previous researchers' works [115], [200].

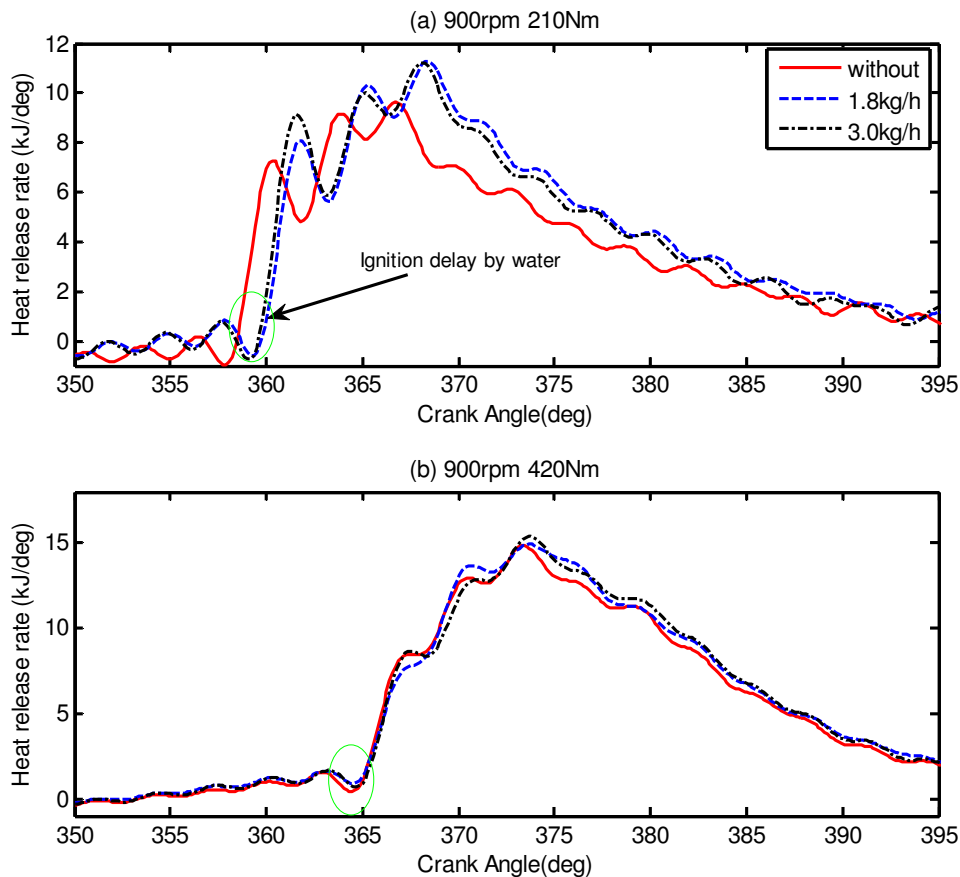


Figure 8-8 Heat releases rate of CI engine versus crank angle running with biodiesel (100B) and water at range of engine speeds and engine loads

The ignition delay, being the time (or crank angle) interval between the start of injection and the start of combustion, is seen to rise with an increase in the water injection flow rate. In the

author opinion the ignition delay is due to the cooling effect of water on the inlet air temperature.

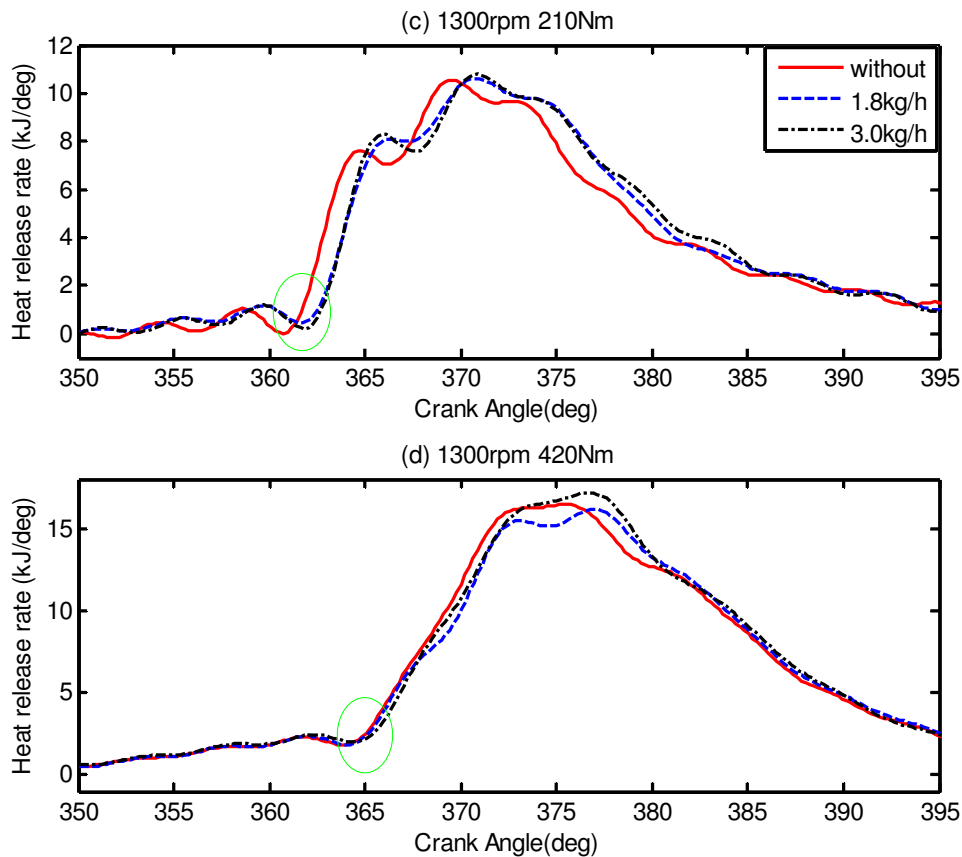


Figure 8-8 Heat releases rate of CI engine versus crank angle running with biodiesel(100B) and water at range of engine speeds and engine loads

Furthermore, addition of water can also have had a significant effect on the chemical kinetics within the combustion chamber. At higher loads (as seen in Figure 8-8(c) and Figure 8-8(d)), combustion was almost purely diffusive and the influence of water injection on ROHR was less. In this case, with water injected together with air, the spray entrained a water-air mixture instead of pure air, so that an increase in combustion duration was expected.

The cumulative heat release is an important parameter to characterise the efficiency of the combustion process. The variation of cumulative heat release rate with crank angle is shown in the Figure 8-9. The figure showed that at lower engine speeds engine running with water injection, had slightly higher cumulative heat release rate than the engine running without water injection. At higher loads, the water injection did not show any significant change in the cumulative heat release rate.

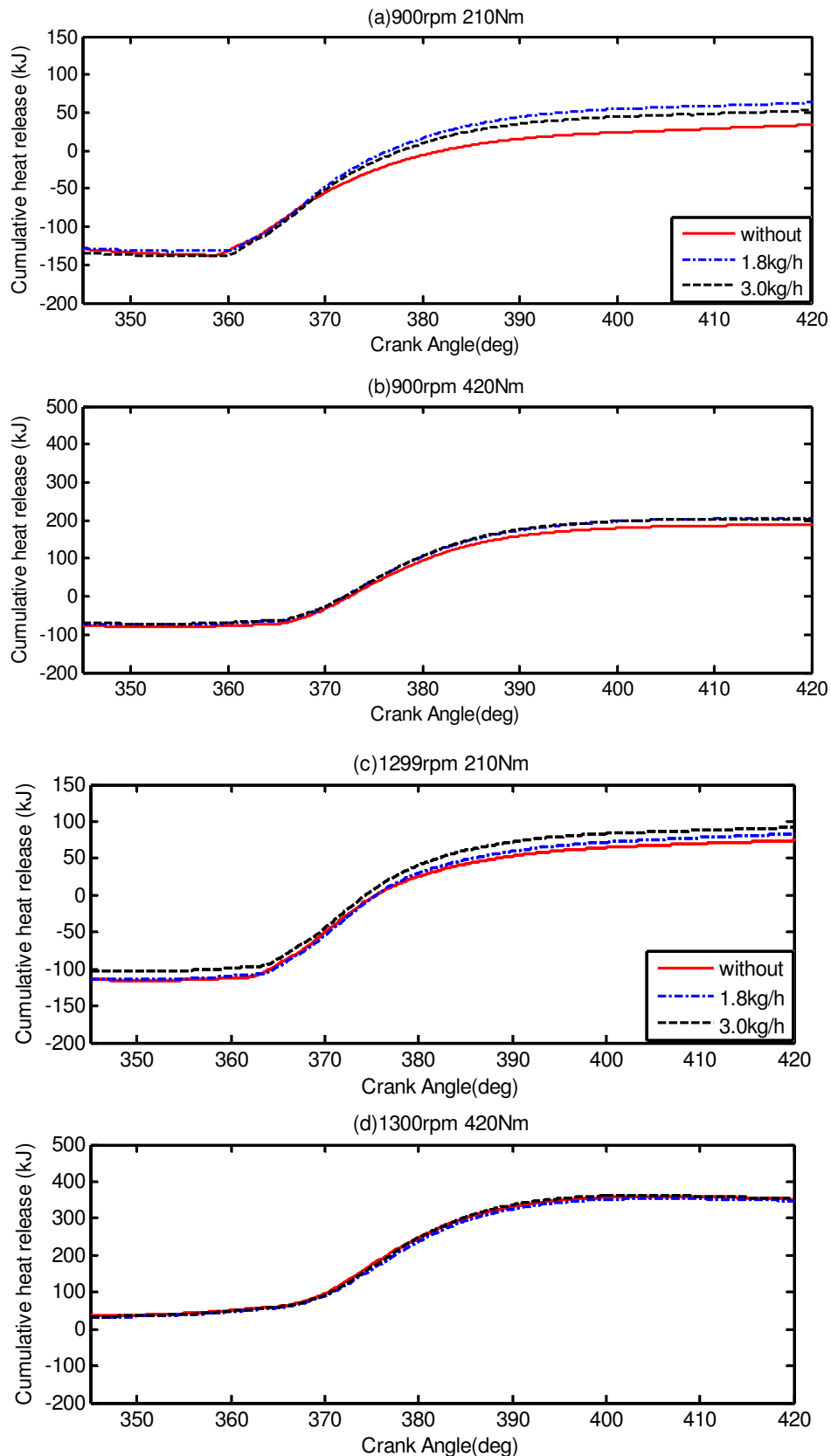


Figure 8-9 Cumulative heat release of CI engine versus crank angle running with biodiesel(100B) and water at range of engine speeds and engine loads

8.3 Effects of Water Injection on Engine Performance

To monitor the effects of water injection on the engine performance, two parameters namely, brake specific fuel consumption and thermal efficiency have been investigated. The brake specific fuel consumption shows the effects of water injection on the efficiency of fuel use. The thermal efficiency is the reciprocal of brake specific fuel consumption and heating value. In this section the effects of the water injection on the brake specific fuel consumption and thermal efficiency have been investigated. The variation of the brake specific fuel consumption (BSFC) with speeds for different water injection conditions (without water, with 1.8kg/h water, and 3kg/h water) at different loads is depicted in Figure 8-10.

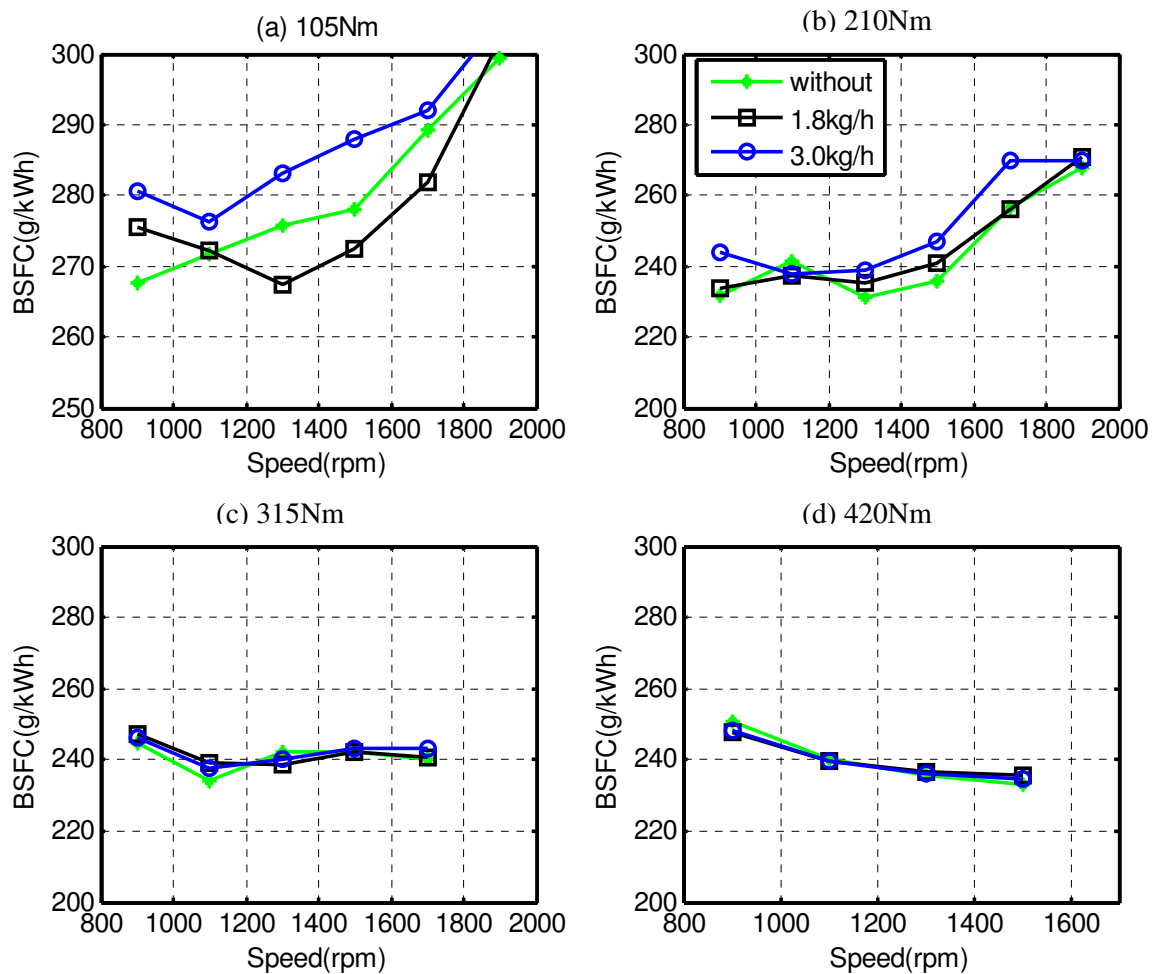


Figure 8-10 Brake specific fuel consumption (BSFC) of CI engine running with biodiesel(100B) and water at range of engine speeds and various engine loads

The BSFC was estimated from the brake power output of the engine and the mass flow rate of the fuel. It can be seen from Figure 8-10 that the BSFC decreased as the engine speed increased, reaching its minimum and then increased at high engine speeds. This can be

explained on the basis that at low speeds, the heat loss through the combustion chamber walls is proportionally greater and the combustion efficiency is poorer. These result in higher fuel consumption for the same amount of power produced. At higher speeds, the power required to overcome friction increased at a higher rate, resulting in a slower increase in output power with a consequent increase in BSFC [160], [205]. The percentage change in BSFC due to water injection is depicted in Figure 8-11. It can be seen that at lower engine loads (105Nm and 210Nm), the BSFC was at a minimum for the engine operating without water injection and with water injection at 1.8 kg/h. At higher loads (315Nm and 420Nm), the injection of water did not show any significant changes in BSFC.

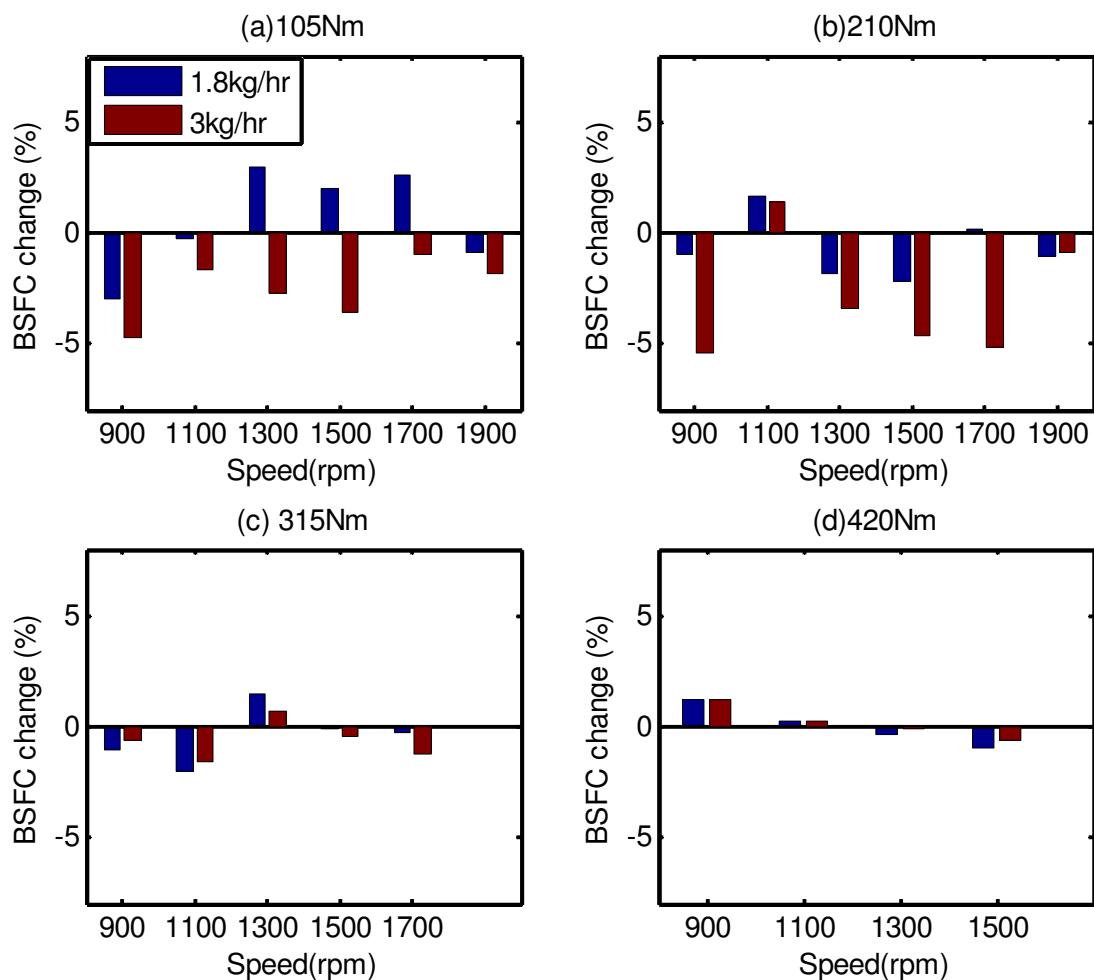


Figure 8-11 Brake specific fuel consumption (BSFC) change of CI engine due to water injection at range of engine speeds and engine loads

The effects of water injection on the thermal efficiency of engine running with biodiesel with and without water injection are shown in figure 10. The brake thermal efficiency was calculated from the BSFC and lower heating value of the fuel, as shown in equation (8-1):

$$\eta = \frac{3600}{BSFC \times LHV} \times 100 \quad (8-1)$$

Where η is the thermal efficiency (%), BSFC is brake specific fuel consumption (g/kWh) of the biodiesel and LHV is lower heating value (kJ/kg) of the biodiesel.

It can be observed from Figure 8-12 that at all the operating conditions the thermal efficiency increases at lower engine speeds, reaches its higher point and then decreases.

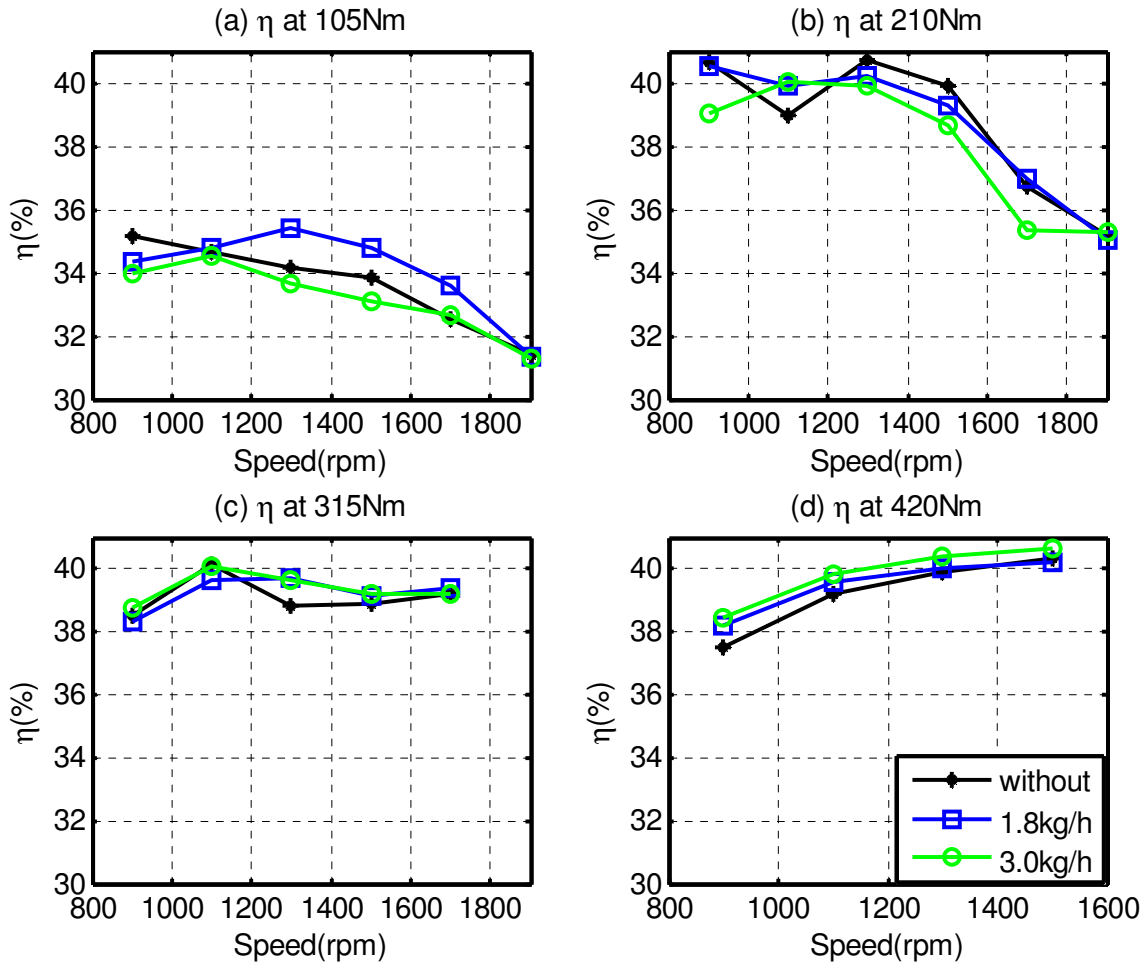


Figure 8-12 Thermal efficiency values of CI engine running with biodiesel(100B) and water at range of engine speeds and engine loads

At lower loads, the engine brake thermal efficiency corresponding to 3kg/h water injection decreased by an amount of 3% as compared to the thermal brake efficiency of the engine running without water as shown in Figure 8-13(a-b). At higher loads (210Nm and 420Nm), the thermal efficiency of engine running with water injection was slightly

higher as compared to the no-water injection condition. This shows that the effect of water injection on the thermal efficiency of the engine is insignificant.

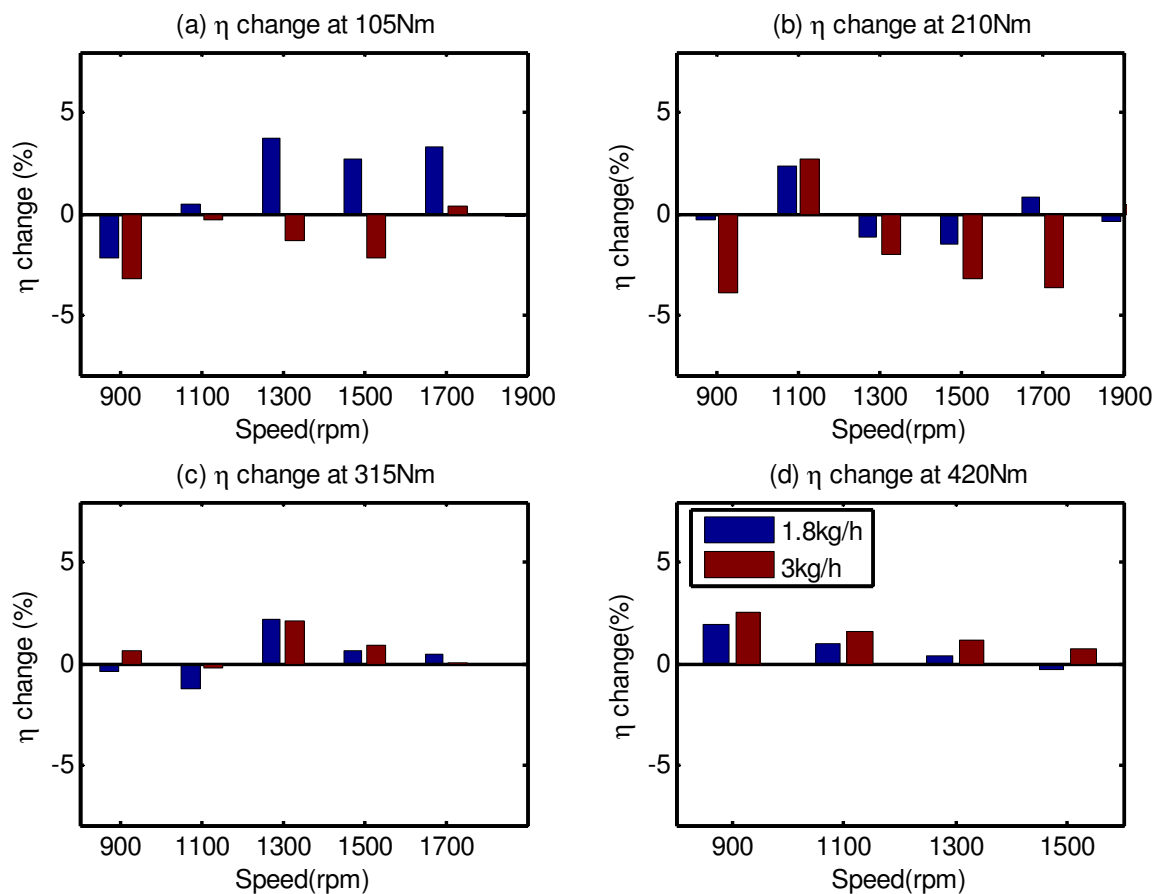


Figure 8-13 Thermal efficiency change of CI engine due to water injection at range of engine speeds and engine loads

8.4 Summary on Effects of Water Injection on CI engine Performance

In this chapter the effects of water injection on NOx emission coming out of the engine running with biodiesel have been investigated and discussed. The following summary can be drawn:

1. The in-cylinder pressure analysis shows the peak cylinder pressures have only minor differences in magnitude for different water flow rates under given operating conditions. As a result the water injection into the intake manifold does not affect the peak flame temperature considerably during combustion. This further validates the theory which states that water injection mainly affects the premixed combustion flame temperature.

2. Water injection has resulted in increasing of the ignition delay. The higher ignition delay leads to accumulation of fuel in the combustion chamber at the time of combustion resulting in higher ROHR.
3. The BSFC of CI engine shows a slight increase under lower engine loads (105Nm and 210Nm), while at higher loads (315Nm and 420Nm), the injection of water did not show any significant changes in BSFC.
4. The water injection into the intake manifold reduced the NOx exhaust emission by around 20% and 40%, at 1.8kg/h and 3kg/h water injection rates, respectively. The main reason for NOx reduction is the cooling effect of water in pre-combustion and the delay of ignition.
5. The water injection into the intake manifold increases the CO emission by up to 25% during 3kg/h water injection. However, the 1.8kg/h injection rate did not show significant change in CO emission.

The next chapter includes conclusion and future work of this thesis. The main contributions, conclusions and future works have been summarized for each section of work.

CHAPTER NINE

9. CONCLUSIONS AND FUTURE WORKS

This chapter summarizes the review of research objectives and achievements, the conclusions and the future of work in this research area. For each specific objective the achievements have been described. The conclusions on biodiesel characterisation, performance and emission characteristics of the engine during both steady and transient operations, the newly developed NOx emission prediction model and the effects of water injection on the engine performance and emission have been included. Furthermore an explicit summary of the novel contributions of the research conducted by the author has been included. Finally, the chapter ends by addressing the future work that would help in further understanding of engine operations with biodiesel as a fuel.

9.1 Review of Research Objective and Achievements

The main achievements of this work have been presented below in the same order they appear in Section 2.5.

Objective 1: To analyse the physical properties such as density, viscosity and lower heating value of biodiesel and its blends experimentally by considering biodiesel content and temperature variation.

Achievement 1: The effects of biodiesel blend content and temperature on the specific gravity, kinematic viscosity and lower heating value have been measured using hydrometer, Cannon-Fenske Viscometer tube (size B) and Bomb Calorimeter respectively in Applied Science laboratory, University of Huddersfield. The experimental data analyses have shown a variation in the physical properties at different biodiesel blend fractions values and temperatures. The understanding of the physical behaviour of these two critical parameters has huge importance in the preparation of biodiesel blends for direct application in the engine. In addition, understanding of the temperature effects on biodiesel will have high importance in design of pre-heater for biodiesel application to manage physical properties.

Objective 2: To develop prediction models for physical properties of biodiesel and its blends from the experimental data which can correlate the physical properties with biodiesel content and temperature.

Achievement 2: Prediction models have been developed for density, kinematic viscosity and lower heating values and compared with current models available in literature. In addition, new density and viscosity prediction models have been developed by considering the combined effect of biodiesel content and temperature. All the empirical models have shown a fair degree of accuracy in estimating the physical properties of biodiesel compared with the experimental results. These models can be used in engine design stage for combustion, performance and emission characterisation. It can also be used to develop thermo-physical models to be used in engine simulation software.

Objective 3: To investigate numerically the effects of the biodiesel physical properties on the fuel supply system such as fuel filter, fuel pump and engine combustion chamber.

Achievement 3: Mathematical models have been developed to investigate the effect of density, viscosity and lower heating value on the fuel supply system such as fuel pump, fuel filter and in-cylinder air mix phenomena. These models can be used to understand the effects of changes in the physical properties on the fuel supply system. In addition, the integrated fuel supply system can be analysed for its performance during the design stage of fuel pump, fuel filter and injection systems to optimise its performance.

Objective 4: To analyse experimentally, the combustion characteristics such as in-cylinder pressure, heat release rate and cumulative heat release of CI engine fuelled with biodiesel and its blends during both steady and transient conditions.

Achievement 4: A comprehensive diesel engine test rig has been developed featuring key instrumentation along with emission analyser in the Automotive Laboratory, University of Huddersfield. The engine speed, in-cylinder pressure, air mass flow rate, inlet conditions and the exhaust conditions have been measured. Detailed analyses on the in-cylinder pressure, heat release rate, ignition delay have been carried out. As a result, the effects of biodiesel content on in-cylinder pressure, heat release rate and ignition delay have been quantified.

Objective 5: To examine analytically the brake specific fuel consumption, thermal efficiency and in-cylinder peak pressure of CI engine systems from experimental data obtained from engine using biodiesel and its blends as a fuel during both steady and transient conditions.

Achievement 5: The CI engine has been tested with three biodiesel sources and six biodiesel blends. The engine performance parameters such as the fuel mass flow rate, brake specific fuel consumption, exhaust temperature and in-cylinder pressure have been measured experimentally. The thermal efficiency has been calculated from the brake specific fuel consumption and the lower heating value. The effects of biodiesel feed stock sources and biodiesel content on brake specific fuel consumption, thermal efficiency, in-cylinder pressure and exhaust temperature have been investigated and quantified.

Objective 6: To examine numerically and experimentally the emissions of CI engine systems which is running with biodiesel and its blends during both steady and transient conditions.

Achievement 6: The emissions of CI engine fuelled with various biodiesel feed stock and its blends have been measured by HORIBA EXSA-1500 during both steady and transient

operations. A detailed analysis has been carried out on the emission behaviour of the CI engine emission for both steady and transient operations. During this analysis, the emission changing rate during the transient time span has been investigated. The effects of biodiesel feed stock sources and biodiesel content on CO₂, NO_x, CO and THC have been investigated and quantified. Furthermore, a transient emission prediction model has been developed using associated steady and transient emission data.

Objective 7: To develop a method to estimate NO_x emission under steady and transient operation using in-cylinder pressure, specific heat and mass air flow rate.

Achievement 7: A new on-line prediction model for NO_x has been developed using the in-cylinder pressure generated within a CI engine along with air mass flow rate experimentally. This model has been validated using experimental data obtained from a NO_x emission analyzer and shows good agreement. This model can be used for prediction of NO_x during both steady and transient conditions.

Objective 8: To develop direct water injection system for use on CI engine running with biodiesel and investigate the combustion characteristics, performance and NO_x emission of the engine during steady state mode of operation.

Achievement 8: A direct water injection system has been developed for use on the engine test rig where it is installed and can be used to inject water into the intake manifold. Water has been injected through the intake manifold over a range of volumetric flow rates. The effects of water injection on in-cylinder pressure, heat release rate, brake specific fuel consumption and thermal efficiency have been investigated. A detail analysis has been carried out on the effect of water injection and NO_x emission when the engine is fuelled with biodiesel.

9.2 Conclusions

This research is directed towards the characterisation of physio-chemical properties of biodiesel, combustion, performance and emission characteristics of CI engine running with biodiesel during both steady and transient operations. Furthermore, to overcome problems experienced with high NO_x emission from CI engine running with biodiesel, to monitor the NO_x emission during steady and transient operation, a NO_x prediction model has been developed. Furthermore a novel water injection technique has been developed to

manage the NO_x emission. In this study, the following conclusions have been drawn for each research area:

9.2.1 Conclusions on Biodiesel Characterisation

In this section, the key conclusions associated with biodiesel characterisation are summarised which are based on the experimental results.

Conclusion 1: The density, kinematic viscosity and lower heating value of biodiesel blends (0B, 5B, 10B, 20B, 50B, 75B, and 100B) from the three biodiesel feed stocks have been measured over a range of temperatures. It was noticed that when the biodiesel content increases, the density and the viscosity of the biodiesel increases. However, the lower heating value decreases with increasing the biodiesel content. It was also observed that the density and viscosity of each blend decreased with an increase in the temperature. The density, viscosity and heating value of neat biodiesel are 1.03, 1.56 and 0.90 times the diesel respectively. Based on the above results it can be concluded that biodiesel fraction and temperature highly affect the physical properties of the fuel.

Conclusion 2: It was found that the empirical equations which have been developed from the experimental data for prediction of density, viscosity and lower heating value as a function of biodiesel fraction and temperature have matched closely with the experimental results. Furthermore, the Grun-Nissan viscosity equation has been further modified to predict the kinematic viscosity of biodiesel blends from the biodiesel fraction and operating temperature values. The modified models have shown a reasonable degree of accuracy. The developed model can be used in numerical investigation of engine design and performance evaluation.

Conclusion 3: Using a newly developed fuel supply system model, it has been found that the density and viscosity of the biodiesel affect the performance of the fuel supply system which includes fuel pump, fuel filters and air-fuel mixing behaviour. It has been found that when the density and viscosity of biodiesel increase, the fuel pump head loss also increases. Furthermore with increase in density and viscosity, the fuel flow rate through the filter reduces and the sauter mean diameter increases. These finding show that

density, viscosity and lower heating value have considerable effect on the fuel supply system.

9.2.2 Conclusions on Combustion, Performance and Emission

Characteristics of the Test CI Engine during Steady and Transient Operations

The effects of biodiesel blend fraction and its physical properties on the CI engine's in-cylinder pressure, brake specific fuel consumption, thermal efficiency and the exhaust emissions (CO_2 , NO_x , CO , THC and O_2) have been investigated during steady and transient state operations. The following conclusions have been drawn from the analysed data.

Conclusion 4: After investigating the combustion, performance and emission characteristics of the CI engine running with three biodiesel from different feed stocks; it has been found that the values of brake specific fuel consumption, thermal efficiency, in-cylinder pressure and emissions have not shown any significant differences. It can be concluded that the feed stock of biodiesel and its associated effects on the combustion, performance and emission are in-significant.

Conclusion 5: It has been found that peak in-cylinder pressure of the engine running with biodiesel blends is slightly higher than the engine running with diesel. The main reason for a higher in-cylinder pressure in the CI engine running with biodiesel is due to the advanced combustion process being initiated by the easy flow-ability of biodiesel and its other relevant physical properties such as viscosity, density and bulk modulus.

Conclusion 6: It has been seen that the engine running with diesel and biodiesel blends show the same combustion stages at all load conditions except for the slight variation in peak heat release rate and ignition delay. When using biodiesel, the ignition is seen to be advanced when compared to diesel fuel. These finding suggest that the application of biodiesel does not have negative impact on the combustion behaviour of the engine.

Conclusion 7: The effects of the physical properties of biodiesel have been investigated and it was noticed that when the density and viscosity of biodiesel is increased an increase in brake specific fuel consumption of CI engine has been observed at all load conditions investigated. However, when the heating value increases, brake specific fuel consumption

decreases. It was also noticed that when the biodiesel content increases the brake specific fuel consumption of the CI engine increases while the thermal efficiency decreases. These results indicate that the physical properties of biodiesel result in significant impact on the performance of the engine.

Conclusion 8: It was found that during the speed transient operations for both acceleration and deceleration operations the difference between the exhaust temperature of engine running with diesel and biodiesel blend is insignificant. However during torque transition operations, the exhaust temperature of the engine running with biodiesel is higher than that running with diesel by 7%. Based on this result it can conclude that exhaust temperature is more sensitive for change torque than speed.

Conclusion 9: The emission behaviours have been investigated for various transient operation conditions and biodiesel blends. It has been found that the biodiesel and its blends have trends of reducing the CO₂, CO and THC emission during all the transient operations. However, the use of biodiesel as a fuel in CI engine increases the NO_x emission during the speed transient and torque transition operations. This results leads to conclude that the biodiesel have potential to reduce the major emission when it is used in CI engine.

Conclusion 10: It has been found that the post transient emission time for NO_x and CO is relatively higher than other emissions. Based on the experimental results, it can be concluded that the transient operation resulted in a long 'term' effects on the post-transient emission characteristics.

9.2.3 Conclusions on NO_x Prediction Model

The following section describes the key conclusions drawn from the NO_x prediction model study. In this study, the measured in-cylinder pressure has been used to predict the NO_x emission for a compression ignition (CI) engine running with different fuels including biodiesel. These conclusions from this study are summarised below:

Conclusion 11: The NO_x prediction model has been developed using the in-cylinder pressure along with air mass flow rate. The predicted data obtained from NO_x prediction model has been compared with measured data and it has been observed that the deviation is

less than to 4.06% for diesel and 4.39% for biodiesel respectively. Based on the acceptable error between measured and predicted NO_x values, it can conclude that the in-cylinder pressure data can be used to predict the real-time NO_x emission estimation for engine transient operation condition.

9.2.4 Conclusions on Effects of Water Injection on NO_x Reduction

The following section describes the conclusions drawn from the experimental investigation into combustion, performance and emission characteristics of a CI engine running with biodiesel with an integrated water injection system. Based on the experimental results the main effects of the water injection are summarized as follows:

Conclusion 12: The water injection at the intake manifold does not result in any significant difference in the peak cylinder pressure and heat release rate of CI engine running with biodiesel. From these results it can be concluded that the water injection into the intake-manifold does not affect the peak temperature; instead it affects the pre-mixed combustion temperature which is mainly the cause of NO_x emission.

Conclusion 13: It has been found that water injection at intake manifold does not show any significant change in the brake specific fuel consumption and thermal efficiency of the engine at intermediate and higher engine loads. However, it was seen that the brake specific fuel consumption increased by a maximum of 4% and the thermal efficiency decreased by a maximum of 3% at low loads due to the water injection.

Conclusion 14: Intake manifold water injection reduces NO_x emission by up to 50% over the entire operating range. Based on the above it can concluded that water injection into the intake manifold can be employed to reduce NO_x emission without loss of power and any negative effect on fuel consumption.

9.3 Thesis contribution to the Knowledge

This thesis has many new aspects that have not been considered in previous research and has made significant contributions to the knowledge in the area of biodiesel physical characterisation, combustion, performance and emission characteristics of CI engines and management of the NO_x emission. A summary of these contributions is given below.

Contribution 1: New density and viscosity prediction models have been developed by considering the combined effect of biodiesel content and temperature to estimate the physical properties of biodiesel mixture at various temperatures. In addition, new lower heating value models have been developed by which LHV can be computed from the known density and viscosity of biodiesel blends. No work has been found in the literature to predict the density, kinematic viscosity and lower heating value as a function of temperature and biodiesel blend fraction.

Contribution 2: The application of mathematical models for investigating the effects of density and viscosity have not previously been used on the fuel pump, fuel filter and air-fuel mixing behaviour. Even though some experimental results have been reported, there are no mathematical models considering the fuel supply system as one unit.

Contribution 3: The emission characteristics of CI engine fuelled with biodiesel blends during transient operations have been investigated. The effect of transient operation on the post-transient condition has also been quantified. Finally, a universal transient emission prediction model has been developed using steady state data for range of engine operation conditions. This model can be used to predict the emissions of CO₂, NO_x, CO and THC for any transient operation. Both the investigation of the transient emission behaviour and transient emission predicting models are novel. Understanding this transient emission phenomenon is very important for the biodiesel producers, engine manufacturers and environment policy makers.

Contribution 4: An on-line prediction model for NO_x using in-cylinder pressure generated within a CI engine along with air mass flow during both steady and transient phenomena is a novel work. This model will be very important to monitor the NO_x emission by integrating the engine dynamic characteristics with in-cylinder pressure.

Contribution 5: Investigations on reduction of NO_x emission for CI engines fuelled with biodiesel by direct water injection at intake manifold is novel. No work has been found in literature that fully describes the effects of water injection on the combustion, performance and emission characteristics of CI engines.

9.4 Recommended Future Work

The theoretical aspects, numerical models and experimental results presented in this study highlight the potential for biodiesel application to CI engine. From this extensive study, a number of key recommendations are made for future works in this area with a view to improving the application of biodiesel to the CI engine.

Recommendation 1: In this research the physical properties of the biodiesel effects on the engine performance and emission characteristics were investigated. It is crucial that further experimental investigation is conducted into the effects of the biodiesel properties on the fuel penetration, full cone spray and sauter mean diameter (SMD).

Recommendation 2: One of the problems associated to biodiesel application to CI engine is its higher viscosity during winter time. To overcome such problems some authors have proposed using a pre-heater in the fuel supply system. The present work revealed viscosity is directly related with temperature and hence if the biodiesel is heated up to 70°C the viscosity values would become comparable with the petrol diesel. Therefore further investigation is required to integrate the pre-heater with the engine system and to use the heat energy contained in engine coolant to pre-heat the biodiesel.

Recommendation 3: The numerical investigations on the fuel's physical properties effects on fuel supply system revealed that the pump performance, injector behaviour, air-fuel mixture characteristics are dependent on the density and viscosity of biodiesel. Further, experimental investigation is required to quantify the effects of these properties of the fuel supply system.

Recommendation 4: It is documented that biodiesel fuel contains 11% oxygen and hence the heating value of biodiesel is lower than fossil fuels by approximately 10%. Given the importance of fuel heating value, further work should be focussed on reducing this oxygen content in the biodiesel molecule to increase the carbon and hydrogen molecules using additives without affecting the fuel consumption rate.

Recommendation 5: The CI engine emissions during transient operations show unique behaviour. This characteristic requires further investigation to develop numerical models for

each emission during the transient operation. These models can be used in further modification of the European transient cycle.

Recommendation 6: The NO_x emission model has been developed using in-cylinder pressure along with air mass flow rate to predict NO_x emission of the CI engine when running with biodiesel. Further work is required to integrate this model with easily obtainable engine dynamic characteristics such as vibration.

Recommendation 7: In the current study, water injection in the engine cylinder significantly reduced the NO_x emission. This study was carried out with constant water flow rate while the engine speed and loads were varied. Two basic studies are important in these areas: firstly, a detailed study is required on the integration of water injection systems with the fuel control system. This can be done by using one of the operating parameters such engine speed or performance parameters such as boost pressure, exhaust temperature and turbine speed. Secondly, in this study the main heat transfer phenomena in the combustion cylinder have been investigated. However, further investigation is required in the reaction chemistry of the fuel with water addition. This gives an opportunity to understand the effects of water in the performance and emission characteristics and the durability of the engine.

APPENDIX

Appendix A: Heating Value Measurement

The higher heating values of the biodiesel and its blends and diesel were measured by a Parr Adiabatic Model 230/5 Oxygen Bomb Calorimeter using the procedures outlined in the Parr manual. The bucket-filling system, water heater, three decimal weigh, and water cooler included as auxiliaries of the Bomb Calorimeter were used. The general scheme of the bomb calorimeter is shown in Figure 3-2. To measure the heating value, the following summarised procedures were used:

- I. All Bomb calorimeter facilities were prepared and a pellet of benzoic acid weighed to approximately 0.8-1.0 g.
- II. A 10 cm length of fuse wire was cut and weighed. The fuse wire was cut and threaded through the electrodes and configured in a V shape directly above the sample.
- III. Using a pipette, exactly 1.0 ml of pure water was introduced into the clean dry bomb. The wires were tied to the electrodes, the bomb was assembled and pressurised with oxygen to approximately 30 atmospheres.
- IV. A can was placed inside the insulating jacket, the bomb was set inside the can, and electric leads were attached. Exactly 2L of water was poured in at a temperature of about 1-2 degrees below room temperature and the cover closed.
- V. The water in the calorimeter was stirred, and after approximately 2 minutes, the temperature readings at 1 minute intervals for at least 5 minutes were taken.
- VI. The capacitor (ignition unit) was discharged to initiate combustion exactly 30 seconds after the previous reading and the ignition switch released when the red pilot light went out.
- VII. The temperature was recorded 30 seconds after ignition and then every 30 seconds while the temperature was on the rise. After a maximum temperature was observed, temperature readings for a further 5 minutes, reverting to one minute intervals, continued to be taken.

- VIII. Graphs of temperature versus time were plotted using an expanded interrupted temperature scale and extrapolated to determine the temperature change in the given time.
- IX. The heat capacity of the calorimeter was calculated using the data from the benzoic acid run in equation 6.1. The specific energies of combustion of benzoic acid and iron wire are $-26.421 \text{ kJ g}^{-1}$ and -6.694 kJ g^{-1} respectively:

$$W = \frac{m_b * LHV_b + e_1}{\Delta T_b}$$

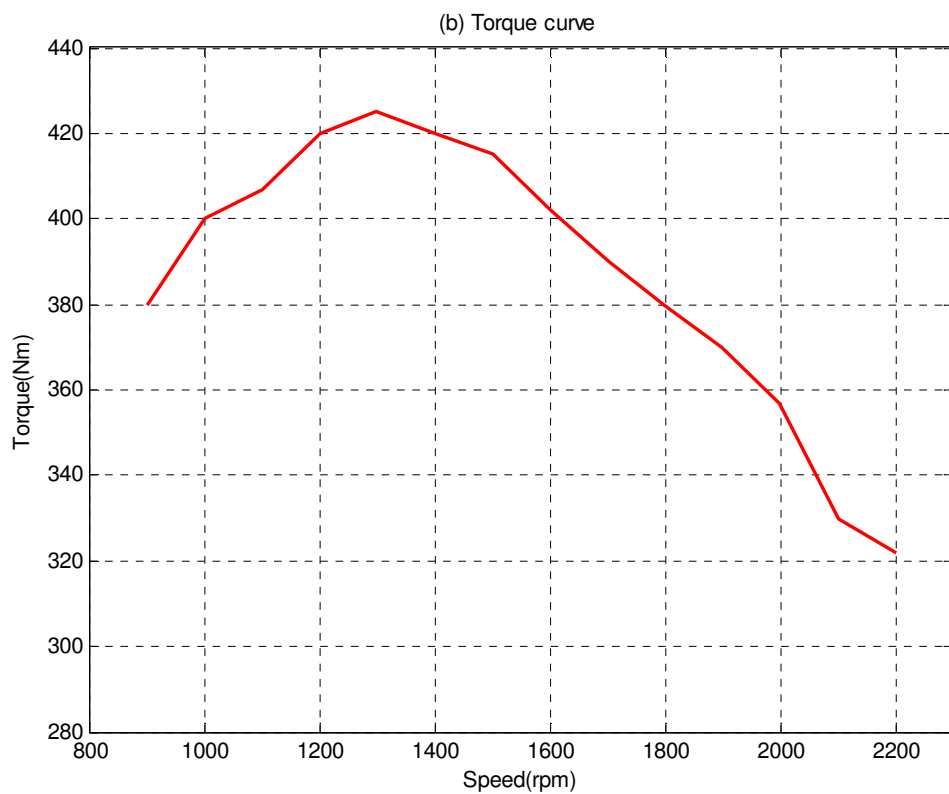
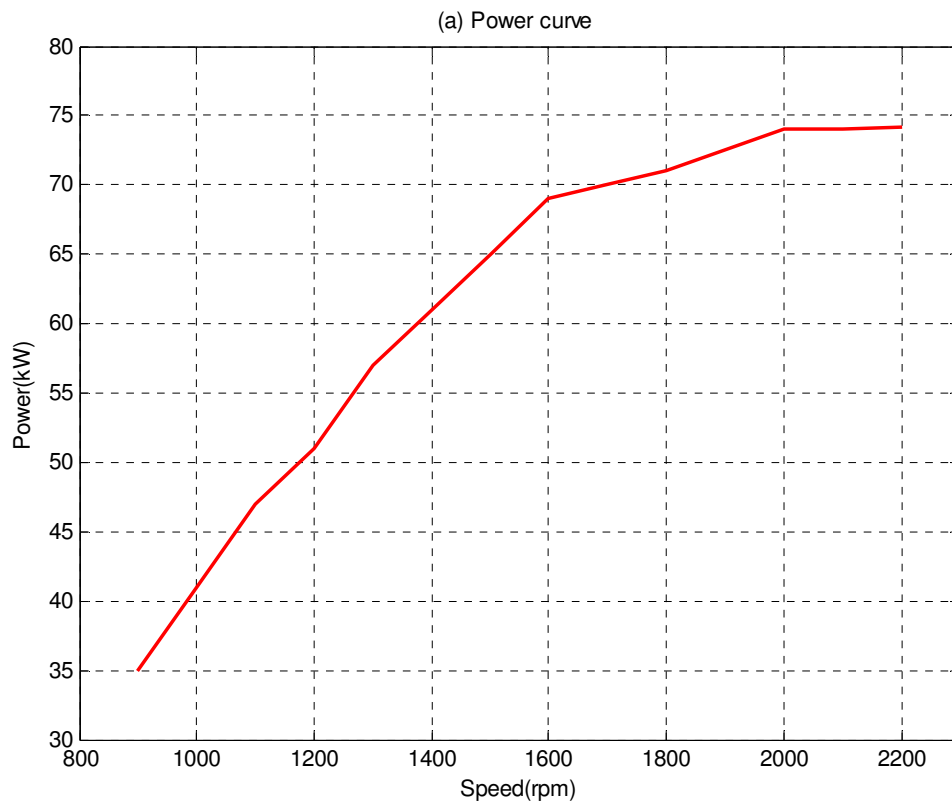
Where W is the energy equivalent of the calorimeter (J/k) being used, m_b is the mass of the benzoic acid and e_1 is the correction for heat produced by burning the fuse wire in the bomb.

- X. Steps I-IX was repeated for biodiesel and its blends. The lower heating value of the biodiesel and its blends were calculated using equation 6.2:

$$LHV = \frac{\Delta T * W - e_1}{m_{bd}}$$

Where LHV is the lower heating value (kJ/kg), ΔT is the temperature raise (K), W is the energy equivalent of the calorimeter being used which is calculated by equation 6-1, e_3 is the correction for heat produced by burning the fuse wire in the bomb.

Appendix B: Power and Torque Curves of CI engine



References

- [1] A. Demirbas, *Biodiesel - A Realistic Fuel Alternative for Diesel Engines*, First. Velag: Springer, 2008.
- [2] K. Dowaki, T. Ohta, Y. Kasahara, M. Kameyama, K. Sakawaki, and S. Mori, "An economic and energy analysis on bio-hydrogen fuel using a gasification process," *Renewable Energy*, vol. 32, no. 1, pp. 80-94, Jan. 2007.
- [3] Daniel Puppen, "Environmental Evaluation of Biofuels," 16-Jun-2008. [Online]. Available: http://www.pp.bme.hu/so/2002_1/pdf/so2002_1_08.pdf. [Accessed: 16-Jun-2008].
- [4] J. J. MacKenzie, "Oil as a finite resource," *Nonrenewable Resources*, vol. 7, no. 2, pp. 97-100, 1998.
- [5] S. Shafiee and E. Topal, "An econometrics view of worldwide fossil fuel consumption and the role of US," *Energy Policy*, vol. 36, no. 2, pp. 775-786, Feb. 2008.
- [6] World metres, "Cars produced in the world - Worldometers." [Online]. Available: <http://www.worldometers.info/cars/>. [Accessed: 22-Feb-2011].
- [7] Q. Wang, "Time for commercializing non-food biofuel in China," *Renewable and Sustainable Energy Reviews*, vol. 15, no. 1, pp. 621-629, Jan. 2011.
- [8] G. Hammond, S. Kallu, and M. McManus, "Development of biofuels for the UK automotive market," *Applied Energy*, vol. 85, no. 6, pp. 506-515, Jun. 2008.
- [9] D. Qi, L. Geng, H. Chen, Y. Bian, J. Liu, and X. Ren, "Combustion and performance evaluation of a diesel engine fueled with biodiesel produced from soybean crude oil," *Renewable Energy*, vol. 34, no. 12, pp. 2706-2713, Dec. 2009.
- [10] F. Ma and M. A. Hanna, "Biodiesel production: a review," *Bioresour. Technology*, vol. 70, no. 1, pp. 1-15, Oct. 1999.
- [11] USA Departemnt of Energy, "Biodiesel Handelling and Use Guidelines," Nov-2004.
- [12] T. Durbin, J. Collins, J. Norbeck, and M. Smith, "Effects of Biodiesel, Biodiesel Blends, and a Synthetic Diesel on Emissions from Light Heavy-Duty Diesel Vehicles," *Environmental Science & Technology*, vol. 34, no. 3, pp. 349-355, Feb. 2000.
- [13] Biofule research Advisory council, "European Union, Avison For 2030 and Beyond," Mar-2006.
- [14] EDD, "The EU Biodiesel Industries," 2010. [Online]. Available: <http://www.ebb-eu.org/stats.php>. [Accessed: 14-Dec-2010].
- [15] EBB, "European Biodiesel Board." [Online]. Available: <http://www.ebb-eu.org/stats.php>. [Accessed: 13-Dec-2010].
- [16] thebioenergysite, "Government Support for Ethanol and Biodiesel in China - Bioenergy Articles from The Bioenergy Site." [Online]. Available: <http://www.thebioenergysite.com/articles/209/government-support-for-ethanol-and-biodiesel-in-china>. [Accessed: 11-Mar-2011].
- [17] W. Thurmond, *Biodiesel Market - Biodiesel 2020: Market Survey With Forecasts and Case Studies* -. 2008.
- [18] EREC, "Renewable Energy Technology Roadmap," 2008.
- [19] I. P. S. HM Revenue and Customs, "Revenue & Customs Brief 18/10." [Online]. Available: <http://www.hmrc.gov.uk/briefs/excise-duty/brief1810.htm>. [Accessed: 11-Mar-2011].

- [20] R. Tate, K. Watts, C. Allen, and K. Wilkie, "The viscosities of three biodiesel fuels at temperatures up to 300 °C," *Fuel*, vol. 85, no. 7, pp. 1010-1015, May. 2006.
- [21] S. A. Basha, K. R. Gopal, and S. Jebaraj, "A review on biodiesel production, combustion, emissions and performance," *Renewable and Sustainable Energy Reviews*, vol. 13, no. 6, pp. 1628-1634, Aug. .
- [22] A. Srivastava and R. Prasad, "Triglycerides-based diesel fuels," *Renewable and Sustainable Energy Reviews*, vol. 4, no. 2, pp. 111-133, Jun. 2000.
- [23] J. Otera, "Transesterification," *Chemical Reviews*, vol. 93, no. 4, pp. 1449-1470, Jun. 1993.
- [24] "Biodiesel - A Realistic Fuel Alternative for Diesel Engines." [Online]. Available: http://www.knovel.com.librouter.hud.ac.uk/web/portal/basic_search/display?_EXT_KNOVEL_DISPLAY_bookid=2085. [Accessed: 14-Dec-2010].
- [25] C. V. McNeff et al., "A continuous catalytic system for biodiesel production," *Applied Catalysis A: General*, vol. 343, no. 1, pp. 39-48, Jul. 2008.
- [26] M. S. Graboski and R. L. McCormick, "Combustion of fat and vegetable oil derived fuels in diesel engines," *Progress in Energy and Combustion Science*, vol. 24, no. 2, pp. 125-164, 1998.
- [27] E. Alptekin and M. Canakci, "Determination of the density and the viscosities of biodiesel-diesel fuel blends," *Renewable Energy*, vol. 33, no. 12, pp. 2623-2630, Dec. 2008.
- [28] M. Tat and J. Van Gerpen, "The specific gravity of biodiesel and its blends with diesel fuel," *JAOCs*, vol. 77, no. 2, 2000.
- [29] G. Knothe and K. R. Steidley, "Kinematic viscosity of biodiesel components (fatty acid alkyl esters) and related compounds at low temperatures," *Fuel*, vol. 86, no. 16, pp. 2560-2567, Nov. 2007.
- [30] M. Canakci, "Performance and emissions characteristics of biodiesel from soybean oil," *Proceedings of the Institution of Mechanical Engineers - D*, vol. 219, no. 7, 2005.
- [31] C. Kaplan, R. Arslan, and A. Surmen, "Performance Characteristics of Sunflower Methyl Esters as Biodiesel," 19-Jun-2008. [Online]. Available: <http://huddersfield.library.ingentaconnect.com/content/tandf/ueso/2006/00000028/00000008/art00006>. [Accessed: 19-Jun-2008].
- [32] A. Ramadhas, C. Muraleedharan, and S. Jayaraj, "Performance and emission evaluation of a diesel engine fueled with methyl esters of rubber seed oil," *Renewable Energy*, vol. 30, no. 12, pp. 1789-1800, Oct. 2005.
- [33] J. Krahl et al., "Comparison of exhaust emissions and their mutagenicity from the combustion of biodiesel, vegetable oil, gas-to-liquid and petrodiesel fuels," *Fuel*, vol. 88, no. 6, pp. 1064-1069, Jun. 2009.
- [34] M. Lapuerta, O. Armas, R. Ballesteros, and J. Fernández, "Diesel emissions from biofuels derived from Spanish potential vegetable oils," *Fuel*, vol. 84, no. 6, pp. 773-780, Apr. 2005.
- [35] O. Armas, J. J. Hernández, and M. D. Cárdenas, "Reduction of diesel smoke opacity from vegetable oil methyl esters during transient operation," *Fuel*, vol. 85, no. 17, pp. 2427-2438, Dec. 2006.
- [36] S. Samuel, D. Morrey, D. Taylor, and M. Flowkes, "Parametric Study into the Effects of Factors Affecting Real-World Vehicle Exhaust Emission Levels," *SAE*, no. 2007, 2007.
- [37] Z. Bazari, "Diesel Exhaust Emissions Prediction Under Transient Operating Conditions," *SAE Paper 940666*, 1994.
- [38] Dieselnets, "Emission Standards: Europe: Cars and Light Trucks." [Online].

- Available: <http://www.dieselnet.com/standards/eu/ld.php>. [Accessed: 29-Sep-2010].
- [39] S. Samuel, L. Austin, and D. Morrey, "Automotive test drive cycles for emission measurement and real-world emission levels-a review," *Proceedings of the Institution of Mechanical Engineers, Part D: Journal of Automobile Engineering*, vol. 216, no. 7, pp. 555-564, 2002.
- [40] An Executive Agency of the Department of Transport, "New Car Fuel Consumption and Emissions Figures,," May-2003.
- [41] S. McGinness, "Climate Change & the Kyoto Protocol," SCIENCE AND ENVIRONMENT SECTION, HOUSE OF COMMONS LIBRARY, 29-Nov-2001.
- [42] Automotive Council, "Grants and incentives." [Online]. Available: <http://www.automotivecouncil.co.uk/invest-in-uk/grants-and-incentives/>. [Accessed: 23-Feb-2011].
- [43] C. Kaplan, R. Arslan, and A. Sürmen, "Performance Characteristics of Sunflower Methyl Esters as Biodiesel," *Energy Sources, Part A: Recovery, Utilization, and Environmental Effects*, vol. 28, no. 8, p. 751, 2006.
- [44] M. Lapuerta, O. Armas, and J. Rodríguez-Fernández, "Effect of biodiesel fuels on diesel engine emissions," *Progress in Energy and Combustion Science*, vol. 34, no. 2, pp. 198-223, Apr. 2008.
- [45] M. Naik, L. Meher, S. Naik, and L. Das, "Production of biodiesel from high free fatty acid Karanja (*Pongamia pinnata*) oil," *Biomass and Bioenergy*, vol. 32, no. 4, pp. 354-357, Apr. 2008.
- [46] L. Meher, D. Vidya Sagar, and S. Naik, "Technical aspects of biodiesel production by transesterification--a review," *Renewable and Sustainable Energy Reviews*, vol. 10, no. 3, pp. 248-268, Jun. 2006.
- [47] Z. Liu, D. Ford, V. Vasys, D. Chen, and T. Johnson, "Influence of Engine Operating Conditions on Diesel Particulate Matter Emissions in Relation to Transient and Steady-State Conditions," *Environmental Science & Technology*, vol. 41, no. 13, pp. 4593-4599, Jul. 2007.
- [48] M. S. Graboski and R. L. McCormick, "Combustion of fat and vegetable oil derived fuels in diesel engines," *Progress in Energy and Combustion Science*, vol. 24, no. 2, pp. 125-164, 1998.
- [49] T. Belachew, M. Rakesh, and F. Gu, "Emission Behavior of a CI Engine Running by Biodiesel under Transient Conditions," *SAE*, vol. 2010, 2010.
- [50] C. Lin and H. Lin, "Diesel engine performance and emission characteristics of biodiesel produced by the peroxidation process," *Fuel*, vol. 85, no. 3, pp. 298-305, Feb. 2006.
- [51] H. C. Krijnsen, W. E. J. van Kooten, H. P. A. Calis, R. P. Verbeek, and C. M. V. D. Bleek, "Prediction of NO_x Emissions from a Transiently Operating Diesel Engine Using an Artificial Neural Network," *Chemical Engineering & Technology*, vol. 22, no. 7, pp. 601-607, 1999.
- [52] S. Fernando, C. Hall, and S. Jha, "NO_x Reduction from Biodiesel Fuels," *Energy & Fuels*, vol. 20, no. 1, pp. 376-382, Jan. 2006.
- [53] EU, "BS EN 14213:2003 - Heating fuels. Fatty acid methyl esters (FAME). Requirements and test methods – BSI British Standards," vol. 14213, 2004.
- [54] ASTM, "ASTM D6751 -10 Standard Specification for Biodiesel Fuel Blend Stock (B100) for Middle Distillate Fuels," ASTM, 2008.
- [55] S. Naik, V. V. Goud, P. K. Rout, and A. K. Dalai, "Production of first and second

- generation biofuels: A comprehensive review,” *Renewable and Sustainable Energy Reviews*, Dec. 2009.
- [56] R. Tate, K. Watts, C. Allen, and K. Wilkie, “The densities of three biodiesel fuels at temperatures up to 300 °C,” *Fuel*, vol. 85, no. 7, pp. 1004-1009, May. 2006.
- [57] B. Freedman and M. Bagby, “Heats of combustion of fatty esters and triglycerides,” *JAOCS*, vol. 66, no. 11, 1989.
- [58] S. Bari, T. H. Lim, and C. W. Yu, “Effects of preheating of crude palm oil (CPO) on injection system, performance and emission of a diesel engine,” *Renewable Energy*, vol. 27, no. 3, pp. 339-351, Nov. 2002.
- [59] J. B. Heywood, *Internal Combustion Engine Fundamentals*. McGraw-Hill, New York, 1988.
- [60] P. V. Bhale, N. V. Deshpande, and S. B. Thombre, “Improving the low temperature properties of biodiesel fuel,” *Renewable Energy*, vol. 34, no. 3, pp. 794-800, Mar. 2009.
- [61] G. Knothe and K. R. Steidley, “Kinematic viscosity of biodiesel components (fatty acid alkyl esters) and related compounds at low temperatures,” *Fuel*, vol. 86, no. 16, pp. 2560-2567, Nov. 2007.
- [62] K. Krisnagkura, “Heats of combustion of fatty esters and triglycerides,” *JAOCS*, vol. 68, no. 1, 1991.
- [63] S. Sadrameli, W. Seames, and M. Mann, “Prediction of higher heating values for saturated fatty acids from their physical properties,” *Fuel*, vol. 87, no. 10, pp. 1776-1780, Aug. 2008.
- [64] A. Demirbas, “Relationships derived from physical properties of vegetable oil and biodiesel fuels,” *Fuel*, vol. 87, no. 8, pp. 1743-1748, Jul. 2008.
- [65] P. Benjumea, J. Agudelo, and A. Agudelo, “Basic properties of palm oil biodiesel-diesel blends,” *Fuel*, vol. 87, no. 10, pp. 2069-2075, Aug. 2008.
- [66] M. Albuquerque et al., “Properties of biodiesel oils formulated using different biomass sources and their blends,” *Renewable Energy*, vol. 34, no. 3, pp. 857-859, Mar. 2009.
- [67] L. Grunberg and A. Nissan, “Mixture Law for Viscosity : Abstract : Nature,” *Nature*, vol. 164, 1949.
- [68] R. M. Joshi and M. J. Pegg, “Flow properties of biodiesel fuel blends at low temperatures,” *Fuel*, vol. 86, no. 1, pp. 143-151, Jan. 2007.
- [69] K. Krisnangkura, C. Sansa-ard, K. Aryasuk, S. Lilitchan, and K. Kittiratanapiboon, “An empirical approach for predicting kinematic viscosities of biodiesel blends,” *Fuel*, vol. 89, no. 10, pp. 2775-2780, Oct. 2010.
- [70] M. R. Riazi and G. N. Al-Otaibi, “Estimation of viscosity of liquid hydrocarbon systems,” *Fuel*, vol. 80, no. 1, pp. 27-32, Jan. 2001.
- [71] K. Raveendran and A. Ganesh, “Heating value of biomass and biomass pyrolysis products,” *Fuel*, vol. 75, no. 15, pp. 1715-1720, Nov. 1996.
- [72] C. Sheng and J. Azevedo, “Estimating the higher heating value of biomass fuels from basic analysis data,” *Biomass and Bioenergy*, vol. 28, no. 5, pp. 499-507, May. 2005.
- [73] P. S. Mehta and K. Anand, “Estimation of a Lower Heating Value of Vegetable Oil and Biodiesel Fuel,” *Energy & Fuels*, vol. 23, no. 8, pp. 3893-3898, 2009.
- [74] A. Demirbas, “A direct route to the calculation of heating values of liquid fuels by using their density and viscosity measurements,” *Energy Conversion and Management*, vol. 41, no. 15, pp. 1609-1614, Oct. 2000.
- [75] A. Demirbas, “Prediction of Higher Heating Values for Biodiesels from Their Physical Properties - Energy Sources, Part A: Recovery, Utilization, and

- Environmental Effects,” *Energy sources*, no. 31, pp. 633-638, 2009.
- [76] M. G. Bannikov, S. I. Tyrlovoy, I. P. Vasilev, and J. A. Chattha, “Investigation of the Characteristics of the Fuel Injection Pump of a Diesel Engine Fuelled with Viscous Vegetable Oil-Diesel Oil Blends,” *Proceedings of the Institution of Mechanical Engineers, Part D: Journal of Automobile Engineering*, vol. 220, no. 6, pp. 787-792, 2006.
- [77] K. Yamane, A. Ueta, and Y. Shimamaoto, “Influence of physical and chemical properties of biodiesel fuels on injection, combustion and exhaust emission characteristics in a direct injection compression ignition engine,” *International Research Journal*, vol. 2, no. 4, 2001.
- [78] Y. Gao et al., “Experimental study of the spray characteristics of biodiesel based on inedible oil,” *Biotechnology Advances*, vol. 27, no. 5, pp. 616-624, Sep. .
- [79] C. S. Lee, S. W. Park, and S. I. Kwon, “An Experimental Study on the Atomization and Combustion Characteristics of Biodiesel-Blended Fuels,” *Energy & Fuels*, vol. 19, no. 5, pp. 2201-2208, 2005.
- [80] B. Kegl, “Experimental Investigation of Optimal Timing of the Diesel Engine Injection Pump Using Biodiesel Fuel,” *Energy & Fuels*, vol. 20, no. 4, pp. 1460-1470, Jul. 2006.
- [81] B. Kegl and A. Hribernik, “Experimental Analysis of Injection Characteristics Using Biodiesel Fuel,” *Energy & Fuels*, vol. 20, no. 5, pp. 2239-2248, 2006.
- [82] Intertek, “Biodiesel Fuel Filter Blocking Problems.” [Online]. Available: <http://www.intertek.com/energy/alternative/biodiesel-fuel-filter-blocking-problems/>. [Accessed: 18-Apr-2011].
- [83] M. Gumus, “A comprehensive experimental investigation of combustion and heat release characteristics of a biodiesel (hazelnut kernel oil methyl ester) fueled direct injection compression ignition engine,” *Fuel*, vol. 89, no. 10, pp. 2802-2814, Oct. 2010.
- [84] P. Benjumea, J. Agudelo, and A. Agudelo, “Effect of altitude and palm oil biodiesel fuelling on the performance and combustion characteristics of a HSDI diesel engine,” *Fuel*, vol. 88, no. 4, pp. 725-731, Apr. 2009.
- [85] J. P. Szybist, J. Song, M. Alam, and A. L. Boehman, “Biodiesel combustion, emissions and emission control,” *Fuel Processing Technology*, vol. 88, no. 7, pp. 679-691, Jul. 2007.
- [86] Y. Zhang and V. G. Van Gerpen, “Combustion Analysis of Esters of Soybean Oil in a Diesel Engine,” *SAE*, vol. 960765, 1996.
- [87] A. Yusuf and H. Milford A, “In-Cylinder Pressure Characteristics of a D.I. Heavy Duty Diesel Engine on Biodiesel Fuel,” *SAE*, vol. 971683, 1997.
- [88] M. P. Dorado, E. Ballesteros, J. M. Arnal, J. G. Gomez, and F. J. Lopez, “Exhaust emissions from a Diesel engine fueled with transesterified waste olive oil [small star, filled],” *Fuel*, vol. 82, no. 11, pp. 1311-1315, Jul. 2003.
- [89] A. Monyem and J. H. Van Gerpen, “The effect of biodiesel oxidation on engine performance and emissions,” *Biomass and Bioenergy*, vol. 20, no. 4, pp. 317-325, Apr. 2001.
- [90] A. Ramadhas, C. Muraleedharan, and S. Jayaraj, “Performance and emission evaluation of a diesel engine fueled with methyl esters of rubber seed oil,” *Renewable Energy*, vol. 30, no. 12, pp. 1789-1800, Oct. 2005.
- [91] J. Xue, T. E. Grift, and A. C. Hansen, “Effect of biodiesel on engine performances and emissions,” *Renewable and Sustainable Energy Reviews*, vol. 15, no. 2, pp. 1098-1116, Feb. 2011.
- [92] C. Hasimoglu, M. Ciniviz, I. Özsert, Y. İçingür, A. Parlak, and M. Sahir Salman,

- “Performance characteristics of a low heat rejection diesel engine operating with biodiesel,” *Renewable Energy*, vol. 33, no. 7, pp. 1709-1715, Jul. 2008.
- [93] O. Armas, K. Yehliu, and A. L. Boehman, “Effect of alternative fuels on exhaust emissions during diesel engine operation with matched combustion phasing,” *Fuel*, vol. 89, no. 2, pp. 438-456, Feb. 2010.
- [94] B. Lin, J. Huang, and D. Huang, “Experimental study of the effects of vegetable oil methyl ester on DI diesel engine performance characteristics and pollutant emissions,” *Fuel*, vol. 88, no. 9, pp. 1779-1785, Sep. 2009.
- [95] M. Gumus and S. Kasifoglu, “Performance and emission evaluation of a compression ignition engine using a biodiesel (apricot seed kernel oil methyl ester) and its blends with diesel fuel,” *Biomass and Bioenergy*, vol. 34, no. 1, pp. 134-139, Jan. 2010.
- [96] Y. Ulusoy, Y. Tekin, M. Cetinkaya, and F. Karaosmanoglu, “The Engine Tests of Biodiesel from Used Frying Oil,” *Energy Sources, Part A: Recovery, Utilization, and Environmental Effects*, vol. 26, no. 10, p. 927, 2004.
- [97] Z. Utlu and M. S. Koçak, “The effect of biodiesel fuel obtained from waste frying oil on direct injection diesel engine performance and exhaust emissions,” *Renewable Energy*, vol. 33, no. 8, pp. 1936-1941, Aug. 2008.
- [98] J. Song and C. Zhang, “An experimental study on the performance and exhaust emissions of a diesel engine fuelled with soybean oil methyl ester,” *Proceedings of the Institution of Mechanical Engineers, Part D: Journal of Automobile Engineering*, vol. 222, no. 12, pp. 2487-2496, 2008.
- [99] A. Pal, A. Verma, S. Kachhwaha, and S. Maji, “Biodiesel production through hydrodynamic cavitation and performance testing,” *Renewable Energy*, vol. 35, no. 3, pp. 619-624, Mar. 2010.
- [100] C. Carraretto, A. Macor, A. Mirandola, A. Stoppato, and S. Tonon, “Biodiesel as alternative fuel: Experimental analysis and energetic evaluations,” *Energy*, vol. 29, no. 12, pp. 2195-2211, Oct. .
- [101] H. Raheman and A. G. Phadatar, “Diesel engine emissions and performance from blends of karanja methyl ester and diesel,” *Biomass and Bioenergy*, vol. 27, no. 4, pp. 393-397, Oct. 2004.
- [102] X. Meng, G. Chen, and Y. Wang, “Biodiesel production from waste cooking oil via alkali catalyst and its engine test,” *Fuel Processing Technology*, vol. 89, no. 9, pp. 851-857, Sep. 2008.
- [103] J. Reyes and M. Sepúlveda, “PM-10 emissions and power of a Diesel engine fueled with crude and refined Biodiesel from salmon oil,” *Fuel*, vol. 85, no. 12, pp. 1714-1719, Sep. 2006.
- [104] P. Sahoo et al., “Comparative evaluation of performance and emission characteristics of jatropha, karanja and polanga based biodiesel as fuel in a tractor engine,” *Fuel*, vol. 88, no. 9, pp. 1698-1707, Sep. 2009.
- [105] K. Ryu, “The characteristics of performance and exhaust emissions of a diesel engine using a biodiesel with antioxidants,” *Bioresource Technology*, vol. 101, no. 1, pp. S78-S82, Jan. 2010.
- [106] M. Kalam and H. Masjuki, “Testing palm biodiesel and NPAA additives to control NOx and CO while improving efficiency in diesel engines,” *Biomass and Bioenergy*, vol. 32, no. 12, pp. 1116-1122, Dec. 2008.
- [107] A. F. Asmus, *Diesel engines and fuel systems* /, 3rd ed. Melbourne :: Longman Cheshire, 1992.
- [108] M. Cetinkaya, Y. Ulusoy, Y. Tekin, and F. Karaosmanoglu, “Engine and winter road test performances of used cooking oil originated biodiesel,” *Energy*

- Conversion and Management*, vol. 46, no. 7, pp. 1279-1291, May. 2005.
- [109] A. Hansen, M. Gratton, and W. Yuan, "Diesel engine performance and NOX emissions from oxygenated biofuels and blends with diesel fuel," *Trans ASABE*, vol. 49, pp. 589-95, 2006.
- [110] S. Murillo, J. Míguez, J. Porteiro, E. Granada, and J. Morán, "Performance and exhaust emissions in the use of biodiesel in outboard diesel engines," *Fuel*, vol. 86, no. 12, pp. 1765-1771, Aug. 2007.
- [111] N. Usta et al., "Combustion of biodiesel fuel produced from hazelnut soapstock/waste sunflower oil mixture in a Diesel engine," *Energy Conversion and Management*, vol. 46, no. 5, pp. 741-755, Mar. 2005.
- [112] M. I. Al-Widyan, G. Tashtoush, and M. Abu-Qudais, "Utilization of ethyl ester of waste vegetable oils as fuel in diesel engines," *Fuel Processing Technology*, vol. 76, no. 2, pp. 91-103, May. 2002.
- [113] A. Agarwal and L. Das, "Biodiesel Development and Characterization for Use as a Fuel in Compression Ignition Engines," *J. Eng. Gas Turbines Power*, vol. 123, no. 2, pp. 440-448, 2001.
- [114] M. N. Nabi and J. E. Hustad, "Influence of Biodiesel Addition to Fischer-Tropsch Fuel on Diesel Engine Performance and Exhaust Emissions," *Energy & Fuels*, vol. 24, no. 5, pp. 2868-2874, May. 2010.
- [115] X. Tauzia, A. Maiboom, and S. R. Shah, "Experimental study of inlet manifold water injection on combustion and emissions of an automotive direct injection Diesel engine," *Energy*, vol. 35, no. 9, pp. 3628-3639, Sep. 2010.
- [116] H. Bayraktar, "Experimental and theoretical investigation of using gasoline-ethanol blends in spark-ignition engines," *Renewable Energy*, vol. 30, no. 11, pp. 1733-1747, Sep. 2005.
- [117] G. Hammond, S. Kallu, and M. McManus, "Development of biofuels for the UK automotive market," *Applied Energy*, vol. 85, no. 6, pp. 506-515, Jun. 2008.
- [118] M. Lapuerta, O. Armas, R. Ballesteros, and J. Fern[un]dez, "Diesel emissions from biofuels derived from Spanish potential vegetable oils," *Fuel*, vol. 84, no. 6, pp. 773-780, Apr. 2005.
- [119] T. Durbin, J. Collins, J. Norbeck, and M. Smith, "Effects of Biodiesel, Biodiesel Blends, and a Synthetic Diesel on Emissions from Light Heavy-Duty Diesel Vehicles," *Environmental Science & Technology*, vol. 34, no. 3, pp. 349-355, Feb. 2000.
- [120] Daniel Puppan, "Environmental Evaluation of Biofuels," 16-Jun-2008. [Online]. Available: http://www.pp.bme.hu/so/2002_1/pdf/so2002_1_08.pdf. [Accessed: 16-Jun-2008].
- [121] H. Hazar, "Effects of biodiesel on a low heat loss diesel engine," *Renewable Energy*, vol. 34, no. 6, pp. 1533-1537, Jun. 2009.
- [122] C. Lin and R. Li, "Engine performance and emission characteristics of marine fish-oil biodiesel produced from the discarded parts of marine fish," *Fuel Processing Technology*, vol. 90, no. 7, pp. 883-888, Jul. .
- [123] M. S. Graboski and R. L. McCormick, "Combustion of fat and vegetable oil derived fuels in diesel engines," *Progress in Energy and Combustion Science*, vol. 24, no. 2, pp. 125-164, 1998.
- [124] W. Marshall, L. Schumacher, and S. Howell, "Engine Exhaust Emissions Evaluation of a Cummins L10E When Fueled with a Biodiesel Blend," *SAE*, vol. 952363, 1995.
- [125] M. Canakci, "Combustion characteristics of a turbocharged DI compression ignition engine fueled with petroleum diesel fuels and biodiesel," *Bioresource*

- Technology*, vol. 98, no. 6, pp. 1167-1175, Apr. 2007.
- [126] M. Cardone, M. V. Prati, V. Rocco, M. Seggiani, A. Senatore, and S. Vitolo, "Brassica carinata as an Alternative Oil Crop for the Production of Biodiesel in Italy: Engine Performance and Regulated and Unregulated Exhaust Emissions," *Environmental Science & Technology*, vol. 36, no. 21, pp. 4656-4662, Nov. 2002.
- [127] M. E. Tat and J. H. Gerpen, "Speed of sound and isentropic bulk modulus of alkyl monoesters at elevated temperatures and pressures," *Journal of the American Oil Chemists' Society*, vol. 80, no. 12, pp. 1249-1256, 2003.
- [128] S. Puhan, N. Vedaraman, G. Sankaranarayanan, and B. V. B. Ram, "Performance and emission study of Mahua oil (madhuca indica oil) ethyl ester in a 4-stroke natural aspirated direct injection diesel engine," *Renewable Energy*, vol. 30, no. 8, pp. 1269-1278, Jul. 2005.
- [129] M. Lapuerta, J. M. Herreros, L. L. Lyons, R. García-Contreras, and Y. Briceño, "Effect of the alcohol type used in the production of waste cooking oil biodiesel on diesel performance and emissions," *Fuel*, vol. 87, no. 15, pp. 3161-3169, Nov. 2008.
- [130] G. Labeckas and S. Slavinskas, "The effect of rapeseed oil methyl ester on direct injection Diesel engine performance and exhaust emissions," *Energy Conversion and Management*, vol. 47, no. 13, pp. 1954-1967, Aug. 2006.
- [131] H. Aydin and H. Bayindir, "Performance and emission analysis of cottonseed oil methyl ester in a diesel engine," *Renewable Energy*, vol. 35, no. 3, pp. 588-592, Mar. 2010.
- [132] W. Wang, D. Lyons, N. Clark, M. Gautam, and P. Norton, "Emissions from Nine Heavy Trucks Fueled by Diesel and Biodiesel Blend without Engine Modification," *Environmental Science & Technology*, vol. 34, no. 6, pp. 933-939, Mar. 2000.
- [133] M. N. Nabi, M. S. Akhter, and M. M. Zaglul Shahadat, "Improvement of engine emissions with conventional diesel fuel and diesel-biodiesel blends," *Bioresource Technology*, vol. 97, no. 3, pp. 372-378, Feb. 2006.
- [134] J. Krahl, A. Munack, O. Schröder, H. Stein, and J. Schröder, "Influence of Biodiesel and Different Designed Diesel Fuels on the Exhaust Gas Emissions and Health Effects," 2003.
- [135] E. Buyukkaya, "Effects of biodiesel on a DI diesel engine performance, emission and combustion characteristics," *Fuel*, vol. 89, no. 10, pp. 3099-3105, Oct. 2010.
- [136] D. Altıparmak, A. Keskin, A. Koca, and M. Gökçe, "Alternative fuel properties of tall oil fatty acid methyl ester-diesel fuel blends," *Bioresource Technology*, vol. 98, no. 2, pp. 241-246, Jan. 2007.
- [137] A. Serdari, K. Fragioudakis, E. Lois, S. Stournas, C. Teas, and F. Zannikos, "Effect of Biodiesel Addition to Diesel Fuel on Engine Performance and Emissions," *Journal of Propulsion and Power*, vol. 15, no. 2, pp. 224-231, 1999.
- [138] K. F. Hansen and M. G. Jensen, "Chemical and Biological Characteristics of Exhaust Emissions from a DI Diesel Engine Fuelled With Rapeseed Oil Methyl Ester (RME)," in *SAE paper*, vol. 971689, 1997.
- [139] S. Chan, Y. He, and J. Sun, "Prediction of transient nitric oxide in diesel exhaust," *Proceedings of the Institution of Mechanical Engineers, Part D: Journal of Automobile Engineering*, vol. 213, no. 4, pp. 327-339, Jan. 1999.
- [140] Fuent, Inc, "Thermal NOx Formation," 2003. [Online]. Available: <http://jullio.pe.kr/fluent6.1/help/html/ug/node624.htm>. [Accessed: 19-Aug-2010].
- [141] "Online Book J B Heywood, Internal Combustion Engine Fundamentals, New York PDF | Online Associate." [Online]. Available:

- <http://onlineassociate.net/pdf/J-B-Heywood,-Internal-Combustion-Engine-Fundamentals,-new-york/>. [Accessed: 17-Aug-2010].
- [142] A. Mellor, J. Mello, K. Duffy, W. Easley, and J. Faulkner, "Skeletal Mechanism for NO_x Chemistry in Diesel Engines," *SAE*, no. 981450, 1998.
- [143] S. Aithal, "Modeling of NO_x formation in diesel engines using finite-rate chemical kinetics," *Applied Energy*, vol. 87, no. 7, pp. 2256-2265, Jul. 2010.
- [144] H. K. Newhall, "Kinetics of engine-generated nitrogen oxides and carbon monoxide," *Symposium (International) on Combustion*, vol. 12, no. 1, pp. 603-613, 1969.
- [145] E. EU, "European emission standard," Diesel net.
- [146] A. Ibrahim and S. Bari, "A comparison between EGR and lean-burn strategies employed in a natural gas SI engine using a two-zone combustion model," *Energy Conversion and Management*, vol. 50, no. 12, pp. 3129-3139, Dec. 2009.
- [147] J. Rodríguez-Fernández, A. Tsolakakis, R. Cracknell, and R. Clark, "Combining GTL fuel, reformed EGR and HC-SCR aftertreatment system to reduce diesel NO_x emissions. A statistical approach," *International Journal of Hydrogen Energy*, vol. 34, no. 6, pp. 2789-2799, Mar. 2009.
- [148] A. K. Agrawal, S. K. Singh, S. Sinha, and M. K. Shukla, "Effect of EGR on the exhaust gas temperature and exhaust opacity in compression ignition engines," *Sadhana*, vol. 29, no. 3, pp. 275-284, 2004.
- [149] S. Fernando, C. Hall, and S. Jha, "NO_x Reduction from Biodiesel Fuels," *Energy & Fuels*, vol. 20, no. 1, pp. 376-382, Jan. 2006.
- [150] B. Martin, "Emissions Control Techniques Applied to Industrial Vehicles," 2005. [Online]. Available: <http://www.ifp.fr/antidot/search?context=default&keywords=emission+control+techniques&x=0&y=0>. [Accessed: 17-Aug-2010].
- [151] W. Muller, H. Klein, E. Lox, T. Kreuzer, and K. Ostgathner, "Catalytic NO_x Reduction on a Passenger Car Diesel Common Rail Engine," *SAE*, vol. 980191, 1998.
- [152] J. C. Conklin and J. P. Szybist, "A highly efficient six-stroke internal combustion engine cycle with water injection for in-cylinder exhaust heat recovery," *Energy*, vol. 35, no. 4, pp. 1658-1664, Apr. 2010.
- [153] V. Subramanian, J. Mallikarjuna, and A. Ramesh, "Effect of water injection and spark timing on the nitric oxide emission and combustion parameters of a hydrogen fuelled spark ignition engine," *International Journal of Hydrogen Energy*, vol. 32, no. 9, pp. 1159-1173, Jun. 2007.
- [154] E. Radloff, "NO_x Emissions Reduction Through Water Injection," *Naval Engineers Journal*, vol. 118, no. 3, pp. 65-76, 2006.
- [155] D. Hountalas, G. Mavropoulos, T. Zannis, and S. Mamalis, "Use of Water Emulsion and Intake Water Injection as NO_x Reduction Techniques for Heavy Duty Diesel Engines," *SAE 2006-01-1414*, 2006.
- [156] K. Breda and P. Stanislav, "Reduction of Diesel Engine Emissions by Water Injection," *SAE 2001-01-3259*, 2001.
- [157] G. Andrews, K. Bartle, S. Pang, A. Nurein, and P. Williams, "The Reduction in Diesel Particulate Emissions Using Emulsified Fuels," vol. 880348, 1988.
- [158] J. Park, K. Huh, and K. Park, "Experimental study on the combustion characteristics of emulsified diesel in a rapid compression and expansion machine," *Proc IMechE, Part D: Journal of Automobile Engineering*, vol. 214, no. 5, pp. 579-86, 2000.
- [159] N. Samec, B. Kegl, and R. W. Dibble, "Numerical and experimental study of

- water/oil emulsified fuel combustion in a diesel engine,” *Fuel*, vol. 81, no. 16, pp. 2035-2044, Nov. 2002.
- [160] C. Lin and L. Chen, “Engine performance and emission characteristics of three-phase diesel emulsions prepared by an ultrasonic emulsification method,” *Fuel*, vol. 85, no. 5, pp. 593-600, 2006.
- [161] M. Y. E. Selim and S. M. S. Elfeky, “Effects of diesel/water emulsion on heat flow and thermal loading in a precombustion chamber diesel engine,” *Applied Thermal Engineering*, vol. 21, no. 15, pp. 1565-1582, Oct. 2001.
- [162] T. Kadota and H. Yamasaki, “Recent advances in the combustion of water fuel emulsion,” *Progress in Energy and Combustion Science*, vol. 28, no. 5, pp. 385-404, 2002.
- [163] R. H. Stanglmaier, P. J. Dingle, and D. Stewart, “Cycle-Controlled Water Injection for Steady-State and Transient Emissions Reduction From a Heavy-Duty Diesel Engine,” *J. Eng. Gas Turbines Power*, vol. 130, no. 3, 2008.
- [164] C. J. Chadwell and P. J. Dingle, “Effects of diesel and water co-injection with-real control time control on diesel engine performance and emission,” *SAE Paper 2008011190*, 2008.
- [165] O. Armas, R. Ballesteros, F. Martos, and J. Agudelo, “Characterization of light duty Diesel engine pollutant emissions using water-emulsified fuel,” *Fuel*, vol. 84, no. 7, pp. 1011-1018, May. 2005.
- [166] N. Sawa and S. Kajitani, “Physical Properties of Emulsion Fuel (Water/Oil-Type) and Its Effect on Engine Performance under Transient Operation,” vol. 920198, 1992.
- [167] The Institute of petroleum and BSI, “Crude petroleum and liquid petroleum products -- Laboratory determination of density -- Hydrometer method. BS EN 3675, The Institute of petroleum and BSI 1996,” 1996.
- [168] The Institute of petroleum and BSI, “Methods of test for Petroleum and its products: Transparent and opaque liquids- Determination of kinematic viscosity and calculation of dynamic viscosity. BS EN ISO 3104:1996, The Institute of petroleum and BSI 1996,” 1996.
- [169] F. Payri, J. Luján, J. Martín, and A. Abbad, “Digital signal processing of in-cylinder pressure for combustion diagnosis of internal combustion engines,” *Mechanical Systems and Signal Processing*, vol. 24, no. 6, pp. 1767-1784, Aug. 2010.
- [170] Z. G. Liu, T. A. Swor, J. J. Schauer, J. A. Debilzen, and C. L. Severance, “A Source Dilution Sampling System for Characterization of Engine Emissions under Transient or Steady-State Operation,” *Aerosol Science and Technology*, vol. 42, no. 4, p. 270, 2008.
- [171] J. Benajes, J. Luján, V. Bermúdez, and J. Serrano, “Modelling of turbocharged diesel engines in transient operation. Part 1: insight into the relevant physical phenomena,” *Proceedings of the Institution of Mechanical Engineers, Part D: Journal of Automobile Engineering*, vol. 216, no. 5, pp. 431-441, Jan. 2002.
- [172] M. Lindgren, “A Transient Fuel Consumption Model for Non-road Mobile Machinery,” *Biosystems Engineering*, vol. 91, no. 2, pp. 139-147, Jun. 2005.
- [173] O. Armas, R. Ballesteros, F. Martos, and J. Agudelo, “Characterization of light duty Diesel engine pollutant emissions using water-emulsified fuel,” *Fuel*, vol. 84, no. 7, pp. 1011-1018, May. 2005.
- [174] “Combustion Analysis of Esters of Soybean Oil in a Diesel Engine.”
- [175] M. Lindgren and P. -. Hansson, “Effects of Transient Conditions on Exhaust Emissions from two Non-road Diesel Engines,” *Biosystems Engineering*, vol. 87,

- no. 1, pp. 57-66, Jan. 2004.
- [176] C. Rakopoulos, A. Dimaratos, E. Giakoumis, and D. Rakopoulos, "Evaluation of the effect of engine, load and turbocharger parameters on transient emissions of diesel engine," *Energy Conversion and Management*, vol. 50, no. 9, pp. 2381-2393, Sep. 2009.
- [177] J. Arregle, V. Bermudez, J. Serrano, and E. Fuentes, "Procedure for engine transient cycle emissions testing in real time," *Experimental Thermal and Fluid Science*, vol. 30, no. 5, pp. 485-496, May. 2006.
- [178] A. J. MARTYR and M. A. PLINT, *Engine Testing: Theory and Practice*, 3rd ed. A Butterworth-Heinemann Title, 2007.
- [179] C. Lin and L. Chen, "Engine performance and emission characteristics of three-phase diesel emulsions prepared by an ultrasonic emulsification method," *Fuel*, vol. 85, no. 5, pp. 593-600, Mar. .
- [180] X. Tauzia, A. Maiboom, P. Chesse, and N. Thouvenel, "A new phenomenological heat release model for thermodynamical simulation of modern turbocharged heavy duty Diesel engines," *Applied Thermal Engineering*, vol. 26, no. 16, pp. 1851-1857, Nov. 2006.
- [181] J. M. Bland and D. G. Altman, "Statistics Notes: Measurement error and correlation coefficients," *BMJ*, vol. 313, no. 7048, pp. 41 -42, Jul. 1996.
- [182] M. Rakesh, "Lecture not on Automotive Power Units (NIA 2270)," Univeristy of Huddersfield.
- [183] J. Coulson, J. Richardson, J. Backhurst, and J. Harker, *Chemical Engineering: Particle Technology and Separation Processes v. 2*, 4th ed. Butterworth-Heinemann Ltd, 1996.
- [184] H. Hiroyasu, M. Arai, and M. Tabata, "Empirical Equations for the Sauter Mean Diameter of a Diesel Spray," in *SAE paper*, vol. 890464, 1989.
- [185] H. Hiroyasu, "Diesel Engine Combustion and its Modelling. In Diagnostics and modelling of combustion in Reciprocating Engines," in *COMODIA 85*, 1985.
- [186] C. Baumgarten, *Mixture formation in internal combustion engines*. Birkhäuser, 2006.
- [187] S. H. Park, H. J. Kim, H. K. Suh, and C. S. Lee, "Atomization and spray characteristics of bioethanol and bioethanol blended gasoline fuel injected through a direct injection gasoline injector," *International Journal of Heat and Fluid Flow*, vol. 30, no. 6, pp. 1183-1192, Dec. 2009.
- [188] B. M.F.J, R. Harjit, and E. Andrew L., "The Calculation of Heat Release Energy from Engine Cylinder Pressure Data," in *SAE paper*, vol. 981052, 1998.
- [189] J. Desantes, J. Galindo, C. Guardiola, and V. Dolz, "Air mass flow estimation in turbocharged diesel engines from in-cylinder pressure measurement," *Experimental Thermal and Fluid Science*, vol. 34, no. 1, pp. 37-47, Jan. 2010.
- [190] M. Gumus, "A comprehensive experimental investigation of combustion and heat release characteristics of a biodiesel (hazelnut kernel oil methyl ester) fueled direct injection compression ignition engine," *Fuel*.
- [191] A. Monyem, J. Van Gerpen, and M. Cankci, "The Effects of Timing and Oxidation on Emissions from biodiesel-Fueled Engines," *Transactions of the ASAE*, vol. 44, no. 1, pp. 35-42, 2001.
- [192] B. Kegl, "Numerical analysis of injection characteristics using biodiesel fuel," *Fuel*, vol. 85, no. 17, pp. 2377-2387, Dec. 2006.
- [193] M. Gumus, C. Sayin, and M. Canakci, "Effect of Fuel Injection Timing on the Injection, Combustion, and Performance Characteristics of a Direct-Injection (DI) Diesel Engine Fueled with Canola Oil Methyl Ester–Diesel Fuel Blends," *Energy*

- & *Fuels*, vol. 24, no. 5, pp. 3199-3213, May. 2010.
- [194] M. Balat, "Potential alternatives to edible oils for biodiesel production - A review of current work," *Energy Conversion and Management*, vol. 52, no. 2, pp. 1479-1492, Feb. 2011.
- [195] M. Abu-Zaid, "Performance of single cylinder, direct injection Diesel engine using water fuel emulsions," *Energy Conversion and Management*, vol. 45, no. 5, pp. 697-705, Mar. 2004.
- [196] M. Canakci, "Combustion characteristics of a turbocharged DI compression ignition engine fueled with petroleum diesel fuels and biodiesel," *Bioresource Technology*, vol. 98, no. 6, pp. 1167-1175, Apr. 2007.
- [197] F. Wu, J. Wang, W. Chen, and S. Shuai, "A study on emission performance of a diesel engine fueled with five typical methyl ester biodiesels," *Atmospheric Environment*, vol. 43, no. 7, pp. 1481-1485, Mar. 2009.
- [198] M. Abu-Qudais, "Exhaust gas temperature for knock detection and control in spark ignition engine," *Energy Conversion and Management*, vol. 37, no. 9, pp. 1383-1392, Sep. 1996.
- [199] F. Morey and P. Seers, "Comparison of cycle-by-cycle variation of measured exhaust-gas temperature and in-cylinder pressure measurements," *Applied Thermal Engineering*, vol. 30, no. 5, pp. 487-491, Apr. 2010.
- [200] S. Brusca and R. Lanzafame, "Evaluation of the Effects of Water Injection in a Single Cylinder CFR Cetane Engine," in *SAE paper*, 2001.
- [201] T. AL-Shemmeri and S. Oberweis, "Correlation of the NO_x emission and exhaust gas temperature for biodiesel," *Applied Thermal Engineering*.
- [202] C. Lin and K. Wang, "Diesel engine performance and emission characteristics using three-phase emulsions as fuel," *Fuel*, vol. 83, no. 4, pp. 537-545, Mar. 2004.
- [203] F. Payri, J. Luján, J. Martín, and A. Abbad, "Digital signal processing of in-cylinder pressure for combustion diagnosis of internal combustion engines," *Mechanical Systems and Signal Processing*, vol. 24, no. 6, pp. 1767-1784, Aug. 2010.
- [204] M. Lapuerta, O. Armas, and J. Rodríguez-Fernández, "Effect of biodiesel fuels on diesel engine emissions," *Progress in Energy and Combustion Science*, vol. 34, no. 2, pp. 198-223, Apr. 2008.
- [205] M. Abu-Zaid, "Performance of single cylinder, direct injection Diesel engine using water fuel emulsions," *Energy Conversion and Management*, vol. 45, no. 5, pp. 697-705, Mar. 2004.